Universidad de Valladolid
Facultad de Ciencias

Departamento de Física de la Materia Condensada, Cristalografía y Mineralogía.

Laboratorio CellMat

Tesis Doctoral

Improving the stiffness and strength of porous materials by enhancement of the matrix microstructure and cellular morphology

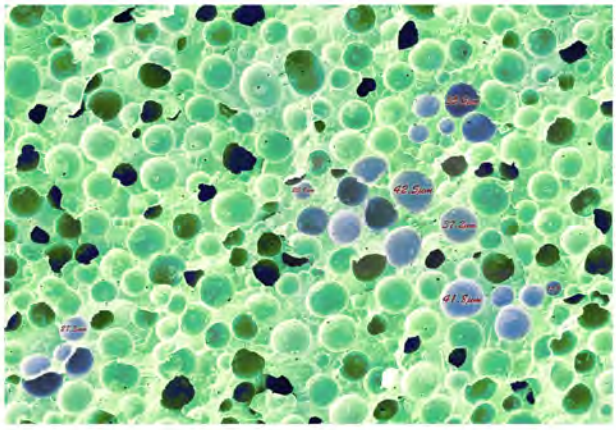

Juan Lobos Martín

Noviembre de 2012

Universidad de Valladolid

FACULTAD DE CIENCIAS

DEPARTAMENTO DE FÍSICA DE LA MATERIA CONDENSADA, CRISTALOGRAFÍA Y MINERALOGÍA

TESIS DOCTORAL:

Improving the stiffness and strength of porous materials by enhancement of the matrix microstructure and cellular morphology.

Presentada por Juan Lobos Martín para optar al grado de doctor por la Universidad de Valladolid

Dirigida por:
Miguel Ángel Rodríguez Pérez

Despite all the work presented in this thesis, the only thing that I am aware at this time are all the things that I have yet to learn to move forward.

Acknowledgements

Quizás la parte más difícil de todo el trabajo sea escribir los reconcimientos, ya que no es posible agradecer a todos aquellos con los que he compartido esta fase de mi vida. Si he sido capaz de finalizar la escritura de esta tesis ha sido gracias al apoyo que he recibido por parte de todos ellos, ya sea directo (familia, profesores, compañeros, amigos, etc,) o indirecto (proveedores, técnicos, especialistas, agricultores, etc). No me olvido de los que me ayudaron indirectamente, pero debido al espacio disponible me limitaré a hablar de los primeros.

Sin mis padres, quienes siempre han estado atentos y me han querido, nunca hubiese imaginado que los sueños de mi infancia podrían hacerse realidad solo con esfuerzo y determinación. Gracias por todos estos años.

El apoyo de estos últimos años junto a mi esposa, quien no solo desea compartir su vida conmigo, sino que también me ayuda constantemente con aquellos pequeños detalles que están a la vista de todos pero que nadie aprecia, así como con con mi inglés y el formato de esta tesis.

Quiero agradecer a Jose Antonio de Saja por darme la oportunidad de trabajar con él, permitiendome seguir aprendiendo.

También agradecer todos aquello que he aprendido gracias a la inestimable ayuda de M.A. Rodriguez-Perez y su paciencia a la hora de corregir mi trabajo (incluyendo esta tesis).

I also wanted to thank the exceptional treatment and opportunity offered to me by Hideo Nakajima-sensei, allowing me to work in his laboratory and teaching many things that are now in this thesis.

There is much to be grateful, not only by me but for more people, to Suzuki-sensei. Thanks to him I learned to organize my job. Although sometimes I have the feeling that I did not as well as I can under his supervision.

Personally I have much to thank to Utsunomiya-sensei. He was an important adviser during my stay in Japan, and it's a shame that we could not start any

common project, because I think I can still learn a lot from him on matters currently I can only guess.

I also want to thank all those who shared my stay in Nakajima laboratory at Osaka University, students and teachers, with whom I shared unforgettable moments and now will always be in my heart.

Son muchas las personas en CellMat a las que aprecio y que me han asistido siempre que lo he necesitado, puede que estas palabras sean escasas para agradeceros. Pero, ¿qué son unas pocas palabras en comparación con vuestra presencia? Mi estancia aquí hubiese sido bien distinta de no haber sido por vosotros: Jorge, Eusebio, Cristina, Silvia, Javi, Jaime, Cesar, Natalia, Cesar II, Alberto, Josias, Dani, Sergio Pinto, Samu, Belen, Ester (por favor ignorad el orden, ya que es el orden aproximado en que os fui conociendo). Gracias por todo.

No quiero olvidarme de Blanca y Laura, sin ellas no hubiese podido caracterizar millares de muestras, siempre han estado enseñándome a conocer todos los detalles de la caracterización con una sonrisa y ahora soy capaz de hacerlo por mi mismo. Más recientemente comencé a trabajar con Puri y Haritz, quienes me han ayudado y han soportado mi presencia en la misma sala.

Para finalizar no quiero olvidar a Emi, no es solo que nos ayude en los tramites burocráticos para que perdamos el mínimo tiempo posible para resolverlos, se preocupa antes que nosotros en resolver todas las trabas administrativas antes que nos veamos atrapados por ellas. Todos los años que he estado en el departamento siempre he notado como nos cuidaba en todo momento.

Tampoco quiero olvidar a los muchos amigos que me han apoyado incondicionalmente todos estos años. También os he tenido presentes a la hora de realizar este trabajo.

Gracias a todos por compartir conmigo estos años, y espero que nos sigamos encontrando en el futuro.

Thank you to everyone for sharing these years with me, i hope we continue to meet again in the future.

Indice (Index)

1 Introducción

1.1 Introducción

Existe una cantidad significativa de materiales porosos en la naturaleza, como es el caso de la madera, huesos, tallos y hojas. Las celdas o poros en estos materiales poseen múltiples funciones, como aligerar el peso de la estructura, permitir que exista permeabilidad a los fluidos, lograr aislamiento térmico, mejorar en masticabilidad, etc.
Un ejemplo muy interesante es el hueso. Superficialmente los huesos tienen un aspecto sólido, pero al explorarlos detenidamente la mayoría de los huesos presentan una estructura más elaborada compuesta de una corteza más densa y compacta, envolviendo un núcleo poroso de celdas o tejido esponjoso. La composición base del hueso es un compuesto aligerado relativamente duro, formado en su mayoría por fosfato cálcico ordenado en la estructura cristalográfica de la hidroxiapatita de calcio, $Ca_5(PO_4)_3(OH)$[1]. Esta configuración minimiza el peso del hueso a la vez que permite una amplia superficie de apoyo, un diseño que reduce los puntos de acumulación de esfuerzos en las uniones [3].

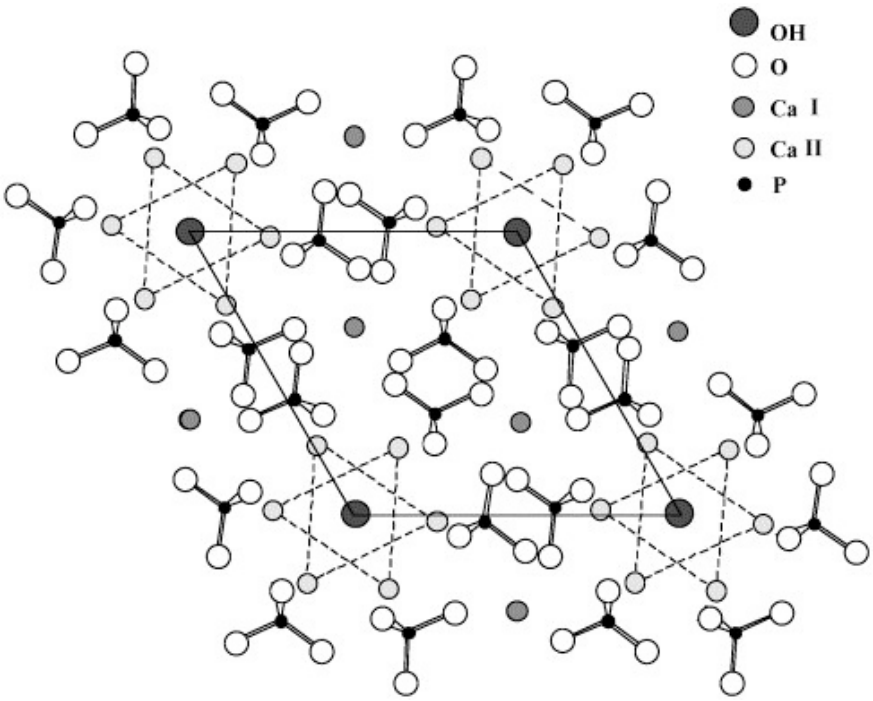

Figura 1: *Proyección en el plano (001) de la estructura de la hidroxiapatita* de calcio.*[2]*

Los materiales celulares naturales tienen por matriz sólidos muy diversos. Por ejemplo, la madera está compuesta básicamente de celulosa y lignina [4,5]. La celulosa es un polímero orgánico consistente en una larga cadena de glucosa (Figura 1a). La lignina es un complejo polímero orgánico; el monómero original es el ácido aminofenilpropanoico (Figura 1b). El enlace intermolecular entre la celulosa y la lignina es la razón principal de la rigidez en la estructura de la madera.

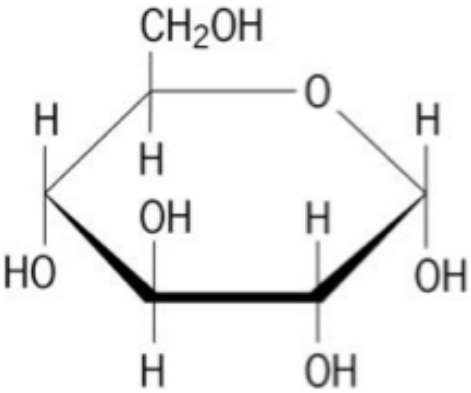

Figura 1a: *Estructura química de la glucosa*

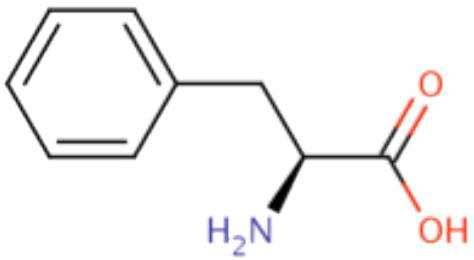

Figura 1b: *Estructura química del ácido amino-fenilpropanoico*

Pese a las diferencias en su composición química la función primaria de ambos materiales, madera y hueso, es estructural.

Los materiales sintéticos celulares, tanto poliméricos como metálicos, se utilizan principalmente como materiales funcionales para aislamientos térmico, aislamiento acústico, absorción de impactos y vibraciones, etc [6-8]. No obstante, **la presente tesis se centra en materiales sintéticos celulares cuyo uso sería principalmente estructural**. Esta función estructural para los materiales celulares, muy común en la naturaleza, no es tan habitual en nuestros diseños. De hecho estos diseños usuales utilizan materiales macizos con fines estructurales, a pesar de que hay una clara tendencia a cambiar este concepto clásico [9,10].

El objetivo principal de esta investigación es mejorar la rigidez y la resistencia de dos clases de materiales celulares.
El primero es cobre poroso tipo lotus (como ejemplo de un metal). Para estos materiales el estudio se centró en mejorar la microestructura y propiedades de la matriz metálica, manteniendo al mismo tiempo la estructura celular.

El segundo es un material celular, basado en polietileno de baja densidad (como ejemplo de un termoplástico). En este caso particular el principal propósito es producir un material sin reticulación con una estructura celular mejorada mediante la reducción del tamaño de celda y una mayor homogeneidad en ña distribución de tamaños celulares. Para poder obtener estos materiales se ha desarrollado un nuevo proceso de espumado.

El presente trabajo se ha desarrollado en dos localizaciones distintas:

El **metal poroso** estructural se desarrolló y caracterizó en el Nakajima Laboratory perteneciente al ISIR (Institute for Scientific and Industrial Research), de la Universidad de Osaka, en Japón, bajo la supervisión del profesor H. Nakajima.

El **polímero celular** basado en el polietileno se desarrolló y caracterizó en el CellMat Laboratory en el Departamento de Física de la Materia Condensada de la Universidad de Valladolid, en España, bajo la supervisión del profesor M.A. Rodríguez-Perez.

Aunque la matriz de los dos tipos de materiales analizados es muy diferente, existen varios aspectos comunes en la fabricación y caracterización de ambos tipos de materiales celulares. Estos son algunos aspectos en común:

a) En ambos casos la densidad relativa (densidad del material dividida por la densidad del material sólido no poroso) de los materiales analizados era alta, entre 0.27 y 0.92 (porosidades de 73% a 8%). Esto es porque queremos conservar al máximo las propiedades de la matriz de soporte.
b) La producción del material se llevó a cabo en un proceso en el que la matriz es fundida.
c) El análisis de las propiedades mecánicas se ha realizado utilizando el mismo marco teórico.

La tesis se ha dividido en 9 capítulos conteniendo la siguiente información:

El Capítulo 2 introducen varios conceptos necesarios para entender el trabajo. Algunos de ellos tratan sobre sobre las propiedades mecánicas de los metales, los polímeros y sus características estructurales. Ademas se introducen los conceptos básicos asociados a las propiedades mecánicas de los materiales celulares y cómo pueden utilizarse para aligerar el peso total de una determinada estructura manteniendo el comportamiento mecánico.

Los Capítulos 3 a 5 describen la investigación llevada a cabo sobre metales porosos tipo lotus (metales lotus). La introducción (capítulo 3) muestra entre

otros aspectos cómo los metales porosos tipo lotus consiguen una dependencia lineal entre las propiedades mecánicas y la porosidad[11].

Los metales para uso estructural se fabrican mediante un proceso de forjado. El forjado puede producir una pieza más resistente que una de la misma forma conseguida mediante relleno de un molde con metal fundido.
Para conseguir su estructura porosa, los metales porosos tipo lotus fueron fabricado mediante fundición del metal, de modo que la matriz metálica del material resultante es más dúctil que la que se consigue en los metales forjados. Esta investigación se centró en mejorar las propiedades mecánicas de la matriz metálica para que se asemejen a aquellas de los metales forjados, sin deteriorar la estructura celular del cobre poroso tipo lotus.

El Capítulo 4 es un intento de hacer una mejora parcial de la estructura metálica mediante un proceso de tratamiento en la superficie de las piezas basada en la aplicación de deformación mediante un cepillo de alambre (wire-brush technique).

El Capítulo 5 introduce una técnica diseñada para la forja de metales, ECAE (Equal Channel Angular Extrusion), la cual fue modificada para poder aplicarla a metales porosos sin alterar la estructura porosa.

Los Capítulos 6, 7 y 8 describen la investigación llevada a cabo en espumas poliméricas en CellMat. Las espumas poliméricas convencionales no mantienen la relación lineal entre propiedades mecánicas y porosidad. Nam Suh [12] propuso la idea de desarrollar plásticos microcelulares los cuales mantendrían las propiedades mecánicas mas próximas a las de los polímeros sólidos. Habitualmente estas espumas poliméricas microcelulares han sido producidas con polímeros amorfos [13]. En nuestro caso el objetivo de la investigación era obtener una espuma microcelular a partir de un polímero semicristalino como el polietileno, siguiendo la idea principal de mejorar sus propiedades mecánicas.
El Capítulo 6 es una introducción a los procesos industriales utilizados en la actualidad para producir espumas poliméricas; y espumas microcelulares tras las cuales entramos en profundidad en el nuevo proceso de moldeado desarrollado para producir las espumas de esta tesis. Esta técnica permite producir espumas estructurales no reticuladas con una densidad baja.
El Capítulo 7 se centra en el análisis de las propiedades mecánicas de las espumas resultantes.
El Capítulo 8 estudia en profundidad la estructura celular resultante, la conductividad termica y los efectos globales de usar mas cantidad de agente espumante.

El Capítulo 9 hace un resumen de las conclusiones obtenidas durante esta investigación.

1.2 Investigación desarrollada en esta tesis

El trabajo desarrollado en esta tesis ya ha sido diseminado en varias publicaciones tal como puede verse en la siguiente tabla.

1	*Mechanical Behaviour at Low Strains of LDPE Foams with Cell Sizes in the Microcellular Range: Advantages of Using These Materials in Structural Elements.*	
	Rodríguez Pérez, M. A.; Lobos Martín, J.; Pérez Muñoz, C.; de Saja Sáez, J. A.; González Gutierrez, L. M.; del Carpio, M.A.	
	Cellular Polymers, vol. 27, no.6, pp. 347-362	2008
2	*Mechanical Response of Polyethylene Foams with High Densities and Cell Sizes in the Microcellular Range.*	
	Rodriguez-Perez, M.A.; Lobos, J.; Perez-Muñoz, C.A.; de Saja J.A.	
	Journal of Cellular Plastics. vol. 45 no. 5 pp.389-403	2009
3	*Structural change and improvement of the mechanical properties of a lotus-type porous copper by wire-brushing.*	
	J Lobos, S Suzuki, H Nakajima, Y S Ji, H Fujii, D Terada, N Tsuji,	
	Journal of Physics: Conference Series. Vol 165 no.1	2009
4	*Structure Change and Improvement of the Mechanical Properties of Lotus-Type Porous Copper by ECAE Process.*	
	J Lobos ,S Suzuki, H Utsunomiya, H Nakajima	
	Materials Science Forum. Vol.620 - 622 pp.757-760	2009
5	*Mechanical Behaviour of High Density Polyethylene Based Foams.*	
	Lobos, J.; Rodriguez-Perez, M.A.; del Carpio, M.A.; de Saja J.A.	
	Materials Science Forum. Vol.620 - 622 pp.781-784	2009
6	*Effect of Pass Route and Pass Number of Equal-Channel Angular Extrusion on Structure and Strength of Lotus-type Porous Copper.*	
	S Suzuki, J Lobos Martin, H Utsunomiya, H Nakajima	
	Steel Research International, Vol. 81, No. 9, pp.482-485	2010
7(*)	ECAEによるロータス型ポーラス銅の変形と強化	
	鈴木進補, ファン・ロボス, 宇都宮裕, 中嶋英雄	
	銅と銅合金 49 1 244-248	2010
7 T	Deformation and improvement of mechanical properties of lotus-type porous copper through ECAE *(English title of 7)*	
	Suzuki S, Lobos J, Utsunomiya H, Nakajima H.	
	Copper and copper alloy 49(1), pp.244-248	2010

8(‡)	ロータス型ポーラス金属の塑性加工	
	鈴木進補, Juan Lobos Martin, 宇都宮裕, 中嶋英雄	
	塑性と加工	2011
8 T	*Deformation Processing of Lotus-type Porous Metals. (English title of 8)*	
	Suzuki S, Lobos Martin J, Utsunomiya H, Nakajima H.	
	Japan Society for Technology of Plasticity, Vol.52 pp.206-211	2011
9	*Strengthening of lotus-type porous copper by ECAE process.*	
	J Lobos ,S Suzuki, H Utsunomiya, H Nakajima, MA Rodrigez-Perez	
	Journal of Materials Processing Technology 212 pp.2007-2011	2012
10	*Improving the mechanical behaviour of lotus-type porous copper by wire-brushing.*	
	J Lobos, S Suzuki, H Nakajima, Y S Ji, H Fujii, D Terada, N Tsuji, MA Rodrigez-Perez	
	Journal of Materials Science and Technology	Submitted
11	*Thermal conductivity and cellular structure of polyethylene foams by improved compression moulding route.*	
	J. Lobos, M.A. Rodrigez-Perez	
	journal of polymer science: polymer physics	Submitted

El articulo 7 (*) es una traducción del articulo 6 para la sociedad japonesa de metales, escrito en Japonés por el Dr. Suzuki.

El articulo 8 (‡) es una revisión de todos los métodos de forjado desarrollados para los materiales tipo lotus con los proceedings enviados a los congresos , indicados en la siguiente tabla 4, 5, 7 y 8, junto con el trabajo que se realizóó procesando el cobre tipo lotus por Rolling [14]. Escrito en Japonés por el Dr. Suzuki.
Ademas partes de la investigación se han presentado en los siguientes congresos internacionales.

1	Blowing Agents Conference 2008	
	(Oral presentation)	
	"Mechanical Response of High density Polyolefin based foams"	
	M.A. Rodriguez-Perez, J. Lobos, J.A. de Saja, MAB del Carpio, JF Lopez Díaz	
	Berlin, Germany.	May 2008
2	2008 Fall Annual Meeting of The Japan Institute of Metals	
	(Oral presentation)	
	"Mechanical Properties At Low Strains o Microcellular LDPE Foams"	
	M.A. Rodriguez-Perez, J.Lobos, C. Perez-Muñoz, J.A. de Saja.	
	Kumamoto, Japan.	September 2008

3	Foams 2008	
	(Oral presentation)	
	"Improvement of the mechanical properties of lotus-type porous copper by wire-brushing"	
	J. Lobos, S. Suzuki, H. Nakajima, Y. S. Ji, H. Fujii, D. Terada, N. Tsuji.	
	Charlotte, USA.	September 2008
4	International Conference on Advanced Structural and Functional Materials Design 2008	
	(Poster presentation)	
	"Structural change and improvement of the mechanical properties of a lotus-type porous copper by wire-brushing."	
	J. Lobos, S. Suzuki, H. Nakajima, Y. S. Ji, H. Fujii, D. Terada, N. Tsuji.	
	Osaka, Japan.	November 2008
5	The 10th International Symposium on Eco-materials Processing and Design	
	(Oral presentation)	
	"Structure Change and Improvement of the Mechanical Properties of Lotus-type Porous Copper by ECAE Process"	
	J. Lobos, S. Suzuki, H. Utsunomiya, H. Nakajima.	
	Xi'an, China.	January 2009
6	The 10th International Symposium on Eco-materials Processing and Design	
	(Oral presentation)	
	"Mechanical behaviour of high density Polyethylene based foams"	
	J. Lobos, M. A. Rodriguez-Perez, M. del Carpio, J. A. de Saja.	
	Xi'an, China.	January 2009
7	2009 Spring Annual Meeting of The Japan Institute of Metals	
	(Oral presentation)	
	"Improvement of mechanical properties of Lotus-type porous copper by ECAE"	
	J.Lobos, S.Suzuki, H.Utsunomiya, H.Nakajima	
	Tokyo, Japan.	March 2009
8	6th International Conference on Porous Metals and Metallic Foams METFOAM 2009	
	(Oral presentation)	
	"Improvement of strength of porous copper with directional pores by ECAE"	
	J. Lobos, S. Suzuki, H. Utsunomiya and H. Nakajima.	
	Bratislava, Slovakia.	September 2009

1.3 Estructura de la presente tesis

En esta tesis se ha usado el formato de compendio de artículos. Es decir, parte de los trabajos publicados o enviados se han usado en los diferentes capítulos tal y como se indica en la tabla que sigue.

	Chapter 4	
8	*Improving the mechanical behaviour of lotus-type porous copper by wire-brushing.*	
	J Lobos, S Suzuki, H Nakajima, Y S Ji, H Fujii, D Terada, N Tsuji, MA Rodrigez-Perez	
	Journal of Materials Science and Technology	Submitted
	Chapter 5	
7	*Strengthening of lotus-type porous copper by ECAE process.*	
	J Lobos ,S Suzuki, H Utsunomiya, H Nakajima, MA Rodrigez-Perez	
	Journal of Materials Processing Technology 212 pp.2007-2011	2012
	Chapter 7	
1	*Mechanical Behaviour at Low Strains of LDPE Foams with Cell Sizes in the Microcellular Range: Advantages of Using These Materials in Structural Elements.*	
	Rodríguez Pérez, M. A.; Lobos Martín, J.; Pérez Muñoz, C.; de Saja Sáez, J. A.; González Gutierrez, L. M.; del Carpio, M.A.	
	Cellular Polymers, vol. 27, no.6, pp. 347-362	2008
	Chapter 7	
2	*Mechanical Response of Polyethylene Foams with High Densities and Cell Sizes in the Microcellular Range.*	
	Rodriguez-Perez, M.A.; Lobos, J.; Perez-Muñoz, C.A.; de Saja J.A.	
	Journal of Cellular Plastics. vol. 45 no. 5 pp.389-403	2009
	Chapter 8	
9	*Thermal conductivity and cellular structure of polyethylene foams by improved compression moulding route.*	
	J. Lobos, M.A. Rodrigez-Perez	
	journal of polymer science: polymer physics	Submitted

1.4 Técnicas de caracterización usadas en la presente tesis

En la realización de la presente tesis se han usado múltiples técnicas de caracterización de la estructura celular, de la matriz de los distintos materiales y en as propiedades. Se resumen brevemente dichas técnicas a continuación.

1.4.1 Caracterización de la estructura celular:

Densidad: La caracterización de la densidad se realizó con el kit de densidad hidrostática de la balanza Mettler Toledo AT261.

Imágenes SEM: Acronimo del ingles Scanning Electron Microscope (Microscopio electrónico de barrido)[15]. Proporcionó imágenes de la estructura celular en detalle de los materiales estudiados, los poliméricos habían sido previamente recubiertos por una fina capa de oro para hacerlos conductores. En el laboratorio de Nakajima se usó un FE–SEM JEOL 9800, Mientras que en CellMat se disponía de un SEM JEOL JSM-820

Microscopía óptica: Las imágenes de la estructura celular de los metales tipo lotus han sido tomadas con una microscopio digital KEYENCE VHX-200. Algunas muestras de cobre han sido atacadas con acido para diferenciar los granos metálicos del cobre y de las espumas lotus.

Reconocimiento de Imagenes: Se utilizo el software gratuito ImageJ [16] con un plugin desarrollado por el CelMat para reconocer las estructuras celulares de los distintos materiales porosos a partir de imágenes de su estructura. Con esta herramienta se logran medidas automáticas y reproducibles de los parámetros básicos de la estructura celular.

1.4.2 Caracterización de las propiedades mecánicas:

Curva esfuerzo-deformación: Para todas las espumas se realizaron ensayos de esfuerzo-deformación con maquinas de ensayo universal para conocer las propiedades elásticas (Módulo de Young) y el comienzo de la deformación plástica (limite elástico) de los materiales estudiados[17]. En Japón se utilizó una maquina Instron 5582 para realizar ensayos de compresión a una velocidad de compresión de 0.15 mm/min y ensayos de tracción con una velocidad de estiramiento de 2 mm/min. En CellMat se utilizó una maquina INSTRON 5500R6025 con una velocidad de compresión de 1 mm/min para las espumas poliméricas.

1.4.3 Caracterización de la matriz polimérica:

Termogravimetria (TG): Se usó para determinar el contenido de azodicarbonamida en la formulación original de los precursores y verificar que las formulaciones preparadas eran correctas [18,19].

Calorimetría de barrido diferencial (DSC): La calorimetría diferencial de barrido puede ser utilizada para medir varias propiedades características de una muestra polimerica, como la fusión, la cristalización así como temperaturas de transiciones vítreas (Tg). Se ha utilizado para identificar el polímero que compone la espuma polimérica y ver si se ha alterado el mismo durante el proceso de espumación [18,19].

1.4.4 Caracterización de la matriz metálica:

Dureza: Para medir la dureza Vickers de la matriz metálica se usó un durómetro Akashi MVK-II

EBSD: Acrónimo en ingles de Electron backscatter diffraction (difracción de electrones por retrodispersión). Es una técnica de caracterización cristalográfica y microestructural. En ella, se mide directamente la orientación cristalográfica de un grano mediante indexación automática de su diagrama de difracción, compuesto por varias bandas de Kikuchi [20]. Se uso el microscopio FE–SEM JEOL 9800 como fuente de electrones para la difracción junto a un analizador de los patrones EBSD analyzer Tex SEM Labo. Inc. MSC-2200.

1.5 Referencias

*[1]. S. Bertazzo and C.A. Bertran. Key Engineering Materials, Bioceramics **18**, 309, 2006.*

*[2]. D. Eichert, M. Salomé, M. Banu, J. Susini, C. Rey; Spectrochimica Acta a Part B: Atomic Spectroscopy **60**,15, 2005.*

[3]. L.J. Gibson and M.F. Ashby M.F. "Cellular solids", Cambridge, UK: Cambridge University Press, 1997.

[4]. E. Sjöström "Wood Chemistry: Fundamentals and Application", Academic Press, Orlando, 1993.

*[5]. E. Adler. Wood Science and Technology **11**, 169, 1977.*

[6]. D. Klempner and K.C. Frisch eds. "Handbook of Polymeric Foams and Foam Technology", Hanser, 1991.

[7]. D. Eaves ed. "Handbook of Polymer Foams", Rapra Technology Limited, 2004.

[8]. T.A. Osswald and G. Menges "Materials Science of polymers for Engineers", Hanser Publishers, 2003.

[9]. B. C. Wendle "Structural foam", Marcel Dekker, 1985.

[10]. C. Koerner "Integral Foam Molding of Light Metals", Springer-Verlag Berlin Heidelberg, 2008.

*[11]. Nakajima H., Progress in Materials Science **52**,1091, 2007.*

[12]. N.P. Suh "Innovation in Polymer Processing", Hanser/Gardner Publications, Cincinnati, 1996.

*[13]. V. Kumar and N.P. Suh. Polymer Engineering & Science **30**,1323, 1990.*

*[14]. H. Utsunomiya, T. Yukimoto, T. Sakai, S. Suzuki, H. Nakajima. Materials Science Forum **658**, 328, 2010*

[15]. L. Reimer "Scanning Electron Microscopy: Physics of Image Formation and Microanalysis", Springer-Verlag Heildelberg, 1998.

[16]. http://rsb.info.nih.gov/ij/

[17]. F. Beer, R. Johnston, J. Dewolf and D. Mazurek "Mechanics of materials". , McGraw-Hill, New York, 2009.

[18]. A. Skoog, F. Douglas, J. Holler and T. Nieman "Principles of Instrumental Analysis" , New York, 1998.

[19]. J.P. Hernández-Ortiz "Differential Scanning Calorimetry: Polymers Characterization", Universidad Nacional de Colombia, 2004.

[20]. V. Randle. Materials Characterization **60**, 913, 2009.

1 Introduction (translation)

1.1 Introduction

There are a significant number of porous materials in nature. For instance woods, animal bones, leaves and stalks. The cells or pores in these materials have several functions, providing, lightweight, fluid permeability, thermal insulation, masticability, etc. A very interesting example is bone. Superficially, bones look fairly solid, but with a carefully exploration, most bones are an elaborate construction made up of an outer shell of dense compact bone, enclosing a core of porous cellular, cancellous or trabecular bone. The phosphate minerals are the basic matrix for bones. The primary tissue of bone is a relatively hard and lightweight composite material formed mostly of calcium phosphate in a chemical arrangement termed calcium hydroxyapatite, $Ca_5(PO_4)_3(OH)$[1]. This configuration minimizes the weight of

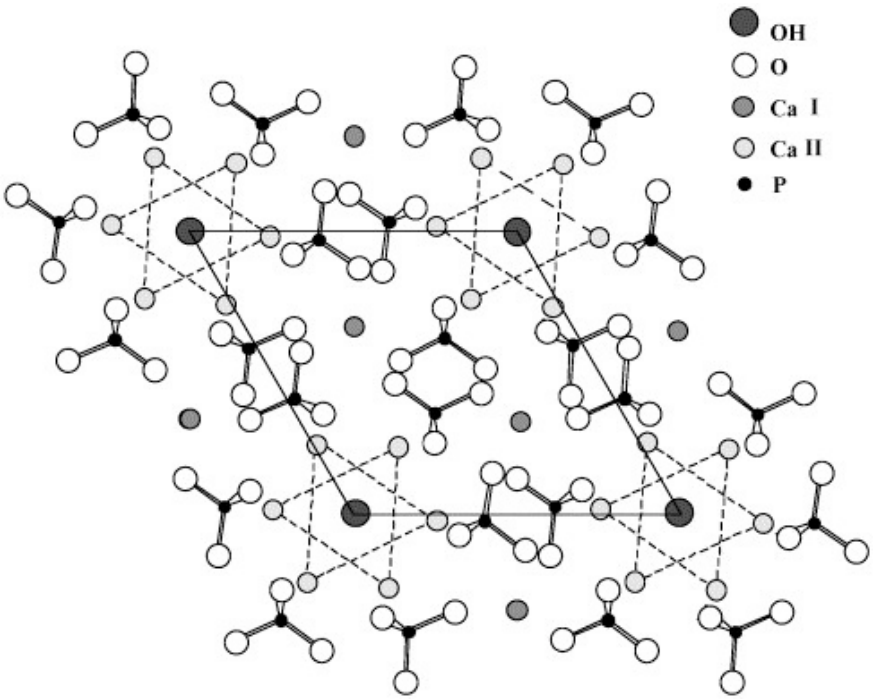

Figure 1: *Projection on the (001) plane of the hydroxyapatite structure.[2]*

bone while still providing a large bearing area, a design which reduces the bearing stresses at the joints [3].

Natural cellular materials are based on different types of solid materials. For instance wood is composed basically by cellulose and lignin[4,5]. Cellulose is an organic polymer, a polysaccharide consisting of a linear chain of glucose units (Figure 1a). Lignin is a complex organic polymer; the original monomer is aminophenylpropanoic acid (Figure 1b). The intermolecular bond between cellulose and lignin is the main reason for the rigid structure of wood.

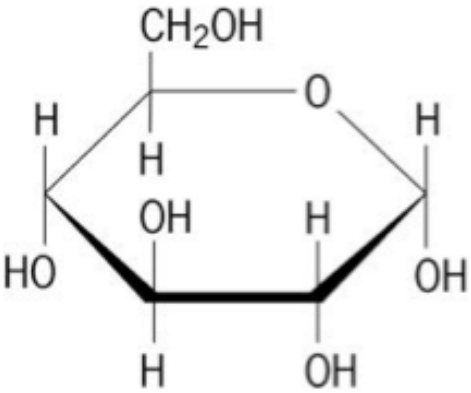

Figure 1a: *Chemical structure of glucose*

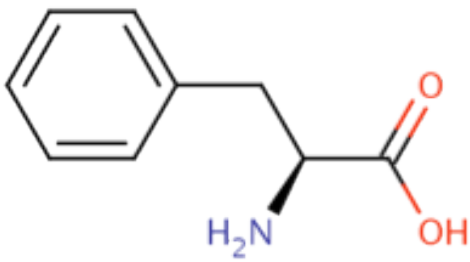

Figure 1b: *Chemical structure of amino-phenylpropanoic acid*

Despite of its cellular structure the primary function of both, wood and bone, is structural.

Synthetic cellular materials, both polymeric and metallic, are mainly used as functional materials for thermal insulation, acoustic management, energy absorption, etc[6-8]. However, **the present thesis is focused on synthetic cellular materials as load-bearing structural materials**. These materials, common in the natural world, wood an bone, are not so common in the current technology. In fact most of our current designs use bulk materials for structural purposes, although there is a clear trend to change this classical concept[9,10].

The main objective of this thesis is improving the stiffness and strength of two different types of cellular materials.
The first type is lotus type porous copper (as an example of metal). For these materials the study has been focused on improving the microstructure and

properties of the metallic matrix keeping at the same time the cellular structure.
The second one is a cellular material, based on a low-density polyethylene (as an example of thermoplastic). In this particular case the main purpose was producing a non-crosslinked material with improved cellular structure by reducing cell size and improving cell size homogeneity. In order to obtain these materials a novel foaming route has been developed

The present work was carried out in two different locations:

The structural **porous metals** were produced and characterized in the Nakajima Laboratory in the ISIR (Institute for Scientific and Industrial Research) at Osaka University in Japan under the supervision of professor H. Nakajima.

The structural **cellular polymers** were produced and characterized in the CellMat Laboratory in the Condensed Mater Physic Department of the University of Valladolid under the supervision of professor M.A. Rodriguez-Perez.

Although the matrix of the two type of materials analyzed is very different there are several common aspect in the fabrication and characterization of both types of cellular materials. These are some of those common aspects:

a) In both cases, the relative density (density of the material divided by the density of the non porous solid material) of the analyzed materials was high, between 0.27 and 0.92 (Porosities between 73% to 8%). This is caused because high relative densities are needed for keeping up to some extend the mechanical properties of the matrix.
b) The production of the material was carried out in a process in which the matrix is molten.
c) The analysis of the mechanical properties has been done using the same theoretical framework.

The thesis has been divided in 9 chapters containing the following information

Chapter 2 will introduce several concepts needed to understand the work. Some of them are related to the mechanical properties of metals and polymers as structural support. In addition basic concepts about the mechanical properties of cellular materials and the advantages of using them in structural applications are included

Chapters 3 to 5 will describe the research conducted on lotus-type porous metals (lotus metals). The introduction (chapter 3) will show how Lotus-type porous metals archived the necessary linear dependence between the mechanical properties and the porosity[11]. In general structural metals are post-processed by forging. Forging can produce a piece that is stronger than an equivalent cast or machined part. Lotus-type porous metals were processed by casting, so the metallic matrix of the resultant material is softer than the typical obtained in forged metals. The research was focused on improving the strength characteristics of the matrix to obtain similar values than that of typical forged metals, without deteriorating the cellular structure.

Chapter 4 is an attempt to make a partial improvement of the metal matrix by producing a small alteration of the surface using a wire-brush technique.

Chapter 5 introduces a technique designed for metal forging, ECAE (Equal Channel Angular Extrusion), which was modified to be applied to porous metals leaving unchanged the porous structure of the lotus-type copper.

Chapters 6 to 8 will describe the research conducted on cellular polymers at CellMat Laboratory. Polymeric foams did not archive the linear relationship between mechanical properties and porosity. Nam Suh [12] proposed the idea of developing microcellular plastics to promote the material toughness by tiny spherical cells that act as crack arrestors by blunting the crack tip. Typically these microcellular polymeric foams had been produced by using amorphous polymers [13]. In this case the objective of the research was to obtain a microcellular foam from a semi-crystalline polymer such as low density polyethylene with the objective of improving the mechanical performance.

Chapter 6 is an introduction to industrial processes currently used to produce semi-crystalline polymer foams, and microcellular foams after which we enter fully into the novel moulding process developed to produce the foams of this thesis. This technique allows producing non-crosslinked structural foams with relatively low-density.

Chapter 7 focuses on the analysis of the mechanical properties of the resulting foams.

Chapter 8 focuses on the analysis of the cellular structure of the foams, the effect of using different amounts of blowing agent, and the thermal conductivity of the foams produced.

Chapter 9 summarizes the conclusions of the conducted research.

1.2 Research conducted in this thesis

The work conducted in this thesis has been already disseminated in several publications as it can be seen in the following table.

1	*Mechanical Behaviour at Low Strains of LDPE Foams with Cell Sizes in the Microcellular Range: Advantages of Using These Materials in Structural Elements.*	
	Rodríguez Pérez, M. A.; Lobos Martín, J.; Pérez Muñoz, C.; de Saja Sáez, J. A.; González Gutierrez, L. M.; del Carpio, M.A.	
	Cellular Polymers, vol. 27, no.6, pp. 347-362	2008
2	*Mechanical Response of Polyethylene Foams with High Densities and Cell Sizes in the Microcellular Range.*	
	Rodriguez-Perez, M.A.; Lobos, J.; Perez-Muñoz, C.A.; de Saja J.A.	
	Journal of Cellular Plastics. vol. 45 no. 5 pp.389-403	2009
3	*Structural change and improvement of the mechanical properties of a lotus-type porous copper by wire-brushing.*	
	J Lobos, S Suzuki, H Nakajima, Y S Ji, H Fujii, D Terada, N Tsuji,	
	Journal of Physics: Conference Series. Vol 165 no.1	2009
4	*Structure Change and Improvement of the Mechanical Properties of Lotus-Type Porous Copper by ECAE Process.*	
	J Lobos ,S Suzuki, H Utsunomiya, H Nakajima	
	Materials Science Forum. Vol.620 - 622 pp.757-760	2009
5	*Mechanical Behaviour of High Density Polyethylene Based Foams.*	
	Lobos, J.; Rodriguez-Perez, M.A.; del Carpio, M.A.; de Saja J.A.	
	Materials Science Forum. Vol.620 - 622 pp.781-784	2009
6	*Effect of Pass Route and Pass Number of Equal-Channel Angular Extrusion on Structure and Strength of Lotus-type Porous Copper.*	
	S Suzuki, J Lobos Martin, H Utsunomiya, H Nakajima	
	Steel Research International, Vol. 81, No. 9, pp.482-485	2010
7(*)	ECAEによるロータス型ポーラス銅の変形と強化	
	鈴木進補, ファン・ロボス, 宇都宮裕, 中嶋英雄	
	銅と銅合金 49 1 244-248	2010
7 T	Deformation and improvement of mechanical properties of lotus-type porous copper through ECAE *(English title of 7)*	
	Suzuki S, Lobos J, Utsunomiya H, Nakajima H.	
	Copper and copper alloy 49(1), pp.244-248	2010

8(‡)	ロータス型ポーラス金属の塑性加工	
	鈴木進補, Juan Lobos Martin, 宇都宮裕, 中嶋英雄	
	塑性と加工	2011
8 T	*Deformation Processing of Lotus-type Porous Metals. (English title of 8)*	
	Suzuki S, Lobos Martin J, Utsunomiya H, Nakajima H.	
	Japan Society for Technology of Plasticity, Vol.52 pp.206-211	2011
9	*Strengthening of lotus-type porous copper by ECAE process.*	
	J Lobos ,S Suzuki, H Utsunomiya, H Nakajima, MA Rodrigez-Perez	
	Journal of Materials Processing Technology 212 pp.2007-2011	2012
10	*Improving the mechanical behaviour of lotus-type porous copper by wire-brushing.*	
	J Lobos, S Suzuki, H Nakajima, Y S Ji, H Fujii, D Terada, N Tsuji, MA Rodrigez-Perez	
	Journal of Materials Science and Technology	Submitted
11	*Thermal conductivity and cellular structure of polyethylene foams by improved compression moulding route.*	
	J. Lobos, M.A. Rodrigez-Perez	
	journal of polymer science: polymer physics	Submitted

Article 7 (*) is a translation of Article 6 for metal Japanese society, written in Japanese by Dr. Suzuki.

Article 8 (‡) is a review of all forging methods developed for lotus-type metals. This work is based on on the conference proceedings (4, 5, 7 and 8) indicated in the following table with the work made by Rolling [14], written in Japanese by Dr. Suzuki .

In addition, part of the research has been presented in international conferences. The following table summarize this aspect.

1	Blowing Agents Conference 2008	
	(Oral presentation)	
	"Mechanical Response of High density Polyolefin based foams"	
	M.A. Rodriguez-Perez, J. Lobos, J.A. de Saja, MAB del Carpio, JF Lopez Díaz	
	Berlin, Germany.	May 2008
2	2008 Fall Annual Meeting of The Japan Institute of Metals	
	(Oral presentation)	
	"Mechanical Properties At Low Strains o Microcellular LDPE Foams"	
	M.A. Rodriguez-Perez, J.Lobos, C. Perez-Muñoz, J.A. de Saja.	
	Kumamoto, Japan.	September 2008

3	Foams 2008	
	(Oral presentation)	
	"Improvement of the mechanical properties of lotus-type porous copper by wire-brushing"	
	J. Lobos, S. Suzuki, H. Nakajima, Y. S. Ji, H. Fujii, D. Terada, N. Tsuji.	
	Charlotte, USA.	September 2008
4	International Conference on Advanced Structural and Functional Materials Design 2008	
	(Poster presentation)	
	"Structural change and improvement of the mechanical properties of a lotus-type porous copper by wire-brushing."	
	J. Lobos, S. Suzuki, H. Nakajima, Y. S. Ji, H. Fujii, D. Terada, N. Tsuji.	
	Osaka, Japan.	November 2008
5	The 10th International Symposium on Eco-materials Processing and Design	
	(Oral presentation)	
	"Structure Change and Improvement of the Mechanical Properties of Lotus-type Porous Copper by ECAE Process"	
	J. Lobos, S. Suzuki, H. Utsunomiya, H. Nakajima.	
	Xi'an, China.	January 2009
6	The 10th International Symposium on Eco-materials Processing and Design	
	(Oral presentation)	
	"Mechanical behaviour of high density Polyethylene based foams"	
	J. Lobos, M. A. Rodriguez-Perez, M. del Carpio, J. A. de Saja.	
	Xi'an, China.	January 2009
7	2009 Spring Annual Meeting of The Japan Institute of Metals	
	(Oral presentation)	
	"Improvement of mechanical properties of Lotus-type porous copper by ECAE"	
	J.Lobos, S.Suzuki, H.Utsunomiya, H.Nakajima	
	Tokyo, Japan.	March 2009
8	6th International Conference on Porous Metals and Metallic Foams METFOAM 2009	
	(Oral presentation)	
	"Improvement of strength of porous copper with directional pores by ECAE"	
	J. Lobos, S. Suzuki, H. Utsunomiya and H. Nakajima.	
	Bratislava, Slovakia.	September 2009

1.3 Structure of the present thesis

This thesis is presented as a compendium of articles and some of the items included in the first table are incorporated in the various chapters of the thesis as follows.

	Chapter 4	
8	*Improving the mechanical behaviour of lotus-type porous copper by wire-brushing.*	
	J Lobos, S Suzuki, H Nakajima, Y S Ji, H Fujii, D Terada, N Tsuji, MA Rodrigez-Perez	
	Journal of Materials Science and Technology	Submitted
	Chapter 5	
7	*Strengthening of lotus-type porous copper by ECAE process.*	
	J Lobos ,S Suzuki, H Utsunomiya, H Nakajima, MA Rodrigez-Perez	
	Journal of Materials Processing Technology 212 pp.2007-2011	2012
	Chapter 7	
1	*Mechanical Behaviour at Low Strains of LDPE Foams with Cell Sizes in the Microcellular Range: Advantages of Using These Materials in Structural Elements.*	
	Rodríguez Pérez, M. A.; Lobos Martín, J.; Pérez Muñoz, C.; de Saja Sáez, J. A.; González Gutierrez, L. M.; del Carpio, M.A.	
	Cellular Polymers, vol. 27, no.6, pp. 347-362	2008
	Chapter 7	
2	*Mechanical Response of Polyethylene Foams with High Densities and Cell Sizes in the Microcellular Range.*	
	Rodriguez-Perez, M.A.; Lobos, J.; Perez-Muñoz, C.A.; de Saja J.A.	
	Journal of Cellular Plastics. vol. 45 no. 5 pp.389-403	2009
	Chapter 8	
9	*Thermal conductivity and cellular structure of polyethylene foams by improved compression moulding route.*	
	J. Lobos, M.A. Rodrigez-Perez	
	journal of polymer science: polymer physics	Submitted

1.4 Characterization techniques used in this thesis

Multiple characterization techniques have been used to study the cell structure, the matrix and the properties of the materials produced in this research. A brief description of these techniques is given in the following paragraphs.

1.4.1 Characterization of cellular structure:

Density: The density characterization was performed with the balance Mettler Toledo AT261 and the hydrostatic density kit for this system.

SEM images: Scanning Electron Microscopy[15] provide images in detail of the cell structure, the polymer were previously coated with a thin layer of gold to make them conductive. In the Nakajima's laboratory a FE-SEM JEOL 9800 was used, while in the CellMat Lab a JEOL JSM-820 was available.

Optical microscopy: images of cellular structure of lotus-type porous metals have been taken with a digital microscope KEYENCE VHX-200. Some samples have been etched with acid to differentiate grains of copper and to study the grain size of the metallic matrix.

Image Recognition: We used the free software ImageJ [16] with a plugin developed by CelMat Lab. to recognize cellular structures of different porous materials using images of its structure. By using this software it is possible to accurately determine the key parameters of the cellular structure.

1.4.2 Characterization of the mechanical properties:

Stress-strain curves : Tension or compression tests were performed using universal testing machines to measure the elastic properties (Young's modulus) and the yield strength (elastic limit) of the materials studied[17]. An INSTRON 5582 machine was used to perform compression test with a compression speed of 0.15mm/min for ECAE samples and to carry out tension tests with a tension speed of 2mm/min for Wire-brush samples. An INSTRON 5500R6025 was used with a compression rate of 1 mm/min to characterize the polymeric foams.

1.4.3 Characterization of the polymeric matrix:

Thermogravimetry (TG) was used to determine the content of azodicarbonamide in the original formulation of the foam precursors and validate the production of these precursors [18,19].

Differential Scanning Calorimetry (DSC) can be used to characterize several properties of a polymer sample, such as melting temperature (Tm), glass transitions temperature (Tg) etc. It is an useful technique to identify the

polymer and to analyze if the polymer has been affected by the foaming process [18,19].

1.4.4 Characterization of the metallic matrix:

A **Hardness tester** was used to measure the Vickers hardness of the metallic matrix. The used equipment was the Akashi MVK-III.

Electron backscatter diffraction (EBSD) is a microstructural-crystallographic technique used to examine the crystallographic orientation of many materials. It is a very useful technique to measure the size of the metal grains in the metallic matrix[20]. The FE-SEM JEOL 9800 was used as electron source for the electron diffraction, and completed with a patterns analyzer Labo Tex. Inc. MSC-2200.

1.5 References

*[1]. S. Bertazzo and C.A. Bertran. Key Engineering Materials, Bioceramics **18**, 309, 2006.*

*[2]. D. Eichert, M. Salomé, M. Banu, J. Susini, C. Rey; Spectrochimica Acta a Part B: Atomic Spectroscopy **60**,15, 2005.*

[3]. L.J. Gibson and M.F. Ashby M.F. "Cellular solids", Cambridge, UK: Cambridge University Press, 1997.

[4]. E. Sjöström "Wood Chemistry: Fundamentals and Application", Academic Press, Orlando, 1993.

*[5]. E. Adler. Wood Science and Technology **11**, 169, 1977.*

[6]. D. Klempner and K.C. Frisch eds. "Handbook of Polymeric Foams and Foam Technology", Hanser, 1991.

[7]. D. Eaves ed. "Handbook of Polymer Foams", Rapra Technology Limited, 2004.

[8]. T.A. Osswald and G. Menges "Materials Science of polymers for Engineers", Hanser Publishers, 2003.

[9]. B. C. Wendle "Structural foam", Marcel Dekker, 1985.

[10]. C. Koerner "Integral Foam Molding of Light Metals", Springer-Verlag Berlin Heidelberg, 2008.

*[11]. Nakajima H., Progress in Materials Science **52**,1091, 2007.*

[12]. N.P. Suh "Innovation in Polymer Processing", Hanser/Gardner Publications, Cincinnati, 1996.

*[13]. V. Kumar and N.P. Suh. Polymer Engineering & Science **30**,1323, 1990.*

[14]. H. Utsunomiya, T. Yukimoto, T. Sakai, S. Suzuki, H. Nakajima. Materials Science Forum ***658****, 328, 2010*

[15]. L. Reimer "Scanning Electron Microscopy: Physics of Image Formation and Microanalysis", Springer-Verlag Heildelberg, 1998.

[16]. http://rsb.info.nih.gov/ij/

[17]. F. Beer, R. Johnston, J. Dewolf and D. Mazurek "Mechanics of materials". , McGraw-Hill, New York, 2009.

[18]. A. Skoog, F. Douglas, J. Holler and T. Nieman "Principles of Instrumental Analysis" , New York, 1998.

[19]. J.P. Hernández-Ortiz "Differential Scanning Calorimetry: Polymers Characterization", Universidad Nacional de Colombia, 2004.

[20]. V. Randle. Materials Characterization **60**, 913, 2009.

2 Background

Resumen (Spanish):

En este capitulo se hace una introducción a los materiales que vamos a utilizar durante toda la tesis, polímeros y metales. Así mismo introducimos como se procesan dichos materiales cuando se quieren usar en aplicaciones estructurales, forjado para los metales y reforzados con fibras para los polímeros. Terminamos la introducción con las propiedades especificas de los materiales celulares así como el estudio particular de dos casos donde el uso del material es estructural, una viga y una plancha sometidos a una carga en su centro, y como la espumación del material puede conseguir una reducción del material necesario para construir dicha pieza conservando su capacidad de soportar esa carga.

2.1 Materials:

The new Oxford American dictionary[1] has as first meaning for **material**: "(noun) the matter from which a thing is or can be made" Given this broad definition, coupled with our management in the daily surroundings, we know that "materials" are use to do everything , our tools, our clothes, our homes, our furniture, etc.

Throughout history, materials have limited design. The ages in which man has lived are named for the materials used: stone, bronze, iron. The history of the humanity has been named by their options to choose and processed the materials. Now the number of materials available to make different products is vast: something over 120000 is at disposal[2], and although standardization strives to reduce the number, the continuing appearance of new materials with novel, exploitable, properties expands the options further.

This evolution is illustrated in Figure 2.1. The materials of pre-history (>10,000 BC, the Stone Age) were ceramics and glasses, natural polymers, and composites. Weapons—always the peak of technology — were made of wood and flint; buildings and bridges of stone and wood. Naturally occurring gold and silver were available locally and, through their rarity, assumed great influence as currency, but their role in technology was small. The development of rudimentary thermo-chemistry allowed the extraction of, first, copper and bronze, then iron (the Bronze Age, 4000–1000 BC and the Iron Age, 1000 BC–1620 AD) stimulating enormous advances in technology. Cast iron technology (1620s) established the dominance of metals in engineering; and since then the evolution of steels (1850 onward), light alloys (1940s) and special alloys, has consolidated their position. By the 1960s,

"engineering materials" mean "metals". Engineers were focused on metallurgy; other materials were rarely mentioned[3]. But in the last 50 years the metals have lost their position of leadership and industry dedicated to polymers and composites has experienced exceptional growth and projections of the growth in production of the new high-performance ceramics suggests continued expansion here also.

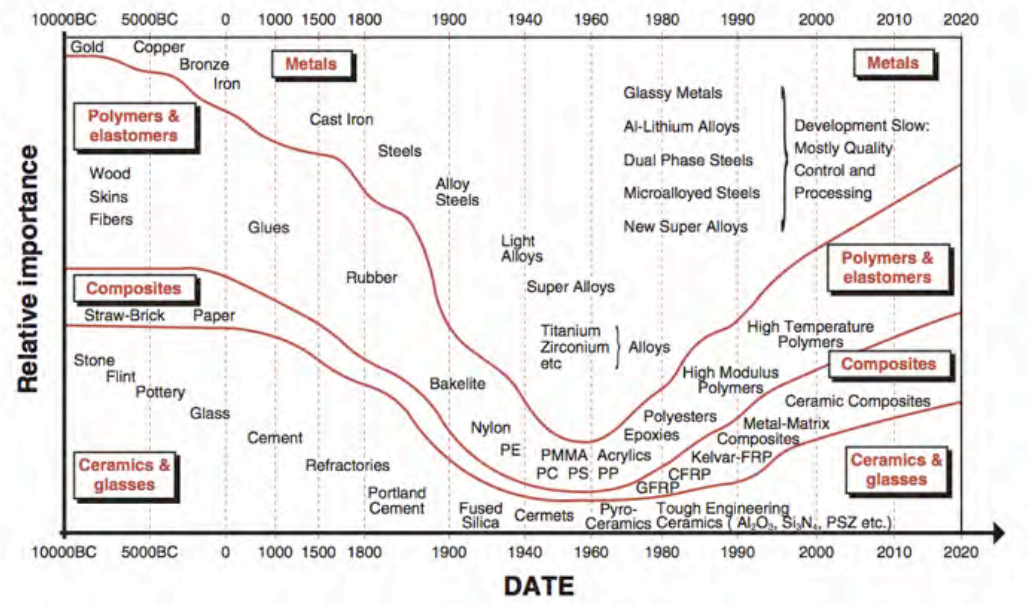

Figure 2.1: *Relative importance of materials though the history [2]*

2.2 Metallic and non-metallic materials.

While engineering materials are often grouped as metals, as are named in Figure 2.1, a simpler distinction might be to separate them into metallic and non-metallic. The common metallic materials include iron, copper, aluminum, magnesium, nickel, titanium, lead, tin, and zinc as well as the alloys of these metals, such as steel, brass, and bronze. They possess the metallic properties of lustre, high thermal conductivity, and high electrical conductivity; they are relatively ductile. Some common non-metals are wood, brick, concrete, glass, rubber, and plastics. Their properties vary widely, but they generally tend to be weaker, less ductile, and less dense than metals and to have poor electrical and thermal conductivities.

Although metals had the leadership in the first times of the industrial revolution, the non-metallic materials have become increasingly important after the Second World War. Advanced ceramics, composite materials, and engineered plastics have emerged in a number of applications. In many cases, metals and non-metals are viewed as competing materials, with selection being based on how well each is capable of providing the required properties. Where both perform adequately, total cost often becomes the deciding factor, where total cost includes both the cost of the material and the cost of fabricating the desired component. Factors such as product lifetime, environmental impact, energy requirements, and recyclability are also considered.

2.2.1 Metals

Most of the elements in the periodic table are metals. Metals have "free" electrons – electrons that flow in an electric field – so they conduct electricity well, they reflect light and they are completely opaque. The metals used in product design are, almost without exception, alloys. Steels account for more than 90% of all the metals consumed in the world; aluminum comes next, followed by copper, nickel, zinc, titanium, magnesium and tungsten[3].

No material was as important to the history of the human as metals. For millennia the history and technical evolution of human societies have been linked to the processing and production of metal tools.
From about 7000 BC a few neolithic communities begin hammering copper into crude knives and sickles, which work as well as their stone equivalents and last far longer. I took several millennia to improve the way to produce metal tools and first technological revolution comes with an entire period of early civilization has become known as the Bronze Age [4].
The cast alloy of copper and tin is bronze. A bronze blade will take a sharper edge than copper and will hold it longer. And bronze ornaments and vessels can be cast for a wide variety of purposes.

The next great development in the tool production involves a metal which is the most abundant in the earth's surface but which is much more difficult to work than copper or tin. It is iron, with a melting point too high for primitive furnaces to extract it in pure form from its ore. The best that can be achieved is a cluster of globules of iron mixed with sludgy impurities. This unpromising substance can be turned into a useful metal by repeated heating and hammering, until the impurities are literally forced out.

A few iron objects dating from before 2000 BC have been found (beads, a ring, some blades), but it is not until about 1500 BC that the working of iron is done anywhere on a regular basis. The Hittites are the first people to work iron[4].

By the 11th century BC it has been discovered that iron can be much improved. If it is reheated in a furnace with charcoal (containing carbon), some of the carbon is transferred to the iron. This process hardens the metal; and the effect is considerably greater if the hot metal is rapidly reduced in temperature, usually achieved by quenching it in water. The new material is steel. It can be worked (or 'wrought') just like softer iron, and it will keep a finer edge, capable of being honed to sharpness.

Iron and steel was the most important material in Ancient History, being the most resourceful metal for the ancient Roman Empire, mining up to 82,500 tones per year and producing a huge variety of tools. Roman production techniques are preserved throughout the Mediterranean until early in the 11th century innovations [5].

Thus far in the story iron has been heated and hammered, but never melted. Its melting point (1528°C) is too high for primitive furnaces, which can reach about 1300°C and are adequate for copper (melting at 1083°C). This limitation is overcome when the Chinese develop a furnace hot enough to melt iron, enabling them to produce the world's first cast iron - an event traditionally dated in the Chinese histories to 513 BC.

In this they are a thousand and more years ahead of the western world. The first iron foundry in England, for example, dates only from AD 1161. By that time the Chinese have already pioneered the structural use of cast iron, using it sometimes for the pillars of full-size pagodas.

Advances in steel production remained constant until the industrial revolution (1800-1850) where the advances of steel works becomes the Iron and carbon the most important materials for industry.

In 1807, the English chemist Sir Humphrey Davy established the existence of aluminium – although the name only came into common usage some time later. In 1825, the Danish physicist H.C. Oersted produced the first nodules of aluminium. In 1831, P. Berthier discovered bauxite in the village of Les Baux – hence the name. By 1854, the Frenchman Henri Sainte-Claire Deville had developed a process that allowed the production of this high-cost metal in limited quantities. Finally, in 1886, the smelting process that is still used today

was discovered almost simultaneously by Charles Martin Hall in the US and Paul Louis Toussaint Héroult in France. In 1888, Karl Bayer further improved the process, which greatly reduced the cost of aluminium – by around 80% – making it a commercial commodity[6].

Compared to all other classes of material, metals are stiff, strong and tough, but they are heavy. They have relatively high melting points, allowing some metal alloys to be used at temperatures as high as 2200°C. Only one metal – gold – is chemically stable as a metal; all the others will, given the chance, react with oxygen or sulphur to form compounds that are more stable than the metal itself, making them vulnerable to corrosion. There are numerous ways of preventing or slowing this to an acceptable level, but they require maintenance. Metals are ductile, allowing them to be shaped by rolling, forging, drawing and extrusion; they are easy to machine with precision; and they can be joined in many different ways. This allows a flexibility of design with metals that is only now being challenged by polymers.

Primary production of metals is energy intensive. Many, among them aluminum, magnesium and titanium, require at least twice as much energy per unit weight (or 5 times more per unit volume) than commodity polymers. [2,7] But metals can generally be recycled, and the energy required to do so is much less than that required for primary production. Some are toxic, particularly the heavy metals – lead, cadmium, mercury. Some, however, are so inert that they can be implanted in the body: stainless steels, cobalt alloys and titanium alloys, for example.

2.2.2 Polymers

The few non-metallic elements of the periodic table could make strong bonds between atoms. The same bodings than are used in the organic compounds. Polymers (From the Greek, poli which means many, and meros which means parts) are prepared by joining a large number of small molecules called monomers. Monomers are generally simple organic molecules containing a double bond or a minimum of two active functional groups. The presence of the double bond or active functional groups act as the driving force to add one monomer molecule upon the other repeatedly to make a polymer molecule.

The difference in behaviour between ordinary organic compounds and polymeric materials is due mainly to the large size and shape of polymer molecules. Common organic materials such as alcohol, ether, chloroform,

sugar, and so on, consist of small molecules having molecular weights usually less than 1,000. The molecular weights of polymers, on the other hand, vary from 20,000 to hundreds of thousands. The synonym term 'plastics', describes the compound of a polymer with one or more additives[8,9].

Natural polymeric materials, such as rubber, have been in use for thousands of years. Natural rubber also known as caoutchouc (crying trees) has been used by South American Indians in the manufacture of waterproof containers, shoes, torches, and squeeze bulb pumps. The first Spanish explorers of Haiti and Mexico reported that natives played games on clay courts with rubber balls [10]. Rubber trees were first mentioned in De Orbe Novo, originally published in Latin, by Pietro martire d'Anghiera in 1516.

However, it was not until the 20th century that the molecular architecture of polymers was well understood. Before that just with the introduction of the rubber in Europe, various uses were proposed. Gossart manufactured the first polymer tubes in 1768 by wrapping rubber sheets around glass pipes. During the same time period small rubber blocks where introduced to erase lead pencil marks from paper. In fact, the word rubber originates from this specific application – rubbing.

These new materials slowly evolved from their novelty status as a result of new applications and processing equipment, Although the screw press, the predecessor of today's compression molding press, was patented in 1818 by McPherson Smith [11], the first documented polymer processing machinery dates to 1820 when Tomas Hancock invented a rubber masticator. This masticator, consisting of a toothed rotor in a toothed cylindrical cavity [12], was used to recover rubber scraps that resulted from the manual manufacturing process of elastic straps, perhaps the first recycling effort. In 1833 the development of vulcanization process by Charles Goodyear [13] greatly enhanced the properties of natural rubber, and in 1836 Edwin M. Chaffe invented the two-roll steam heated mill, the predecessor of the actual calender. It was used to continuously mix additives into rubber for the manufacture of rubber-coated textiles and leathers. As early as in 1845, presses and dies were used to mould buttons, jewelry, dominoes, and other novelties out of shellac and gutta-percha. Gutta-percha (rubber clump), a gum found in trees similar to rubber, became the first wire insulation and was used for ocean cable insulation for many years.

The ram-type extruder was invented by Henry Bewley and Richard Brooman in 1845. The first polymer processing screw extruder, the most influential equipment in polymer processing, was patented by an Englishman named

Mathew Gray in 1879 for the purpose of wire coating. However, the screw pump is attributed to Archimedes and the actual invention of the screw extruder by A.G.DeWolfe of the U.S. dates back to the early 1860's.

Cellulose nitrate plasticized by camphor, possibly the first thermoplastic, was patented by Isaiah and John Hyatt in 1870. Based on experience from metal injection molding, the Hyatt brothers built and patented the first injection molding machine in 1872 to mold cellulose materials [14].

With the mass production of rubber, gutta-percha, cellulose, and shellac articles during the height of the industrial revolution, the polymer processing industry after 1870 saw the invention and development of internal kneading and mixing machines for the processing and preparation of raw materials [15]. A notable invention was the Banbury mixer, developed by Fernley Banbury in 1916. This mixer, with some modifications, is still used for rubber compounding.

Bakelite, developed by Leo Baekeland in 1907, was the first synthetically developed polymer. Bakelite, also known as a phenolic, is a thermoset resin that reacts by condensation polymerization occurring when phenol and formaldehyde are mixed and heated.

In 1924, hermann Staudinger proposed a model that described polymers as linear molecular chains. Once this model was accepted by others scientists, the concept for the synthesis of new materials was realized. In 1927 cellulose acetate and polyvinyl chloride (PVC) [16] were developed. Because of its higher wear resistance, polyvinyl chloride replaced shellac for phonograph records in the early 1930s. Wallace Carothers pioneered condensation polymers such a polyesters and polyamides. It was not until this point that the scientific world was finally convinced of the validity of Staudinger's work. polyamides, first called Nylon, were set into production in 1938. Polyvinyl acetate acrylic polymers, polystyrene (PS), polyurethanes, and melamine were also developed in the 1930s [17].

The first single-screw extruder designed for the processing of the thermoplastic polymers was built in 1935 at the Paul Troester Maschinenfabrik [18]. Around that same time period, Roberto Colombo developed a twin-screw extruder for thermoplastics.

World War II and the post-war years saw accelerated development of new polymeric materials. polyethylene (PE), polytetrafluoroethylene, epoxies, and acrylonitrile-butadiene-styrene (ABS) were developed in the 1940s, and

linear polyethylene, polypropylene (PP), polyacetal, polyethilene terephthalate (PET), polycarbonate (PC), and many more materials came in the 1950s. The 1970s saw the development of new polymers such as polyphenylene sufide and in the 1980s, liquid crystalline polymers were developed.

2.3 Mechanical properties of Metals and Polymers

In the historical background of the used materials, the preponderance of metals was clear until 1940. At this time new kinds of materials start to grow in applications that metals could not fill.

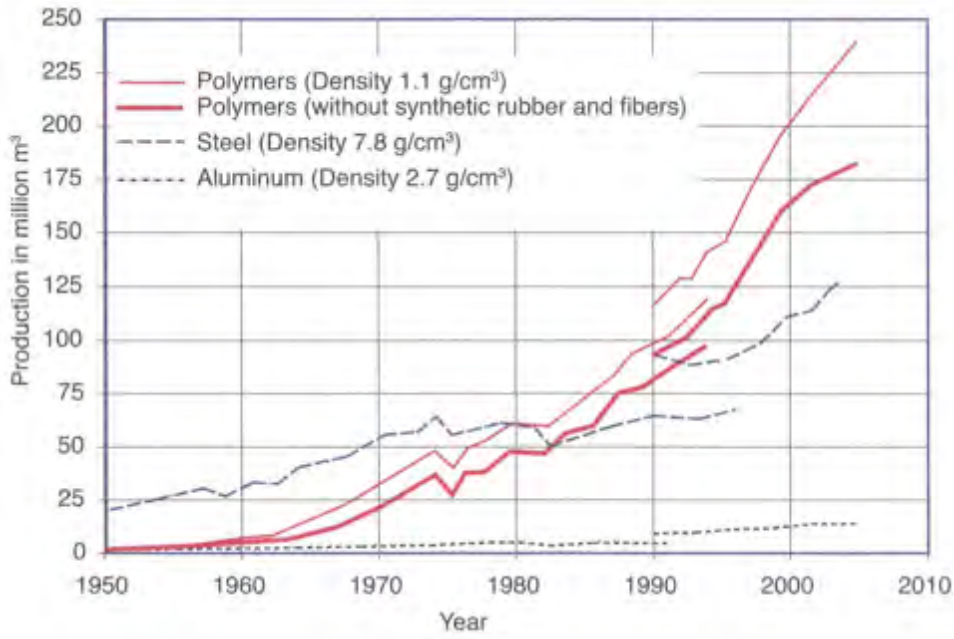

Figure2.2: *Production of the most important metals (Steel and Aluminum) and polymers by volume, from 1950 to 2005.[19]*

Figure 2.2 shows the increase in the production of metals (Steel and Aluminium) and plastics from 1950 to 2005. Before 1990 the figure only includes the production of the western side of the Iron Curtain, the production of the old western block was included when these countries were introduced in the market, making a global market. Before 1980 metals were the most important but now are polymers (at least in volume)[19].

Metals and polymers actually share the market for functional and structural materials, and in many products (examples: hammers, scissors, computers. cars, planes…) both type of materials are used.

Figure 2.3 shows the Young's modulus as function of the density in logarithmic scale. As it can be observed metals and polymers are in separate parts of the diagram.

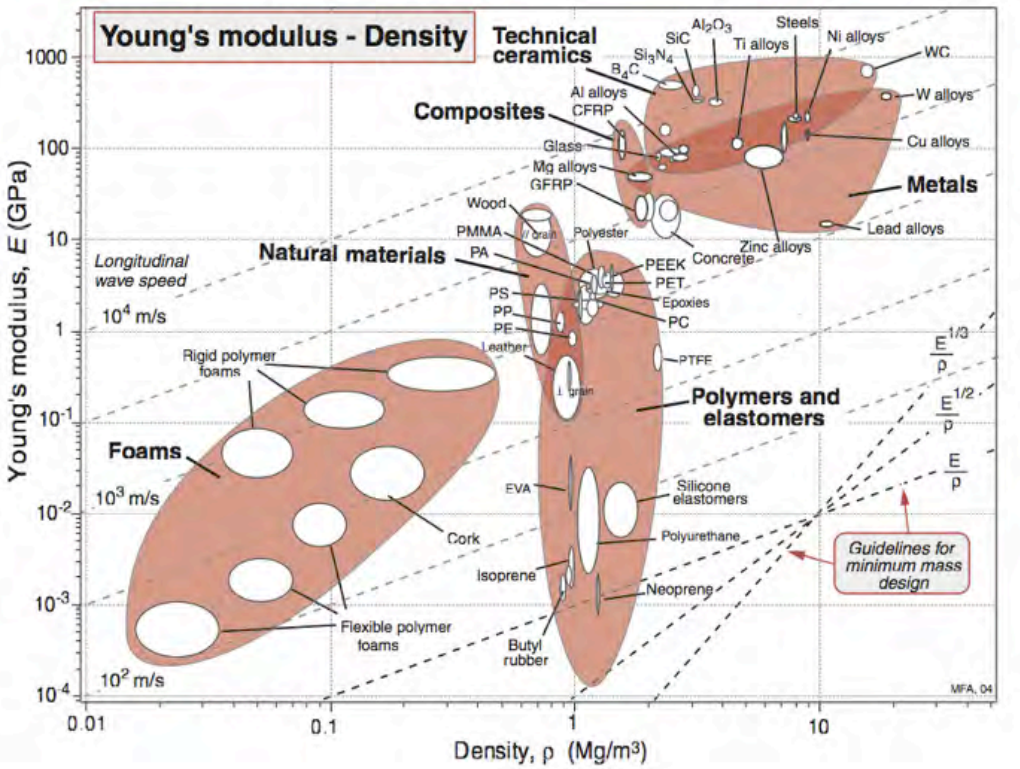

Figure 2.3: *Young's modulus as function of the density for several materials.[2]*

2.4 Metals as structural support (Metal forging)

The metallic bonding constitutes the electrostatic attractive forces between the delocalized electrons (Valence electrons of each atom), called conduction electrons, gathered in an electron cloud, and the positively charged metal ions. The atoms in metals have a strong attractive force between them.

The atoms with this bonding are well packet and have a large a regular structure. But except for very exceptional cases the mass of metal does not crystallize together with all atoms having the same orientation. Several

crystals start growing in the mass of molten metal until growth is interrupted by the presence of neighbouring crystals; the frontier (Grain boundary) is solidified without a perfect orientation. So metals are formed by a multiplicity of crystals each one with a different orientation of the crystallographic axes to the direction of their neighbors (polycrystalline solid) [20].

One of the properties of the grain boundary is disrupt the motion of dislocations through a material, so reducing crystallite size is a common way to improve strength, as described by the Hall–Petch relationship[21], (equation 2.1). So one important strategy to improve the mechanical properties of metals is reducing the grain size.

$$\sigma_y = \sigma_0 + \frac{k_y}{\sqrt{d}} \tag{2.1}$$

where σ_y is the yield stress, σ_0 is a constant associated to the initial stress for dislocation movement (or the resistance of the lattice to dislocation motion), k_y is the strengthening coefficient (a constant unique to each material), and d is the average grain diameter.

Forging is a manufacturing process involving the shaping of a metal using localized compressive forces in which new grain boundaries are form. Forging is often classified according to the temperature at which it is performed: "cold", "warm", or "hot" forging.

Many metal forging processes are suitable for processing large quantities of material, and their suitability depends not only upon the shape and size control of the product but also upon the surface finish produced. There are many different metal forging processes and some processes yield a better geometry (i.e., shape and size) and surface-finish than some others. In general, cold working metal forging processes result in better shape, size and surface finish as compared to hot working processes. Hot working results in oxidation and decarburisation of the surface and lack of size control due to contraction of the work piece while it cools to room temperature[22].

The use of mechanical working processes give some advantages to the final parts:

1. Mechanical working improves several mechanical properties of material such as ultimate tensile strength, wear resistance, hardness and yield

point while it lowers ductility. This phenomenon is called "strain hardening".

2. It results in grain flow lines being developed in the part. The grain flow improves the strength against fracture when the part is in actual use. This is the best explained by taking illustration of a crankshaft. If the crankshaft is manufactured by machining from a bar of large cross-section the grain flow lines get cut at bends whereas in a crankshaft which is shaped by forging (which is a mechanical working process), the grains flow lines follow the full contour of the crankshaft making it stronger. This is illustrated in Figure 2.4.

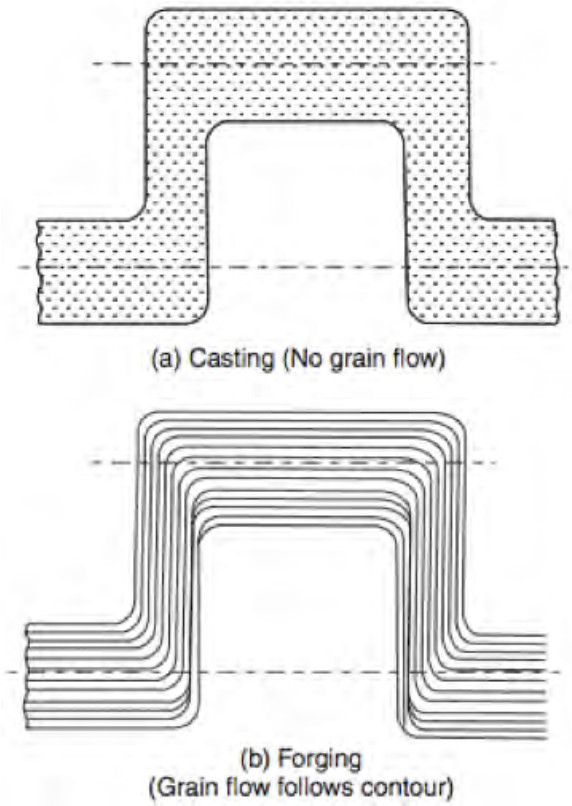

Figure 2.4: *Comparison of grain flow for casting and forging[22]*

During mechanical working, the grains of the metal get deformed and lengthen in the direction of metal flow. Hence they offer more resistance to fracture across them. Due this, mechanically worked components have better mechanical strength in a certain orientation i.e., across the grain flow. Figure 2.5 shows the forging process made by rolling In this process it is possible to reduce the grain size.

For these advantages load-bearing structural metals are always forged. To make an interesting porous metal to support a load is necessary to give to

the cellular matrix the strength of the forging metals. This will be one of the key topics of this research.

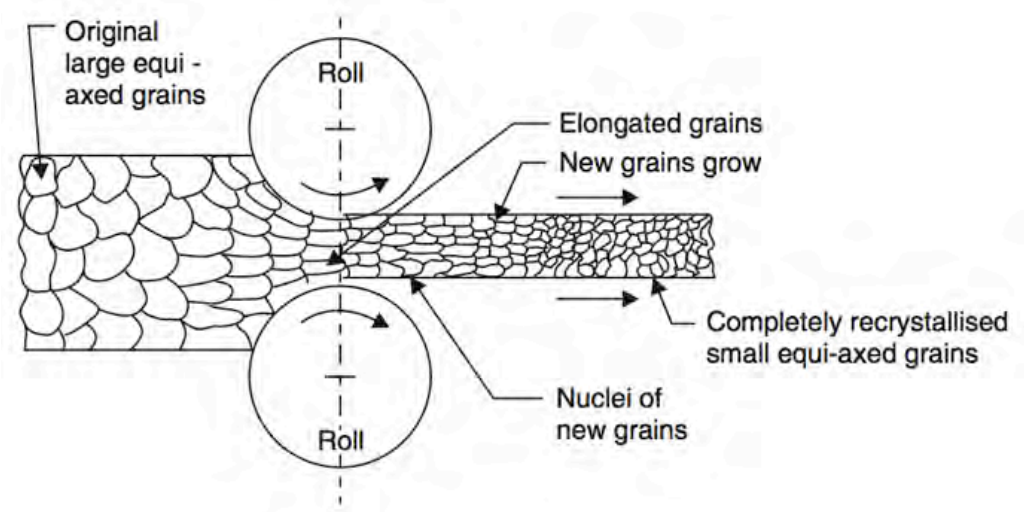

Figure 2.5: *Example of grain refinement by forging during Rolling[21]*

2.5 Polymers as structural support (Reinforcing Processes)

Reinforced plastics are composites in which a resin is combined with a reinforcing agent to improve one or more properties of the polymer matrix. The polymer may be either a thermoset or a thermoplastic.

The reinforcement used is usually a strong inert material bound into the plastic to improve its strength, stiffness, or impact resistance. The reinforcing agent can be fibrous, powdered, spherical, crystalline, or whisker, and made of organic, metallic, or ceramic material. Fibrous reinforcements are usually glass, although, sisal, cotton, nanoparticles (carbon nano tube, graphene, nanoclays) and high-performance fibres are also used[23-25]. To be structurally effective, there must be a strong adhesive bond between the resin and the reinforcement. Most reinforcements are thus treated to provide maximum adhesion to the polymer matrix.

Typical polymeric composites used for structural purposed used carbon fiber or glass fibers as reinforcing agents. These materials are nowadays in use in the aeronautic[1], automobile and naval industries[26,27].

[1] The fuselage of the new Boeing 787 Dreamliner [28] and Airbus A350 XWB [29]

2.6 Structure properties relationships in cellular materials

Four important physical properties (density, elastic modulus, thermal conductivity and compression strength) for materials such as ceramics, metals and polymers, and for cellular materials that use these materials as supporting matrix are shown in figure 2.6. It can be observed that foaming dramatically extends the range of properties available[30].

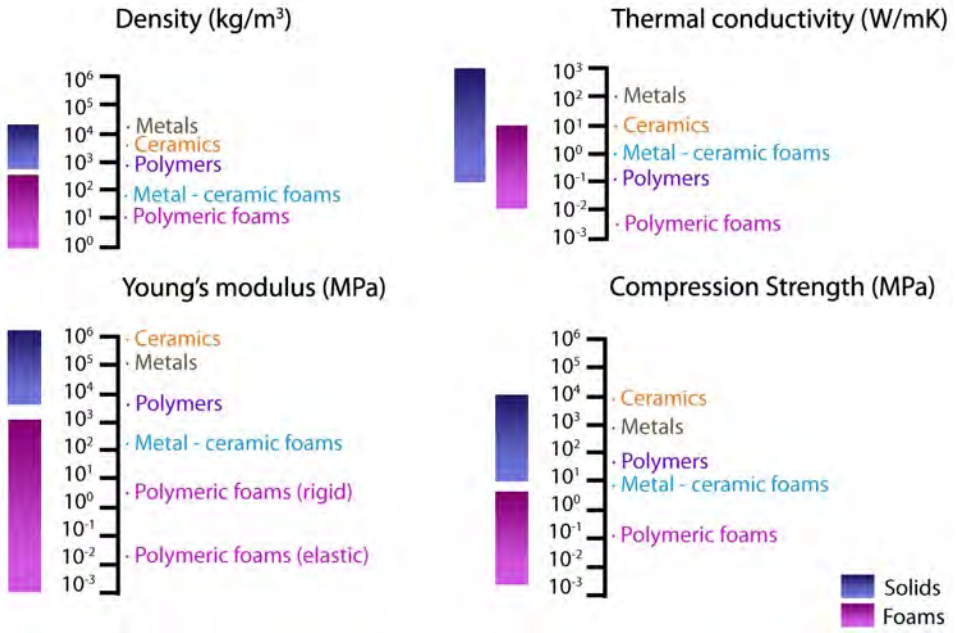

Figure.2.6: *General properties of solid materials and their foams.*

This enormous extension of properties creates applications for cellular materials which cannot easily be filled by fully dense solids, and offers potential for engineering ingenuity. The low densities permit the design of light, stiff components such as sandwich panels. The low thermal conductivity allows cheap, reliable thermal insulation. The low stiffness makes foams ideal for a wide range of cushioning applications. The low strengths and large compressive strains make foams attractive for energy-absorbing applications; there is an immense market for cellular solids for the protection of almost everything.

Nowadays, qualitative knowledge over physical mechanisms that control several physical properties, (thermal expansion, thermal conductivity, mechanical behavior in compression tests, drop impact tests, etc.), and some approximate theoretical models have been developed[31,32].

Theoretical or semi-empirical models for the prediction of mechanical properties are not accurate enough, due to the complex cellular structure of real foams. For example regarding stiffness, at low densities, experimental results indicate that Young's modulus (E) of cellular solids is related to their density (ρ) through the relation[33,34]:

$$\frac{E}{E_s} = C \cdot \left(\frac{\rho}{\rho_s}\right)^n \tag{2.2}$$

where E_s and ρ_s are the Young's modulus and density of the solid skeleton (matrix of the cellular material). The constants C and n depend on the microstructure of the solid material. The value of n generally lies in the range $1 < n < 4$, giving a wide range of properties at a given density. The complex dependence of C and n on microstructure is not well understood, but seem to depend on :

1. **At the cellular structure scale**. Important variables include the cell character (e.g. opened or closed), cell size distribution, cell anisotropy, distribution of material in walls and edges, the shape of the cell struts or walls, presence of defects, etc.
2. **A mesoscopic scale.** The geometrical arrangement of the cells is also crucial. The values of both C and n depend on whether the material is periodic or disordered. Density gradients are also important.

For the evolution of mechanical properties with the porosity, n is the most important factor. If C=1 and n=1, the evaluated mechanical property will evolve linearly with the porosity, in this case the specific mechanical (E_s/ρ_s) property will not change. When the material is intended to be a load bearing structural material n=1 is the ideal case. If n>1, when the porosity increases the mechanical property decreases quickly and the specific property decreases when density is reduced.

2.7 Weight reduction in structural applications

This section analyses how the use of a cellular material allows weight reduction in structural elements. The analyses is focused on two examples, a bar loaded in bending and a thin plate also loaded in bending. We compare the stiffness of a solid sample and of cellular materials with different densities. Calculating the weight reduction that is possible to archive when the cellular material is used. The main criteria used for the calculation is that

both structures (the solid one and the cellular one) should have the same stiffness.

Figure 2.7 shows the first case, a bar loaded by bending. The bending stiffness of a bar, k, is defined by the equation 2.3

$$k = \frac{C_1 \, E \, b \, h^3}{12 \, l^3} \tag{2.3}$$

E is the Young's modulus, $b \cdot h^3/12$ is the second moment of inertia where b is base width, h the height (thickness), and l is the distance between the supports (span).

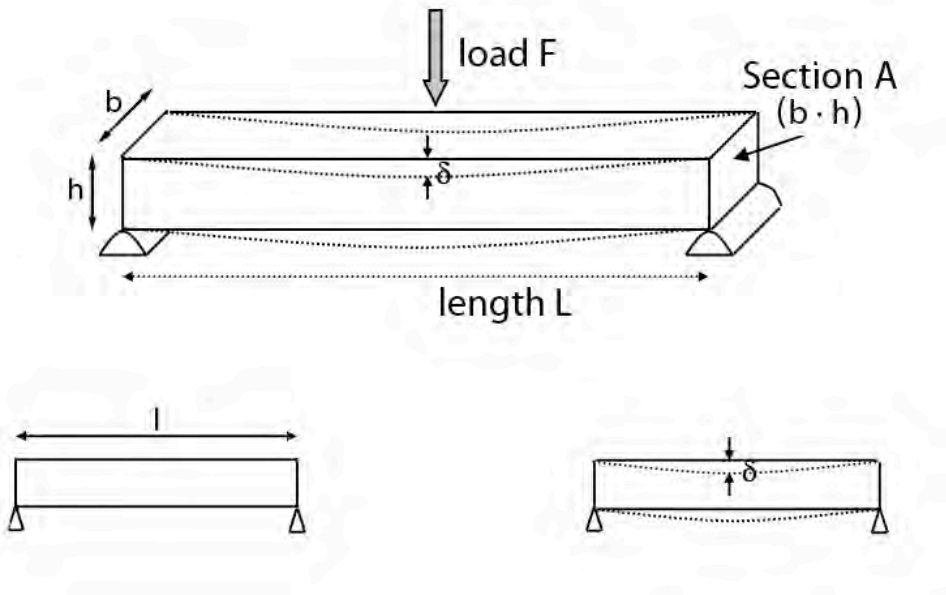

Figure 2.7: *A bar loaded in bending*

Using the equations 2.2 and 2.3, it is possible to find the relationship between the weight of the beam and the relative density of the foam to have the same stiffness, than the solid bar. The calculation is made assuming that the solid beam, and porous beam will have the same width and different thickness. Using this relationship the weight reduction archived has ben calculated, Figure 2.8.

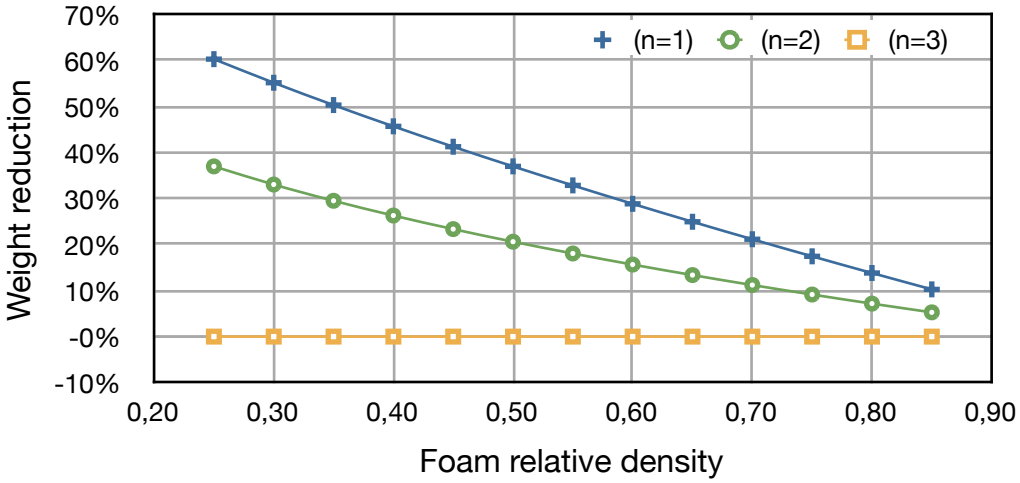

Figure 2.8: *Weight reduction as a function of the relative density to produce a beam with the same stiffness than one produced from the solid material. Results for different values of n are given.*

Clear differences are observed as function of n value. If n=1, it is possible to obtain near to 40% of weight reduction if the relative density of the foamed beam is 0.5, the half of the density of the solid material. Weight reduction is only 20% when n=2, and there is no weight reduction when n=3.

It is also possible to make a similar study in a thin plate. Figure 2.9 show the deformation by bending of a thin plate, supported at the edge and loaded by a cylinder at the centre.

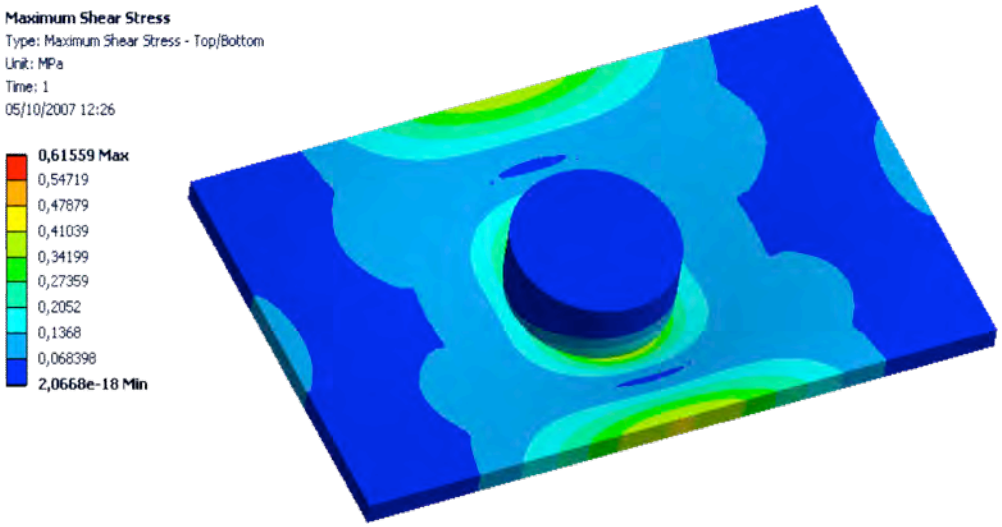

Figure 2.9: *deformation by bending of a thin plate*

The equation of the bending stiffness of a thin (isotropic) plate is:

$$k = \frac{2h^3 E}{3(1-\nu)} \tag{2.4}$$

Where E is the Young's modulus, 2h is the thickness of the plate, and ν is the Poisson's Ratio of the material. In this case it is more difficult to calculate the weight reduction as a function of relative density because the Poisson's Ratio of the material could change when the solid material is foamed[31]. If the pores are small and the relative density is high the Poisson's Ratio of the foam will be similar to that of the solid material, but if the pores are large and the relative density low the Poisson's Ratio will be near zero for the foamed material. The results of the calculated weight reduction are showed in Figure 2.9.

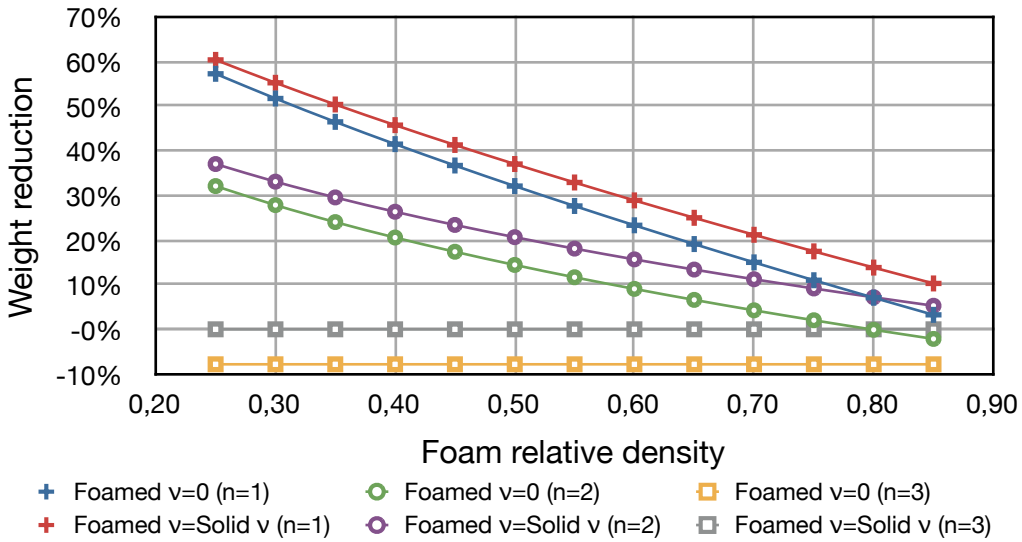

Figure 2.10: *Weight reduction as a function of the relative density for a thin plate produced using cellular materials with different values of 'n' in the Young's modulus relationship, and different values of the Poisson's Ratio.*

Figure 2.10 presents the two extremes of values of the Poisson's Ratio. The lines with the same representation of dots have the same 'n' in the equation of the Young's modulus as function of density. Once again the optimum weight reduction is achieved when n=1. A large value of Poisson's Ratio improve the mechanical performance.

The previous calculations prove that "It is possible to reduce weight by using cellular materials". One of the main aspects in which this thesis is focussed is developing cellular materials with n as close as possible to 1, which allows the maximum weight reduction.

2.8 References

[1]. Oxford University "New Oxford American Dictionary", Oxford University Press, Inc, 2005.

[2]. M. F. Ashby "Materials Selection in Mechanical Design", Elsevier's Science and Technology, 2005.

[3]. M. Ashby and K. Johnson "Materials and Design: The Art and Science of Material Selection in Product Design", Butterworth-Heinemann, 2002.

[4]. W. Hilgemann and H. Kinder "Atlas zur Weltgeschichte" Deutscher Taschenbuch Verlag, Munchen, 1974 (Spanish translated in 1984)

[5]. P. T.Craddock. "The Oxford Handbook of Engineering and Technology in the Classical World", Oxford University Press, 2008.

[6]. I.J. Polmear. "Light Alloys: From Traditional Alloys to Nanocrystals" Elsevier, Oxford, 2006

[7]. D.A. Colling and T. Vasilos "Industrial Materials," Volume i and ii, Prentice Hall, 1995.

[8]. T.A. Osswald and G. Menges "Materials Science of polymers for Engineers", Hanser Publishers, 2003.

[9]. H.J. Stern "Rubber: Natural and Synthetic", Maclaren and Sons, LDT London, 1967.

[10]. C.M. de la Condamine "Relation Abregee D'un Voyage Fai dans l'interieur de l'Amerique Meridionale", Academie des Sciences Paris, 1745.

[11]. J.H. Dubois "Plastics History U.S.A", Cahners Publishings Co., Inc. Boston, 1972.

[12]. Z. Tadmor and C.G Gogos "Principles of Polymer Processing", John Wiley & Sons, New York, 1979.

[13]. A.T. McPherson and A. Klemin "Engineering Uses of Rubber", Reinhold Publishing Corporation, New York, 1965.

*[14]. R. Sonntag, Kunstsoffe **75**, 4, 1985.*

*[15]. H. Herrmann, Kunstsoffe **75**, 2, 1985.*

*[16]. H.V. Regnault, Liebigs Ann **14**, 22, 1835.*

[17]. H. Ulrich, "Introduction to Industrial Polymers", Hanser Publishers, Munich, 1993.

[18]. C. Rauwendaal "Polymer Extrusion", Hanser publishers, Munich, 1990.

[19]. T.A. Osswald "Understanding Polymer Processing", Hanser Publications, Munich, 2011.

[20]. H.N. Gupta; R.C. Gupta; A. Mittal "Manufacturing processes", New Age International, 2009.

[21]. William F. Smith and Javad Hashemi "Foundations of Materials Science and Engineering", McGraw-Hill, 2006.

[22]. J. T. Black and R. A. Kohser "DeGarmo's Materials and Processes in Manufacturing", Wiley, 2007.

[23]. G. Lubin "Handbook of Composites", Van Nostrand Reinhold, New York, 1982.

*[24]. W.J. Lee, J.C. Seferis, and D.C. Bonner. Prepreg processing science, SAMPE Quarterly **17**, 58, 1986.*

[25]. G.P. Daumit "Latest in carbon fibers for advanced composites", Performance Plastics' 87 First International Ryder Conference on Special Performance Plastics and Markets, Atlanta, 1987.

[26]. B. Ilschner et al.. "Composite Materials". Ullmann's Encyclopedia of Industrial Chemistry Weinheim, Germany: Wiley-VCH Verlag GmbH & Co. KGaA, 2002.

[27]. G. Lubin "Handbook of Composites", Van Nostrand Reinhold, New York.1982.

[28]. G. Norris, G. Thomas, M. Wagner and C. Forbes Smith "Boeing 787 Dreamliner – Flying Redefined" Aerospace Technical Publications International, 2005.

[29]. "Taking the lead: A350XWB presentation". EADS. December 2006.

[30]. L.J. Gibson and M.F. Ashby "Cellular Solids", Cambridge University Press, 1997.

[31]. M.F. Ashby, A.G. Evans, N.A. Fleck, L.J. Gibson, J.W. Hutchinson and H.N.G. Wadley "Metal Foams: A Design Guide", Butterworth-Heinemann, 2000.

[32]. B. C. Wendle "Structural foam", Marcel Dekker, 1985.

[33]. D. Klempner and K.C. Frisch eds. "Handbook of Polymeric Foams and Foam Technology", Hanser, 1991.

*[34]. B. Brandel and R. S. Lakes, Journal of Materials Science **36**, 5885, 2001.*

3 Lotus-type porous metals

Resumen (Spanish):

En este capitulo introducimos el cobre poroso tipo lotus, que es el material que hemos usado para parte de la investigación. Describimos las distintas técnicas de fabricación y exponemos parte de sus propiedades mecánicas, las cuales se puede ver que son excepcionales para un material poroso. Pero este material poroso no esta forjado, así que es un metal mucho mas dúctil que el que se usa en aplicaciones estructurales. Lo cual nos dará pie a introducir la investigación que se realizó con este tipo de material usando métodos de forjado que no suprimiesen su estructura celular.

3.1. Introduction

The first reported aluminum foams were produced at Bjorksten Research Laboratories in 1952[1]. Although the first prototypes were available in the 50s, commercial production was started only in the 90s by Shinko Wire company in Japan. Metallic foams are rather new materials, without a massive industrial development and however many different industrial process has been competing, and new methods have been developed so far.

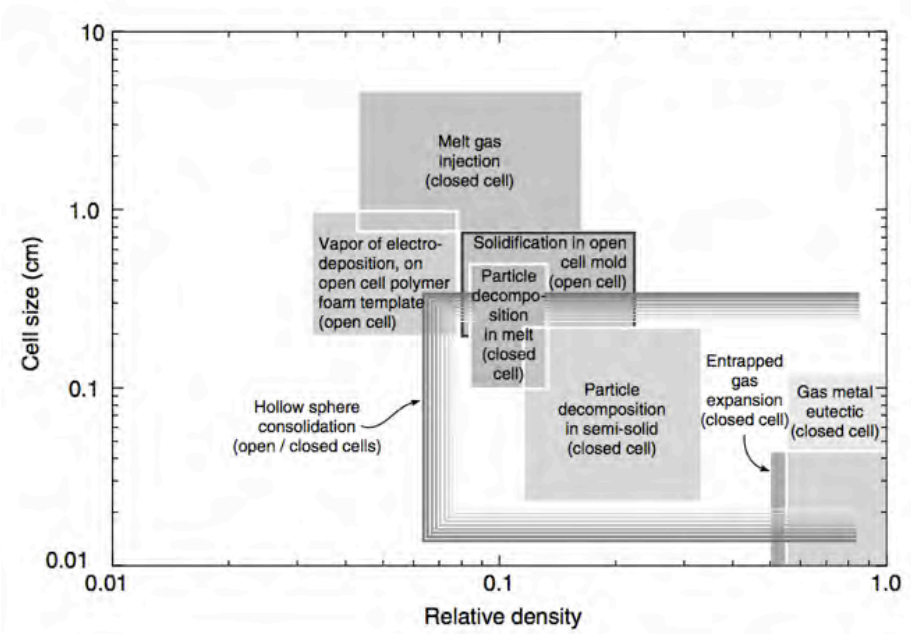

Figure 3.1: *The range of cell size and relative density for the different metal foam manufacturing techniques.*

Each technique can be used with a small subset of metals to create a porous material with a limited range of relative densities and cell sizes. Figure 3.1 summarizes the ranges of cell size, cell type (open or closed), and relative densities that can be manufactured with different methods[2].

3.2 Lotus-type porous metals

One of the most interesting cellular metals developed until now are lotus-type porous-metal[3] these metals are named "Gas metal eutectic" in Figure 3.1. The production process for these materials is based on the variation of the gas solubility in a metal between the liquid and the solid phase. Figure 3.2 shows the temperature dependence of hydrogen solubility of various metals [4]. The solubility of hydrogen increases with increasing temperature, and the variation is smooth except at the temperature of a phase transformation (Solidification-melting). This gap in the hydrogen solubility is used to produce the porous structure.

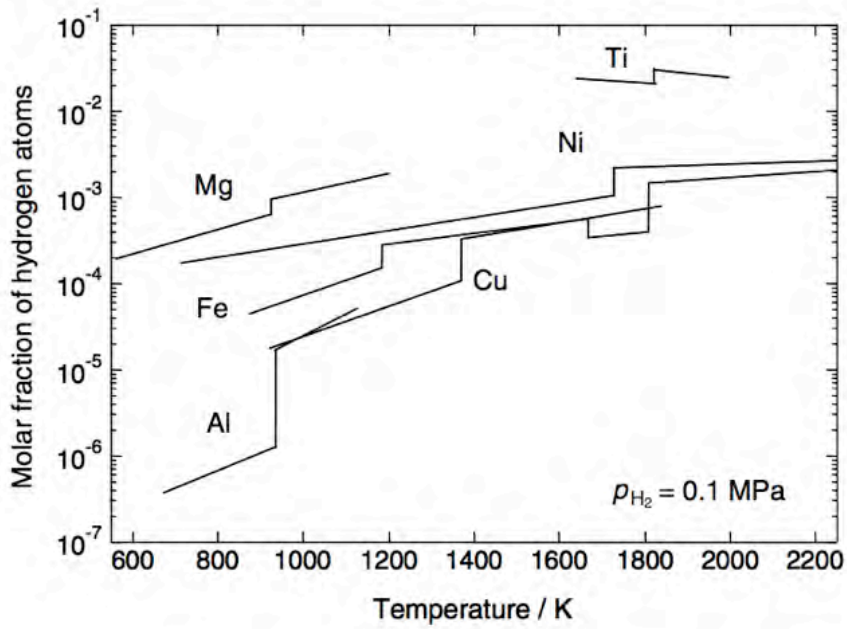

Figure 3.2: *Hydrogen solubility of various metals as function of the temperature under the hydrogen pressure of 0.1 MPa. [3,7-9]*

The steps used to produce a lotus-type porous metal are as follows: inside a gas-tight chamber, with a controlled atmosphere (usually, a mix of Ar and H_2) the metal is melted and a gas is dissolved in the melt. Then the melt is cooled down and starts to solidify, because the solubility in the melt is higher than that in the solid, the excess of the gas that cannot be dissolved in the solid

phase form bubbles in the meal. The metals and available gases, to make this type of porous structures are compiled in Table 1.

The solid-gas eutectic solidification phenomena, is common to make 'Lotus-type' and Gasar (Russian acronyms for 'solid–gas eutectic solidification') porous metals [3,5,6,10]. The binary phase diagram for copper an hydrogen can be seen in figure 3.3. The presence of the phase Cu+H_2 down the solidification temperature of the copper (1075ºC) when a critical concentration of hydrogen (0.01) is reached is the key aspect allowing the production of lotus-type porous metals.

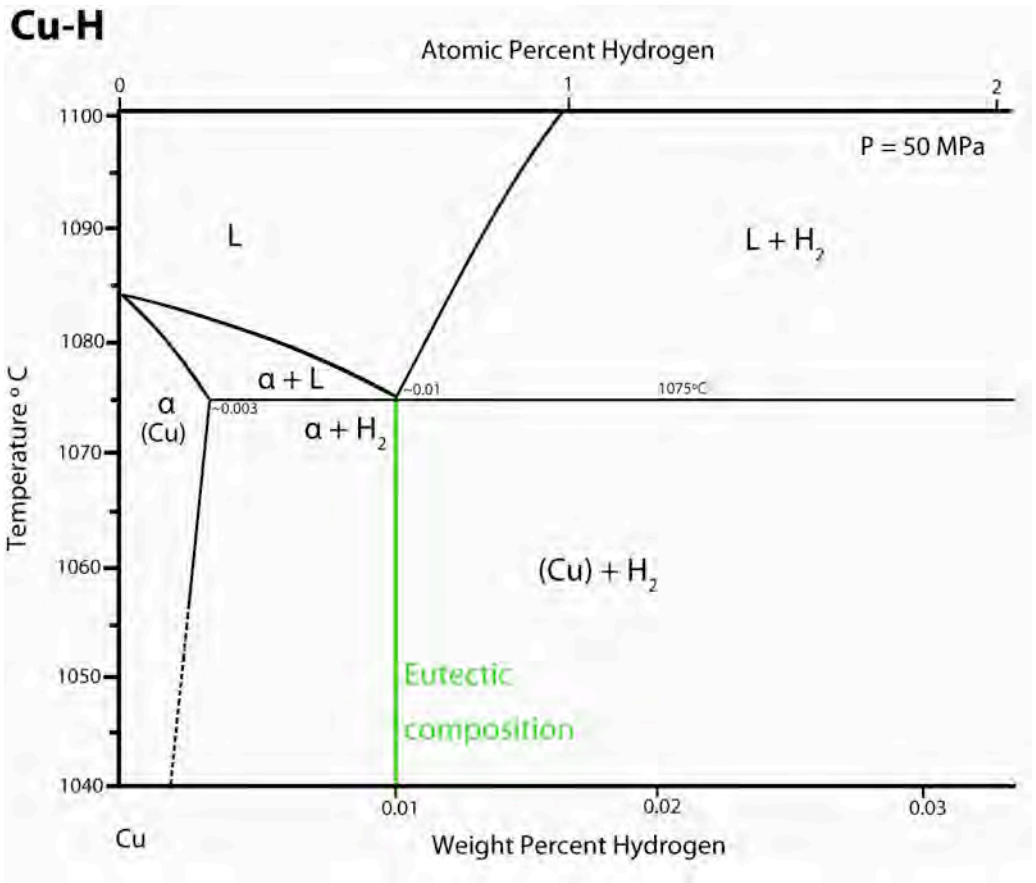

Figure 3.3: *Binary phase diagram for a mixture of Copper and Hydrogen for a pressure of hydrogen of 50MPa.[11,12]*

One option to introduce the gas inside the molten metal is the use of a decomposing blowing agent that decomposes at the temperature of the molten metal by releasing hydrogen (TiH_2 for instance)[13,14]. But the most typical method is introducing the gas, at high pressure, in the chamber were the metal is melted. The gas will dissolve in the metal until reach to the

equilibrium between the gas pressure in the surface of the melt and the concentration of the gas in the melt. For hydrogen, and other diatomic gases, Sievert's law is used to evaluate this equilibrium[15].

Table 1: *Metals and gases used to produce porous metals [3,5,7]*

Gas	Metal			
Hydrogen (H_2)	Aluminum	Copper	Manganese	Titanium
	Beryllium	Fe (Iron)	Molybdenum	Tungsten
	Chromo	Fe-C (Steel)	Nickel	Wolfram
	Cobalt	Magnesium		
Oxygen (O_2)	Copper	Fe-C (Steel)	Gold	Silver
Nitrogen (N_2)	Copper	Fe (Iron)	Manganese	Nickel

Sievert found that the dissolution of the gas in the metal involves dissociation of the molecule of the gas (for a diatomic gas):

$$H_2(gas) \leftrightharpoons 2H(disolved) \tag{3.1}$$

The diffusion rate for the gas in the molten metal is very high, in several seconds the equilibrium is obtained. At constant temperature, the equilibrium solubility of hydrogen is governed by Sievert's law, which states that the hydrogen concentration in molten metal is proportional to the square root of the partial pressure of diatomic hydrogen above the melt:

$$H_{eq}(wt\%) = K_{eq}\sqrt{P_{H_2}} = exp\left(-\frac{\Delta G_0^1}{RT}\right)\sqrt{P_{H_2}} \tag{3.2}$$

$H_{eq}(wt\%)$: is the hydrogen concentration in the melt, in the equilibrium. It can be measured as percentage by mass or molar fraction.
K_{eq}: is the equilibrium constant for reaction 3.1.
P_{H2}: is the partial pressure of H_2 in the chamber.
$\Delta G^1{}_0$: is the Gibbs free energy for the absorption and dissociation of the gas in the metal 3.1.
R: is the gas constant.
T: is the temperature of the melt.

The diatomic gases follow the Sievert's law, but different gases change the constant of equilibrium of the reaction.

3.3 Use of other gasses instead of hydrogen

There are reported systems of metals and gases that also present good solubility, and a gap in solubility between the solid and liquid phases of the metal. For instance nitrogen has been used to produce lotus-type porous iron, nickel, copper and manganese. In addition some few metals, with low oxidation rates, can be processed with oxygen.

Since hydrogen is inflammable and explosive when oxygen is present, its use is not convenient from the industrial point of view. Use of other gases than hydrogen is desirable.

In the case of iron the use of nitrogen is a good option to produce lotus-type porous iron, the maximum concentration of gas is similar and the solubility changes, with temperature in the same way as in hydrogen, as can be see in Figure 3.4. The advantage of using nitrogen is alloying the reaction between Fe–N (Nitriding)[16], when part of the nitrogen is adsorbed in the metallic structure. A small amount of nitrogen increase the yield strength of iron [17,18] with no significant decrease in toughness or ductility[19]

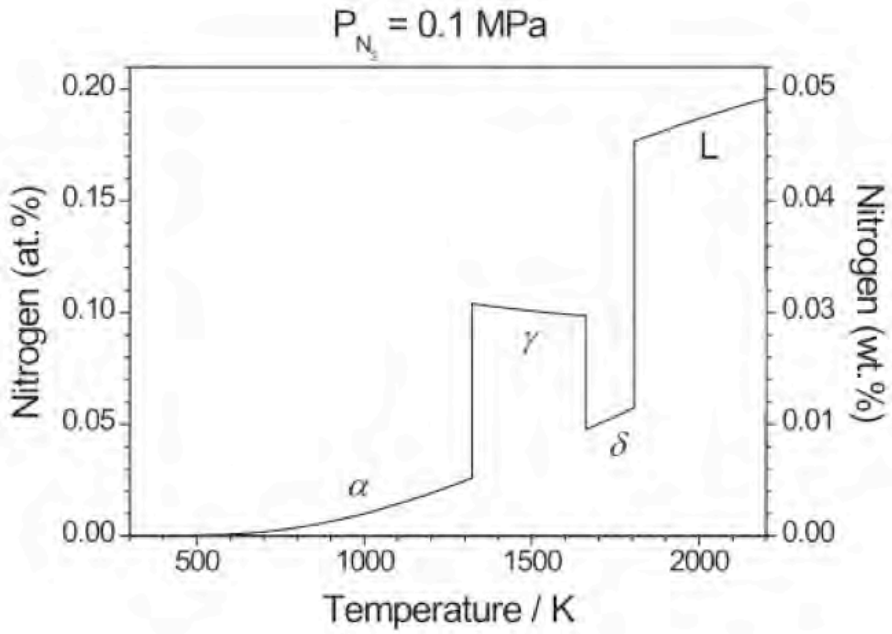

Figure 3.4: *Nitrogen solubility in solid and liquid iron under a pressure of 0.1 MPa. [1,20]*

Other gases like helium and argon do not show the solubility gap between solid and liquid phase. Due to this reason, argon is used to increase the pressure inside the chamber, but does not produce the cellular structure.

3.4 Methods of production of the lotus metals

The direct solidification in a mould of a metal-gas blend to make porous metals is called, "Mold casting technique". In this process the metal is melted inside a chamber with a controlled atmosphere and cooled inside of a mould, without exiting the chamber. This basic process is able to produce a good porous structure for metals with high thermal conductivity like copper. For metals with a lower conductivity the cellular structure is more inhomogeneous. This technique is explained in detail in the section 3.4.1 and it has been used to produce the samples of the chapter 4.

Nakajima Laboratory at Osaka University developed a new process that allows producing porous metals using low thermal conductivity metals. This method is called "continuous casting technique". This technology is explained in the section 3.4.2 and it has been used to produce the samples of chapter 5.

3.4.1 Mold casting technique

The mold casting method is one of the main options to fabricate lotus and GASAR metals [3,4]. This technique uses a slow crystallization of the liquid metal inside a hydrogen atmosphere in a pressurized chamber. As mentioned above, when the molten metal solidifies the gas concentration surpass the maximum of solubility for the solid crystalline structure. The excess of gas in the solid is stabilized in pores in the interface between molten and solidified metal.

Figure 3.5 shows a schematic drawing of this technique. A metal inside a crucible is melted by induction heating in a high-pressure gas atmosphere, usually between 0.5-1.5MPa[2]. The gas in the atmosphere of the chamber is dissolved into the molten metal to obtain the equilibrium concentration according to the Sieverts' law, equation 3.2. The melt saturated with gas is poured into the mold. The metal is solidified in the mold, and pores start to grow everywhere distributed randomly. An improvement is obtained when the mold is cooled from the bottom part, Figure 3.5, the melt starts the solidification in the vicinity of the cooling part, the pores appear in the interface between solid and liquid phase and grows unidirectionally at the

[2] Chambers could work until 3MPa, there also exist high pressure chambers prepared to work below 10MPa. During the description of the nucleation process the reason to work with this pressure will be explained.

same time that the solid phase grows. This process make elongated pores for copper as can be seen in Figure 3.6.

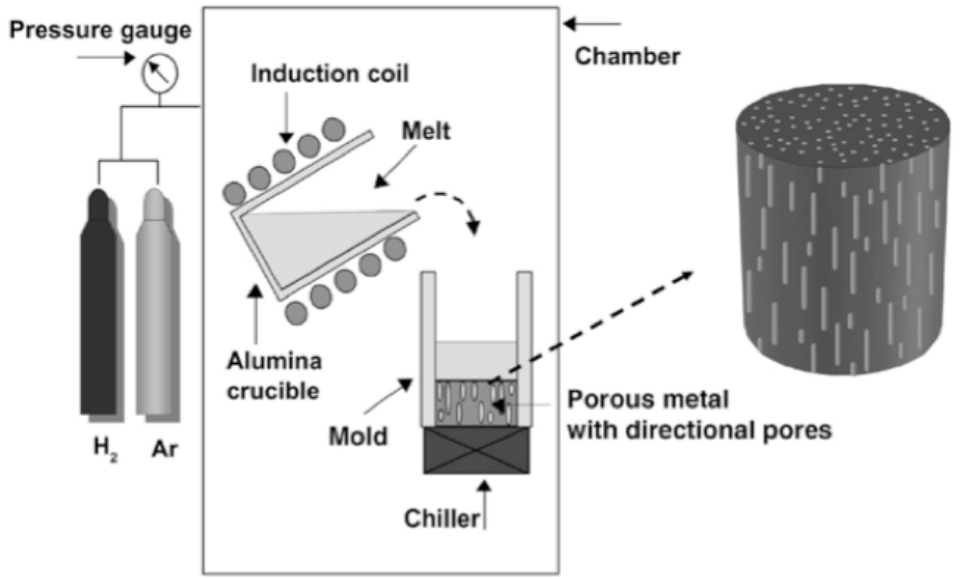

Figure 3.5: *Mold casting technique for producing lotus-type and gasar-type porous metals.*

In general, cellular metals are characterized by pore growth direction, pore size and porosity, and those parameters are not easy to control by conventional fabrication methods. The lotus-type process has a good control of the porosity and pore size.

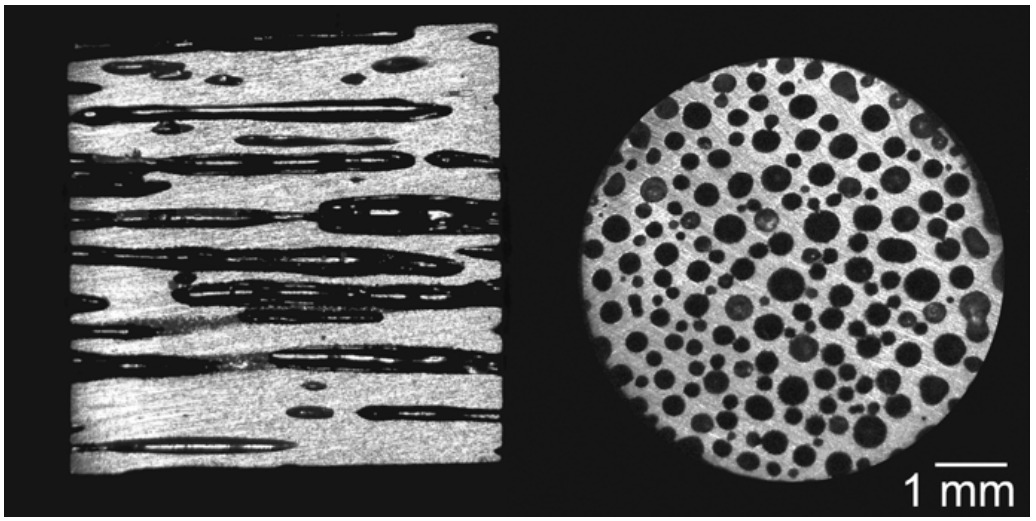

Figure 3.6: *Side view, and top view of lotus copper.*

Control parameters used are:

* The melt temperature.
* The dissolving gas pressure during melting and solidification.
* The inert gas pressure during melting and solidification.
* Solidification rate (cooling rate) and cooling geometry.

With the change in those parameters it is possible to modify the pore morphology and porosity, obtaining very homogenous and reproducible cellular structures.

Figure 3.7 illustrates three different types of moulds and position of the chillers to obtain different pores orientation. As it is observed the orientation of the pores can be controlled by modifying the cooling method.

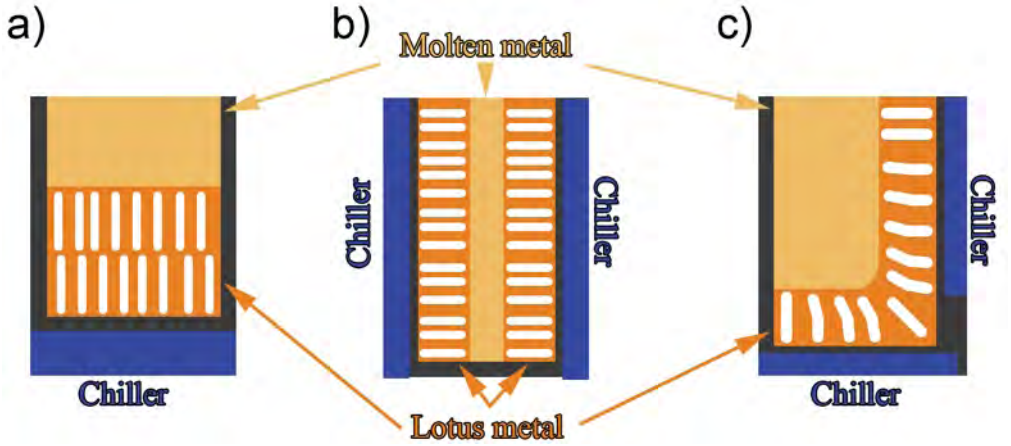

Figure 3.7: *Three different types of moulds with different cooling system. a) Chiller in the base of the mould. b) Chiller in the sides of the mould. c) Chiller in the base and in one side of the mould. Different pores orientations are obtained.*

The melt temperature together with the pressure is connected with the quantity of hydrogen, or active gas dissolved in the metal. Most of metals increase the amount of gas dissolved with the temperature, but for others the amount of gas decrease with temperature (see Figure 3.2 for Ti)

The main limitation is related to the maximum solubility. Taking the data represented in the Figure 1 the maximum solubility for the hydrogen in copper allows a porosity larger than 50%, but the small solubility of hydrogen in molten aluminum drop the maximum porosity to lower values, maximum value are around 24% porosity[21].

In some metals it is not convenient to reach the maximum solubility of the active gas. Figure 3.8 shows the binary phase diagram for a mixture of copper

and hydrogen; in that diagram for a pressure of 50MPa there is a eutectic solidification for a concentration of 0.01% by weight of hydrogen. This means that for this concentration of hydrogen the gas bubbles are formed at the same temperature that the copper starts to solidify, eutectic composition (Point A) in the figure 3.8. For that concentration all the pores show similar geometry. Therefore, if the gas concentration is larger (hypereutectic composition), the nucleation starts when the temperature reach the liquid curve (Point A), and the first bubbles appear on the liquid phase lowering the gas concentration to the eutectic concentration; at lower temperature (Point B) the copper starts to solidify and new bubbles are formed. At that point the distribution in pore sizes is more disperse, and if the hypereutectic composition is relatively higher than the eutectic composition it's possible to observe a double population of pores. In order to have a better distribution of pores sizes it is necessary to have the gas concentration level of the eutectic composition; that concentration is obtained for most

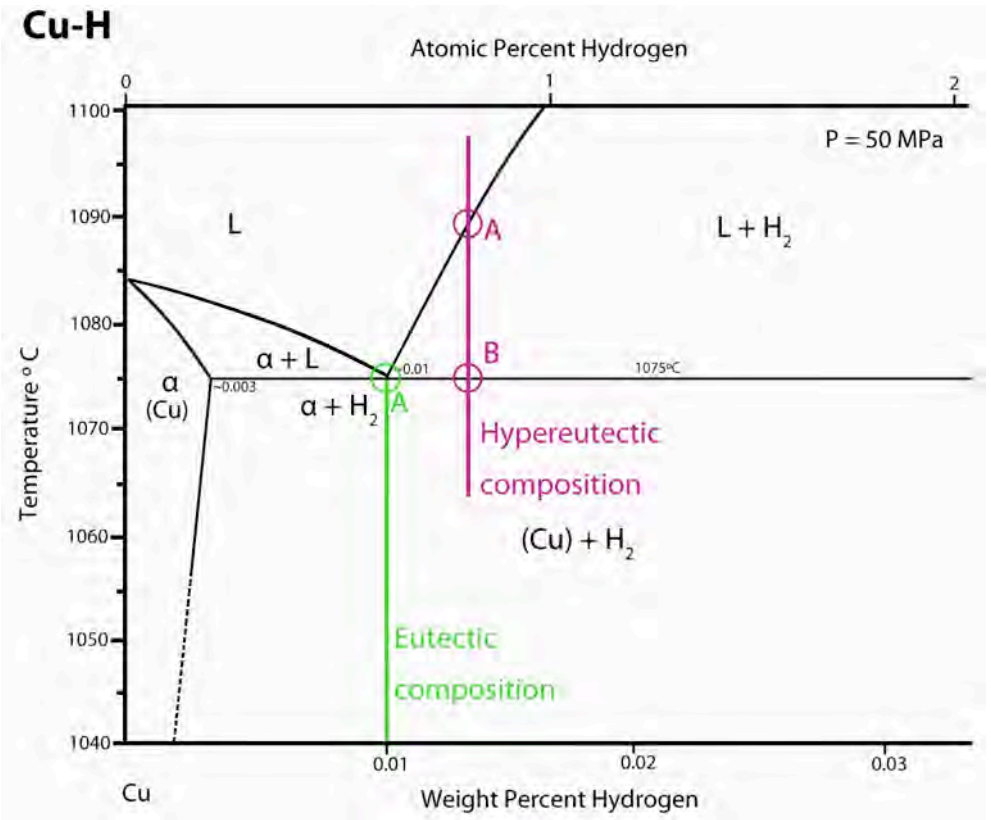

Figure 3.8: *Binary phase diagram for a mixture of Copper and Hydrogen, for a pressure of hydrogen of 50MPa, showing the nucleation points of hydrogen for two compositions, the eutectic composition only have one but the hypereutectic composition has two. [3,11,12]*

metals with low pressure of the active gas (0,5-1,5MPa). To obtain a good pore structure for lotus type porous metals it is necessary to know the eutectic concentration for the active gas.

The use of an inert gas, with no gap in the solubility, like argon has direct effect on the pore size and porosity of the sample. For instance some of the samples of this thesis were produced changing the internal atmosphere, one of the samples was made in relative hydrogen pressure of 0.5MPa and argon relative pressure of 0.5MPa; the second was made in relative hydrogen pressure of 0.5MPa and argon relative pressure of 0.3MPa. The first sample had a porosity of 38±0.4% and average pore size of 173±79μm; the second

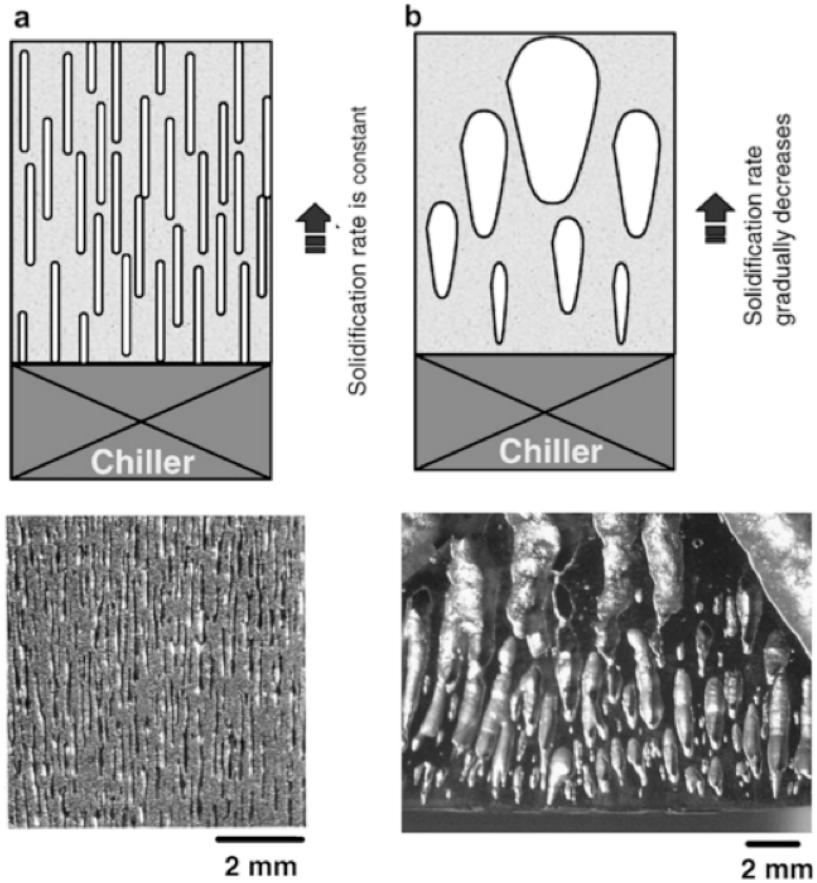

Figure 3.9: *Comparison of the evolution of pores in porous metals fabricated by the mold casting technique in gas atmosphere. The figure shows schematic drawings of pore evolution during the unidirectional solidification, and optical micrographs of the sectional views perpendicular to the solidification. On the left the metal is copper (high thermal conductivity) and on the right is stainless steel (low thermal conductivity).*

had a porosity of 46.3±0.4% and pore size of 388±131μm. Both samples had the same amount of hydrogen dissolved in the molten metal, determined by the Sieverts' law. The difference in the total pressure makes the change in the porosity and in the average diameter of the pores, the total pressure go down from 1MPa to 0.8MPa. The pores grow less if the pressure of the chamber is higher.

The other issue is related to the thermal properties of the metals. This technique allows producing a few porous metals such as copper [22,23] and magnesium [24] with a regular porous structure, because these metals exhibit high thermal conductivity and as a consequence the solidification proceeds with almost constant rate through the whole ingot as illustrated in Figure 3.9a. The same technique applied to fabricate porous metals and alloys of low thermal conductivity such as stainless steel [25], produce a non-regular porosity. The cooling rate becomes slower at the upper part of the solidified ingot that is far from the cooling part and thus the pores become coarse in this area. As a result only porous metals and alloys with non-uniform pore size and porosity can be produced as illustrated in Figure 3.9b.

3.4.2 Continuous casting technique

This technique was developed by Nakajima's Laboratory in order to overcome the previous mentioned limitation showed by metals and alloys with low thermal conductivity. The strategy to overcome this issue was a modification in the geometry of the cooling system.

Figure 3.10 shows a schematic drawing of this process. The fabrication apparatus consists of a high-pressure chamber containing a crucible heated by an induction coil, the crucible is made of graphite for nonmagnetic metals, and alumina for magnetic metals and alloys. The crucible has a hole at the bottom connecting it to a water-cooled mold. A stopper prevents the melt flow though the hole, during the gas dissolution step.

The metal is melted in the crucible by induction heating in a high-pressure mixture of gas. After enough time to make hydrogen (or nitrogen) to dissolve into the molten metal, the metal is pulled down, downloading the stopper, through the cooled mold at a given velocity. The molten metal solidifies in this mould. Then, directional elongated pores are evolved by precipitation of insoluble gas (hydrogen or nitrogen) in the solidified specimen.

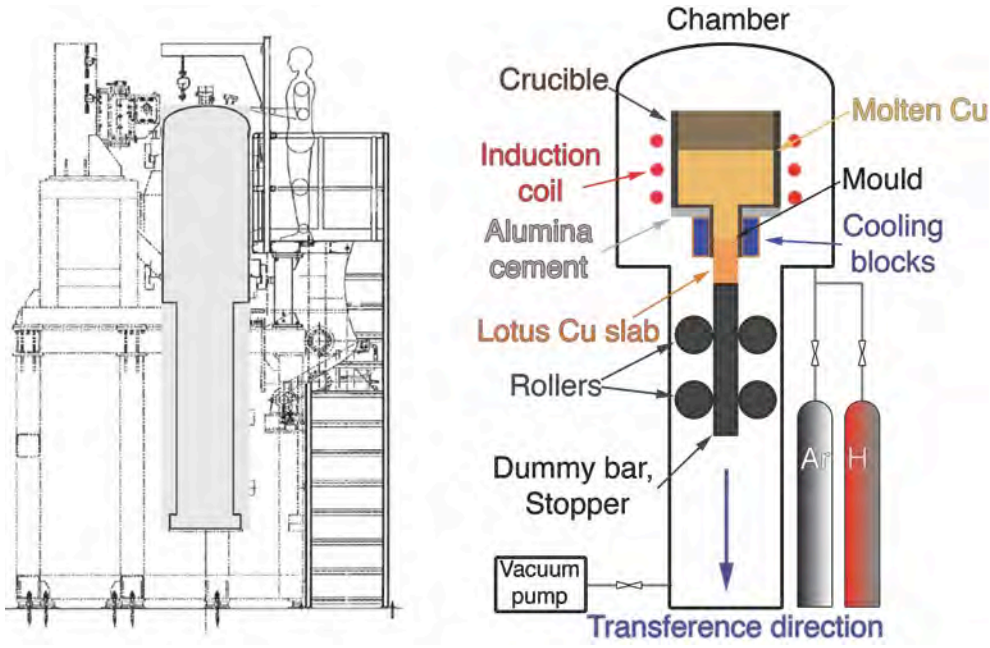

Figure 3.10: *Schematic drawing of the fabrication apparatus to produce lotus metals using the continuous casting technique. Large crucible and induction heating coil are located in the upper part of the pressure vessel, while the mould with cooling blocks and movable mechanism is at the bottom part. The height of the apparatus is about 7m. About 1m lotus ingot in length can be produced. The dummy bar is connected together with the melt at the mould.*

Figure 3.11 shows the interface surface between the liquid an solid phase. The transfer velocity of the stopper and the thermal conductivity of the metal determine the exact shape of the interface between solid and liquid phases. The pores grow perpendicular to the interface surface. The pores formed near the centre are parallel to the transference direction (pore 'a' in the figure) The pore 'b' shows a small deviation, and the pore 'c' shows a higher deviation and turns in its length because the angle of the interface surface change when the pore is growing and moving away from the surface of chiller. In this process the thermal conductivity limit the thickness (distance between the chillers) of the lotus rods. During the solidification process the induction heating for the crucible is still on, until all the metal comes out though the mould.

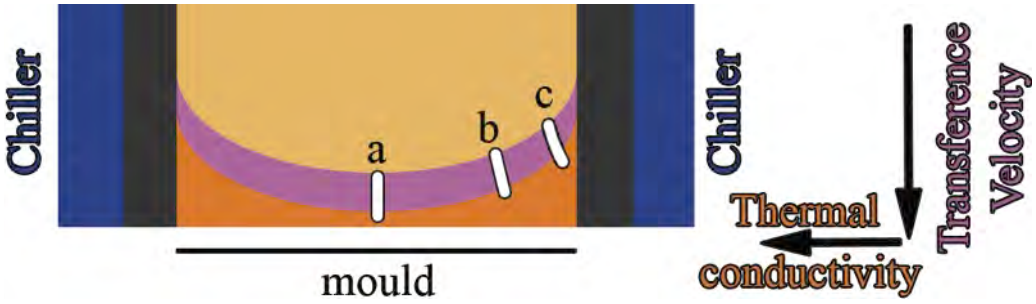

Figure 3.11: *Detail of the solidification in the continuous casting technique. The exact form of the interface, between solid and liquid phases, is function of the transference velocity of the stopper and the heat transfer of the metal. The pores evolve perpendicular to the interface surface between solid and liquid. (a, b, c represent the shape of the pores appearing during solidification in a typical experiment)*

J.S Park made a deeper study for lotus copper[26]. The lotus copper slabs present a skin layer of solidify copper without pores with a thickness that can be controlled by varying the transfer velocity of the stopper. The thickness of the skin layer is showed in Figure 3.12 and Figure 3.13.

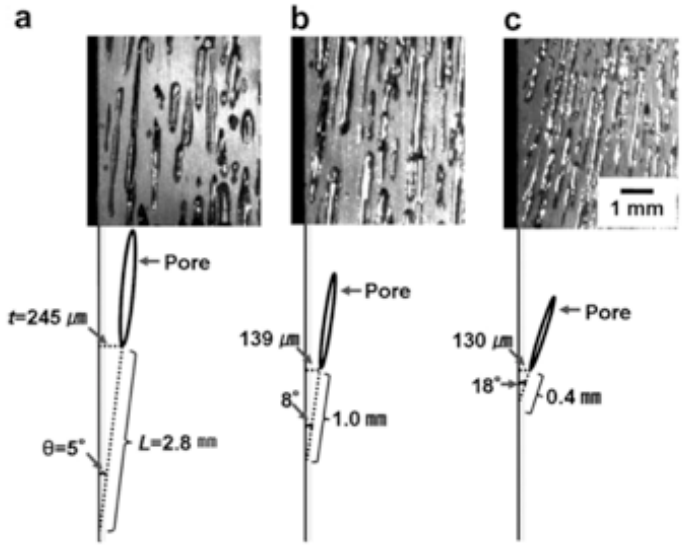

Figure 3.12: *Photographs (upper row) and schematic (lower row) of the pore formation position near the surface at different transfer velocities:*
a) 20 mm min^{-1}
b) 50 mm min^{-1}
c) 100 mm min^{-1}
under a hydrogen pressure of 1.0 MPa.

Also Park measured the angle of the pores as a function of the distance to the center of the rod, as can be seen in figure 3.14.

The angles of the pores on lotus metals are directly related to the angles of the interface between liquid and solid phases during the solidification, and changes for the metal or alloy used. As expected when the heat conductivity of the metal is large the pores of the lotus metal have low angles. When the

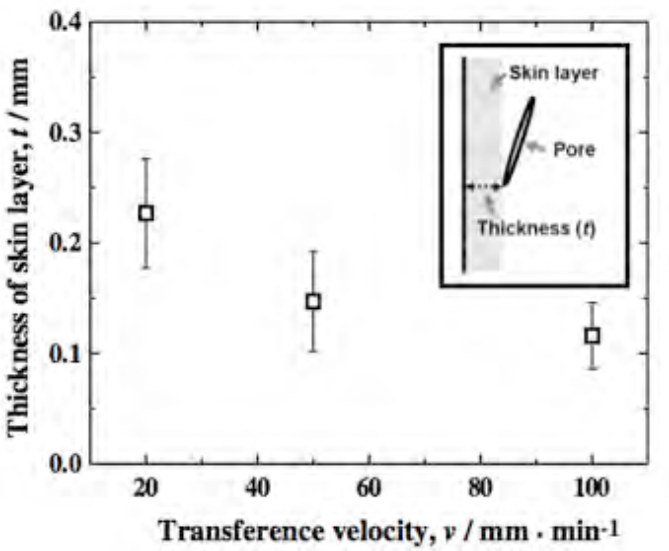

Figure 3.13: *Thickness of the skin layer as a function of the transference velocity for lotus-type porous copper fabricated under a hydrogen gas pressure of 1.0 MPa.*

transfer velocity increases, the solidification in the walls of the mould is quick, but the metal in the center of the mould is still liquid, increasing the angle of the interface and therefore the angle of the pores.

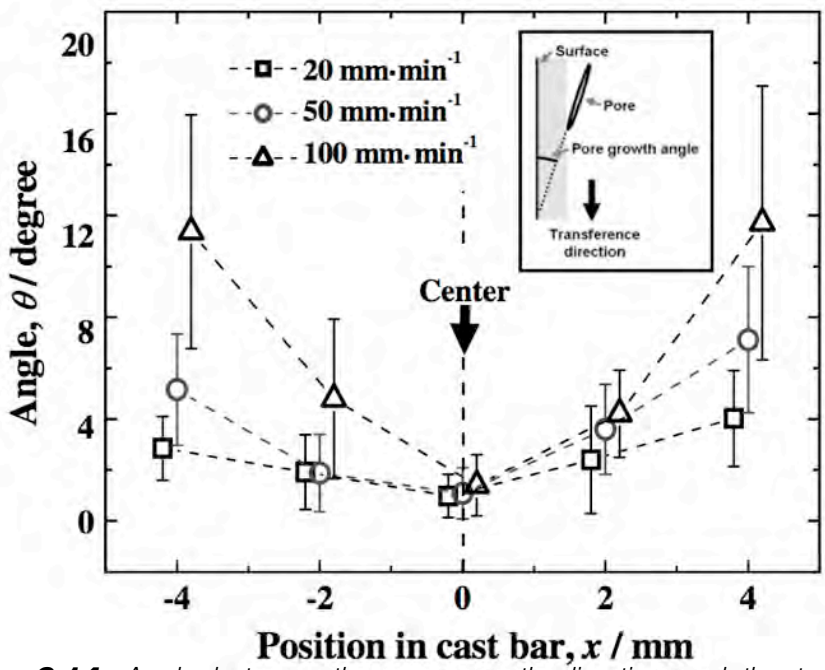

Figure 3.14: *Angle between the pore growth direction and the transference direction in various positions of the slab in a direction perpendicular to the transference direction; the slab was fabricated at various transference velocities under a hydrogen gas pressure of 1.0 MPa. (Angles at x = 0, ± 2 and ±4 mm are measured. The slab surface is at x = ±5 mm. Error bars are the standard deviations.)*

The transfer velocity of the stopper also changes the size of the pores. Figure 3.15 show photographs of several samples of the same alloy (pure copper), produced in the same conditions, except transference velocity. It can be observed that a higher transference velocity reduces the pore size [3, 26]. It is important to mention that the porosity does not depend on transference velocity; this parameter is mainly controlled by the partial pressure of the active gas. i.e. the amount of gas dissolved.

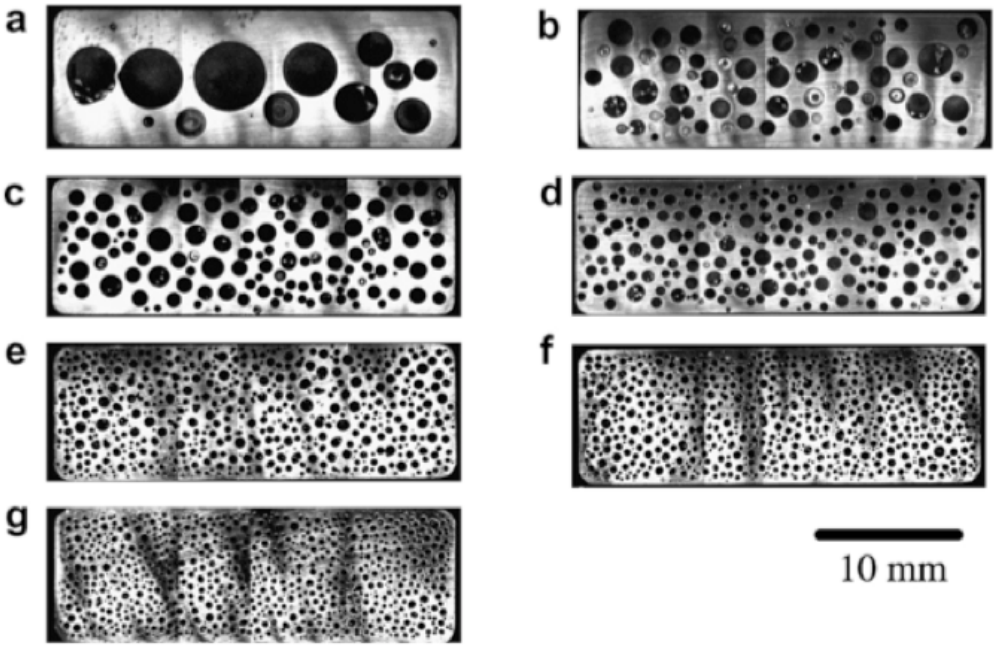

Figure 3.15 *Cross-sections perpendicular to the transference direction of the lotus-type porous copper fabricated using hydrogen at 0.25 MPa and argon 0.15 MPa by the continuous casting technique. Transference velocities are (a) 1 mm min^{-1}, (b) 5 mm min^{-1}, (c) 10 mm min^{-1}, (d) 20 mm min^{-1}, (e) 50 mm min^{-1}, (f) 100 mm min^{-1} and (g) 200 mm min^{-1}.*

Figures 3.16 and 3.17 shows the porosity of copper samples processed at the same velocities and with two different hydrogen pressures[27]. The porosity and average cell diameter are reduced by the total pressure in the chamber.

Summing up the previous description, it is possible to point out that the continuous casting technique allows fabricating rods of metals and alloys, with almost the same porosity and pore morphology on all its length. The maximum length of the rod is only limited by the length of the chamber.

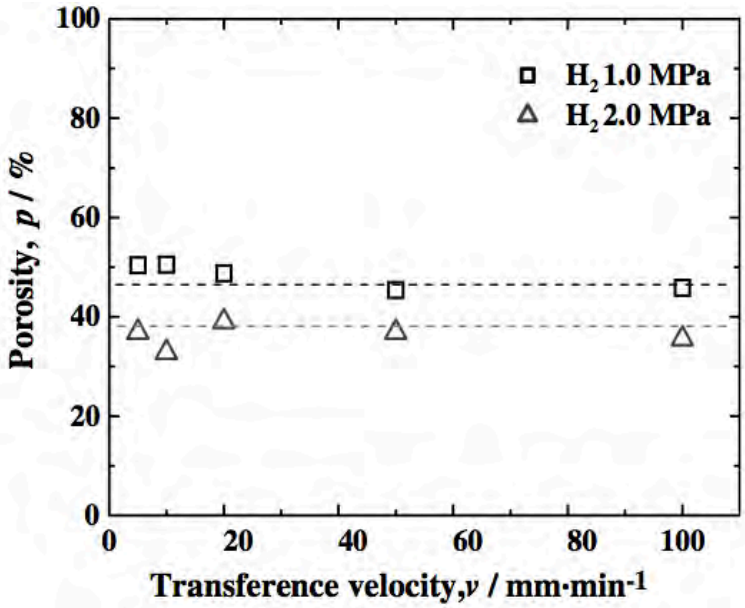

Figure 3.16: *Porosity Vs. transference velocity of lotus-type porous copper fabricated under hydrogen gas pressures of 1.0 and 2.0 MPa*

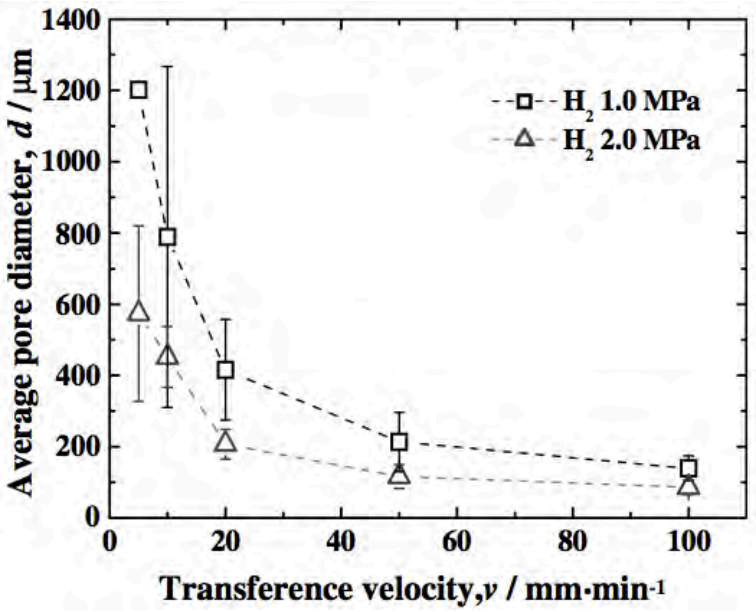

Figure 3.17: *Average pore diameter Vs. transference velocity of lotus-type porous copper fabricated under hydrogen gas pressures of 1.0 and 2.0 MPa.*

3.5 Mechanical properties of lotus-type porous metals

Effect of pores orientation and porosity.

Usually conventional porous metallic materials possess almost nearly spherical pores and as a consequence mechanical properties are usually isotropic [2]. But the shape of pores is not always round and the structure presents several type of defects (broken cell walls, accumulation of metal in few walls, etc.) The overall uniformity of the pore size and the porosity is not maintained in all the volume of the sample, dropping the value of the yield stress, and ultimate strength.

Lotus-type porous metals have regular elongated cylindrical pores aligned unidirectionally, in addition the metallic matrix has an uniform microstructure in all the sample. When the lotus metals are investigated various mechanical properties are remarkably different from those of isotropic porous materials, and show significant anisotropic behavior. Although the data on the mechanical properties of lotus metals are not so much accumulated compared with those of isotropic porous materials, it is at present, good enough to review some of the most significant findings related to their properties.

3.5.1 Elastic properties

Members of the Nakajima laboratory[3, 28, 29], measured the anisotropic elastic constants of lotus iron, with a regular distribution of elongated pores. The specimens were cut out of the ingots, and machined into rectangular parallelepipeds with the surfaces normal to the pore (solidification) direction. Figure 3.18 present the results obtained in the experiments in two different directions, perpendicular and parallel to the pores direction. For materials produced using hydrogen.

The materials also show the power-law formula typically used to describe the physical properties (Young's modulus, yield stress, thermal conductivity, etc.) of all cellular materials as function of the relative density, presented in section 2 (2.2), we write again this equation here for a general mechanical property M;

$$\frac{M_p}{M_0} = C \cdot \left(\frac{\rho}{\rho_s}\right)^n \qquad (3.3)$$

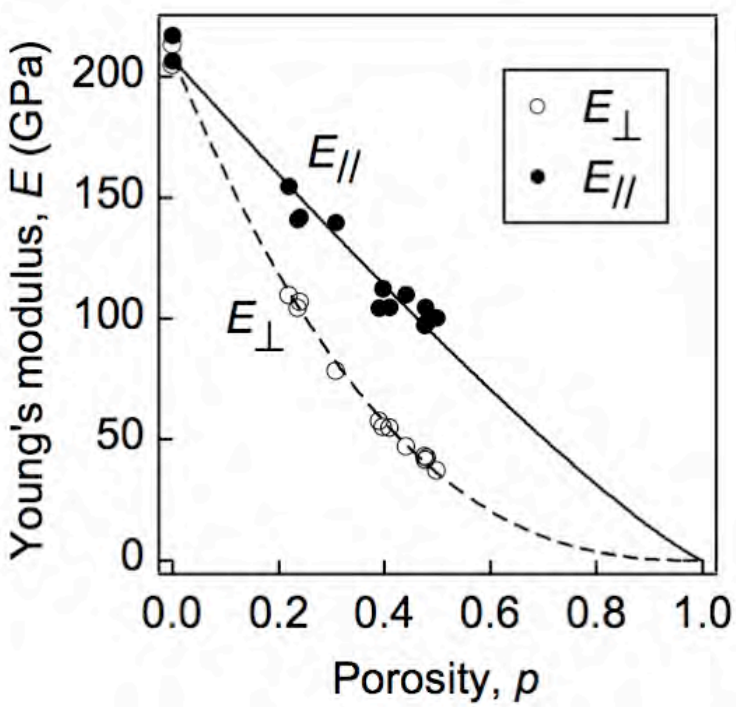

Figure 3.18: *Young's modulus of lotus iron produced with hydrogen as a funtion of porosity. Where $E_{\perp}$ and $E_{//}$ indicate the Young's modulus in the directions parallel and perpendicular to the pore direction, respectively. The Young's modulus decreases, with the increase of the porosity but with a different behavior for $E_{\perp}$ and $E_{//}$.*

Using the definition of porosity:

$$\phi = 1 - \frac{\rho}{\rho_s} \tag{3.4}$$

The equation 3.3 can be written as function of the porosity of the material:

$$M_p = C \cdot M_0 \cdot (1 - \phi)^n \tag{3.5}$$

Where M_0 is the physical property of the solid material; ϕ is the porosity of the material, and n is a coefficient that depends on the cellular structure, and the constant C is close to 1 for materials of high relative densities[30,31].

In lotus iron, Figure 3.18, the Young's modulus evaluated in the parallel direction ($E_{//}$) has a linear dependence with porosity $n \approx 1$, and the Young's modulus evaluated in the perpendicular direction ($E_{\perp}$) shows an exponent $n \approx 2.4$.

3.5.2 Tensile strength

Figure 3.19 shows the typical stress–strain curves for lotus copper specimens in the parallel and perpendicular direction to the pore orientation and different porosities, measured by Hyun [32].

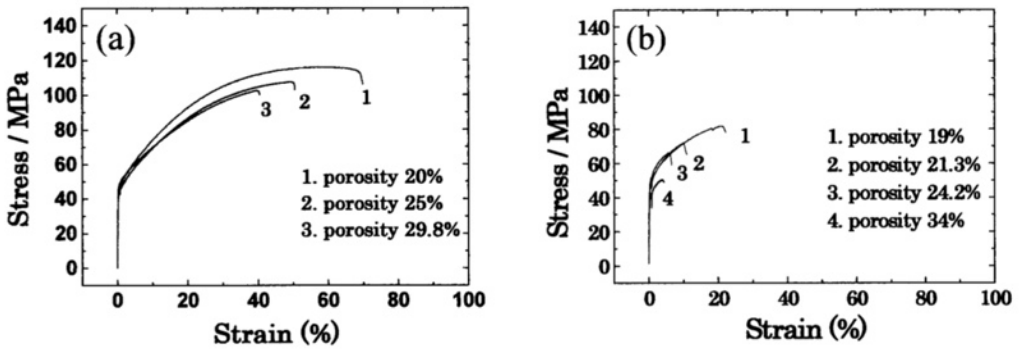

Figure 3.19: *Stress–strain curves for lotus copper specimens with the pore orientation (a) parallel and (b) perpendicular to the tensile direction.*

The curves show linear elastic behavior at small strains (elastic behavior), followed by yield and strain hardening up to failure. The ductility of the specimens decreases with increasing porosity. Similar to the analysis of the Young's modulus, the specimens show a different behavior if the applied stress is parallel to the pores longer axis or perpendicular to them. It is clear that the ductility is lower in the perpendicular direction. The yield strength (σ_t) and the ultimate tensile strength (σ_y) are plotted as a function the porosity in Figure 3.20. There are no differences in the yield strength for the samples perpendicular or parallel to the force, both curves follow a lineal trend with the porosity.

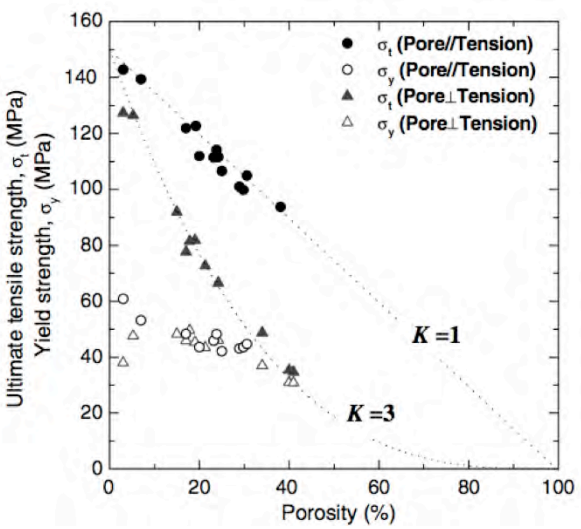

Figure 3.20: *Ultimate tensile strength (σ_y) and yield strength (σ_t) of lotus copper in the parallel and perpendicular direction to larger pore axis versus porosity.*

For the ultimate tensile strength there is a basic difference. When the stress is applied parallel to the pores the ultimate tensile strength changes linearly with the porosity, but when the stress is applied perpendicular to the pore direction the decrease is quicker with the porosity. If the data are fitted to equation 3.5.

$$\sigma_p = \sigma_0 \cdot (1 - \phi)^k \tag{3.6}$$

the exponent is k≈1 when the force is applied in the parallel direction and k≈3 when the force is applied in the perpendicular direction to the larger pore axis. Baccaccini et al. [33] suggested that the empirical constant k is related with the stress concentration around the pores. The stress concentration factor of the pores depends on the pore geometry and orientation with respect to the direction of applied stress and can be expressed by:

$$k = {}^{\sigma_{max}}/_{\sigma} \tag{3.7}$$

Where σ_{max} is the maximum value of the stress, which is given by equation 3.8, (Figure 3.21).

$$\sigma_{max} = \sigma \cdot \left(1 + 2\frac{a}{b}\right) \tag{3.8}$$

If we suppose that the different behavior is determined by the different shape of the pores; for the specimen with the cylindrical pores aligned parallel to the tensile direction, since b becomes large (in ideal case infinite),

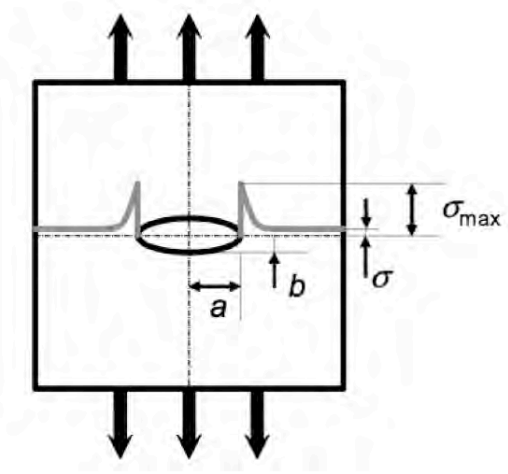

Figure 3.21: *Stress concentration in the vicinity of an elliptical pore in an infinitely large sample. The pore is located in the center. The stress is concentrated in both edges of the pore.*

the value of k approaches unity. Thus equation (3.6) can be simply rewritten as:

$$\sigma_p = \sigma_0 \cdot (1 - \phi) \quad (3.9)$$

For the specimen with cylindrical pores it is possible to assume a = b, so that the value of k approaches 3. Then, the stress can be expressed as:

$$\sigma_p = \sigma_0 \cdot (1 - \phi)^3 \quad (3.10)$$

Therefore, it can be assured that the different behavior in the ultimate tensile strength is due to the stress concentration in the cellular structure. This is a general trend for lotus-type porous metals.

3.6 Mechanical properties for lotus metals produced using different gases

It is normal the use of hydrogen to produce lotus metals, because the solubility of hydrogen in the melt is larger than that of other gases. But the gases present during the solidification could bring different properties; for this reason some times it is better to use other gases. One typical example is steel. Figure 3.22 shows the yield strength and the ultimate tensile strength of lotus iron fabricated in hydrogen and nitrogen atmosphere. The doted lines are equations (3.9) and (3.10) for steel. The samples made in hydrogen atmosphere follow those equations, but the samples made in nitrogen atmosphere give similar strength than the values of non-porous samples. The samples made in nitrogen contains a 0.0873% of nitrogen. Such remarkable enhancement of the tensile strength is attributed to solid solution strengthening due to solute nitrogen atoms. Therefore, the technique of gas dissolution to produce the porous metal can also be used to improve the proprieties of the metallic matrix.

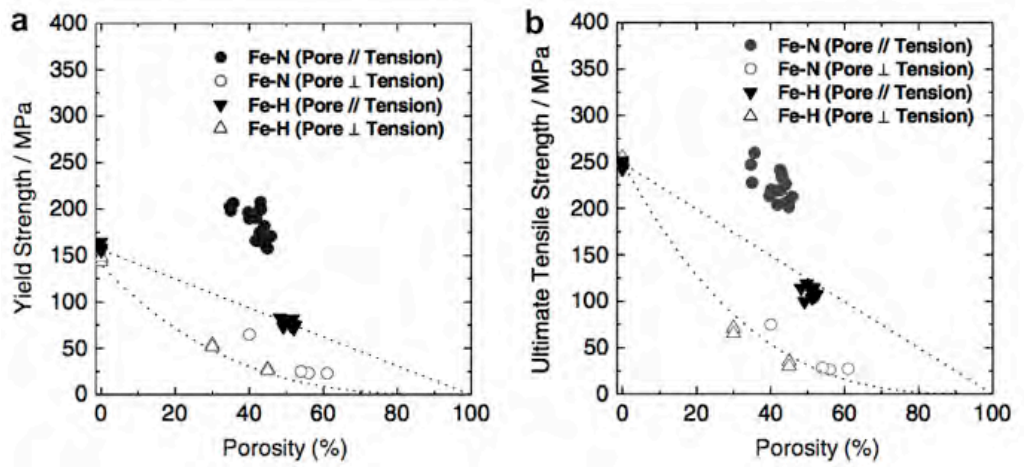

Figure 3.22: *Porosity dependence of (a) yield strength and (b) ultimate tensile strength of lotus iron fabricated in hydrogen or nitrogen atmosphere in the direction parallel and perpendicular to pore larger axis.[29]*

3.7 Microstructure of the metallic matrix (Grain size)

As it was explained in the section 2.4, the crystal size is directly related with harness and strength. A metal with larger crystal size have a larger ductility but lower hardness and strength than other of the same alloy with lower grain size [34-37].

In metals produced for structural applications, it is common to design quick cooling rates with hot rolling, or post-processing treatments to reduce the crystal size. In the process to produce lotus metals all variables are chosen to obtain a uniform porous structure. The election of those parameters also affect the crystallization of the metallic matrix.

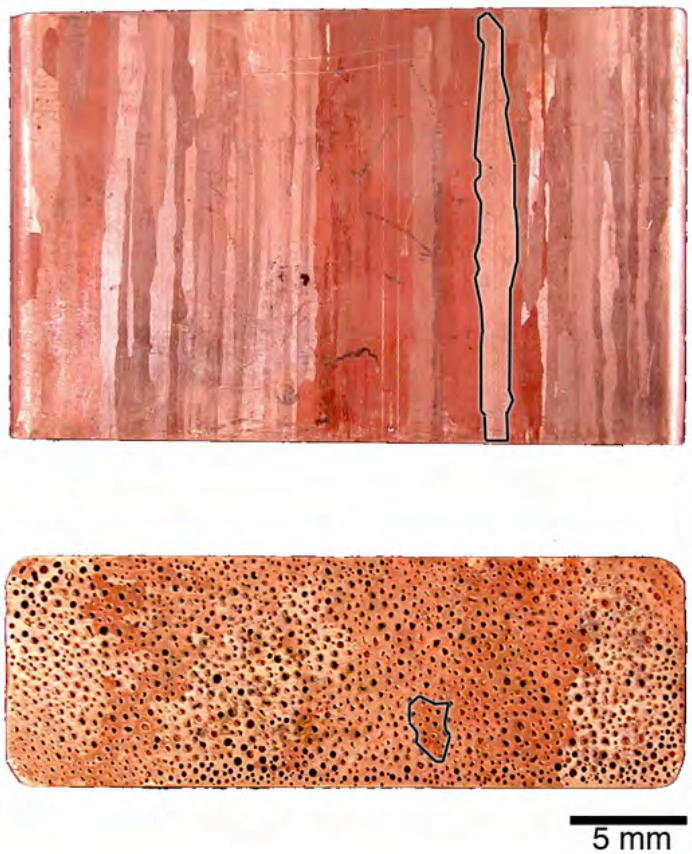

Figure 3.23: *Micrographs showing two perpendicular views the grain size of a lotus pure-copper bar produced by the continuous casting process, at 20mm·min^{-1}, in atmosphere of H_2 0.5MPa and Argon 0.3MPa. The copper was melted at 1573K.*

Figure 3.23 shows the crystal size of a lotus copper bar produced by the continuous casting. The grain size has more than 20mm in length and more

than 3mm in diameter. These sizes are a consequence of the slow cooling rates needed to obtain the cellular structure. Non-porous pure copper samples cooled using the same conditions showed the same crystal shapes and sizes.

The low crystallization rate for the lotus copper, and the subsequent large grain crystals made a soft metallic matrix. The focus of this thesis is to replace the bulk materials used as structural support for foamed materials that retain the mechanical materials with the porosity. So we need to compare our porous samples of pure copper with another copper with high mechanical properties.

Oxygen-free high thermal conductivity (OFHC) copper is a high purity copper with small grain size used basically for applications in electrical engineering. The acronym for the term, oxygen-free high conductivity copper, OFHC™, is a registered trademark of Phelps Dodge Specialty Copper Products. Comparable generic products are generally referred to simply as OF (oxygen-free) copper. In copper, the conductivity is related with the grain size of the metal in similar terms than yield strength, when the crystal size is reduced the conductivity grows. Also OF copper is 99.9% pure copper, the same alloy used to produce lotus copper. So we can compare the strength of the lotus copper with this special copper[38]. The OFHC copper has been also annealed to increase the grain size in the sample decreasing the yield strength.

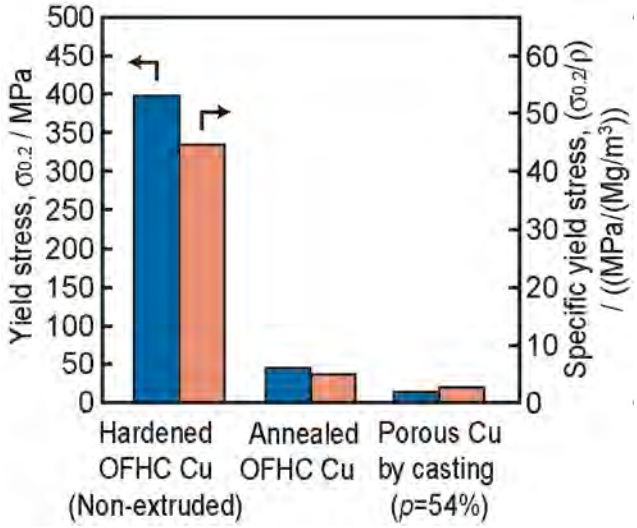

Figure 3.24: *Comparative of the yield stress of several copper samples. A hardened nonporous copper, annealed OFHC copper and lotus copper (99.99% pure copper).*

Figure 3.24 shows the yield stress, and specific yield stress in compression for different types of solid and porous copper.

The lotus-type porous copper did not match to the yield strength of the Oxygen-free high thermal conductivity copper, but also is lower than the annealed OFHC copper, the same result is valid for the specific yield stress. Lotus copper is far away to substitute the bulk metal in an structural application.

3.8 Objectives of the thesis

In this chapter, a short review about the processing methods and the basic mechanical properties of lotus-type porous metals has been presented.

As a summary we can conclude that lotus metals have a homogenous and anisotropic porous structure giving to a good mechanical performance in the parallel direction to the long axis of the cells. As a consequence, these metals are good candidate for their use in structural applications as substitutes of bulk metals. However when we make the direct comparison between the metallic matrix of the lotus metals and structural metals, we found that the lotus metals are far away from the necessary mechanical properties asked for a metallic structural part. The specific strength of lotus copper is around 8 times lower than structural copper, as is show in Figure 3.24. The reason is connected with the low cooling rate needed to produce the lotus-type porous metal that results in a large grain size.

This thesis, in the next chapters, will show two fundamental scientific studies aiming at overcoming this basic problem in the mechanical properties of lotus metals, trying to improve the metallic matrix microstructure and properties, without losing or deteriorating the porous structure.

1. The first approach used a near surface severe plastic deformation [39,40] treatment developed by the Joining and Welding Research Institute at Osaka University. This treatment produce a refined grain site at the skin (Chapter 4).
2. The second approach uses the well know ECAE (Equal channel angular extrusion) process [41-43], sometimes also called equal-channel angular pressing (ECAP) process [44], to improve the hardness and strength of the porous metals (Chapter 5).

3.9 References

[1] J. Bjorksten, J.C. Elliott and R.J. Roth; "Foamed Metal Low-Density Core Material for Sandwich Construction", Wright Air Develop. Center Technical Report 52-51. 1952.

*[2] J. Banhart, Progress in Materials Science **46**, 559, 2001.*

*[3] H. Nakajima, Progress in Materials Science **52**,1092, 2007.*

[4] D.P. Smith ed. "Hydrogen in metals", The University of Chicago Press, 1947.

*[5] V. Shapovalov, MRS Symposium Proceedings Volume **521**, 281, 1998.*

*[6] V. Shapovalov and L. Boyko; Advanced Engineering Materials **6**, 407, 2004.*

[7] T.B. Massalski ed. "Binary alloy phase diagrams", Metals Park: American Society for Metals, 1986.

[8] Y. Levinsky "Pressure dependent phase diagrams of binary alloys", Materials Park: ASM International, 1997.

*[9] A.H. Satir-Kolorz and H.K. Feichtinger; Z Metallkde **82**, 689, 1991.*

[10] R.E. Reed-Hill ed. "Physical metallurgy principles". Princeton: D. Van Nostrand Company, Inc., 1964.

[11] V. Shapovalov. Proceedings of the 1999 International symposium on Liquid Metal Processing and Casting, Santa Fe, 1999.

[12] H. Okamoto "ASM Handbook, Volume 03 - Alloy Phase Diagrams", ASM International, 1992.

*[13] S.Y. Kim, J.S. Park, H. Nakajima. Metallurgical and Materials Transactions A **40**, 937, 2009.*

*[14] H. Nakajima, T. Ide. Metallurgical and Materials Transactions A **39**, p.390, 2008.*

[15] C. K. Gupta "Chemical metallurgy: principles and practice", Wiley-VCH, 2003.

*[16] H. Nakajima. Materials Transactions **42**, 1827, 2001.*

*[17] R.P. Reed; JOM **41**, 3,16, 1989.*

*[18] V.F. Zackay, J.F. Carlson and P.L. Jackson; Transactions of the American Society for Metals **8**, 508, 1956.*

*[19] R.K. Okagawa, R.D. Dixon, D.L. Olson. Welding Journal **62**, 204, 1983.*

[20] L. Coudurier, D.W. Hopkins, I. Wilkomirsky "Fundamentals of Metallurgical Processes", Pergamon Press, Oxford, 1985.

*[21] H. Nakajima, T. Ikeda and S.K. Hyun. Advanced Engineering Materials **6**, 377, 2004.*

[22] S.K. Hyun, Y. Shiota, K. Murakami, H. Nakajima. In: M. Koiwa, K. Otsuka, T. Miyazaki eds. Proceedings of the conference on solid–solid phase transformations'99 (JIMIC-3). Kyoto: Japan Institute of Metals, 341, 1999.

*[23] H. Nakajima, S.K. Hyun, K. Ohashi, K. Ota, K. Murakami. Colloids and Surfaces A: Physicochemical and Engineering Aspects **179**, 209, 2001.*

*[24] T. Ikeda, H. Nakajima. Journal of Japan Foundry Engineering Society **74**, 812, 2002.*

*[25] T. Ikeda, M. Tsukamoto, H. Nakajima. Materials Transactions **43**, 2678, 2002.*

*[26] J.S. Park, S.K. Hyun, S. Suzuki, H. Nakajima; Acta Materialia **55**, 5646, 2007.*

*[27] T. Nakahata, H. Nakajima. Materials Science and Engineering: A **384**, 373, 2004*

*[28] M. Tane, S. K. Hyun, T. Ichitsubo, H. Nakajima; Materials Science Forum **486-487**, 489, 2005.*

*[29] M. Tane, T. Ichitsubo, S.K. Hyun, H. Nakajima; Journal of Materials Research **20**, 135, 2005.*

[30] L.J. Gibson and M.F. Ashby "Cellular Solids", Cambridge University Press, 1997.

[31] M.F. Ashby, A.G. Evans, N.A. Fleck, L.J. Gibson, J.W. Hutchinson and H.N.G. Wadley "Metal Foams: A Design Guide", Butterworth-Heinemann, 2000.

*[32] S.K. Hyun, K. Murakami, H. Nakajima; Materials Science and Engineering: A **299**, 241, 2001.*

*[33] A.R. Boccaccini, G. Ondracek, E.J. Mombello; Journal of Materials Science Letters **14**, 534, 1995.*

*[34] E. O. Hall, Proceedings of the Physical Society. Section B Volume **64**, 747, 1951.*

*[35] N. J. Petch, Journal of the Iron and Steel Institute **174**, 25, 1953.*

[36] W.F. Smith and J. Hashemi "Foundations of Materials Science and Engineering" , McGraw-Hill, 2006.

[37] H.N. Gupta, R.C. Gupta and A. Mittal "Manufacturing processes", New Age International, 2009.

*[38] H. Utsunomiya, H. Koh, J. Miyamoto and T. Sakai. Advances Engineering Materials **10**, 775, 2008.*

*[39] M. Sato, N. Tsuji, Y. Minamino, Y. Koizumi. Science and Technology of Advanced Materials **5**, 145, 2004.*

*[40] Y.S. Sato, Y. Kurihara, S.H.C. Park, H. Kokawa, N. Tsuji; Scripta Materialia **50**, 57, 2004.*

[41] V.M. Segal "Methods of Stress–Strain Analysis in Metalforming", Sc.D. Thesis, Minsk, 1974.

*[42] V.M. Segal. Materials Science and Engineering: A **271**, 322, 1999.*

*[43] R.Z. Valiev. Nature Materials **3**, 511, 2004.*

*[44] R.Z. Valieva, T.G. Langdon. Progress in Materials Science **51**, 881, 2006.*

4 Modification of lotus copper by Near Surface Severe Plastic Deformation: Wire-Brush method

Resumen (Spanish):

En el artículo presentado en este capitulo se recoge la primera experiencia de usar un proceso de NS·SPD (acrónimo en ingles de "deformación plástica severa cercana a la superficie") en metales porosos tipo lotus. Dicha deformación superficial se lleva a cabo con un cepillo metálico, de esta forma la superficie de la pieza sufre un proceso de forjado que deja intacta la estructura porosa del interior. El resultado de las pruebas mecánicas realizadas muestra una mejora de las mismas, pero al ser un tratamiento solo superficial dichas mejoras se reducen a medida que el volumen total de la pieza aumenta.

4.1 Introduction

Since pioneering works of Hall and Petch [1,2] the effect of grain size on mechanical properties of metals is still being discussed in terms of various models. As it was introduced in the section 2.4, for conventional polycrystals the strength dependence with the mean grain size can be described by the Hall-Petch (H-P) relationship[3,4].

$$\sigma_y = \sigma_0 + \frac{k_y}{\sqrt{d}} \tag{4.1}$$

where σ_y is the yield stress, d is the average grain size and σ_0 and k are material constants. As it can be seen in the equation, when the grain size is reduced the yield strength increases.

The grain boundaries act as pinning points impeding further dislocation propagation[4]. Since the lattice structure of adjacent grains differs in orientation, it requires additional energy for the dislocation to change directions and move into the adjacent grain. The grain boundary is also much more disordered than inside the grain which also prevents the dislocations from moving in a continuous slip plane. Impeding this dislocation movement hinders the onset of plasticity and hence increase the yield strength of the material.

The Hall-Petch (H-P) relation is well followed until the average crystal diameter is around 1μm. At smaller sizes new phenomena take place. When

the grain size is around several nanometers (10nm for nickel), only one or two dislocations can fit inside a grain[5]. This scheme prohibits dislocation pile-up and never results in grain boundary diffusion. The lattice resolves the applied stress by grain boundary sliding, resulting in a decrease in the material yield strength.

It is well known that heavy deformations, for example, by cold rolling or drawing, can result in significant refinement of microstructure. Severe plastic deformation (SPD)[6] involves very large strains and usually a significant change in the overall dimensions of the specimen or work-piece. Therefore these kind of processes reduce the porosity of the bulk metal, one advantage in general, but a great step backwards for it use with lotus-type porous metals.

Nobuhiro Tsuji work a few years ago on SPD research using accumulative roll-bonding (ARB)[7,8]. The process of the samples in such research is showed in Figure 4.1.

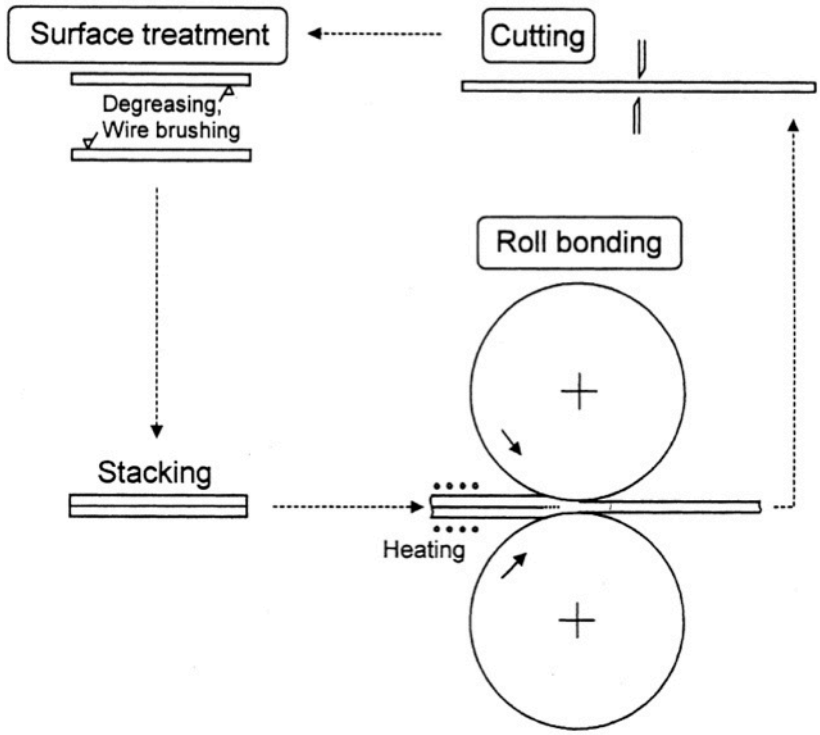

Figure 4.1: *Simpliefied scheme of the accumulative roll-bonding (ARB) process.*

Between each pass through the rolls the metallic plate is cleaned by wire-brushing. In a carefully research on the microstructure of the samples it was

detected that the wire-brush process produced a grain refinement on the surface of the metallic samples, similar to the grain refinement obtained by ARB.

The new process of grain refinement was a NS·SPD process, similar to the friction-stir welding (FSW) [9] used to join two pieces of metal, but less localized.

The new NS·SPD process was denominated wire-brush technique. The wire-brush changes the surface layers of the metallic materials. If the high strain is limited to the surface of the sample it is expected that the porous structure and the bulk density will remain unchanged. Taking into account the papers published on this topic on nonporous materials[10,11] it is expected a thin deformed layer and low changes in the overall mechanical properties. The grain refinement obtained by wire-brush will be significant, with a grain size around 100nm or less in the surface, but the deformed layer will be only a small part of the whole thickness of the sample. In the nonporous samples studied in the previous papers the deformed layer was only 10-30 μm in depth. Taking into account the previous results, we decided to apply this technique to lotus copper. The results are in the following paper submitted to "The Journal of Materials Science".

4.2 Paper: Improving the mechanical behaviour of lotus-type porous copper by wire-brushing.

Improving the mechanical behaviour of lotus-type porous copper by wire-brushing.

J Lobos[1,5], S Suzuki[1,2], H Nakajima[1], Y S Ji[3], H Fujii[3], D Terada[4], N Tsuji[4], M A Rodriguez-Perez[5]
[1]The Institute of Scientific and Industrial Research, Osaka University, Ibaraki, Osaka 567-0047, Japan.
[2]Waseda Institute for Advanced Study, Waseda University, Shinjuku, Tokyo 169-8555, Japan
[3]Joining and Welding Research Institute, Osaka University, Ibaraki, Osaka 567-0047, Japan.
[4]Dept. of Adaptive Machine Systems, Graduate School of Engineering, Osaka University, Suita, Osaka 565-0871, Japan.
[5]Cellular Materials Laboratory, Condensed Matter Physics Department, University of Valladolid, 47011 Valladolid, Spain

E-mail: obi@fmc.uva.es

Abstract. The surface of lotus-type porous copper plates with cylindrical open pores in the thickness direction (porosity 50.4%, average pore diameter 144 μm) was processed by wire-brushing. Due to this surface treatment a nonporous thin layer comprised by ultra-fine grains closed the open pores on the surface of the lotus copper. The Vickers hardness increased in the deformed area due to the grain refinement. The mechanical behaviour of the porous materials (yield strength and ultimate tensile strength) was improved by around 30% due to the surface treatment with no significant increase of the bulk density (increments lower than 10%). The obtained results have showed that wire-brushing is an effective process for improving the mechanical properties of lotus metals without affecting in a significant extend the internal cellular structure.

1. Introduction

Porous metals have been actively studied in recent years because of their promising properties such as light–weight, vibration and acoustic energy damping, and impact energy absorption [1]. However, for many kinds of porous metals the specific strength decreases with increasing porosity because spherical pores cause stress concentrations[2,3]. On the other hand, lotus-type porous metals with long cylindrical pores aligned in one direction have superior mechanical properties compared with porous metals with spherical pores. The specific strength does not decrease with increasing porosity in the pore growth direction [3]. Therefore, lotus metals are expected to be used as light-weight structural materials.
However, as lotus metals are fabricated by solidification processes, their as-cast microstructure has lower strength than that of commonly used structural metals, which are usually produced by forging [4]. It is, therefore, desirable to find methods to improve the hardness and strength of the metallic matrix keeping at the same time the low density of the porous metal.
It has been recently reported that the Vickers hardness of lotus copper increases when the materials are processed by ECAE (equal-channel angular extrusion) with a limited increase in the bulk density [5,6]. These works showed the positive effect of severe plastic deformation on the strength of these materials . On the other hand, wire-brushing process has been recently used to produce near surface severe plastic deformation (NS·SPD) of bulk metals [7,8]. It was reported that wire-brushed nonporous metals have surfaces with smaller grain sizes. Therefore, it is expected that this process could provide severe plastic

deformation to the metallic matrix of lotus metals without destroying the porous structure.
Bearing the previous ideas in mind, lotus copper plates have been treated by wire-brushing. The effects of angular velocity, and number of revolutions per unit length of the wire-brush treatment on mechanical properties such as the Vickers hardness, yield strength and ultimate tensile strength have been analysed. The improvement of mechanical properties has been discussed considering the structural changes taking place during the treatment.

2. Experimental

2.1. Fabrication and preparation of lotus copper samples.

A lotus copper ingot was produced by the mould casting technique, Figure 1a [9]. Four kg of copper were melted in a pressurized hydrogen atmosphere of 0.5 MPa. Inside the chamber, the melt was poured into a cylindrical mould (100mm in diameter) with the chillier in the base which produces and unidirectional solidification in the gravity direction. Because of the solubility gap of hydrogen between solid and liquid phases the pores evolved in the solidification direction. The resulting lotus copper ingot had 114mm in height, with an average porosity of 50.4%, and average pore diameter of 144 μm. After production, the lotus copper ingot was sliced in discs of different thickness (1.45, 1.72, 2.10, 2.74 and 3.74 mm), Figure 1b. The pores were orientated in the thickness direction and due to this open pores were visible on the surface, the average porosity of the samples was 47.51±2.37% for all the discs used.

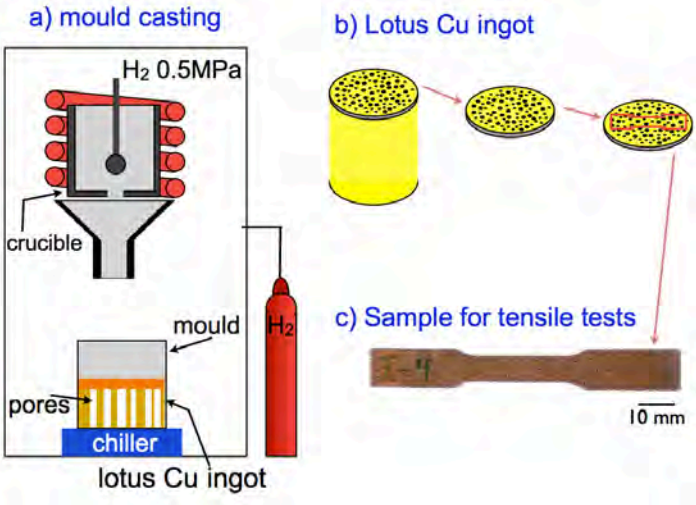

Figure1: a) Mold casting technique to produce lotus-type porous metals. b)The lotus copper ingot was sliced in thin disks. c)The samples for tensile tests were cut from the thin disks.

2.2. Samples for the tensile test and wire-brush treatments.

The samples for the tensile tests and for the wire brushing treatments were cut from the sliced discs of porous copper in a shape that can be seen in Figure 1c. Some samples were tested as produced (reference values) and others were treated by wire-brushing, by both sides, before the mechanical testing.

2.3. Wire–brushing

A schematic illustration of the wire-brushing process used in this study is shown in Fig. 2. A sample of lotus copper with the shape of the tensile specimen (see previous section) was fixed on a table. A rotating stainless steel wire cup brush (grade CN- 16, cup diameter 70 mm, length of the wires 18 mm and diameter of the wires 0.3 mm); was transferred in the direction of the sample width. The rate of the wire–brush was set at 2500, 3750 or 5000 rpm. The transference velocity of the wire-brush was set to maintain the revolutions per unit length constant at 100 mm^{-1} or 200 mm^{-1}. The revolutions per unit length (R.L.) are defined by:

$$R.L. = \frac{angular\ velocity[min^{-1}]}{linear\ velocity\ [mm \cdot min^{-1}]} = \frac{angular\ velocity}{linear\ velocity}[mm^{-1}]$$

The wire-brush rotates clockwise and the axis of the wire-brush was tilted 7 degrees from the vertical during movement. The height was set for all the experiments. The wires were located 1mm below the surface of the sample. With this geometry only half of the circumferential part of the wires hit the sample simultaneously. The time of wire-brushing for one surface of the one sample is between 0.4s for the samples processed at 2500rpm (100 mm^{-1}) to 0.2s in the samples processed at 500rpm (100 mm^{-1})

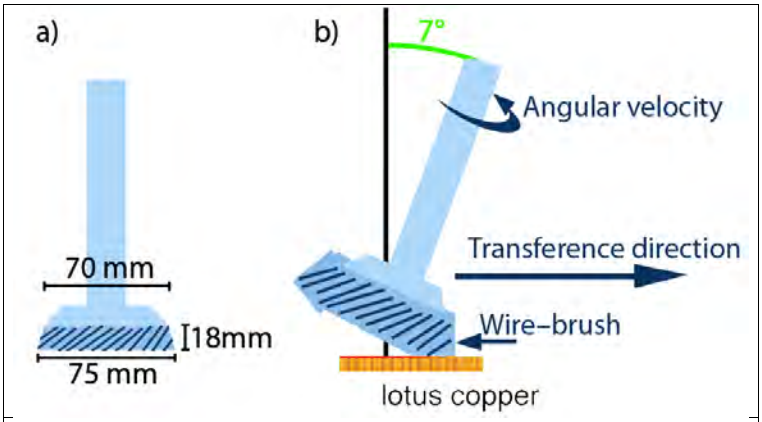

Figure 2: a) Geometry and dimensions of the wire-cup and wire-brush b) Diagram of the wire-brush process on a lotus copper sample.

2.4. Samples processed.

Table 1 summarizes the wire-brush treatments performed. The experiments were designed to obtain information on the effect of three key parameters affecting the process, namely, transference velocity (R.L), angular speed and specimen thickness. The initial samples (type 1 in table 1) were of 2.10 mm in thickness and were treated at 5000rpm using two different values of R.L: 100 mm^{-1} and 200 mm-1. A second set of samples (type 2 in table 1) with 2.10 mm in thickness were processed with different rotational speeds (2500, 3750 and 5000 rpm^{-1}) at a constant R.L. value of 100 mm^{-1}. Finally, a third set of samples (type 3) were treated using the optimum conditions for improving the mechanical behaviour (found in the study of set 1 and 2) to analyze the effect of thickness on the mechanical improvement.

Session	Thickness (mm)	Angular velocity (rpm)	R.L. (mm^{-1})
#1	2.10	5000	**100**
#1	2.10	5000	**200**
#2	2.10	**5000**	100
#2	2.10	**3750**	100
#2	2.10	**2500**	100
#3	**1.45**	3750	100
#3	**1.72**	3750	100
#3	**2.74**	3750	100
#3	**3.74**	3750	100

Table 1: Treated samples by wire-brushing and main parameters used for the treatment.

2.5. Characterization of the processed samples

The surface of the processed lotus copper was observed with a digital microscope (KEYENCE VHX-200). The microstructure of processed lotus copper plate cross sections was observed with a FE–SEM JEOL 9800 and EBSD analyzer Tex SEM Labo. Inc. MSC-2200. The results of the EBSD are presented as Inverse Pole Figure (IPF) map in which the colours correspond to the crystal orientations as shown in the projection.

The Vickers hardness was measured on the processed surface of the lotus copper plates by a hardness tester (AKASHI MVK-III). The testing force was 1 N and the testing time was 20 s. Ten areas on the each sample were tested and the average value was obtained.

The tensile tests were carried out using a universal testing machine (INSTRON 5582). The crosshead speed was set at 2 mm min^{-1}. From the obtained stress-strain curve, the yield strength (0.2% offset) and the ultimate tensile strength were measured. The tensile tests were performed four times for each processing condition and for each thickness.

3. Results

3.1. Surface of the lotus copper plates

Figure 3 shows images of the samples after treatments with different angular speed and constant transference velocity (100 mm^{-1}). The surface porosity was

obtained by image analysis of the micrographs. The open pores are clearly observed in the as–cast material; however the pores are partially closed when the treatments are applied. In fact, the initial porosity of 47% is reduced up to a value of 0.5% for the sample treated at 3750 rpm and 100 mm^{-1}. Therefore, it is possible to conclude that the wire-brush treatment creates a solid skin that partially closed the open porosity of the materials. This effect is maximized for intermediate values of the angular speed as it is clearly observed in figure; for higher speed the pores are reopened and deformed in an ellipsoidal shape with the large axis in the direction in which the wires hit the surface.

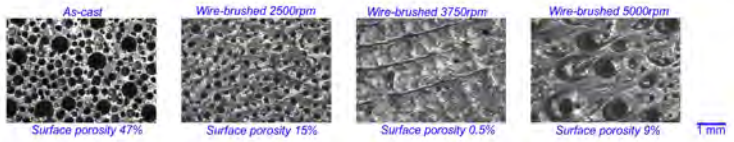

Figure 3: Surface porosity for samples processed at different rotating speeds and the same transference velocity. The surface porosity values are obtained by image analysis processing.

The bulk density of the samples was not significantly increased by the wire-brushing technique; the maximum increase detected in density was 7.7% for the material treated at 3750 rpm.

3.2. Vickers hardness

Figure 4 shows the Vickers hardness of samples treated with different processing parameters compared with the value for the as-cast material. It is clear that the application of the treatment allows a significant increase of the Vickers hardness from 70 (as cast material) to 160 for samples processed at a transference velocity of 100mm-1. In addition, Vickers hardness values do not change with the increase of the angular speed of the wire-brush. However, the value increases significantly (from 160 to 240) when the transference velocity increases from 100mm-1 to 200mm-1.

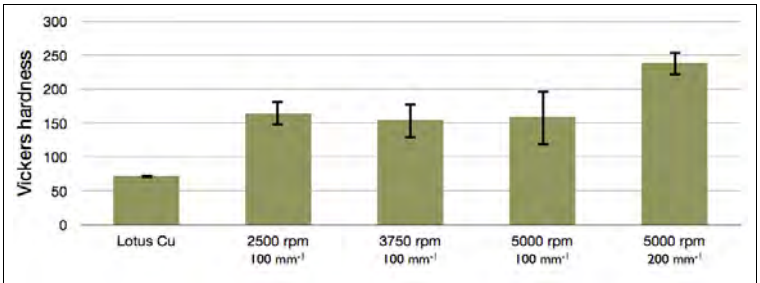

Figure 4: Average Vickers hardness of the surface of the samples treated with different rotating speeds and different transference velocities.

3.3. Microstructure of the metallic matrix.

The SEM images of the cross section of the materials showed that the wire-brush process was able to create a new layer on the surface of the material (figure 3). The microstructure of this new layer has been analyzed by SEM and EBSD mapping. Figure 5 shows a typical example of changes produced by the treatment.

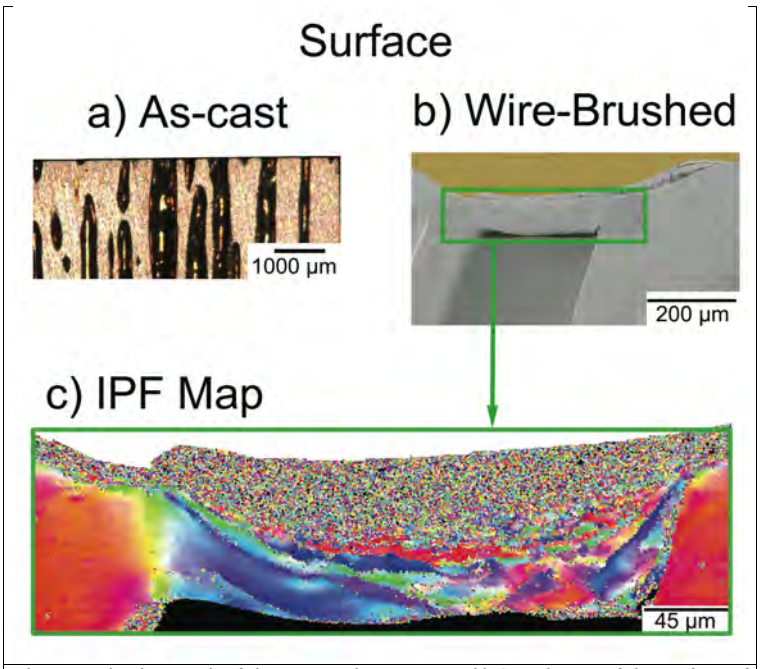

Figure 5: a) Micrograph of the As-cast lotus copper. b) SEM image of the surface of porous copper showing the deformed layer that appears due to the wire-brushing process. c) IPF map of the deformed layer showing the average crystals size in this area. The specific sample of this figure was processed at 3750rpm and 100mm^{-1}.

The cross section image of figure 5b clearly shows that a new deformed layer closing the pores is formed during the wire-brush treatment. The IPF map shows that ultrafine grains are located in this deformed layer. The thickness of this layer is around 45µm in the area closing the pores and 25µm in other areas. The grain refinement has a similar depth than that showed in previous studies on nonporous metals [7-8].

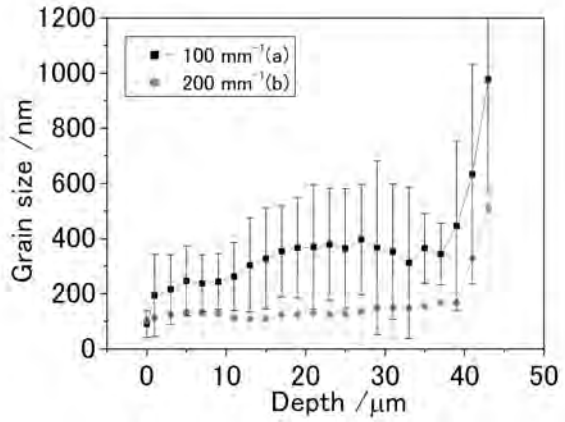

Figure 6: Average grain size of the copper crystals as a function of the depth from the surface. The samples were processed at 5000 rpm and different transference velocities.

Figure 6 shows the grain size as a function of the depth (from the samples surface) for materials processed at 5000 rpm. The values are small for depths below 45 μm. Grains with sizes below 200 nm are formed when the material was treated with a transference velocity of 200 mm^{-1}, the grains are slightly larger (sizes below 400 nm) when the treatment was carried out at 100 mm^{-1}. It seems that the grain refinement increases when the number of times that the wires hit the surface increases.

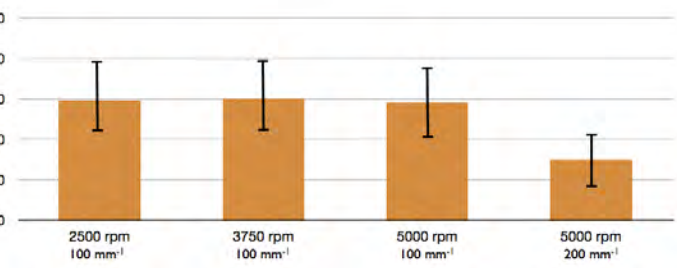

Figure 7: Average grain size of the copper crystals in the 35μm of the deformed layer for several samples.

To perform a more detailed comparison between samples the average grain size in the first 35μm of the deformed layer was determined. Results are summarized in figure 7. From this figure it can be concluded that the angular speed does not play a significant role in reducing the grain size, being the transference velocity the critical parameter here. It is also important to point out that the grain size

measurements are well correlated with the higher Vickers hardness results (figure 3). The sample with lower grain size is the one with higher Vickers hardness.

3.4. Tensile tests

Figure 8a shows typical examples of the stress-strain curves for the as-cast porous material and for one of the treated samples (5000 rpm and 100 mm^{-1}). The figure shows a clear improvement of both yield strength and ultimate tensile strength for the treated sample. An increase of around 30% is obtained for this particular material. This type of trend is also observed for the other analyzed materials. A summary of the results for the ultimate tensile strength increase (in percentage) of the samples treated (all of them with the same thickness (2.10 mm)) is provided in Figure 8b. It is interesting to observe that there is an optimum angular speed to maximize the UTS and that an increase of the transference velocity reduces this property. The same trends were also observed for the yield strength.

Finally, the optimum parameters found in the previous figure, 3750rpm and 100mm-1, were chosen to evaluate the effect of the sample thickness on the yield strength and ultimate tensile strength. The results are summarized in figure 8c where it is possible to observe that the improvements increase when the sample thickness is reduced.

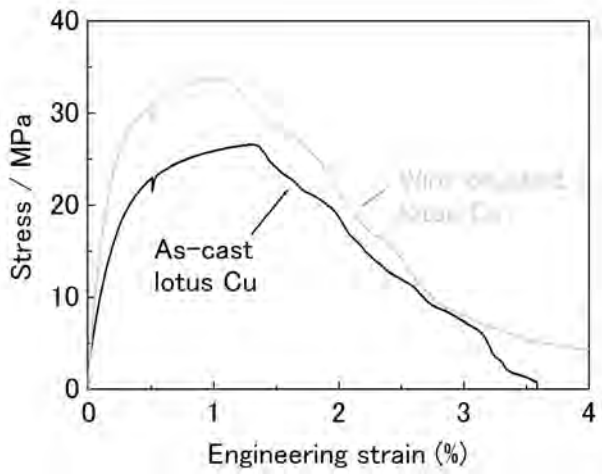

Figure 8a: Stress- Strain curves of two samples, with the same thickness, one as cut from the lotus copper ingot, and the other cut and processed by wire-brush at 5000rpm and 100mm^{-1}.

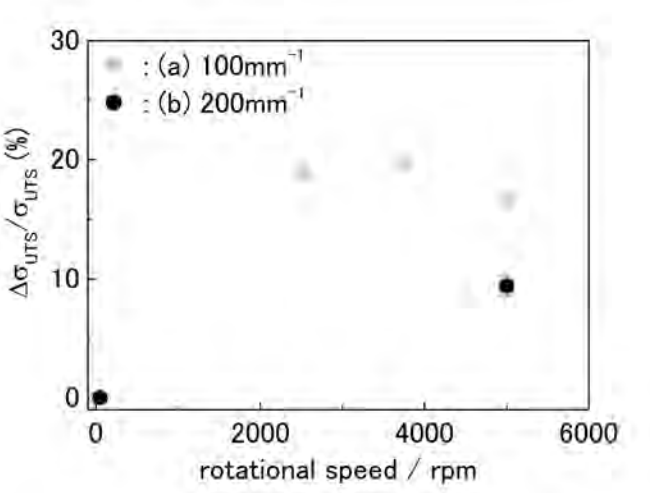

Figure 8b: Increase in the σ_{UTS} (in percentage) for samples of the same thickness 2. (2.1mm) at different processing parameters.

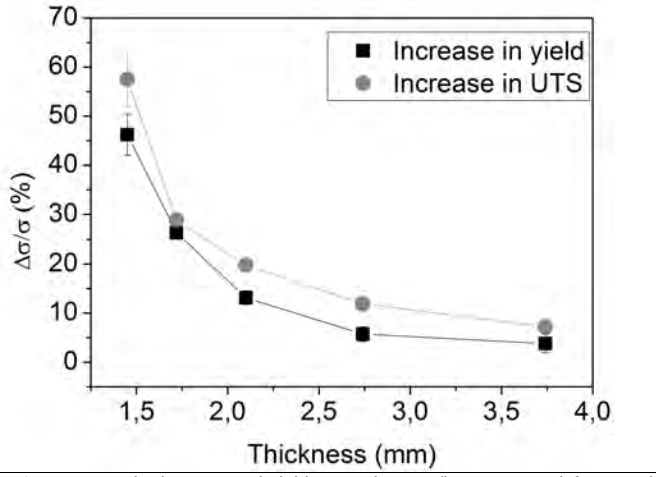

Figure 8c: Increase in the σ_{UTS} and yield strength $\sigma_{0.2\%}$ (in percentage) for samples of different thickness.

4. Discussion

The wire-brushing treatment applied in this research modified the lotus-type porous metals from two different points of view. On the one hand, a solid outer layer of around 45 μm is formed in the surface of the samples. On the other hand, this surface consist of ultra-fine grains with sizes below 400 nm, much smaller than the crystal size of the as cast material (higher than 1 mm). It has been proved that the hardness of the materials treated (measured in the new solid outer layer) increase several times (between 3 and 5 times) over the values measured for the non-treated porous copper. In addition, it has also been proved that these modifications take place with only a marginal increment of the material density.

All these changes have a significant effect on the mechanical behaviour, in particular the tensile strength and ultimate tensile strength of the treated specimens is higher (around 30% higher) than that of the initial porous copper. This increment is justified by the new mesostructure and microstructure of the treated porous material, the presence of hard solid outer layers seems to be the key reason for this significant increment. There are some other results that can be explained taking into account the skin-core structure of the treated materials. For instance, the mechanical properties improvement is much higher for the materials with lower thickness. As the outer layer thickness and their intrinsic characteristics depend on the processing parameters and are independent on the sample thickness, the same outer layer would be formed in samples with 1 mm in thickness than in samples with 2.1 mm. Therefore, the influence of the outer layer on the final properties would be more significant for the material in which the proportion of outer layer is higher, i.e. the samples with lower thickness.

Other interesting result that is connected to this skin-layer morphology is the decrease of the properties when the angular speed or the transference velocity are high. In those cases, the outer layer is not completely regular, in fact it is destroyed at several areas in the samples (see figure 3) and the properties are clearly affected by this effect. Therefore, this result shows that there are optimum processing parameters forming a well develop skin with fine-grains promoting a better mechanical behaviour of the lotus-type porous samples.

5. Conclusions

Samples of lotus-copper were sliced in plates, perpendicular to the pore direction, and the surface of those plates were processed by near surface severe plastic deformation using the wire-brushing technique. The treated samples showed interesting new characteristics in comparison with the as cast porous copper. The main findings were:

1) A deformed layer of copper in the surface closes the pores. At 3750rpm and 100mm-1 almost all the pores were closed with this layer, and therefore a solid outer skin was formed.
2) The new formed layer presents ultrafine grains, very similar to the reported ones in the nonporous materials. This new layer is clearly harder than the original material.

3) The materials characterized by the presence of this thin layer with ultrafine grains present higher tensile strength and ultimate tensile strength than the original materials with only marginal increments in density.

Therefore, it is possible to conclude that processing lotus-type copper by the wire-brush technique is a simple and effective method to improve the mechanical performance of these cellular materials.

Acknowledgement
This work was supported by the Global COE Program (Project: Centre of Excellence for Advanced Structural and Functional Materials Design) from the Ministry of Education, Culture, Sports, Science and Technology, Japan and by the Spanish Agency for International Cooperation (AECI).

References

[1] J. Banhart 2001 Prog. in Mater. Sci. **46** 559
[2] A.R. Boccaccini, G. Ondracek, E. Mombello. J Mater Sci Lett **14**, p.534, 1995.
[3] H. Nakajima 2007 Prog. Mater. Sci. **52** 1091
[4] E.P. Degarmo, J.T. Black, R.A. Kohser. Materials and Processes in Manufacturing (9th ed.), Wiley, 2003.
[5] S. Suzuki, H. Utsunomiya, H. Nakajima. Mater. Sci. Eng. A **490,** p.465, 2008.
[6] J. Lobos, S. Suzuki, H. Utsunomiya, H. Nakajima, M. A. Rodrigez-Perez. Mater Proces Tech, **212**, 10, p2007, 2012.
[7] M. Sato, N. Tsuji, Y. Minamino and Y. Koizumi. Mater. Sci. Forum **246–432,** p.2753, 2003.
[8] M. Sato, N. Tsuji, Y. Minamino and Y. Koizumi. Sci. Tech. Adv. Mater. **5**, p.14, 2003.
[9] S.K. Hyun, H. Nakajima Mater Lett **57**, 21, p.3149,

4.3 Young's modulus

In the previous paper the stress-stain curves were used to evaluate the yield strength and the ultimate tensile strength of the samples. It is also possible to obtain data for the Young's modulus but in general with a high dispersion. In Nakajima's laboratory the elastic properties of metals are measured used resonant ultrasound spectroscopy (RUS) [12, 13] and mode-selective electromagnetic acoustic resonance (EMAR) [14]. To measure the Young's modulus with these techniques it is necessary a fixed cubic geometry of the sample, that we could not obtain for the samples under study. Due to this, we used the values of the Young's modulus from the stress-strain curves as a rough estimation of the real values. The values of the Young's modulus of several samples are showed in figure 4.2

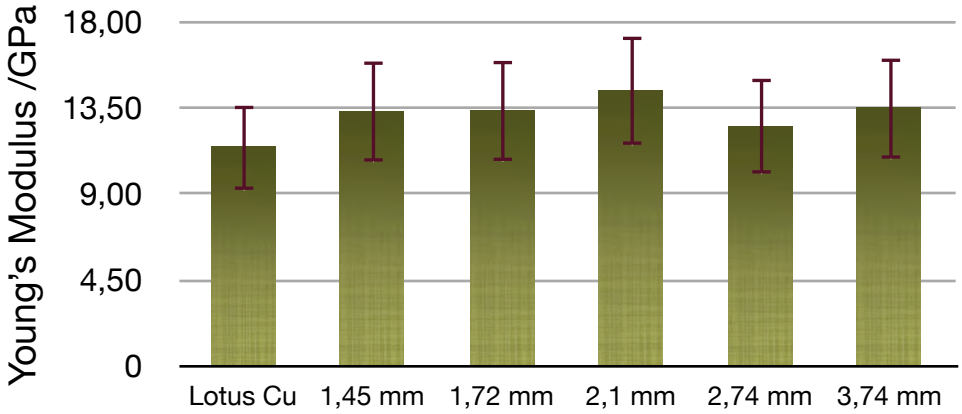

The reduction in the grain size of the metal did not show any change in the value of the elastic modulus[15]. The apparent increase on the Young's modulus is inside of the error of the measurement in the stress-strain curves.

4.4 Conclusions

Using the wire-brushing process it has been possible to produce a new composite with a hard skin formed by ultrafine grains and soft porous core, this technique allow improving the mechanical properties but as expected, this improvement depends on the final thickness of the sample. The deformed layer is only 45 μm depth and due to this the thickness of the samples determines the global behavior.

In the present research, the improvement on the mechanical properties in the perpendicular direction to the pore growth was 10% for samples of 3.7mm in thickness and of 55% for the samples of 1.5mm in thickness. The

advantage of this post processing technique is its simplicity and the possibility of having only marginal increment of the bulk density. However, the final material is far away from the metals that are used in structural applications.

The technique is especially interesting for porous metals with very low thickness. If the sample is only 1mm in thickness and is processed by wire-brushing in a surface parallel to the pore growth direction it would be possible to increment the ultimate tensile strength in values of around 100%.

4.5 References

[1] E. O. Hall, Proceedings of the Physical Society. Section B ***64****, 747 1951.*

[2] N. J. Petch, The Journal of the Iron and Steel Institute ***174****, 25,1953.*

[3] H.N. Gupta, R.C. Gupta and A. Mittal "Manufacturing processes", New Age International, 2009.

[4] W.F. Smith and J. Hashemi "Foundations of Materials Science and Engineering", McGraw-Hill, 2006.

[5] C. Schuh, T.G. Nieh and T. Yamasaki Scripta Materialia ***46****, 735, 2002.*

[6] A. Azushima, , R. Kopp, A. Korhonen, D.Y. Yang, F. Micari, G.D. Lahoti, P. Groche, J. Yanagimoto, N. Tsuji, A. Rosochowski and A. Yanagida; CIRP Annals - Manufacturing Technology ***57****, 716, 2008.*

[7] Y. Saito, H. Utsunomiya, N. Tsuji and T. Sakai; Acta Materiali ***47****, 579, 1999.*

[8] N. Tsuji, Y. Saito, H. Utsunomiya and S. Tanigawa; Scripta Materialia Volume ***40****, 795, 1999.*

[9] W.M. Thomas, E.D. Nicholas, J.C. Needham, M.G. Murch, P. Temple-Smith and C.J. Dawes. Friction-stir butt welding, GB Patent No. 9125978.8, International patent application No. PCT/GB92/02203, 1991.

[10] M. Sato, Science Technology Advanced Materials ***5****, 145, 2004.*

[11] Y. Minamino, Materials Science Forum ***502****, 117, 2005.*

[12]. H.H. Demarest Jr., Journal of the Acoustical Society of America ***49****, 768, 1971.*

[13]. I. Ohno, Journal of Physics of the Earth ***24****, 355, 1976.*

[14]. H. Ogi, H. Ledbetter, S. Kim, M. Hirao. Journal of the Acoustical Society of America ***106****, 660, 1996.*

[15]. P.G. Sanders, J.A. Eastman, J.R. Weertman. Acta Materialia ***45****, 4019, 1997.*

5 Modification of lotus copper by ECAE processing

Resumen (Spanish):

En este capítulo introducimos el proceso ECAE (acrónimo de: "extrusión entre canales iguales" en ingles) y su aplicación a los metales porosos tipo lotus. El cual, como su nombre indica, consiste en hacer pasar la pieza metálica, metal poroso tipo lotus en nuestro caso, por dos canales de la misma sección a través de un ángulo de 150°, que altera de forma marginal la porosidad de la muestra. La deformación producida en el ángulo, debido a la contracción en el lado interno y el estiramiento en el lado externo induce un trabajo en la estructura metálica que aumenta su dureza y resistencia. Para conseguir un forjado adecuado se hace pasar 4 veces la muestra por el canal, pero dadas las diferencias existentes en que el metal pase por el interior, o el exterior, del ángulo se escogen 3 formas distintas de introducir la muestra para ver cual de ellas obtiene una mayor mejora de las propiedades mecánicas. Las muestras producidas se caracterizan mediante medidas de la dureza Vickers y ensayos a compresión.

5.1 Introduction

After the research conducted using the wire-brushing technique we focused our attention in other SPD techniques able to improve the metallic matrix of lotus copper. Over all the different process Equal Channel Angular Extrusion (ECAE)[1-3] was selected. This technique is sometimes also called, equal-channel angular pressing (ECAP)[4,5] or Equal-Channel Angular Forging (ECAF)[6]. ECAE is unique because significant cold work can be accomplished without reduction in the cross sectional area of the deformed work piece. In conventional deformation processes like rolling, forging, extrusion, and drawing, strain is introduced by reduction in the cross sectional area. For ECAE the cross section of the channel is equal at the entry and exit; the angle inside the extrusion channel produces the strain.

In an ECAE process, the die consists in a channel with the same section throughout its length; the channel has an angle between entry channel and the exit channel (Figure 5.1). The strain produced in the sample is a function of the angle (ϕ) larger angles produce lower strain and smaller angles produce a higher strain, usually ECAE experiments choose an angle between 120 and 60 degrees [1-6].

Because the section of the metal does not change in the process, the extrusion could be repeated several times with the same die. In fact, to increase the plastic strain in the samples the ECAE process is usually repeated several times. In that case the chosen orientation of the sample inside the die in the subsequent passes is important to know the direction of the total strain accumulated in the materials[1-5]. The different chosen orientations are called routes and are showed in Figure 5.1.

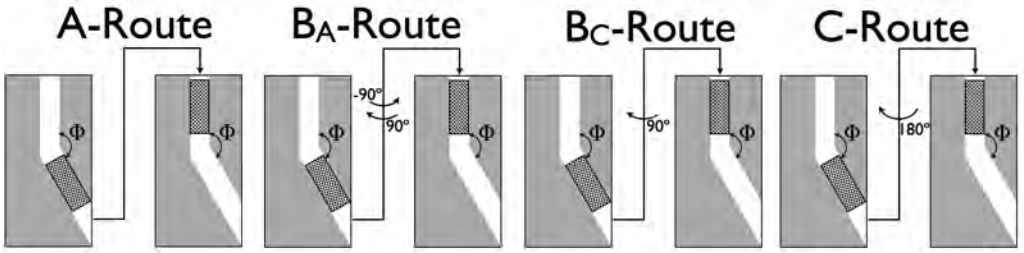

***Figure 5.1**: Different routes for ECAE processing [1-6]*

In the bisection of the angle of the ECAE-die a slip-plane induced by ECAE process is created (figure 5.2(a)). To show the deformation induced by the ECAE process one circular area of the metal was chosen. During the ECAE process the circle will be deformed by the shearing plane as is showed in the figure. The ECAE routes allow different ways to deform the samples.

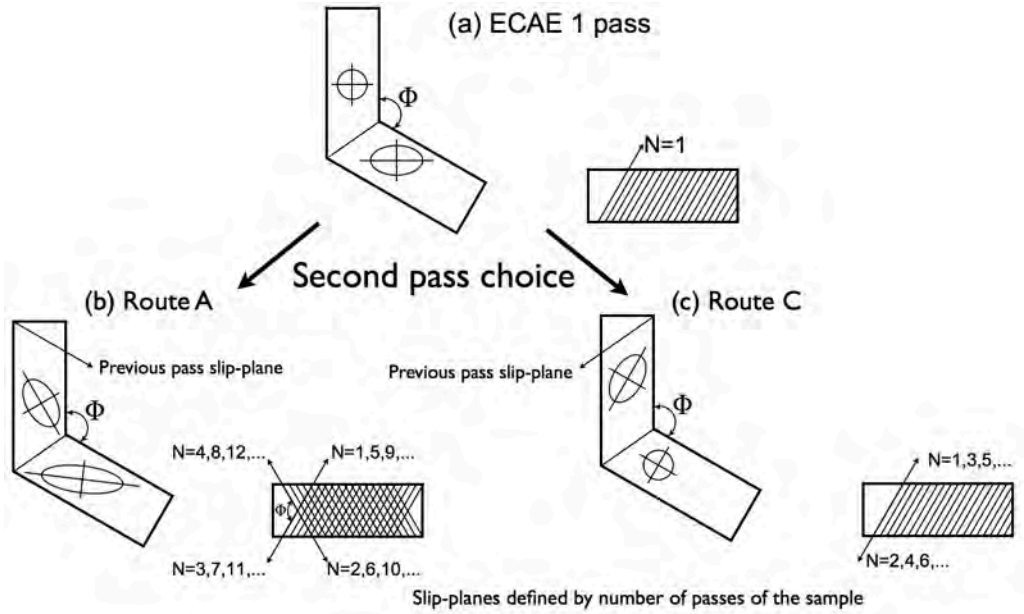

***Figure 5.2**: Deformation induced by ECAE processing. (a) First pass (b) Second pass by Route A (c)Second pass by Route C. The slip-lanes after several passes are marked with N, for the A route and C route.[5,6]*

A and C routes have a symmetry plane in the ECAE process defined by the entry point, the position of the angle, and the exit point. So, it is possible to study the slip-plane and the induced deformation perpendicular to that plane. As it is showed in Figure 5.1 in the A route the sample always is introduced in the same way in the die, the shearing plane induced in the previous pass have the orientation showed by the arrow in the figure 5.2 (b and c) and the original circular portion is more directionally deformed in the second pass, after 4 passes the shearing plane is the same of the first pass as it is showed in the figure 5.2(b.2). In the route C the sample turns 180 degrees every pass, due to this the slip plane in all the passes is the same, and the original circular shape recover the original form, as it is show in the Figure 5.2 (c.1).

The routes B (B_A and B_C) make a tridimensional deformation creating slip-planes in two perpendicular direction by the rotation of 90 degrees, the B_A route make a double A deformation in two sides of the sample and B_C route makes a double C deformation after four passes of the sample in the ECAE-die, as is show in the figure 5.3. After the passes showed in the figure, the next slip-plane coincides with the first and repeat all in order.

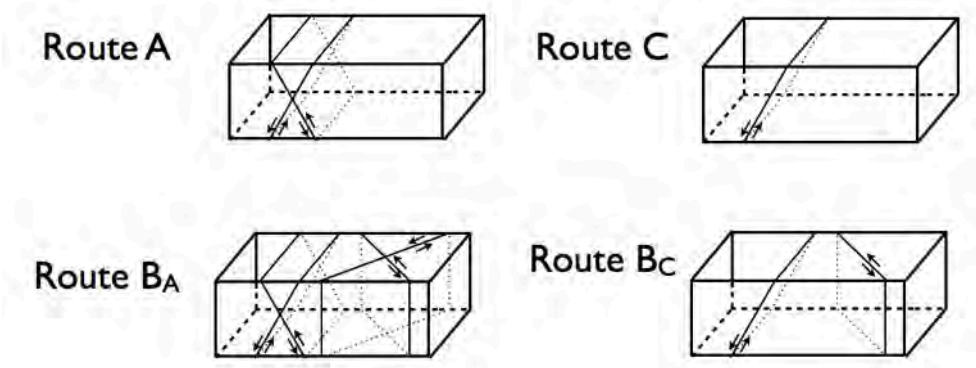

Figure 5.3: *Slip planes induced by ECAE processing. After several passes in routes A (4 passes), C (2 passes), B_A (8 passes) and B_C (4 passes).*

Because of this many slip planes in this process this route is very useful in forging metals. One route may be much better than the other for a given angle of the ECAE-die and a given alloy. For this research we have chosen several routes A, C and B_C.

5.2 Preliminary research

In a previous paper Dr. S. Suzuki [7] processed a 50% porosity lotus-type porous copper with a 90 degrees die. As expected the sample reduces its porosity, from 50% to 17% by uniaxial compression, the sample is first

compressed before continuing through the channel angle, and later sheared in the angle of the die (Figure 5.4).

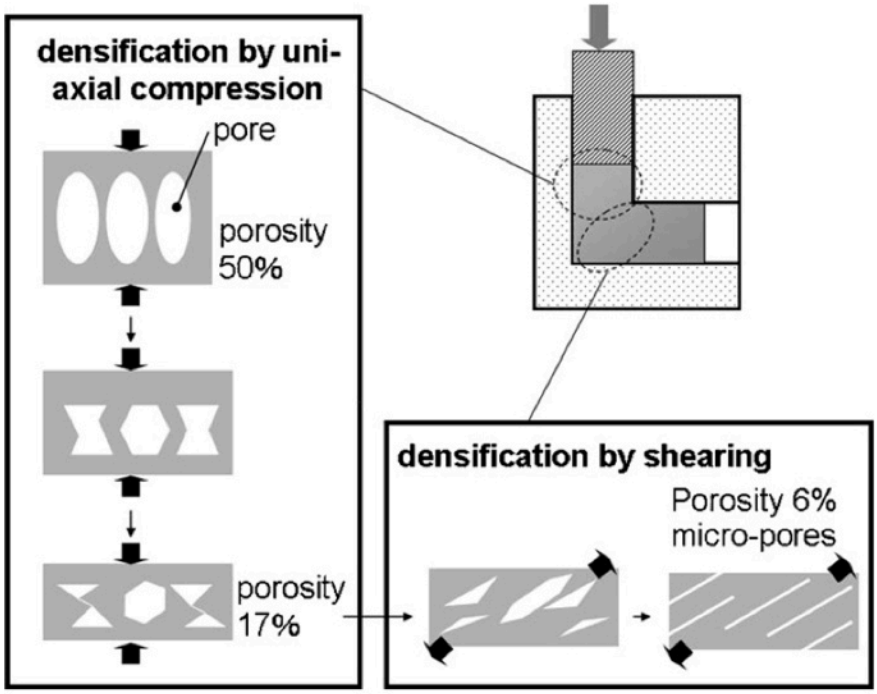

Figure 5.4: *Schematic illustration of deformation of lotus-type porous metals through ECAE process with a channel angle 90°. It demonstrates the case of porosity 50% before the extrusion, as an example.*

To avoid this very high densification, a new 150° ECAE-die was built, and new samples were processed to complete the paper presented by Dr. Suzuki. The research conduced using this new die has been published in the "Journal of material processing technology"and it is included in the following pages.

5.3 Paper: Strengthening of lotus-type porous copper by ECAE process

Journal of Materials Processing Technology 212 (2012) 2007–2011

Contents lists available at SciVerse ScienceDirect

Journal of Materials Processing Technology

journal homepage: www.elsevier.com/locate/jmatprotec

Strengthening of lotus-type porous copper by ECAE process

J. Lobos [a,b,*], S. Suzuki [a,c], H. Utsunomiya [d], H. Nakajima [a], M.A. Rodrigez-Perez [b]

[a] The Institute of Scientific and Industrial Research, Osaka University, Ibaraki, Osaka 567-0047, Japan
[b] Cellular Materials Laboratory, Condensed Matter Physics Department, University of Valladolid, 47011 Valladolid, Spain
[c] Waseda Institute for Advanced Study, Waseda University, Shinjuku, Tokyo 169-8555, Japan
[d] Division of Materials and Manufacturing Science, Graduate School of Engineering, Osaka University, Suita, Osaka 565-0871, Japan

ARTICLE INFO

Article history:
Received 9 February 2011
Received in revised form 2 March 2012
Accepted 28 April 2012
Available online 11 May 2012

Keywords:
Lotus-type porous copper
Equal-channel angular extrusion
Porous metals
Vickers hardness
Yield strength

ABSTRACT

Lotus-type porous copper with directional cylindrical pores was fabricated by unidirectional solidification in a pressurized hydrogen atmosphere. Improvements in microstructure and mechanical properties of the lotus-type porous copper by equal-channel angular extrusion (ECAE) were investigated using a die with a channel angle of 150°. The porosity decreases with increasing pass number, and decreases from 46% to 30% by four passes. It means that pore closure in the ECAE process is not significant. Both the specific compressive yield strength $\sigma^*_{0.2\%}$ and the Vickers hardness HV of the lotus copper increase with increasing pass number of ECAE. The ECAE processed porous copper shows improved $\sigma^*_{0.2\%}$ and HV comparable to those of the extruded nonporous copper. It is suggested that ECAE is a promising method to strengthen porous metals without significant pore closure.

1. Introduction

In recent years, porous and foamed metals have attracted much attention because of their unique features. These metals are expected to be used as lightweight materials, catalyst carriers, electrodes, vibration and acoustic energy damping materials, impact energy absorption materials, etc. Gibson and Ashby explained in detail these excellent properties in their text book (Gibson and Ashby, 1997). Most of the porous and foamed metals have isotropic spherical pores. Stress concentration under loading easily occurs around the pores so that these metals suffer from insufficient mechanical properties. Among these materials, lotus-type and Gasar porous metals have unique pore morphology with long cylindrical pores aligned in one direction. Shapovalov proposed a unidirectional solidification process using pressurized hydrogen (Shapovalov, 1994). Nakajima et al. performed a systematic study on the fabrication using various pressurized gases (Nakajima et al., 2001) and succeeded in continuous fabrication of the porous metals (Nakajima, 2007). Instead of pressurized gas, Nakajima and Ide (2008) proposed to use thermal decomposition of compounds such as hydrides. The pores evolve, from the insoluble gas, when the molten metal is solidified. Compared to conventional porous metals which have nearly spherical and isotropic pores, these metals exhibit superior mechanical properties in one direction.

Segal et al. (1981) proposed ECAE (equal channel angular extrusion/pressing) as a metal forming process to introduce shear deformation into bars or rods without cross-sectional change. Valiev and Langdon (2006) showed severe plastic deformation of bulk metal by repetition of ECAE, as a consequence ultra grain refinement and an increase of hardness and strength was archived. In a previous paper, Suzuki et al. (2008) reported that porous copper with directional pores processed by ECAE (using a die with an angle of 150°) maintained its porous structure to some degree increasing the Vickers hardness. Strengthening of the porous metals is very important because the as-cast metal is much weaker than wrought metals due to casting defects and coarse-grained microstructure. Lower hydrostatic pressure is an important processing condition to suppress pore closure in cold working, so that ECAE is supposed to be preferable for porous metals. However, effects of the number of passes and route of ECAE on deformation behaviour and mechanical properties have not been investigated in detail for porous metals.

This study was undertaken to investigate the evolution of microstructure and mechanical properties of porous copper with directional pores through several passes of ECAE. The aim is to investigate the validity of ECAE as a strengthening method for porous metals with small decrease in porosity.

* Corresponding author at: Cellular Materials Laboratory, Condensed Matter Physics Department, University of Valladolid, 47011 Valladolid, Spain.
Tel.: +34 659364113.
E-mail addresses: obi@fmc.uva.es (J. Lobos), suzuki-s@aoni.waseda.jp (S. Suzuki), uts@mat.eng.osaka-u.ac.jp (H. Utsunomiya), nakajima@sanken.osaka-u.ac.jp (H. Nakajima), marrod@fmc.uva.es (M.A. Rodrigez-Perez).

0924-0136/$ – see front matter © 2012 Elsevier B.V. All rights reserved.
http://dx.doi.org/10.1016/j.jmatprotec.2012.04.024

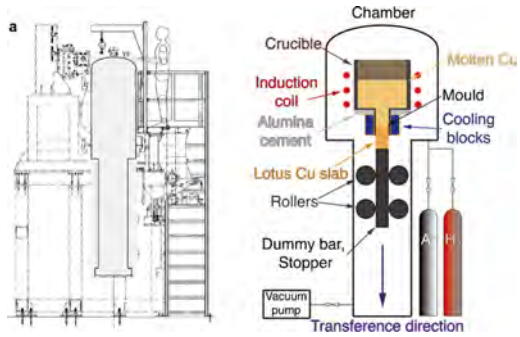

Fig. 1. Schematic drawing of the fabrication apparatus to produce lotus metals using the continuous casting technique. Large crucible and induction heating coil are located in the upper part of the pressure vessel, while the mould with cooling blocks and movable mechanism are in the bottom of the crucible. The height of the apparatus is about 7 m. About 1 m lotus ingot in length can be produced. The dummy bar is connected together with the melt at the mould.

2. Experimental

Electrolytic cathode copper (purity 99.99%) was obtained from Sumitomo Metal Mining Co. Ltd. A slab (600 mm length, 30 mm wide and 10 mm thick) of lotus copper was fabricated by the continuous casting technique, Fig. 1. According to the paper reported by Park et al. (2007), the casting was conducted under a pressurized mixture of hydrogen (0.5 MPa) and argon (0.2 MPa) at a transfer velocity of 20 mm/min. The porosity and the average pore diameter were $46.3 \pm 0.4\%$ and 388 ± 131 μm, respectively. As reference materials, sample rods of nonporous copper were also fabricated by the continuous casting method in an argon atmosphere (0.1 MPa).

The fabricated porous copper slab with directional pores and the nonporous copper were cut into cylinders (8.0 mm in diameter and 45.0 mm in length) with a spark-erosion wire-cutting machine (Model AQ325L-LN1W, Sodick Co.). The pores were oriented in the parallel direction to the cylinder axis (Fig. 2(a)). The cylindrical sample was inserted into a sheath of nonporous copper with 10.8 mm in outer diameter, and 50.0 mm in total length in order to suppress crack formation of porous copper inside the channel during the ECAE process. The inner part of the sheaths were machined in U shape with 8.0 mm of diameter and 45.0 mm of length, the 5 mm of nonporous copper were introduced first during all passes. The porous and nonporous coppers covered with the sheath were supplied to the ECAE channel with a channel angle of 150° as shown in Fig. 2(b). The ECAE channel die was coated with PTFE (Teflon®) and lubricated with lanoline prior to each extrusion. The sample rods were extruded several times through the ECAE-die. The sample was passed through the channel at a speed of 5 mm/min.

After one pass of ECAE, three routes were adopted as shown in Fig. 3. In route A, the orientation of the sample rod was maintained in all the extrusions. In route C, the sample rod was rotated by 180° around the cylinder axis after each extrusion. In route B_C, the sample rod was rotated 90° around the cylinder axis after each extrusion. Valiev and Langdon (2006) reported that Route B_C is the most effective route for severe plastic deformation or grain refinement of nonporous metals. The structure and mechanical properties of porous copper samples after each extrusion were investigated. The nonporous copper samples were processed by routes C and B_C.

The samples processed by ECAE were cut by spark-erosion wire-cutting machine (Model AQ325L-LN1W, Sodick Co.) to remove the external sheath. The test specimens were cut with a cylindrical

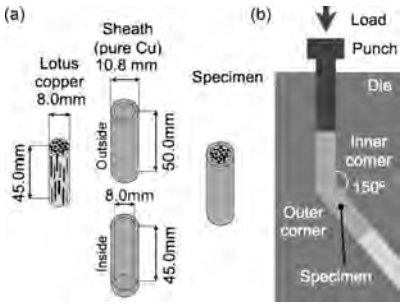

Fig. 2. Schematic drawings of the samples (a) and ECAE process (b).

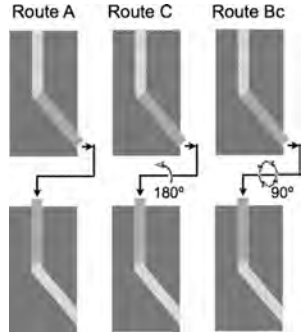

Fig. 3. Schematic drawings of the different ECAE routes used in the present study.

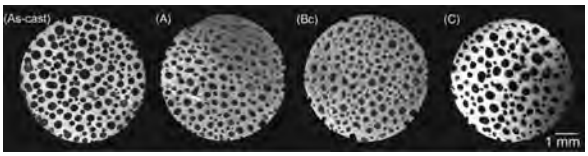

Fig. 4. Cross-sectional views perpendicular to the extrusion direction for the as-cast porous copper and porous copper after 3rd pass through various routes (A, B_C and C). The upper side of the views is the area of the samples that was in contact with the inner corner of the die at 3rd pass.

shape of 6 mm in diameter and 6 mm in length. The axis of the specimens was parallel to the extrusion direction.

The density was measured from the weight and volume, and the porosity (ϕ), Eq. (1), was calculated using the measured density of nonporous copper.

$$\phi = 1 - \left(\frac{\rho_{sample}}{\rho_{bulk}}\right) \quad (1)$$

The pore morphologies were observed with a digital microscope (Keyence VHX-200). Vickers hardness was measured on the plane perpendicular to the extrusion direction using a hardness tester (Akashi MVK-III). The indentation was made on matrix copper with a force of 1 N and a holding time of 20 s. Ten experiments were performed for each specimen.

Compression tests were carried out following the standard (Japanese Industrial Standards H-7902, 2008) using a universal testing machine (Instron 5582) at a crosshead speed of 0.15 mm/min. The compression direction was parallel to the extrusion direction. The compressive force was divided by the initial cross sectional area to obtain the nominal compressive stress. The yield strength was measured at a strain of 0.2% ($\boldsymbol{\sigma_{0.2\%}}$). The specific compressive yield strength $\sigma^*_{0.2\%}$ was obtained by dividing the yield strength $\boldsymbol{\sigma_{0.2\%}}$ by the density Eq. (2).

$$\sigma^*_{0.2\%} = \frac{\sigma_{0.2\%}}{\rho_{sample}} \quad (2)$$

Compression tests were performed five times for each processing condition and a statistical analysis of the data was performed to obtain the average values.

3. Results and discussion

Fig. 4 shows the cross-sectional views in perpendicular to the extrusion direction for the as-cast porous copper and the porous copper after the 3rd pass of ECAE through various routes (A, B_C and C). The upper side of each image is the area of the sample that was in contact with the inner corner of the die after the 3rd pass. It is observed that the pores in the upper side of the samples processed by route A were closed by the severe deformation. Since the upper side of the sample was passed near the same inner corner of the ECAE-die through the extrusion, this area was deformed by successive extrusions repeatedly. The upper sides of the samples processed through B_C and C routes do not exhibit severe deformation; these samples maintain more homogeneous porous structure.

Fig. 5 shows the porosity change of porous copper as a function of the pass number of ECAE. The porosity slightly decreases with increasing pass number; the porosity only decreases from 45% to 30% by four passes. Utsunomiya et al. (2010) processed a lotus copper with a porosity of 40% by multi-pass cold rolling and reported that the porosity almost linearly decreases to less than 5% with increasing total reduction up to 60%. Furthermore, the pores were closed mostly when the total reduction reached 80%. Compared with such cold rolling, the pore closure in ECAE was not significant. This is due to lower hydrostatic pressure in ECAE without back

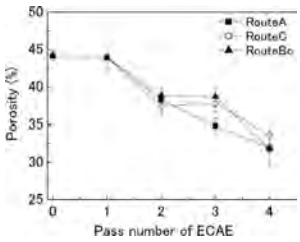

Fig. 5. Porosity change as a function of the pass number of ECAE.

pressure (Bowen et al., 2000). It is suggested that ECAE is useful process for strengthening of porous metal with a small decrease in porosity.

Fig. 6 shows specific compressive yield strength (compressive yield strength divided by nominal density, Eq. (2)) as a function of the pass number of ECAE. While the nonporous copper was extruded through the route B_C, the porous copper samples were processed by extrusion through different three routes (A, B_C, and C). The specific compressive yield strength $\sigma^*_{0.2\%}$ of both the porous and the nonporous copper increases with increasing pass numbers of ECAE. $\sigma^*_{0.2\%}$ of the nonporous copper reaches the maximum after the 2_{nd} pass and then the value remains constant. However, $\sigma^*_{0.2\%}$ of the porous copper delays to reach the maximum value after the 3rd pass. The $\sigma^*_{0.2\%}$ of the porous copper is lower than that of the nonporous copper. This result suggests that the effective strain cause by ECAE in the metallic part of the porous copper is lower than that in the nonporous copper under the same extrusion conditions. This result can be understood taking into account the volume change of the porous samples during ECAE. In the porous coppers, the $\sigma^*_{0.2\%}$ in route C is higher than those in route A or B_C. It is well known that hardening by repeated deformations in similar direction is more apparent than the deformation with strain-path

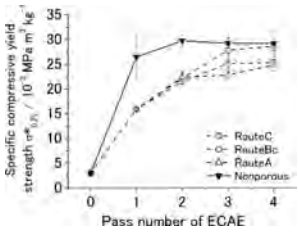

Fig. 6. Specific compressive yield strength as a function of the pass number of ECAE. Nonporous copper was processed by route C, while lotus copper was processed by routes A, B_C or C.

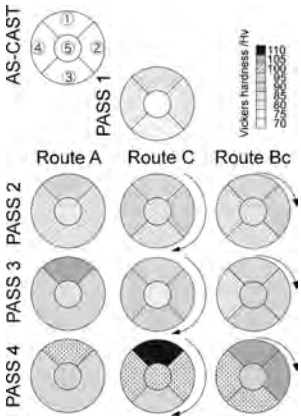

Fig. 7. Hardness map of the porous copper by three different pass. The map shows the plane perpendicular to the extrusion direction. The numbers specify the position in relation to the last ECAE extrusion; 1 is the side close to the inner angle of the die, 3 is the side close to the outer angle of the die, 5 is the centre of the sample, 2 and 4 are the sides that finish the outer ring.

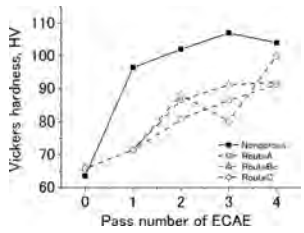

Fig. 8. Vickers hardness in the central parts (region 5 in Fig. 7) as a function of the pass number of ECAE for nonporous copper by route C and the porous copper processed by routes A, B_C and C.

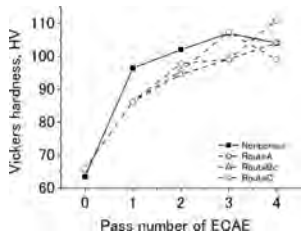

Fig. 9. Vickers hardness in region 1 (see Fig. 7) as a function of the pass number of ECAE. Nonporous copper processed by route C and porous copper processed by the routes A, B_C or C.

change (Baushinger effect). However the Route C with strain-path change gives higher specific strength than the Route A without strain-path change after the third pass. The reason for this anti-Baushinger effect is not completely understood at this stage. The higher $\sigma^{+}_{0.2\%}$ in route C may be due to the fact that elongation direction of pores does not change much in ECAE. In other words, the elongation direction of pores rotates with simple shear deformation in ECAE in route A or C. Therefore, geometrical softening (lower strength in longitudinal direction) may take place by ECAE due to the anisotropy of strength.

The Vickers hardness of the porous copper and the nonporous copper was measured on the cross-section plane perpendicular to the extrusion direction as shown in Fig. 7. The distribution of hardness after the 1st pass is non-homogeneous. The hardness is higher in the region (1) near the inner corner due to the frictional shear stress. On the other hand, the hardness is lower in the region (3) near the outer corner due to the under-filling at the outer corner and the bending. After the 2nd pass, various distributions of the hardness were observed, depending upon the pass routes. The hardness distribution was classified into five regions as a hardness map. In the route A, after 2nd pass only three different regions were found. In the route C after the 2nd pass four different regions were observed, while in the route B_C after the 2nd pass, five different regions were found. In the route A, the upper region showed highest hardness than all the other regions, whilst the centre is the softest. This may be explained by less effective strain in the central region through ECAE. Moreover, when pores in the upper region start to close, the hardness starts to decrease. In the route C, the hardness of the region that went through the inner channel angle after the 4th pass has the higher value, while the hardness of the region which went through the outer channel angle exhibits the lowest in hardness. In the route B_C, the hardness of the quadrants increased in all the passes, but there is a significant increase in hardness of the specific region which went through the inner channel angle.

Fig. 8 shows the relationship between the Vickers hardness and the pass number of ECAE through different routes. The Vickers hardness shows the hardness measured in the central region. The hardness of porous copper processed by route A was low, but after the 4th pass the hardness in the central region increases by the densification of the upper part of the sample. In the route B_C, the Vickers hardness of the centre increased continuously (Zone 5 in Fig. 7). In the route C, the hardness of the centre showed fluctuations; by every two passes the hardening reached a local maximum. This behaviour is explained by the accumulative deformations by every two extrusions. In other words, decrease in dislocation density by the deformation in the opposite direction (typical Bauschinger effect).

Fig. 9 shows the Vickers hardness of the region that went through the inner angle. After the first pass, the Vickers hardness of the porous copper was lower than that of the nonporous copper. The B_C route produce a more regular increase of Vickers hardness without differences between regions, but the final hardness (measured by Vickers hardness or specific yield strength) is lower than that produced by route C. This corresponds to the higher compressive yield strength by the route C.

4. Summary

The ECAE process is an effective forming process that can be used to improve the strength of porous copper with directional pores, maintaining the porous structure. The Vickers hardness and specific compressive yield strength increase with increasing pass number of ECAE reaching a maximum value after four passes.

Both the Vickers hardness and the specific compressive yield strength of the porous copper processed by ECAE are lower than those of nonporous copper, even under the same extrusion conditions. This discrepancy is due to the different

deformation behaviour between the nonporous and the porous copper. While porous copper is deformed by both shear and pore closure, nonporous copper is mainly deformed by shear which is a most effective mechanism to increase hardness. The increase in hardness is considered to be caused by work hardening.

The deformation patterns processed through various routes of ECAE were observed. The deformation starts on the walls of the porous copper samples, and due to the porous structure, shear deformation penetrates into the centre of the samples incompletely. The region that passes close to the inner corner of the die had a higher densification and higher Vickers hardness than the other region. The Bauschinger effect was observed in the C route but not in the A route, which causes higher values of Vickers hardness and specific compressive strength for route C.

Acknowledgements

The present work was supported by Global COE Program (Project: Center of Excellence for Advanced Structural and Functional Materials Design) from the Ministry of Education, Culture, Sports, Science and Technology, Japan and by the Spanish Agency for International Cooperation (AECI). The authors would like to thank Mr. J. Miyamoto of Osaka University for the technical support.

References

Bowen, J.R., Gholinia, A., Roberts, S.M., Prangnell, P.B., 2000. Analysis of the billet deformation behaviour in equal channel angular extrusion. Materials Science and Engineering A 287, 87–99.
Gibson, L.J., Ashby, M.F., 1997. Cellular Solid. Cambridge University Press, Cambridge, UK.
Japanese Industrial Standards Committee, 2008. JIS H 7902 Method for Compressive Test of Porous Metals. Japanese Standards Association, Tokyo.
Nakajima, H., 2007. Fabrication, properties and application of porous metals with directional pores. Progress in Materials Science 52, 1091–1173.
Nakajima, H., Hyun, S.K., Ohashi, K., Ota, K., Murakami, K., 2001. Fabrication of porous copper by unidirectional solidification under hydrogen and its properties. Colloids and Surfaces A179, 209–214.
Nakajima, H., Ide, T., 2008. Fabrication of porous copper with directional pores through thermal decomposition of compounds. Metallurgical and Materials Transactions A 39, 390–394.
Park, J.S., Hyun, S.K., Suzuki, S., Nakajima, H., 2007. Effect of transference velocity and hydrogen pressure on porosity and pore morphology of lotus-type porous copper fabricated by a continuous casting technique. Acta Materialia 55, 5646–5654.
Shapovalov, V.I., 1994. Porous metals. MRS Bulletin 19, 24–28.
Segal, V.M., Rezinikov, V.I., Drobyshevkiy, A.E., Kopylov, V.I., 1981. Plastic working of metals by simple shear. Russian Metallurgy 1, 99–105.
Suzuki, S., Utsunomiya, H., Nakajima, H., 2008. Equal-channel angular extrusion process of lotus-type porous copper. Materials Science and Engineering A 490, 465–470.
Utsunomiya, H., Yukimoto, T., Sakai, T., Suzuki, S., Nakajima, H., 2010. Pore closure in multi-pass cold rolling of lotus-type porous copper. Steel Research International 81, 158–161.
Valiev, R.Z., Langdon, T.G., 2006. Principles of equal-channel angular pressing as a processing tool for grain refinement. Progress in Materials Science 51, 881–981.

5.4 Results and discussion on grain size

ECAE, as other SPD process produce an ultrafine grain metallic structure, For example, a nonporous copper after several passes, 8 to 12, in a 90 degree ECAE-die by route BC get an average grain size in the range of several hundred of nanometers (150 to 300 nm)[16]. We tested this effect on the lotus-type porous copper. To measure the grain refining in lotus copper two samples were observed by electron backscatter diffraction, one after one pass through a 90 degree ECAE-die (Figure 5.5) and the other after five passes through the 150 degree ECAE-die used in the previous paper (Figure 5.6).

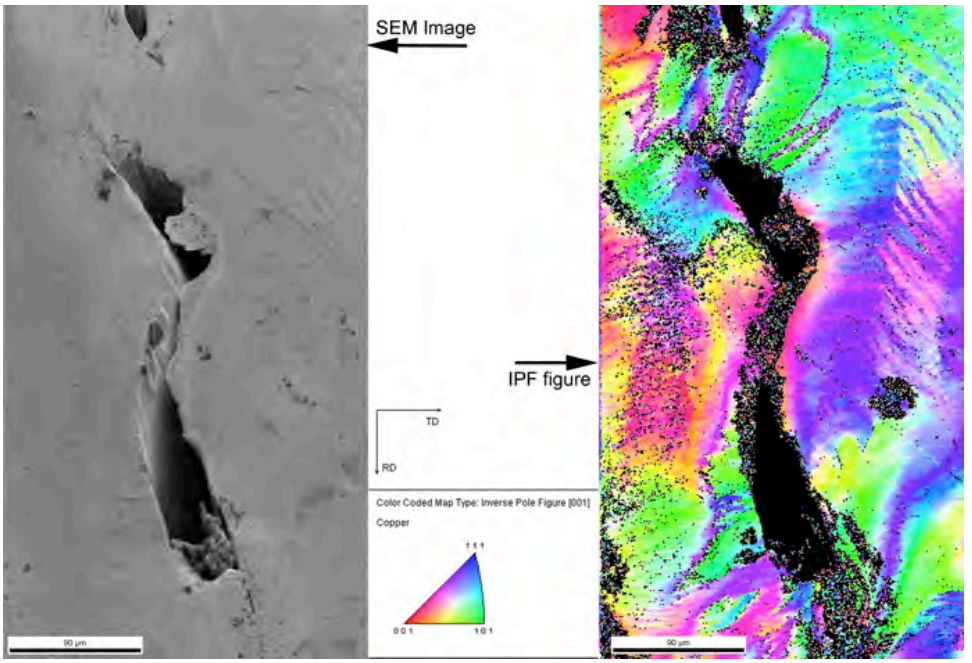

Figure 5.5: *SEM image and IPF map of a lotus copper sample processed by 90 a degree ECAE die (1 pass).*

Figure 5.5 shows a SEM image of a pore in a sample processed by 90 degree ECAE-die and the map of the orientation of the copper crystals. It is possible to observe a collection of dislocations in the copper lattice, but without new boundaries, the crystal size did not change.

In the samples processed by a 150 degree ECAE-die the dislocations are smaller than for the 90 degree ECAE-die,(although it is difficult observe this effect in the IPF map). Figure 5.6 shows the IPF map for a sample processed by route C five times and the miss orientation profile from a point to origin of the line. The red line crosses a grain boundary, when reach one point that changes the orientation of the crystal lattice more than 15º degree. In the

blue line there are no big changes in the orientation from one point to another.

It is clear from this analysis that the ECAE processing increases the strength of lotus metals without a metal grain refinement, only with the introduction of distortions in the lattice.

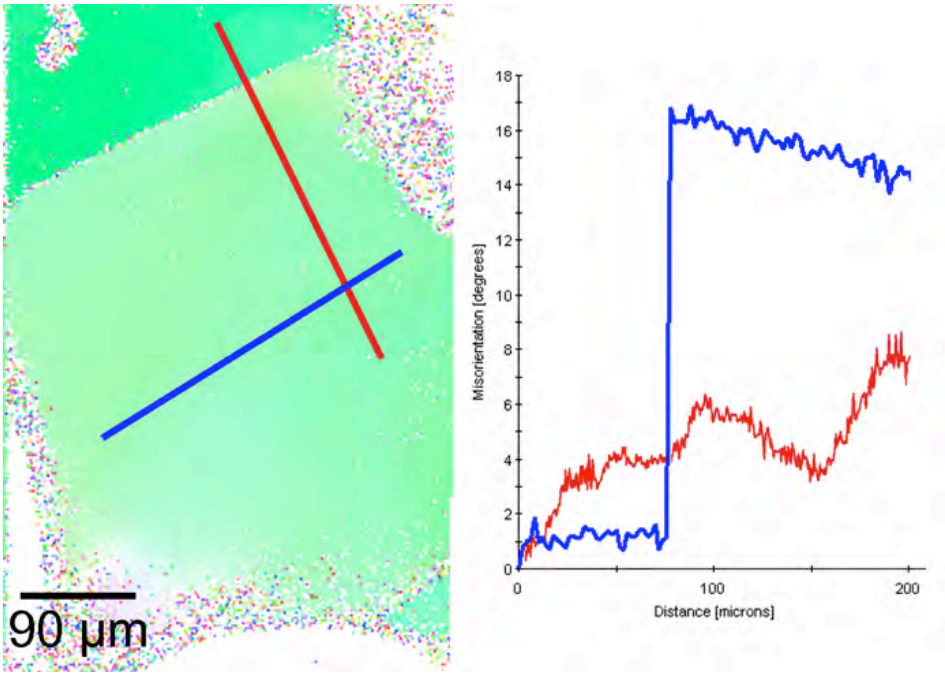

Figure 5.6: *IPF map showing the misorientation in a lotus copper after 5 passes by Route C crossing a grain frontier, and inside the grain. The misorientation is measured point to origin.*

Therefore, we can conclude that the samples experimented a grow in the yield strength without grain refinement.

5.5 Young's modulus

This section summarizes the results obtained for the elastic modulus measured using the stress-strain curves. These approximate data will be compared later with those of polymer foams. Fgure 5.7 show the value of the Young's modulus in compression of the samples studied in the paper included in this chapter. The reference is the Young's modulus of the Hardened OFHC copper that was introduced in the section 3.7. It is clearly observed from the figure that ECAE processing also increased in a significant extend the elastic modulus of the samples. The Young's modulus of the as-cast lotus copper is 7 times lower than that of the Hardened OFHC copper. After one pass by the ECAE-die the difference is reduced to only 4 times

lower. After 4 passes, the Young's modulus of the lotus copper processed by ECAE is half of the one showed by the Hardened OFHC copper but with a porosity of 35%. The non-porous sample cooled as the lotus copper and processed by ECAE had a higher increase in the young modulus until reach a value that is the 72% of the Young's modulus of the reference structural material.

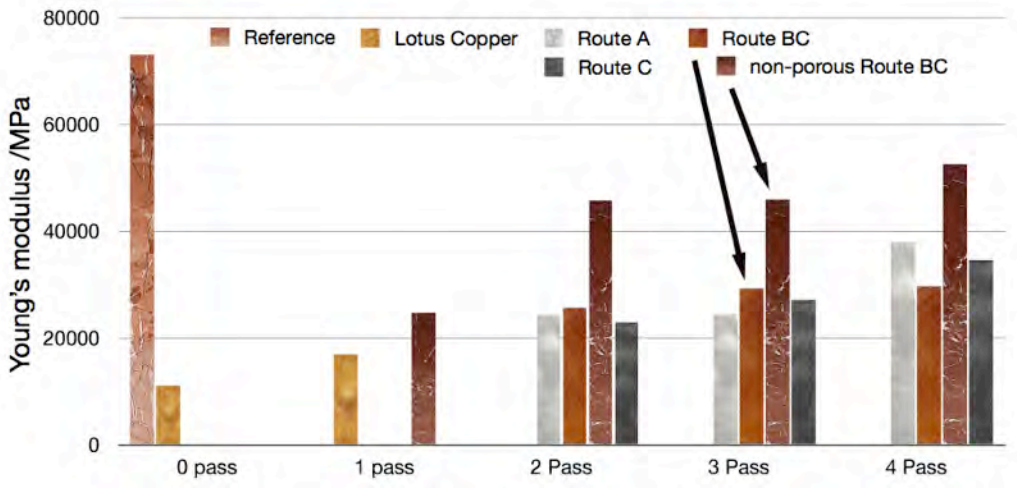

Figure 5.7: *Young's modulus of the samples studied in the previous paper after different passes by ECAE-die compared with the Young's modulus of the Hardened OFHC copper (reference).*

5.6 Conclusions

The main conclusion of this chapter is that the use of the ECAE technique allows a significant improvement of the mechanical properties of porous metals with small increases in density. Therefore, this is a promising technique to improve the performance of these cellular materials.

In section 3.7 we introduced a figure showing the yield strength and the specific yield strength of oxygen-free high thermal conductivity (OFHC) copper compared with that of lotus cooper and that of the annealed OFHC copper, Figure 3.22.

Figure 5.8 shows the results for the previously mentioned materials and the ones obtained after processing the cellular copper by the ECAE technique. It is clearly observed that the values of the materials developed in this chapter are much closer to the ones of the OFHC copper. In fact, the lotus type porous copper processed by 1 pass of ECAE (90°-die) had the 48% specific

yield strength of the OFHC copper and the lotus copper processed by 4 passes of ECAE (150°-die) by C route present the 62% of the specific yield strength of the OFHC copper and 45% of the absolute yield strength of the OFHC copper for a sample with a porosity of 35%.

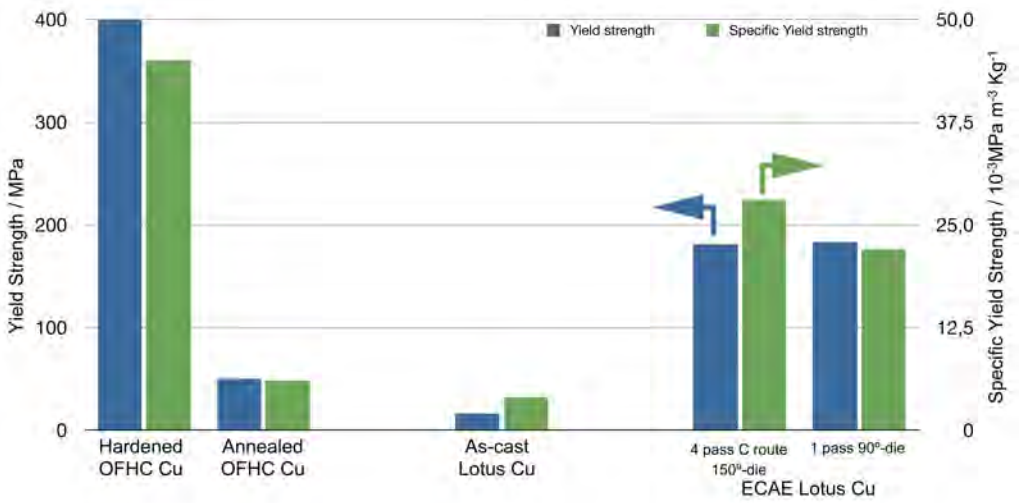

***Figure 5.8**: Yield strength and specific yield strength of the samples presented in this thesis. The OFHC copper is show as a reference of structural metal.*

5.7 References

[1] V.M. Segal, Methods of Stress–Strain Analysis in Metalforming, Sc.D. Thesis, Minsk (1974).

*[2] V.M. Segal. Materials Science and Engineering: A **271**, 322, 1999.*

*[3] R.Z. Valiev. Nature Mater **3**, 511, 2004.*

*[4] R.Z. Valieva and T.G. Langdon. Progress in Materials Science **51**, 881, 2006.*

*[5] M. Furukawa, Z. Horita, M. Nemoto, T. G. Langdon. Journal of Materials Science **36**, 2835, 2001.*

[6] S. R. Agnew, U. F. Kocks, K. T. Hartwig and J. R. Weertman, in "Modelling of Structure and Mechanics of Materials from Microscale to Product," edited by T. Leffers, T. Lorentzen, O. B. Pedersen, B. F. Sørensen and G. Winther. Risø National Laboratory, Roskilde, Denmark, 1998.

*[7] S. Suzuki, H. Utsunomiya, H. Nakajima. Materials Science and Engineering: A **490**, 465, 2008.*

6 Microcellular and structural foams

Resumen (Spanish):

En este capítulo se hace una introducción a las espumas microcelulares, a las espumas structurales y los métodos que se seguían hasta a presente tesis para fabricarlas. Tras lo cual se introduce el sistema de moldeo por compresión mejorado con el cual en esta investigación se han fabricado las espumas que se estudian en los capítulos siguientes.

6.1 Introduction

Plastics can be foamed in a variety of ways[1-4]. The foamed plastics which are also referred to as cellular or expanded plastics, have several inherent features which combine to make them economically important. Thus, a foamed plastic is a good heat insulator by virtue of the low conductivity of the gas (usually air) contained in the system, has a higher ratio of flexural modulus to density than when unfoamed, has greater load-bearing capacity per unit weight, and has considerably greater energy-storing or energy-dissipating capacity than the unfoamed material. Foamed plastics are therefore used in the making of insulation, as core materials for load-bearing structures, as packaging materials used in product protection during shipping, and as cushioning materials for furniture, bedding, and upholstery.

Among those plastics which are commercially produced in cellular form are polyurethane, PVC, polystyrene, polyethylene, polypropylene, epoxy, phenol-formaldehyde, urea-formaldehyde, ABS, cellulose acetate, styrene-acrylonitrile, silicone, and ionomers. However, it is noted that it is possible today to produce virtually every thermoplastic and thermoset material in cellular form. In general, the basic properties of the respective polymers are present in the cellular products except, those changed by conversion to the cellular form [1-4].

Other important aspect is the wide variety of process available to produce polymeric foams (Figure 6.1).A simple option is to dissolve a gas in the polymer and release the pressure at high temperature. The most extended way to make polymeric foams is foaming at the final stage of an extrusion line, that allows high production rates but with a difficult control in the cellular structure. Injection moulding is also used to produce cellular polymers with a defined shaped. Some thermoset foams, such polyurethane or epoxy are produced by reactive polymerization + foaming. Polystyrene

can be foamed by direct extrusion(XPS), but Expanded Polystyrene (EPS) is foamed by boiling the pentane absorbed previously in the polymer beads.

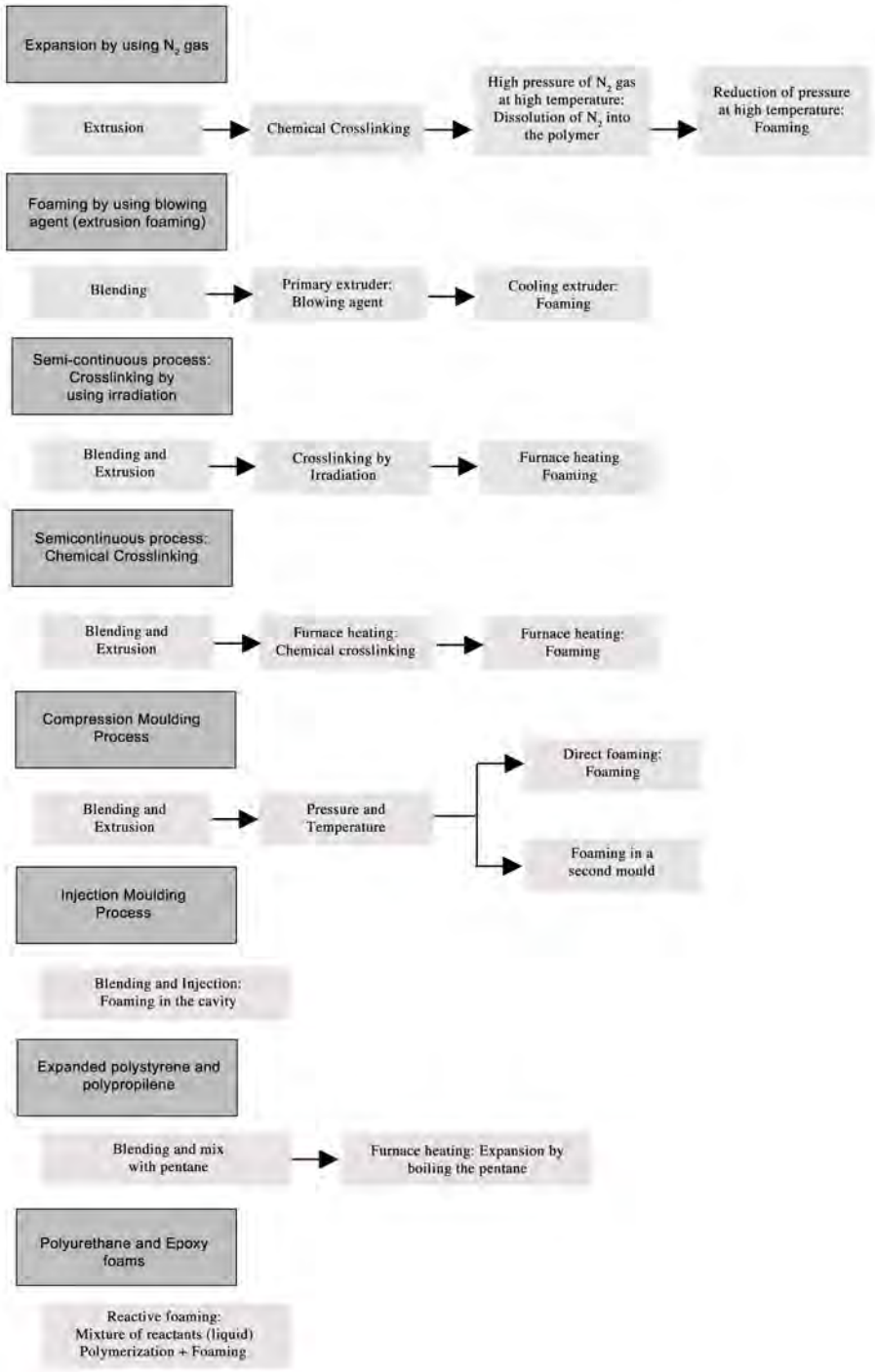

Figure 6.1: *Outline Some foaming processes for polymeric foams*

The group of rigid cellular polymers can be further subdivided according to whether they are used for non-load-bearing applications[5], such as thermal insulation (functional applications); or as load-bearing structural materials, which require high stiffness, strength and impact resistance. The present thesis is related to the second type of cellular polymers.

6.2 Microcellular foams

Microcellular foams refer to thermoplastic foams with cells sizes lower than 100 μm in diameter. Typically these foams are rigid, closed-cell structures. The microcellular process that sparked the growth in this field over the past two decades was invented at Massachusetts Institute of Technology, USA, in the early eighties [6], in response to a challenge by food and film packaging companies to reduce the amount of polymer used in their industries. As most of these applications used solid, thin-walled plastics, reducing their densities by traditional foaming processes that produced bubbles larger than 0.25 mm was not feasible due to excessive loss of strength. Thus was born the idea to create microcellular foam, where we could have, for example, 10 bubbles across 1 mm thickness, and expect to have a reasonable strength for the intended applications.

It would be reasonable to say that the potential of microcellular foams has yet to be realized. These materials have not yet appeared in mass produced plastic items, and the promised savings in materials and associated costs have yet to materialize. This is largely due to manufacturing difficulties encountered in scaling up for large scale production. However, enthusiasm for these materials remains high, and today researchers and commercial enterprises on every continent are in a global race to harness the potential benefits. Much has been learned about the processing and properties of microcellular foams since the first patent was granted in 1984 [7]. An early review of the subject appeared in 1993 [8].

6.3 The Solid-State Batch Process

The basic solid-state microcellular process is a two-stage batch process shown schematically in Figure 6.2. In the first stage, the polymer is placed in a pressure vessel with a high-pressure and a non-reacting gas. This step is usually conducted at room temperature. Over time, the gas diffuses into the polymer, and attains a uniform concentration throughout the polymer specimen. When this specimen is removed from the pressure vessel and brought to atmospheric pressure, a 'supersaturated' specimen that is

thermodynamically unstable due to the excessive gas dissolved into the polymer is produced. In the second stage, the supersaturated specimen is heated to a temperature above the glass transition temperature (Tg) of the polymer-gas mixture, termed the foaming temperature. This step is typically carried out in a heated bath with temperature control. The dissolved gas lowers the Tg of the polymer [9] and the foaming temperature needs only to be above the Tg of the gas-polymer system in order for the bubbles to nucleate and grow.

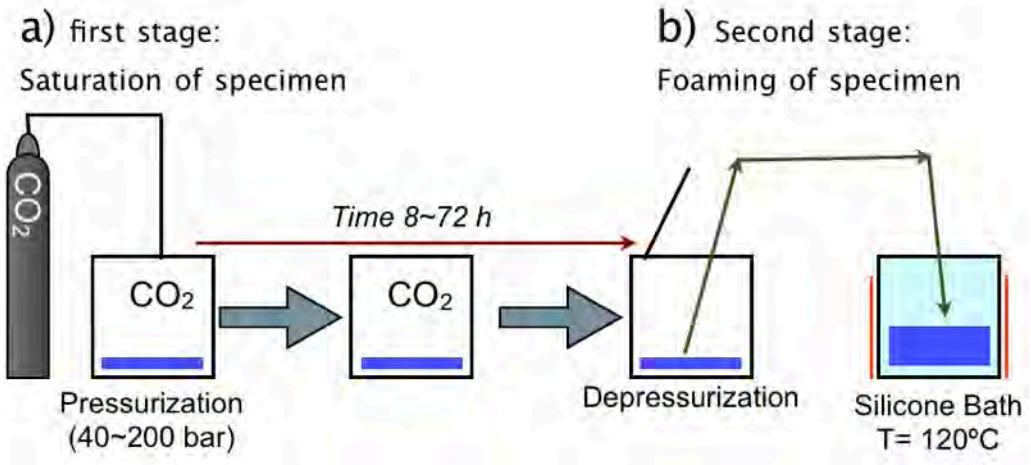

Figure 6.2: *Schematic of the batch process to make solid-state microcellular foams*

Since the polymer is still in a solid state, the foams produced are called 'solid-state foams' to distinguish them from conventional foams that are typically produced in an extruder from a polymer melt. The term 'solid-state' is meant to convey an essential difference from the extrusion processes, namely that in the former process the bubbles are formed in the rubbery state, near the Tg and the polymer is never melted. Thus, while surface tension effects play an important role in the bubble growth dynamics of extrusion foams, these effects are not important in the solid-state process. Instead, the viscoelastic properties of the gas-polymer system become important.

The solid-state batch process has been used to create microcellular foams from a number of amorphous and semi-crystalline polymers, such as polystyrene (PS) [6,11-13], polycarbonate (PC) [11,12], acrylonitrile-butadiene-styrene (ABS) [15], polyethylene terephthalate (PET) [16], glycol-modified PET (PETG) [17], crystallisable polyethylene terephthalate (CPET) [18], and polyvinyl chloride (PVC) [19], etc. Examples of solid- state microcellular structures in several polymers are shown in Figure 6.3. The microcellular structure is remarkably uniform compared to the structure in extruded foams or structural foams.

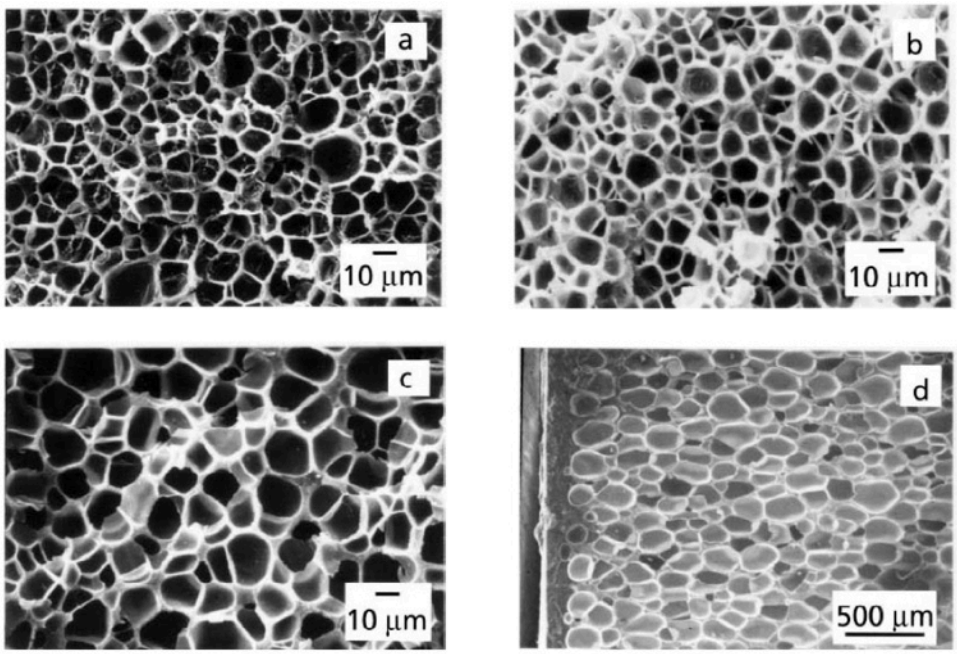

Figure 6.3: *Examples of microcellular foams in a number of thermoplastics: (a) PVC; (b) PC; (c) ABS; (d) PET. All specimens show a remarkable homogeneity in microstructure. The cell sizes range between 1-10 μm except for PET where the cells are in the 100 μm range*

A unique aspect of the batch process is the ability to create an integral unfoamed skin on a foam specimen (structural foam)[20]. This can be understood with reference to Figure 6.4, which shows gas concentration profiles in a saturated specimen, just after it is removed from the pressure vessel (time zero) and at a later time t. During this time, called desorption time, the gas is allowed to escape from the surface layers. Then if C* is the minimum gas concentration needed for bubble nucleation, one can see that there is a surface layer in which bubbles will not nucleate due to a lack of sufficient amount of dissolved gas. Thus a skin of solid polymer with a desired thickness can be created when the specimen is heated after a suitable desorption time. This provides a means to create skin-core structures that can be optimized to achieve the desired properties.

The basic solid-state microcellular process discussed above is called a temperature soak process to signify that after initial saturation of the polymer by gas, bubble nucleation is induced by heating the polymer. The reduction in gas solubility upon heating provides the driving force for bubble nucleation. The bubble nucleation can also be achieved by a sudden reduction of pressure, provided that the gas-saturated specimen is already above the glass transition of the polymer-gas system. This is called the

pressure-quench method, and has also been used to create microcellular foams using supercritical carbon dioxide [21-23].

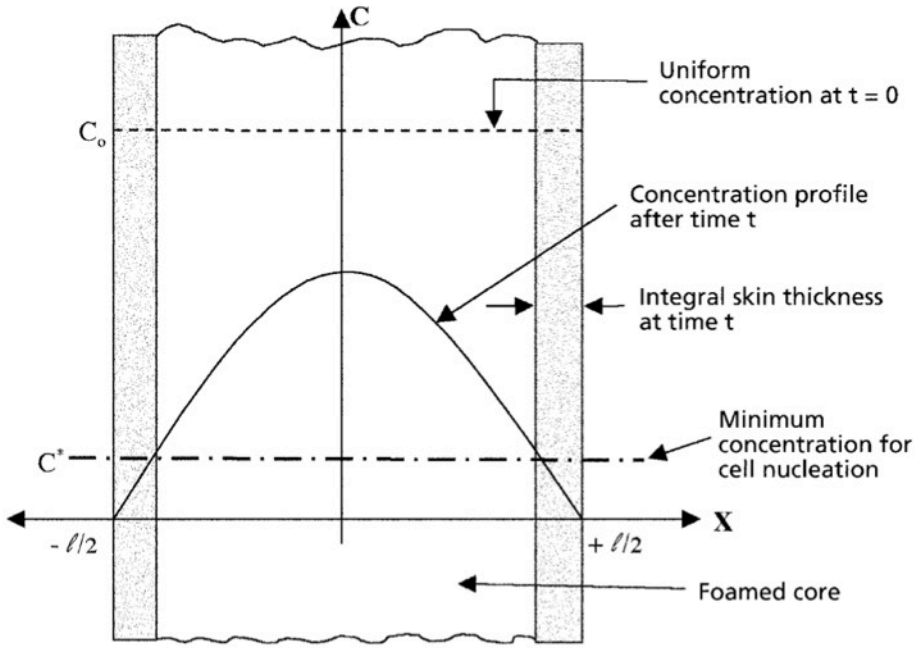

Figure 6.4: *Schematic showing the creation of an integral, unfoamed skin in the batch microcellular process.*

6.4 Structural Foams

The structural foam injection moulding process is schematically showed in Figure 6.5[1-4]. A blowing agent, often nitrogen, is injected into the melt in the extruder, It is also possible to use a chemical blowing agent mixed with the polymer in the barrel of the extruder. The polymer melt, mixed with gas, is then forced into the accumulator[3] where it is maintained at a pressure and temperature high enough to prevent foaming (Figure.6.5a). When a sufficient charge has accumulated it is transferred into the mould (Figure.6.5b). The melt is introduced into the mould at a relatively low pressure compared to the much higher pressure in the accumulator. The lower operating pressures of the moulds make the moulds less expensive than those used for conventional injection moulding. However, the cycle times are usually longer because the foam being a good insulator, takes longer time to cool the part.

[3] Not all the injection molding system for foaming use the accumulator, similar systems are nowdays working without this system.

Structural foams can also be made using a chemical blowing agent rather than an inert gas. In that case, a change in pressure or temperature on entering the mould triggers gas formation. Today structural foam injection moulding is a very fast-growing polymer processing technique that can be used to modify the properties of thermoplastics to suit specific applications.

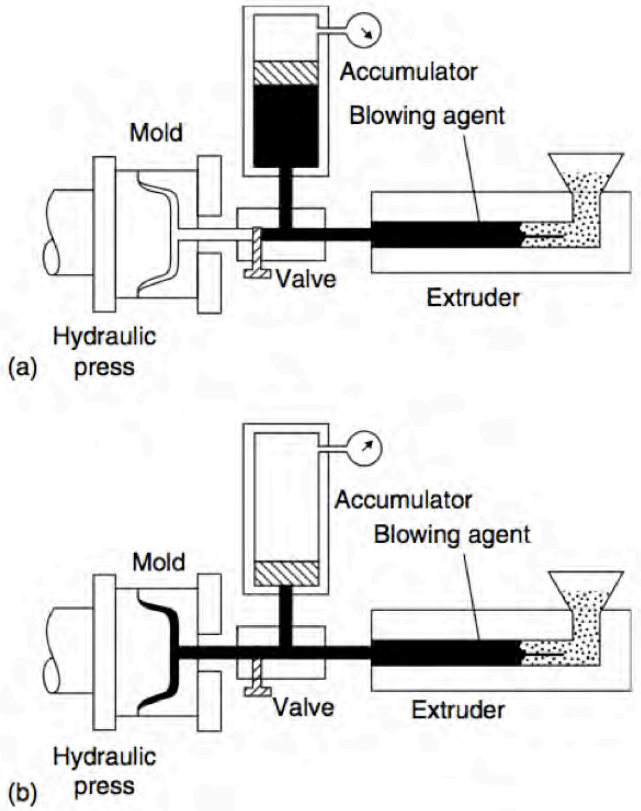

Figure.6.5: *Structural foam process. (a) Filling the accumulator. The blowing agent (usually nitrogen) is injected into the melt in the extruder before it is passed into the accumulator. (b) Filling the mould. The accumulator ram injects the melt into the mould where the reduced pressure allows the gas to foam the resin.*

With the theory of the microcellular plastic developed by the MIT [6], the fundamental theory for microcellular injection molding has been developed for a decade and is still one of major research topics in the plastics industry [24]. Currently the Mucell technology[25] is able to produce microcellular structural foams using specific injection moulding equipment based on similar principles than those explained in the previous paragraphs.

There are four basic steps of microcellular injection molding: using supercritical fluids, mixing and dissolution in the melt; nucleation of cells; cell growth; and shaping in the mold [26–29].

The concept of the continuous process was successfully tried in an extruding process [30]. It basically needs to create the gas–polymer solution first in the barrel. The gas at the supercritical fluid state is metered and injected into the barrel and then dissolved into the molten polymer, as shown in Figure 6.6. The gas is pressurized up to 20 MPa before flowing into the barrel. As the gas flows into molten polymer, it forms big gas droplet in the molten polymer since the flow of the gas is briefly interrupted every time the screw flight wipes over the barrel. The size of the gas droplet in the molten polymer is determined by five major factors: gas pressure and molten polymer pressure; gas flow rate; viscosity of molten polymer; wiping frequency of the flights (screw rotation speed); and diameter of orifice in the gas injector. Then, the large gas droplet is elongated in the barrel through the shear deformation induced by the screw rotation. The elongated gas droplet will be broken up forming many small gas droplets above a critical value of the Weber number, which is a ratio of shear force to the surface force. These gas droplets may be stabilized in the screw channels to form bubbles in the molten polymer matrix. These bubbles, in turn, undergo elongation with additional shear deformation that increases the area-to-volume ratio of each gas bubble. Then, the gas in the bubble diffuses quickly into the molten polymer due to the increased polymer–gas interfacial area and decreased striation thickness of polymer between the gas bubbles.

Eventually, the gas droplets must be small and uniformly distributed in the molten polymer matrix, as shown in Figure 6.6. It may be defined as gas–polymer mixture ready for nucleation. Ideally, the final gas–polymer solution should become the so called single-phase solution [29, 30]. In other words, there are no separate phases such as gas phase and polymer melt phase. However, the real practice in the injection molding machine can create the excellent gas–polymer solution with tiny bubbles in the molten polymer. The single-phase solution of gas and molten polymer may never truly form in such short recovery time in the plasticizing screw [26], and even shorter mixing time with new technology of injecting gas through the nozzle during injection [31, 32]. Therefore, the single-phase solution may be defined as the gas–polymer solution with a uniformity distribution of many tiny bubbles, which has been proven to be a good mixture of gas–polymer solution ready for the next step of microcellular processing in the most current technologies of microcellular injection molding processes [26–32].

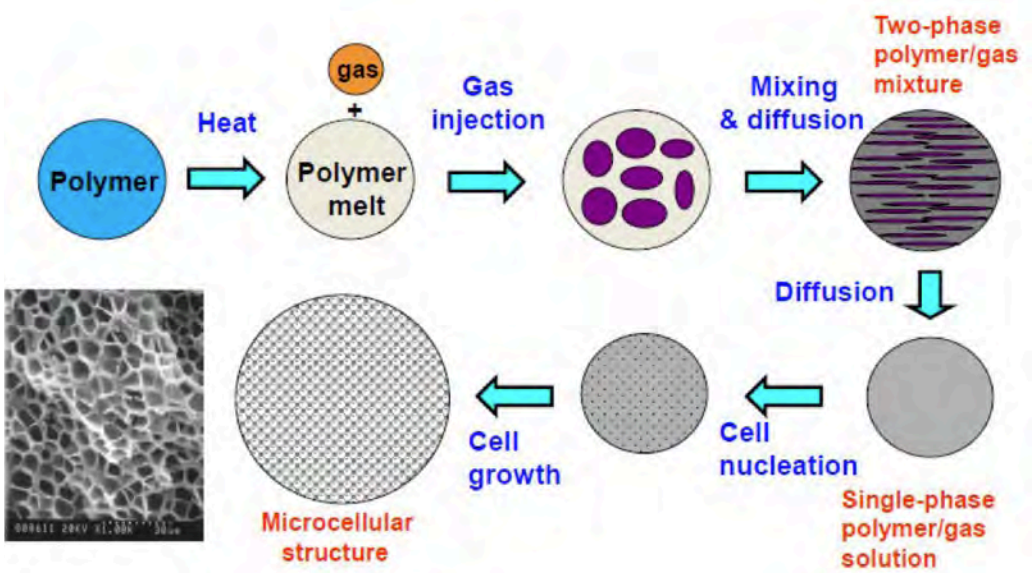

Figure 6.6: *Steps of continuous foaming process using supercritical fluids.*

Then, the next step is nucleating the cells. The thermodynamic instability is generated by either a pressure drop or a temperature change with high rate. Practically, a quick change in the pressure is much easier than a fast change in the temperature in a very short period. Therefore, a very high pressure drop rate occurs in either the nozzle orifice or the valve gate, where the narrow orifice causes a high pressure drop rate up to 1GPa/sec or higher.

Once enough nuclei are created, the nucleated gas–melt mixture is still kept warm for cell growth in the center layer of the part when the skin begins to cool down. In addition, the short shot of injection leaves enough space for cell growth. On the other hand, enough gas is available to provide the necessary gas supply around the nuclei, which is growing further to form a stable cell.

Finally, the part in the mold not only conforms to the shape of the mold but also builds up the skin-cell structure. The cell growth in the part results in a microcellular part. The cells retain their shape and size during the cooling, and also the residual gas pressure inside the cells pushes the part, thereby expanding the cells to overcome the shrinkage of polymer. Then, the expanding of cells inside the part helps the part to contact the cold wall of mold to copy the mold shape exactly and to form the solid skin quickly.

6.5 Mechanical properties of Microcellular Foams

The tensile property data [33] show that the tensile strength of microcellular foams decreases in proportion to the foam density, and can be approximated quite well by the rule of mixtures. Thus a 50% relative density foam can be expected to have 50% of the strength of the solid polymer. Figure 6.7 shows relative tensile strength as a function of relative foam density for a number of microcellular polymers. In this figure the relative tensile strength, is obtained by dividing the tensile strength of the foam by the tensile strength of the solid polymer. Similarly, the relative density is foam density divided by the solid polymer density. In Figure 6.8 we have plotted the strength data on a specific basis. Thus, the specific relative tensile strength for the foam of a given relative density is obtained by dividing the relative tensile strength by the relative density. Figure 6.8 shows that on a specific basis, the tensile strength of microcellular foams is essentially constant over the entire range of foam densities.

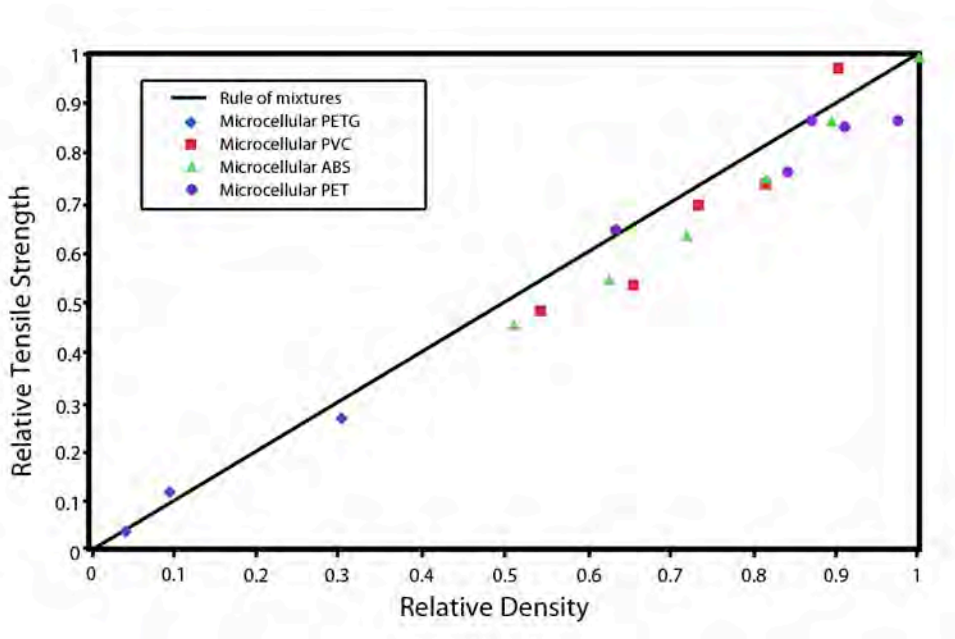

Figure 6.7: *Tensile strength data on microcellular foams produced by the batch process. The tensile strength is closely approximated by the rule of mixtures over the entire range of foam densities.*

A unique aspect of data in Figure 6.7 is that in the relative density range of 0.1 to 0.5, the microcellular foams represent novel materials for the engineer with properties not previously available. Most conventional foams fall either

in the low-density region (relative density less than 0.1) or belong in the structural foams category (relative density greater than 0.5). The modulus of microcellular foams can be reasonably estimated by the Gibson- Ashby cubic cell model [34], which predicts that the relative tensile modulus equals the square of the relative density.

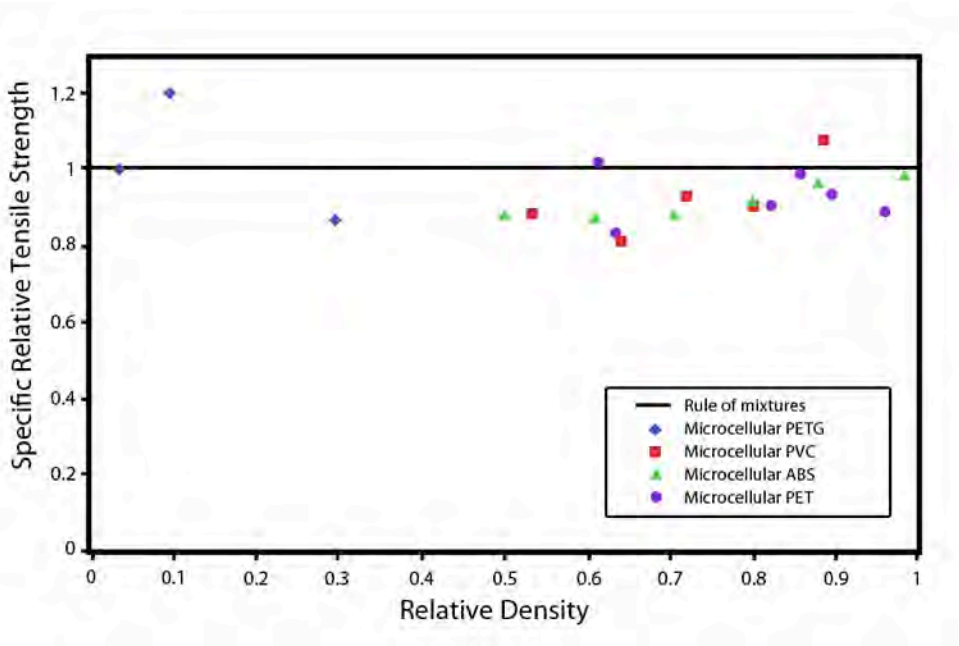

Figure 6.8: *Plot of specific relative tensile strength as a function of relative density of microcellular foams. Note that specific strength is essentially constant over a wide range of foam densities.*

6.6 Compression moulding

Compression moulding (Figure 6.1) is a versatile process suitable for a wide variety of thermoplastic polymeric matrices. Two different variations are commonly used at industrial level [2, 3]. The single stage process involves two steps, first compounding the polymer with the blowing agent and all the required additives, (using a extruder or a Banbury type mixer) and in the second one, the formable compound is placed in a mould and subjected to a temperature higher than the decomposition temperature of the blowing agent, afterwards the polymer is released from the mould, the expansion takes place and the material is foamed. The main advantage of the single-stage variation is its simplicity, however it present several disadvantages being the most important the difficulty of controlling density of the foams. In addition when using low-melt strength thermoplastics, such as polyolefin, or

when high expansion degrees are required, it is necessary to crosslink (either chemically or by irradiation) the polymer for it to bear the extensional forces occurring during expansion, thus avoiding premature collapse of the foam or the presence of a high number of broken cell walls [3].

Using the single stage process, densities lower than 70 kg/m3 can not be achieved. To obtain lower densities, a second variation known as two-stages compression moulding is used [2]. In this process, expansion takes place at two different times and this together with the crosslinking of the polymeric matrix allows lowering the density of the foamed products to values as low as 15 kg/m3. Compounding is carried out as for the single stage process, and the foamable mixture is introduced in a mould and subjected to both pressure and temperature. The polymer is crosslinked and afterwards expanded between 4 and 7 times. Second expansion takes place at atmospheric pressure in a mould having the desired size and shape.

6.7 Objectives of the research

The election of the foaming process is conditioned mainly by the final application of the material which at the same time strongly depends on its relative density. It is well known that foaming process itself as well as the intrinsic characteristics of the polymeric matrix heavily determines the cellular structure of the foamed product [2, 3].

The objective of the research were:

1. Production and characterization of structural foams with fine cells (microcellular size was the target) using as raw material a semicrystalline polymer (low density polyethylene).
2. Low and controlled density with a defined shape, producing the materials using a non-cross-linked thermoplastic matrix.

Injection moulding is the best election to produce structural foams. However, density reductions are limited to a 40%, and in addition they strongly depend on size and shape of the piece [28, 35].

The batch foaming process produces foamed products that have a very high quality, with fine cells and without residues coming from the blowing agent. However, on the other hand, using such process the control of foam density is very complicate, [36]; in addition, the investments at industrial scale are high due to the requirement of a large high-pressure vessel.

Compression moulding, either the single or the two-stages variations presents two main drawbacks. First of all, the control of density of the foamed part which is usually performed by means of blowing agent concentration and hence is far to be precise and second one it is necessary to crosslink the polymeric matrix which harms its recyclability by conventional re-melting techniques, [37].

Due to the absence of a known method to produce the targeted materials of this thesis it was needed to develop a new one, able to obtain all the previously mentioned features. This method has been called 'improved compression molding' (ICM) or 'modified compression modeling'.

6.8 Improved Compression Moulding (ICM)

The Improved Compression Moulding Route, (ICM) could be considered as a variation of the single stage process of compression molding. It is based on a closed control of both temperature and pressure during foaming step as well as on a proper handling of the chemical composition of the sample.

The main difference between the ICM route and the conventional one-step compression moulding lays in the pressure applied to the foam during foaming step, this is, in the ICM route, the foam grows under pressure.

This difference promotes significant advantages of the ICM process over the conventional one. On one hand the possibility of achieving an accurate control of foam density and on the other hand the possibility of modifying the microstructure of the foamed part, (in terms of size and shape) by acting on both foaming parameters and chemical composition.

Foam density is controlled through the use of special moulds known as self-expandable moulds. Those moulds have the ability of applying and retaining pressure to the polymer while the decomposition of the chemical blowing agent and subsequent dissolution into the polymer. In addition, moulds are capable of controlling the expansion degree of the material hence regulating in a very accurate way both size and shape of the foamed part. As the moulds can adopt different geometries, it is possible to obtain net-shaped foams by using the ICM process.

With regard to the second main advantage, it should be said that the control of chemical composition, (mainly blowing agent concentration) time, pressure and temperature during the process make feasible the obtention of foamed products with tailored cellular structures in terms of cell diameters

and cell shapes. Besides, the control of cellular structures can be achieved regardless of which is the density of the foam. Therefore using the ICM route it is possible to obtain customized foams with similar densities but with significantly different cellular structures, so that they would be the most suitable for the desired applications. For example, for structural purposes samples with a good mechanical response, (i.e. with an almost zero open cell content) are desirable, while for sound absorption applications a high degree of interconnection between the cells is preferred.

The ICM route comprises the following steps. In the first one, all raw materials the chemical blowing agent and all the required or desired additives are melt-mixed in a twin-screw extruder or batch mixer at a temperature lower than the decomposition temperature of the blowing agent. So obtained pellets can either be directly foamed or used to produce a precursor that will be afterwards introduced in the final mould and foamed. Precursors are prepared using a mould with the same geometry as the final part but with different dimensions.

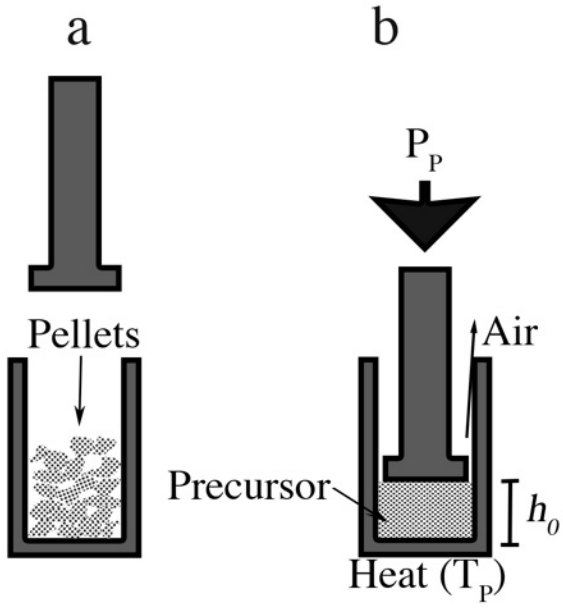

Figure 6.9: *Production of the foam precursor. The pellets of the thermoplastic polymer are introduced in the precursor mold and closes by the piston(a). The mold is heated to a temperature T_P and the pressure of the piston was set to P_P. The piston have enough tolerance to evacuate the air from the mold, the final height of the precursor is h_0 (b).*

A certain amount of the foamable compound is introduced in the mould and subjected to both temperature (T_P) and pressure (P_P) to form a solid sample.

The applied pressure should be high enough to assure a good compaction of the pellets and the temperature lower than the decomposition temperature of the blowing agent in order to prevent its prone decomposition. Figure 6.9.

The final step is the foaming one, so, either pellets or precursors are introduced in the final mould which is at the same time introduced in a hot-plates press. An initial pressure (P_0) is applied to the system while it is heated until foaming temperature (T_F) which is always higher than the decomposition point of the blowing agent. As the temperature increases, the blowing agent starts decomposing and the pressure inside the mould increases up to a higher value (P_F). After a certain time (t_F), when the blowing agent is fully decomposed, and P_F stabilizes, (does not continue increasing), the pressure of the press is released allowing the polymer to expand until to a desired ratio. The mould is then introduced in cool water to cool-down the sample and hence stabilizing cellular structure as fast as possible. Foaming parameters, this is t_F, P_0 and T_F are chosen depending on the polymeric matrix type, chemical composition, (blowing agent concentration) and sample's geometry.

The control of foam density is carried out by means of aforementioned self-expandable moulds. Figure 6.10 shows a schematic draw where it is represented the evolution of both sample and mould during a typical foaming experiment. In the first stage, the precursor or the pellets are introduced in the mould and the initial pressure applied, (P_0). Precursors or equivalently the cavity where pellets are introduced have a defined initial height, (h_0). As the blowing agent decomposes, (second step), the gas starts dissolving in the polymer and the pressure increases above P_0. After the complete decomposition of the blowing agent, the pressure is released allowing the piston to displace vertically and hence the material is able to expand. The distance covered by the piston is defined taking into account the desired expansion ratio *E.R.*:

$$E.R. = \frac{h_f}{h_0} \tag{6.1}$$

So, the final height of the sample is defined as follows:

$$h_f = h_0 + d \tag{6.2}$$

The movement of the piston is restricted to such distance, (d) by the part named "*E.R.* Control Part". Such parts are interchangeable depending on the desired expansion ratio.

The independent control of density and microstructure is probably the greatest advantage of the ICM, also any thermoplastic polymer or

thermoplastic based composite or nanocomposite can be foamed by this process and without the necessity of crosslinking the polymeric matrix. After developing this process it has been used in several investigations by CellMat members. Up to now, pure polymers such as LDPE or EVA, composites such as LDPE/ATH, EVA/ATH or mixtures of EVA and starch, and nanocomposites based on LDPE and silica nanoparticles have been successfully foamed using the ICM process [37-44].

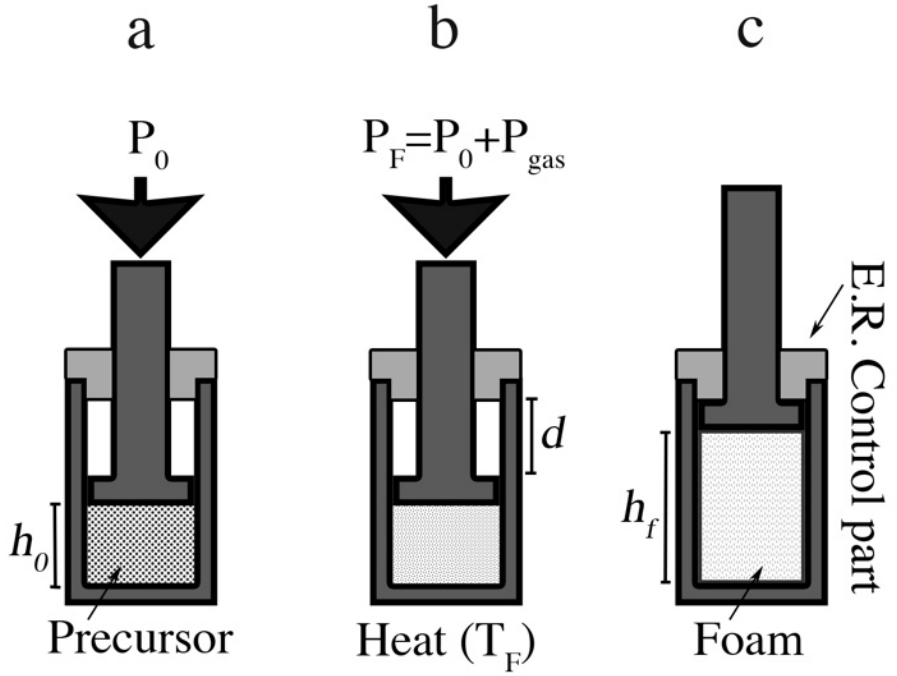

Figure 6.10: *Schematic draw of one self-expandable mould used to develop the improved compression moulding route. (a)The precursor is introduced into the mold and a press introduce the initial pressure P_0.(b) The mold is heated to archive a temperature above the decomposition temperature of the bowling agent T_F. The gas is released and the pressure increases until reach the maximum when all the blowing agent is decomposed.(c) At this time the external pressure is released and the piston goes up until finds the E.R. control part. At this moment the mold is cooled down to solidify the foam.*

6.9 Polyethylene structural foams

To produce the polyethylene structural foams the materials used were:

1. Low density polyethylene (PE008) provided by Repsol Quimica with a melting temperature of 110ºC, MFI=4g/10min at 190ºC, density 923Kg/m3.

2. Azodicarbonamide provided by Urquinsa as blowing agent with an average particle size of 4.9µm.
3. Zinc oxide, Silox Active grade provided by Safin Alcan, used as catalytic of the chemical blowing agent
4. Stearic acid (Stearic Acid 301 supplied by Renichen) used as mixing processing aid.

The high difference between the melting temperature of the polyethylene and the decomposing temperature of the azodicarbonamide allow a wide temperature range to process the precursors of the foams without decomposing the blowing agent.

The polymer, azodicarbonamide, stearic acid (0,15%) and zinc oxide (0,05%) were mixed in a banbury mixer at 145ºC, 25 rpm, by 5 minutes with a total mass of 50 grams. The mixed plastic was pelletized in pieces of 5-8mm^3. The exact composition of the polymers used during the research are in the table 6.1.

Different concentrations of azodicarbonamide were chosen to modify the cellular structure of the foams at given density.

Table 6.1: *Composition of the foams precursors in the present research.*

	Afro a	Afro b	Afro c	Afro d	Afro e
PE	98,62%	93,97%	89,27%	84,25%	79,29%
Azodicarbonamide	1,18%	5,83%	10,53%	15,57%	20,51%
stearic acid	0,15%	0,15%	0,15%	0,15%	0,15%
zinc oxide	0,05%	0,05%	0,05%	0,05%	0,05%

The solid precursor for each foam was produced at T_P= 120ºC inside of the precursor mold, and compressed at P_P=5Tn by high tolerance piston to evacuate the air from the precursor as was show in Figure 6.9. The precursor mold has interior dimensions of 23mm in diameter and 27mm in height. The density of pellets was between 932kg/m^3 to 957kg/m^3 depending on the amount of azodicarbonamide in the solid material.

The precursor was introduced in the mold for foaming, the internal dimensions of this mold were the same than the precursor mold. The piston

was fixed in the position by a hydraulic press at 15Tn, and heated by a heater ring up to 190ºC to decompose all the azodicarbonamide and liberate the gas as was show in Figure 6.10. After 900 seconds the heat is turned off and the piston is released until the foam reaches the desired volume, Figure 6.10. The mould was cooled by water spray and air in 300 seconds to reach room temperature (26ºC). A mould with a maximum height of 27mm (h_f) fixed the final volume of the foam. The different height of the precursors (h_0) produce the differences in the density of the foams.

The pressure inside the mould was 60bar when the mould was close at room temperature, and grows up to 90bar, for 'Afro a', to 125bar, for 'Afro e', when all the azodicarbonamide was decomposed after 900 seconds.

This process produced all non-crosslinked polyethylene foams used for the articles in the following chapters. The relative densities of these foams ranged between 0.27 and 0.92 and cell size between 30 and 100µm.

The next chapter focuses on studying the mechanical properties of the foams.

6.10 References

[1]. Osswald, T.A., and Menges, G., Materials Science of polymers for Engineers, Hanser Publishers, 2003.

[2]. D. Eaves (Editor) "Handbook of Polymer Foams" Rapra Technology Limited 2004

[3]. D. Klempner and K.C. Frisch, K. C. (Editors) "Handbook of Polymeric Foams and Foam Technology" Hanser 1991

[4]. H.N. Gupta; R.C. Gupta; A. Mittal "Manufacturing processes" New Age International 2009

[5]. B. C. Wendle "Structural foam" Marcel Dekker 1985

[6]. J. Martini, F.A. Waldman and N.P. Suh, Proceedings of SPE Antec 82, San Francisco, CA, USA, 1982, 674.

[7]. J.E. Martini-Vvedensky, N.P. Suh and F.A. Waldman, inventors; Massachusetts Institute of Technology, assignee; US 4,473,665, 1984.

*[8]. V. Kumar, Progress in Rubber and Plastics Technology **9**, 54, 1993.*

*[9]. Z. Zhang and Y.P. Handa. Journal of Polymer Science: Polymer Physics Edition **36**, 977, 1998.*

*[10]. J. Colton and N.P. Suh, Polymer Engineering and Science **27**, 485, 1987.*

[11]. V. Kumar. "Process Synthesis for Making Microcellular Thermoplastic Parts: A Case Study in Axiomatic Design" Department of Mechanical Engineering, MIT, USA, 1988.

[12]. J.A. Kweeder, N.S. Ramesh, G.A. Campbell and D.H. Rasmussen, Proceedings of SPE Antec 91, 1398, 1991.

*[13]. V. Kumar, J.E. Weller and H.Y. Hoffer, in Processing of Polymers and Polymeric Composites, Eds., A.A. Tseng and S.K. Soh, Proceedings of the ASME Winter Annual Meeting, Dallas, TX, USA, MD Series **19**, 197, 1990.*

*[14]. V. Kumar and J.E. Weller, Journal of Engineering for Industry **116**, 413, 1994.*

*[15]. R.E. Murray, J.E. Weller and V. Kumar, Cellular Polymers **19**, 6, 413, 2000.*

[16]. V. Kumar and O.S. Gebizlioglu, Proceedings of SPE Antec 92, 1536, 1992.

*[17]. Y.P. Handa, B. Wong, Z. Zhang, V. Kumar, S. Eddy and K. Khemani, Polymer Engineering and Science **39**, 55, 1999.*

*[18]. V. Kumar, R.P. Juntunen and C. Barlow, Cellular Polymers **19**, 25, 2000.*

*[19]. V. Kumar and J.E. Weller. International Polymer Processing **8**, 73, 1993.*

*[20]. V. Kumar and J.E. Weller. Polymer Engineering and Science **34**, 169, 1994.*

*[21]. S.K. Goel and E.J. Beckman. Cellular Polymers **12**, 251, 1993.*

*[22]. K.A. Arora, A.J. Lessor and T.J. McCarthy. Macromolecules **31**, 4614, 1998.*

*[23]. A. Cooper, Journal of Materials Chemistry **10**, 207, 2000.*

[24]. Jingyi Xu "Microcellular Injection Molding" Wiley & Sons 2010

[25]. www.trexel.com

*[26]. Xu, J., and Pierick, P. J. Injection Molding Technology **5**, 152, 2001.*

*[27]. D. Pierick, and K. Jacobsen. Plastics Engineering **57**, 46, 2001.*

[28]. T.K. Okamoto. "Microcellular Processing" Hanser Publications, Cincinnati, 2003.

[29]. N.P. Suh. "Innovation in Polymer Processing", edited by James F. Stevenson, Hanser/Gardner Publications, Cincinnati, 1996.

[30]. N.P. Suh, D.F. Baldwin, S.W. Cha, C.B. Park, T. Ota, J. Yang, and M. Shimbo. Proceedings of the 1993 NSF Design and Manufacturing Systems Conference, Charlotte, NC, January, 1993.

[31]. W. Michaeli, et al. German Patent No. DE 19 853 021 A1, 2000.

[32]. S. Habibi-Naini, and C. Schlummer, C. SPE ANTEC, Technical Papers, 470, 2002.

*[33]. V. Kumar, M. VanderWel, J.E. Weller and K.A. Seeler, Journal of Engineering Materials and Technology **116**, 439,1994.*

[34]. L.J. Gibson and M.F. Ashby "Cellular Solids: Structure and Properties" 2nd Edition, Cambridge University Press, Cambridge, UK, 1999.

[35]. Bayer Material Science "Engineering Polymers: Part and Mold Design" Bayer Material Science, Pittsburgh. 2000

*[36]. R.R. Puri, K. T. Collington. Cellular Polymers **7**, 57, 1988.*

*[37]. M.A. Rodríguez-Pérez, J. Lobos, C.A. Pérez-Muñoz, J.A. de Saja, L. González, B.M.A. del Carpio. Cellular Polymers **27**, 347, 2008.*

*[38] M.A. Rodríguez-Pérez, J. Lobos, C.A. Pérez-Muñoz, J.A. de Saja. Journal of Cellular Plastics **45**, 389, 2009.*

*[39] S. Román-Lorza, M.A. Rodríguez-Pérez, J.A. de Saja. Cellular Polymers **28**, 249. 2009.*

*[40] S. Román-Lorza, M.A. Rodríguez-Pérez, J.A. De Saja, J. Zurro. Journal of Cellular Plastcis **10**, 1, 2010.*

*[41] S. Román-Lorza, J. Sabadell, J.J. García-Ruiz, M.A. Rodríguez-Pérez, J.A. de Saja. Materials Science Forum **636/637**, 98, 2010.*

*[42] M.A. Rodríguez-Pérez, R.D. Simoes, C.J.L. Constantino, J.A. de Saja. Journal of Applied Polymer Science **212**, 2324, 2011.*

*[43] M.A. Rodríguez-Pérez, R.D. Simoes, S. Román-Lorza, M. Alvarez-Lainez, C. Montoya-Mesa, C.J.L. Constantino, J.A. de Saja. Polymer Engineering & Science **52**, 62, 2012.*

[44] C. Saiz-Arroyo, J.A. de Saja, M.A. Rodríguez-Pérez. Composites Part B: Engineering Available online 26 November. In Press (2012).

7 Mechanical properties of polyethylene microcellular foams

Resumen (Spanish):

En este capítulo se presentan los resultados mecánicos que se obtuvieron con las espumas de polietileno producidas con el novedoso método que desarrollamos en la Universidad de Valladolid. El tamaño celular de las espumas esta en el rango de las espumas microcelulares y el módulo de Young evoluciona linealmente con la porosidad de las distintas muestras. También se incluyen los resultados de unas simulaciones de elementos finitos que muestran el ahorro de material que se obtendría por usar estas espumas en una tubería o en una plancha en lugar de usar directamente el polímero sólido.

7.1 Introduction

Two initial papers were focused on the production and mechanical characterization of the foams produced by the Improved compression molding. The foams had different densities and cellular structures by the different amounts of azodicarbonamide in the chemical composition.

The macroscopic characterization was carried out using the compression test (Figure 7.1) measuring the elastic modulus and the collapse strength.

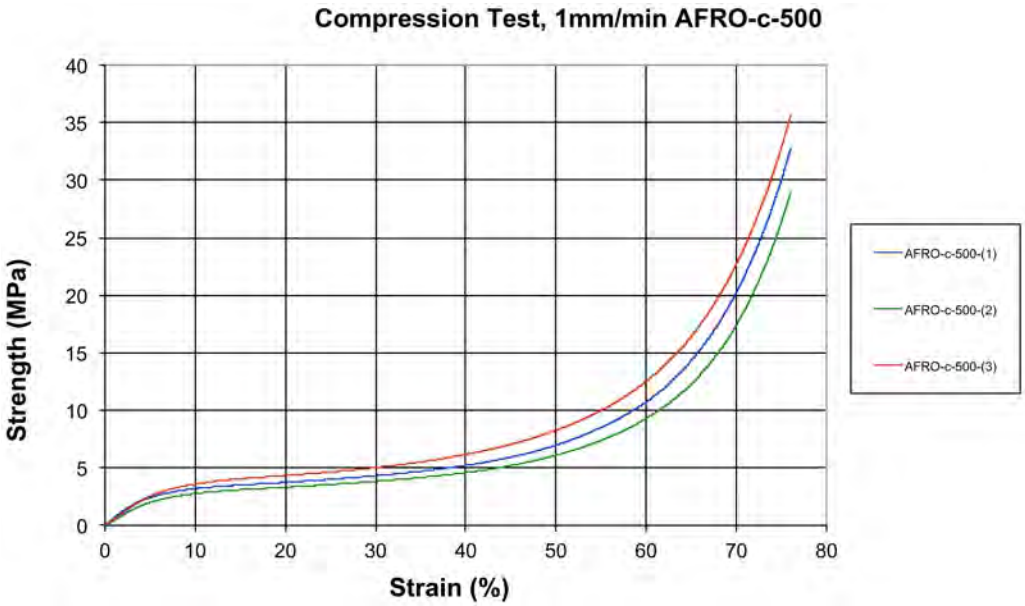

Figure 7.1: *The strength-stress curve for three foams of 0.5 relative density with 10% of azodicarbonamide.*

The key focus was studying the influence of the relative density and cellular size on the mechanical properties.

In addition the possibility of using these materials in structural applications (pipes and panels) was analyzed using FEM (finite element modeling) determining the potential weight reduction that is possible to obtain using cellular polymers.

The first paper was published in Cellular Polymers, and the second in the Journal of Cellular plastics.

7.2 Paper: Mechanical Behaviour at Low Strains of LDPE Foams with Cell Sizes in the Microcellular Range: Advantages of Using These Materials in Structural Elements

Mechanical Behaviour at Low Strains of LDPE Foams with Cell Sizes in the Microcellular Range: Advantages of Using These Materials in Structural Elements

M.A. Rodriguez-Perez[1,*], J. Lobos[1], C.A. Perez-Muñoz[1], J.A. de Saja[1], L. Gonzalez[2] and B.M.A. del Carpio[3]

[1]Cellular Materials Laboratory (CellMat), Condensed Matter Physics Department, University of Valladolid, 47011 Valladolid, Spain
[2]Universidad Politécnica de Madrid, Departamento de Enseñanzas Básicas de la Ingeniería Naval, ETSI Navales, Madrid, Spain
[3]ITPucel, Mar Mediterráneo 72, Majadahonda Madrid 28220

ABSTRACT

This paper presents the production method and the compressive mechanical response at low strains for a collection of polyethylene foams with high densities and cell sizes in the microcellular range. The materials were produced using an improved compression moulding technique that allows and independent control of density and cell size.

The materials had a relative density between 0.27 and 0.92, an homogeneous and multi-structured cellular structure with dense skin and foamed core and cell sizes in the range 30 to 100 microns. The Young´s modulus decreased with density. For relative densities higher than 0.7, the reduced Young's modulus of the foams was higher than that of the solid. In addition, it has been proved that variations in the cell size at constant density did not influence the Young's modulus. The advantages of using these materials for the production of plastic pipes have been analysed. In comparison with a solid pipe a reduction of the weight of foamed pipes loaded in compression of up to 40% can be reached.

1. INTRODUCTION

Microcellular plastics are foamed polymers characterised by cell sizes averaging 100 microns or less, typically between 5 and 50 microns(1). It has been proved

[1]Tel. +34 983 184035, Fax. +34 983 423192, email:marrod@fmc.uva.es

that these materials exhibit high Charpy impact strength, high toughness, high fatigue life, high thermal stability and low thermal conductivity[2] than solid polymers. Because of these unique properties, a large number of innovative applications can be imagined. For instance, food packaging with reduced materials costs, pipes or panels with improved strength to weight ratio, airplane and automotive parts with improved strength and acoustic dampening, sporting equipment with reduced weight and high energy absorption, etc. Due to these potential applications, over the last two decades substantial research and development has been conducted on the topic of microcellular processing and characterisation of microcellular products[3-10].

Microcellular plastics were initially produced at Massachusetts Institute of Technology (MIT) using a batch process[11]. This process has been mainly used to produce microcellular foams of amorphous materials with cells sizes around 10 microns[12].

The previous concept has been extended to the production of microcellular foams by injection moulding and extrusion[1,2,13-15], and although considerable progress has been reached, there is still a need for further research in several areas. For instance, in injection moulding there is a poor surface quality of the produced products in conventional processing[1,15], three is a limitation in the maximum size of the produced parts[1], and a limited weight reduction of the parts, not higher than 30-35%[1]. In extrusion, most of the studies have been performed at a laboratory scale or at a semi-industrial scale and as far as we know microcellular foams of semicrystalline polymers are not produced industrially by extrusion. Only polystyrene has been successfully commercialised[12].

Another open aspect is connected with the physical and mechanical characterisation of these products. Although several investigations have analysed the mechanical properties[1,4,7-10] there is still a need to know, for several polymer systems as polyolefins, the effect of cell size on the elastic response, the effect of the presence of a thick skin on the strength, the influence of the open cell content and the properties of these materials in comparison with foams produced from conventional technologies, etc.

Finally, another open aspect of interest is the identification of industrial areas in which these materials can play a key role[12]. One area of potential interest is plastic pipes of higher stiffness and lower weight with the idea of replacing the solid material. As it is expected that microcellular foams could have better mechanical properties than conventional foams this approach seems to be an interesting way of improving the properties of conventional pipes.

Bearing the previous ideas in mind, this paper focus on the following aspects: first a novel route, improved compression moulding technique or Pucel Technique, to produce foams of semicrystalline polymers with cell sizes in the microcellular range is explained, second the elastic properties of these foams are characterised and third the potential of these materials for the production of plastics pipes is evaluated by performing finite element modelling. The aims of the paper are to gain knowledge on both the production, the structure-property and the potential applicability of high density foams with cell sizes in the microcellular range.

2. MATERIALS

A low density polyethylene (PE008) provided by Repsol Quimica was used as matrix polymer (MFI = 4 g/10 min at 190 ºC, density 920 kg/m^3). Azodicarbonamide with an average particle size of 4.9 μm provided by Urquinsa (Spain) was used as blowing agent. Typical amounts of stearic acid (Stearic Acid 301 supplied by Renichen S.L) and zinc oxide (Silox Active grade provided by Safin Alcan Spain) were used as processing aid and catalyser of the decomposition reaction of the blowing agent respectively[16-18]. No crosslinking agents were used; therefore non crosslinked cellular materials were fabricated.

Foams were produced by an improved compression moulding technique[19]. In this process, first a precursor solid material that incorporates all the chemical compounds needed was produced by melt blending and compression moulding. Then the precursor material was foamed as follows.

The precursor material that contains the blowing agent was inserted in a mould with an internal diameter equal to that of the precursor material (**Figure 1**). During the heating of the precursor material up to the decomposition temperature of the blowing agent (180 ºC in this paper), which yields the blowing agent decomposition, a pressure high enough (around 200 bars) to avoid the foam expansion was applied by using a piston connected to a hydraulic press. When the entire blowing agent was decomposed, pressure was released and the piston moved to its final position. Foaming took place during the piston displacement. After this the mould was cooled and the stabilised foam was extracted from the mould.

In this process, the foams grow under pressure, and the expansion ratio, and as consequence the density, is controlled by the displacement of the piston that applies the pressure. This has a significant advantage over the conventional

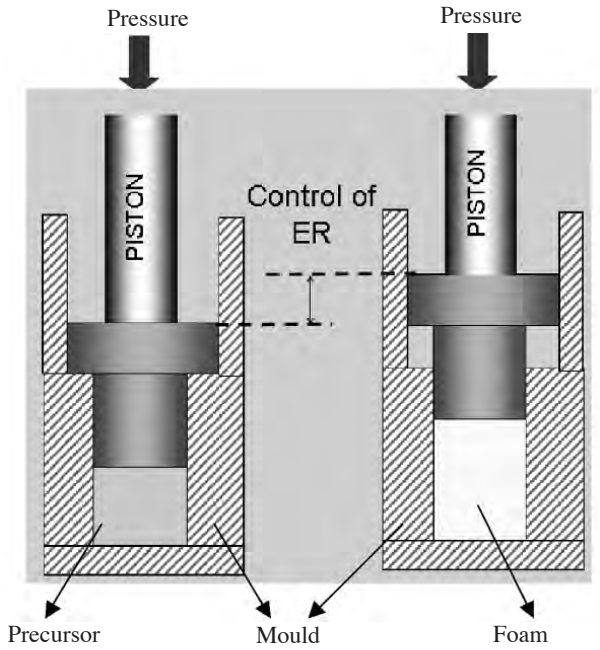

Figure 1. Schematic diagram showing the last step of the improved compression moulding technique. The expansion ratio (ER) is controlled by the piston displacement

compression moulding method[16-18] in which pressure is reduced to atmospheric pressure during decompression and density is controlled by formulation and processing parameters. In this improved compression moulding method density can be easily controlled and it is independent on the formulation. Due to this reason density and cell size can be controlled in an independent way.

Densities of the produced foams ranged between 250 kg/m^3 and 750 kg/m^3, i.e. relative densities in the range 0.27-0.92. Cylindrical samples of 22.8 mm in diameter and 17.5 mm in height were produced.

3. EXPERIMENTAL

Density Measurements

Density measurements were performed by Archimedes principle using the density determination kit for a AT261 Mettler balance.

Scanning Electron Microscopy (SEM)

Quantitative analysis was used to characterize the cellular structure. For this purpose, sections parallel to the cylinders height were microtomed at low temperature to provide a smooth surface that was vacuum coated with gold and examined by SEM using a JEOL JSM 820. Cell size distributions were measured and used to determine the average cell size. Cell density was calculated as the number of cells per unit volume of the unfoamed material using the equation (2):

$$N = \left(\frac{n_b}{A}\right)^{3/2}\left(\frac{\rho_s}{\rho_f}\right) \qquad (1)$$

where n_b is the number of cells in a defined area A, ρ_s is the density of the unfoamed solid and ρ_f is the density of the foam.

Compression Experiments

Compressive stress(s) strain (ε) curves were measured using an Instron machine (model 5500R6025) at room temperature and at a displacement rate of 1 mm/min. The maximum static strain was approximately 75% for all the experiments. These experiments were used to determine the foam Young's modulus[20,21].

Finite Element Modelling (FEM)

The size of the modelled solid pipes was nominal diameter D = 315 mm, thickness 8 mm, modulus of elasticity of the solid material E = 200 MPa, length of the pipe L = 300 mm. The pipe thickness was used as an adjustable parameter in the variational analysis. The compressive applied load was selected in order to have a defection near to 3% of the nominal radius, i.e. 9.45 mm. The simulation was done in three phases.

Initially, the quasi static structural simulation of the configurations was carried out for a 8 mm thick LDPE pipe. The analysis used a normal Lagrange formulation to consider the change in the contact zone . The mesh was generated using Brick 8node 185 and Mapped Face Meshing elements.

In a second step the simulation was performed using the same type of approximations and meshes but in this case foam pipes were simulated. In order to do that, the relationship between Young's modulus and density of the foam was introduced in each model.

In a third step, a variational analysis (Goal Driven Optimization) was performed in order to select the density and thickness of the pipe with optimum performance (similar stiffness than that of the dense pipe and minimum weight). The analysis was carried used a multi-objective genetic algorithm (MOGA) which is able to optimize problems with continuous input parameters.

In all cases, the selected input parameters were the foam density, the Young's modulus and the pipe thickness. The response parameters were the maximum pipe deformation, the maximum stress and the pipe weight. The objective was to find out the pipe (density and thickness) with a similar stiffness to that of the dense pipe and with a minimum weight.

4. RESULTS

Cellular Structure

Figure 2a shows the typical cellular structure of the inner part of one of the foams (density 550 kg/m^3). It can be observed that the foam has a very homogeneous closed cell cellular structure. Cells with diameters lower than 50 microns are observed. In addition, the foams presented skin-core morphology as it can be appreciated in **Figure 2b** for the same material. The skin has a higher density than the core, giving materials with a spatial mass distribution which in general terms optimises mechanical properties and surface quality.

Figures 3a and **3b** summarises several general trends of the average cell size, and cell density for some of the foams under study. As expected for foams produced using chemical blowing agents[22] cell size is reduced and cell density is increased when density is increased. Appreciable values of cell density (higher than 10^8 cells/cm^3) were obtained for high density foams. These values strongly decreased for the lower density foams, which seems to be due to a strong coalescence when the density of the foams was reduced.

By controlling the expansion ratio during the process (**Figure 1**) and the formulation of the precursor materials it was possible to produce foams with relative densities in the range 0.27-0.92 and with average cell sizes in the range 25-100 microns, as it is depicted in **Figure 3c**. The possibility offered

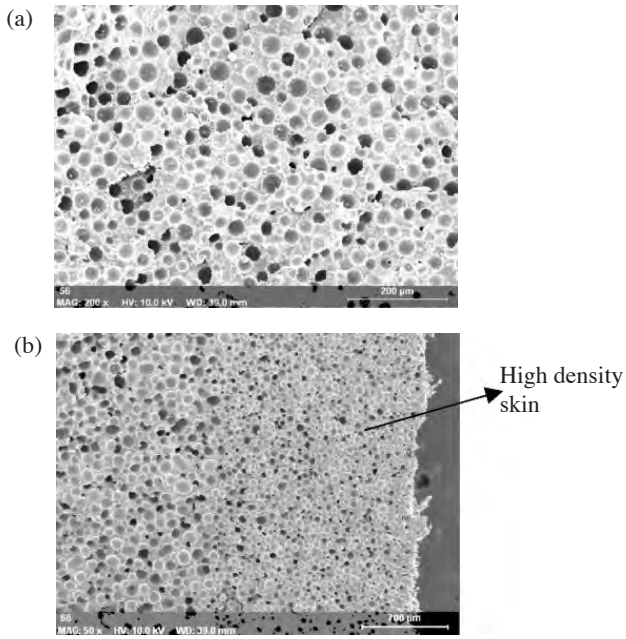

Figure 2. a) SEM micrograph of the inert part of one of the produced foams (density 550 kg/m^3); b) skin of the same material

by the improved compression moulding technique of fabricating foams with a similar density but with a different cellular structures made possible analysing independently the effect on both parameters in the mechanical response as it is explained in the next section.

Mechanical Properties

Figure 4 shows the Young's modulus of the foams as a function of cell size for a given relative density (0.60 in this case). Similar results were found for other densities. It can be observed that Young's modulus showed constant values in the cell size range between 30 and 100 microns. This result that was also found for low density foams[23], has a significant practical importance because indicates that for materials working in the elastic regime controlling the cell size is not the key objective. Other structural parameters such skin

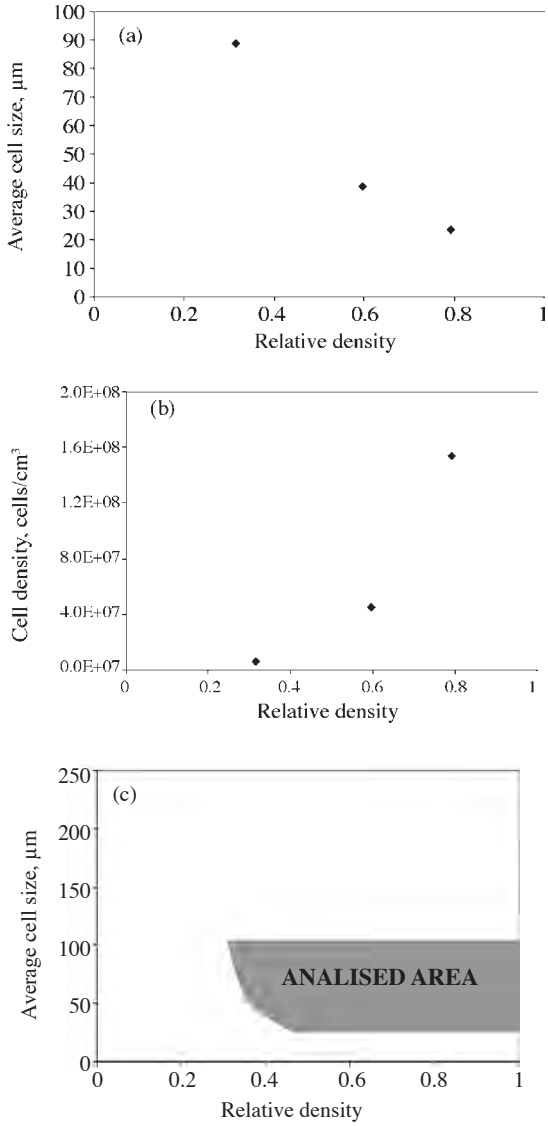

Figure 3. a) Average cell size *vs*. relative density, b) Cell density *vs*. relative density c) Density and cell size of the analysed foams

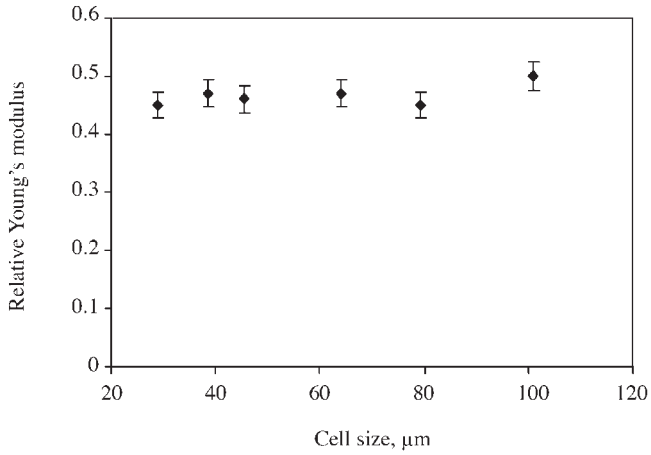

Figure 4. Relative Young's modulus as a function of cell size for foams with a relative density of 0.6

thickness, open cell content, homogenous cellular structure, etc seems to be more important.

As mechanical properties did not showed a dependency with cell size the average values of the Young's modulus for foams of a given density were obtained and analysed as a function of the foams density. **Figure 5a** shows the experimental results compared with two theoretical estimations that were obtained using a potential law of relative Young's modulus versus relative density (equation 2) with exponent n = 1 and exponent n = 2. C was assumed to be 1 in these plots[20].

$$\frac{E_f}{E_s} = C\left(\frac{\rho_f}{\rho_s}\right)^n \qquad (2)$$

where E_f and ρ_f are the foam Young's modulus and the foam density and E_s and ρ_s are the modulus and density of the solid material.

Values of n between 1 and 2 are typical for a wide amount of cellular materials[20], therefore it is expected that most foams, including the ones in this paper, would have properties between these two trends.

The materials under study followed an approximately linear trend given by equation 3.

$$\frac{E}{E_s} = \left[1.292\,\frac{\rho}{\rho_s} - 0.285\right] \qquad (3)$$

The equation has an intercept of -0,285 (the expected value should be close to zero) indicating that the behaviour at lower densities should be different, (i.e. this equation is not able to predict the behaviour of these materials in the whole relative density range; it is only valid for relative densities above 0.3).

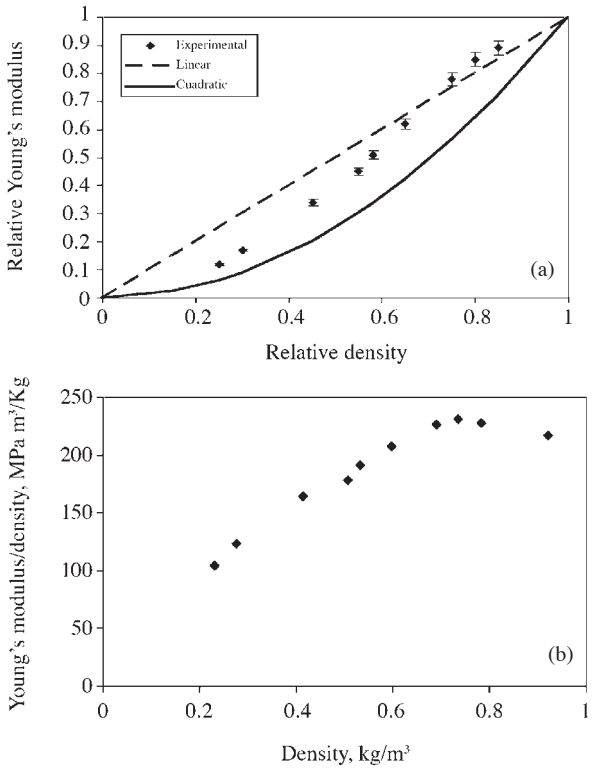

Figure 5. a) Relative Young's modulus as a function of density; b) Reduced Young's modulus as a function of density

A detailed analysis of **Figure 5b** shows different trends depending on the foam density. At high relative densities the mechanical properties of the produced foams are slightly above the linear trend. This shows that in this density range the foams have very good mechanical properties. In fact, it can be observed in **Figure 4b**, that the reduced Young's modulus (modulus divided by density) was higher for these foams than for the solid from which the materials were produced. Two different contributions are the source of this behaviour. First, the solid material (relative density 1) did not include in the formulation the blowing agent; as the blowing agent residues (that are included in the foam) could as a reinforcement, a slightly improvement of the mechanical properties of the solid matrix is expected in the foams in comparison with the solid precursor. In addition, as it is explained in the next paragraph, the foams with higher densities present a solid thick skin which performs as a reinforcement improving the mechanical behaviour.

For relative densities below 0.7 the properties are between the linear trend and the parabolic one. For densities below 0.5 the properties are closer to those of a potential law with exponent 2. Two different structural sources can be the origin of this non-unique trend with foam density. First reason is related with a different thickness of the skin when the foam density was modified. **Figure 6**

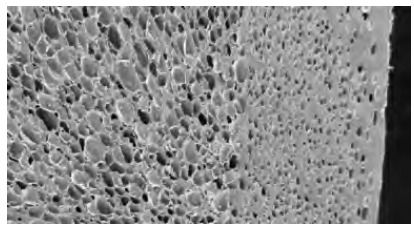

Density 730 kg/m^3

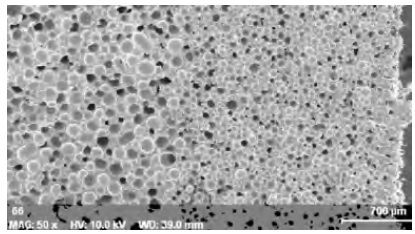

Density 550 kg/m^3

Figure 6. Presence of a more dense skin in samples with a higher density

shows that at low densities the skin seems to have a smaller density, which would reduce the mechanical properties. Second reason would be related with the open cell content in the foams. As the low density polyethylene of this study was not crosslinked, it is expected an increase of the open cell content in the materials when the density was reduced, it is well known that an increase of the open cell content will also reduce the foams stiffness[24].

FEM of the Foams Behaviour in Plastic Pipes

Table 1 shows the results for the finite element modelling comparing the behaviour of a solid pipe with that of the optimum pipe for this application (using a selected material from those produced in the paper). Both pipes were selected with dimensions to assess an equal annular stiffness (the same deformation for a similar compressive load). The pipe produced from the solid material had a density of 920 kg/m^3 and a thickness of 8 mm. The optimum foam had a density of 312 kg/m^3 and a thickness of 14.3 mm. It was calculated (last column) that the pipe produced with the foam has a smaller weight (1.26 kg in spite of 2.1 kg), therefore a 40% reduction in weight was obtained for a similar annular stiffness.

In addition, another advantage is that the maximum stress on the foamed pipe was much smaller (**Table 1** and **Figure 7**). In this case the reduction was much higher, from 1.37 MPa in the solid pipe to 0.42 MPa in the foamed pipe (a 69% reduction).

Finally, a map for pipes with equivalent bending stiffness was obtained (**Figure 8**). In this diagram the mass of the pipe is presented as a function of the foam density, three types of materials are considered. First, ideal materials, following a power law relationship between modulus and density with exponent equal to one, second typical foams that it is known[20] follow a power law relationships between modulus and density with exponent equal to two, and third the materials analysed in this paper that follow the relationship given in equation 3.

Several interesting conclusions are obtained from this figure. On the one hand, it can be concluded than for pipes loaded in compression, the minimum

Table 1.

Case	Thickness (mm)	Density (kg/m^3)	Deformation (mm)	Stress (MPa)	Mass (kg)
Solid Pipe	8	910	9.43	1.37	2.10
Foam Pipe	14.3	312	9.34	0.42	1.26

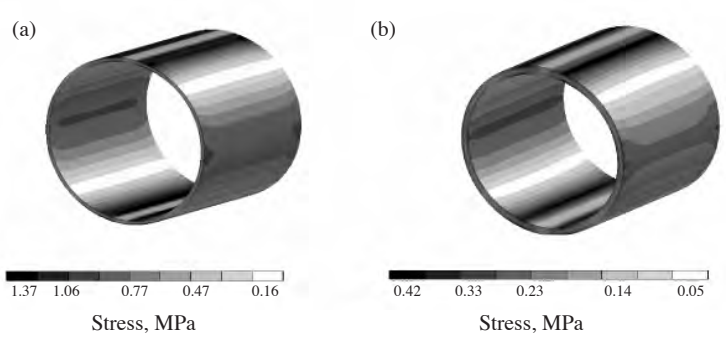

Figure 7. Equivalent stress distribution of a) solid polymer b) foam of 310 kg/m^3 in density. Values in the scale bar are in MPa.

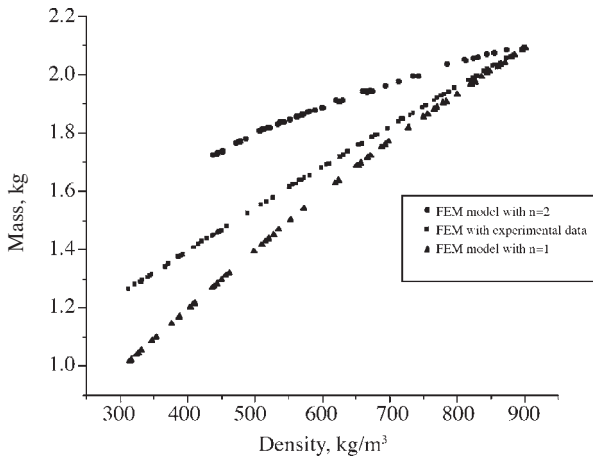

Figure 8. Mass of *vs* foam density for pipes with equal stiffness. The three curves correspond to: (linear) materials following a power law relationships with exponent equal to one, (quadratic) materials following a power law relationships with exponent equal to two, and (experimental data) the materials analysed in this paper that follow the relationships given in equation 3

weight for a given stiffness is reached by using low density foams; in other words it can be said that for this geometry (pipes loaded in compression) foams are stiffer materials than solids at equivalent weight. On the other hand, the maximum weight reduction (minimum panel weight) is obtained for materials with a power law with exponent equal to one, followed by the materials in this study and the materials following a quadratic trend with density. The weights reductions for a relative density of 0.5 are: linear law 38%, experimental data 28%, quadratic law 18%. These data clearly point out the importance of producing foams in which the mechanical properties at low strains take values close to the linear relationship. As it can be observed in the data, the materials produced in this paper give very close weight reductions to the ideal trend for high density foams and intermediate values between the optimum values and the ones obtained using the quadratic trend for mediums and lower density foams.

5. SUMMARY AND CONCLUSIONS

A collection of high density polyethylene foams with cell sizes in the microcellular range have been produced using a novel procedure based on an improved compression moulding technique. This process allows controlling the foam density and the cell size in an independent way.

The cellular structure of the foams was very homogeneous with cell sizes around 50 microns, having the materials a skin-core morphology. The cell size increased and the cell density decreased with a reduction of the density as it is expected for materials produced from a chemical blowing agent. Materials with different cell sizes for a given density were produced, but no improvement of the Young's modulus and the collapse stress was obtained using this strategy. The Young's modulus followed a linear trend with reduced values higher than those of the solid material at high densities. Using finite element modelling it has been demonstrated that the materials can be used to produce light weight structural pipes. Weight reductions up to 40% can be reached using the foams produced in this paper with densities in the range of 300 kg/m^3.

ACKNOWLEDGEMENTS

Financial assistance from the Local Government (Junta of Castile and Leon (VA047A07), Excellence Group (GR39)), Spanish Ministry of Education and Science and FEDER program (project MAT 2006 1614-C03-01) is gratefully acknowledged.

REFERENCES

1. K.T. Okamoto, *Microcellular Processing*, Hanser Publishers, Munich 2004.
2. C.B. Park in: *Foam Extrusion: Principles and Practise*, Ed. S.T. Lee, Technology Publishing Company, USA, 2000, Chapter 11.
3. J. Colton and N.P. Suh, *Polymer Engineering and Science*, **27** (1987) 485.
4. R.E. Murray, J.E. Weller and V. Kumar, *Cellular Polymers*, **19** (2000) 413.
5. V. Kumar and J.E. Weller, *International Polymer Processing*, **8** (1993) 73.
6. K.A. Arora, A.J. Lessor and T.J. McCarthy, *Macromolecules*, **31** (1998) 4614.
7. V. Kumar, M. VanderWel, J.E. Weller, and K.A. Seeler, *Journal of Engineering Materials and Technology*, **116** (1994) 439.
8. G. Wing, A. Pasricha, M. Tuttle and V. Kumar, *Polymer Engineering and Science*, **35** (1995) 673.
9. H. Sun, G.S. Sur, and J.E. Mark, *European Polymer Journal*, **38** (2002) 2373-2378.
10. H. Sun and J.E. Mark, *J. Appli. Polym. Sci.*, **86** (2002) 1692-1701.
11. J.E. Martini, N.P Suh and F.A. Waldman, US patent 4473655, 1984.
12. V. Kumar, in: *Handbook of Polymeric Foams*, Ed: David Eaves, Rapra Technology, UK 2004, Chapter 10.
13. C.B. Park, A.H. Behravesh and R.D. Venter, *Polymeric Foams: Science and Technology*, Ed., K.C. Khemani, *ACS Symposium Series No. 669*, ACS, Washington, DC, USA, 1997.
14. B. Seibig, Q. Huang and D. Paul, *Cellular Polymers*, **19** (2000) 93.
15. A.J. Bledzki, J. Kuhn, H. Kirschiling, and W. Pitscheneder, *Cellular Polymers*, **27** (2008) 91-100.
16. R.R. Puri and K.T. Collington, *Cellular Polymers*, **7** (1988) 57.
17. R.R. Puri and K.T. Collington, *Cellular Polymers*, **7** (1988) 219.
18. D. Eaves, in: *Handbook of Polymeric Foams*, Edited by D. Eaves, Rapra Technology, UK, 2004.
19. M.A. Rodriguez-Pérez, M.A. del Carpio, J.F. Lopez-Díaz and J.A. de Saja, *Procedure to produce moulded pipes with cranial microcellular structure*, Spanish Patent nº P200602638, 2006 (PCT applied 2007).
20. L.J. Gibson and M.F. Ahsby, *Cellular Solids, Structure and Properties*, Cambridge University Press, UK, 1997.
21. M.A. Rodríguez-Pérez, J.I. Velasco, D. Arencón, O. Almanza and J.A. de Saja, *J. Appl. Polymer Sci*, **75** (2000) 156-166.

22. M.A. Rodríguez-Pérez, O. Almanza, J.L. Ruiz-Herrero and J.A. de Saja, *Cellular Polymers*, in press, 2008.

23. M.A. Rodríguez-Pérez, J.I. González-Peña, N. Witten and J.A. de Saja, *Cellular Polymers*, **21** (2002) 165-194 .

24. M.A. Rodríguez-Pérez, *Cellular Polymers,* **21** (2002) 117-136.

7.3 Paper: Mechanical Response of Polyethylene Foams with High Densities and Cell Sizes in the Microcellular Range.

Mechanical Response of Polyethylene Foams with High Densities and Cell Sizes in the Microcellular Range

M. A. RODRIGUEZ-PEREZ,* J. LOBOS,
C. A. PEREZ-MUÑOZ AND J. A. DE SAJA
Celllular Materials Group (CellMat), Condensed Matter Physics Department, University of Valladolid, 47011 Valladolid, Spain

ABSTRACT: This article presents the compressive mechanical response at low strains for a collection of polyethylene foams with high densities and cell sizes in the microcellular range. The materials under study had a relative density between 0.27 and 0.92, a homogeneous and multi-structured cellular structure with a dense skin and a foamed core. The Young's modulus and collapse stress were reduced when density did, the modulus following a linear trend and the collapse stress a quadratic tendency. For relative densities higher than 0.7, the materials showed Young's modulus slightly above the limit given by a potential law with exponent equal to one. In addition, it has been proved that variations in the cell size did not influence the elastic properties. The advantages of using these materials for flat structural panels have been analyzed. A reduction of the weight of flat panels loaded in bending of up to 35% can be reached by using these foams in spite of the solid sheet from which the foam was produced.

KEY WORDS: polyethylene foams, microcellular foams, mechanical properties.

INTRODUCTION

Microcellular plastics are foamed polymers characterized by cell sizes averaging 100 μm or less, typically between 5 and 50 μm [1]. These materials exhibit high Charpy impact strength, high toughness,

*Author to whom correspondence should be addressed. E-mail: marrod@fmc.uva.es
Figure 2 appears in color online: http://cel.sagepub.com

0021-955X/09/05 0389–15 $10.00/0 DOI: 10.1177/0021955X09103946

high fatigue life, high thermal stability, and low thermal conductivity [2] than solid polymers. Because of these unique properties, a large number of innovative applications can be imagined. These include food packaging with reduced materials costs, pipes or panels with improved strength-to-weight ratio, airplane and automotive parts with improved strength and acoustic dampening, sporting equipment with reduced weight and high energy absorption, etc. Due to these potential applications, over the last two decades substantial research and development has been conducted on the topic of microcellular processing and characterization of microcellular products [3–10].

Microcellular plastics were initially produced at Massachusetts Institute of Technology (MIT) using a batch process [11] with three main steps: dissolution of a gas (mainly CO_2 or N_2) in the solid plastic, release of the pressure to create a supersaturated solid with gas, and heating of the material to promote expansion. This process has been mainly used to produce microcellular foams of amorphous materials with cells sizes around 10 μm [12].

The previous concept has been extended to the production of microcellular foams by injection molding and extrusion [1,2,13–15], and although considerable progress has been reached in these areas, there is still a need for further research. For instance, in injection molding there is a poor surface quality of the produced products in conventional processing [1,15], three is a limitation in the maximum size of the produced parts [1], and a limited weight reduction of the parts, not higher than 30–35% [1]. In extrusion, most of the studies have been performed at a laboratory scale or at a semi-industrial scale and as far as we know microcellular foams of semicrystalline polymers are not produced industrially by extrusion. Only polystyrene has been successfully commercialized [12].

One aspect in which the topic microcellular foams needs more detailed studies is connected with the mechanical characterization of these products. Although several investigations have analyzed the mechanical properties [1,4,7–10,16,17] there is still a need to know the effect of cell size on the elastic response, the effect of the presence of a thick skin on the strength, the properties of these materials in comparison with foams produced from conventional technologies, etc.

Finally, another open aspect of interest is the identification of industrial areas in which these materials can play a key role [12]. In order to do this, it is necessary first to establish the structure–property relationships for these materials and second to evaluate the potential advantages of these materials over competitive products in diverse applications. One area of potential interest is the possibility of using the

materials in flat panels of higher stiffness and lower weights with the idea of replacing the solid material. As it is expected that microcellular foams could have better mechanical properties than conventional foams this approach seems to be an interesting way of improving the properties of conventional panels.

This article focuses on these last aspects (mechanical characterization of foams with cell sizes in the microcellular range and identification of potential applications areas for these materials), producing high-density polyethylene foams with cell sizes in the range of 50 μm, characterizing the cellular structure, mechanical properties, and structure property relationships and performing finite element modeling (FEM) of flat panels to show the potential of these materials as structural elements. The aims of the article are to gain knowledge on both the structure–property relationships for foams of high density and with cell sizes in the microcellular range and the potential applicability of these materials.

MATERIALS

A low-density polyethylene was used as the matrix polymer (MFI = 4 g/10 min at 190°C, density 920 kg/m^3). Azodicarbonamide with a particle size of 4.9 μm was used as blowing agent. Typical amounts of stearic acid and zinc oxide were used as processing aid and catalyzer of the decomposition reaction of the blowing agent, respectively [18,19]. No crosslinking agents were used; therefore noncrosslinked cellular materials were fabricated. Foams were produced by a modified compression molding technique [20] in a one-step process. Densities of the produced foams ranged between 250 and 750 kg/m^3, i.e., relative densities in the range 0.27–0.92. Cylindrical samples of 22.8 mm in diameter and 17.5 mm in height were used in the investigation.

EXPERIMENTAL

Density Measurements

Density measurements were performed by Archimedes principle using the density determination kit for a AT261 Mettler balance (ASTM D792-00).

Scanning Electron Microscopy

Quantitative analysis was used to characterize the cellular structure. For this purpose, sections containing the sheets normal were microtomed at low temperature to provide a smooth surface that was vacuum-coated

with gold and examined by scanning electron microscopy (SEM) using a JEOL JSM 820. Cell size distributions were measured and used to determine the average cell size. Cell density was calculated as the number of cells per unit volume of the unfoamed material using the equation:

$$N = \left(\frac{n_b}{A}\right)^{3/2}\left(\frac{\rho_s}{\rho_f}\right) \quad (1)$$

where n_b is the number of cells in a defined area A, and ρ_s is the density of the unfoamed solid, and ρ_f is the density of the foam.

Compression Experiments

Compressive stress (s) strain (ε) curves were measured using an Instron machine (model 5500R6025) at room temperature and at a strain rate of 1 mm/min. The maximum static strain was approximately 75% for all the experiments. These experiments were used to determine the foam Young's modulus and the collapse stress [21,22].

Finite Element Modeling

The size of the modeled sheets was $1000 \times 1000\,mm^2$, the thickness being used as an adjustable parameter in the variational analysis. The sheets were homogeneously supported in their edges. A disk of steel was located in the center of the sheets. This disk has a diameter of 550 mm and a thickness of 100 mm (Figure 1). The applied load was selected in order to have a defection lower than a 1% of the sheets length, i.e., 10 mm.

Initially, the static structural simulation was carried out for a 10 mm thick polyethylene solid sheet. The large-scale effects of inertia and damping were neglected in all calculations. The mesh was generated using Brick 8 node 185 and mapped face meshing elements. In a second step the simulation was performed using the same type of

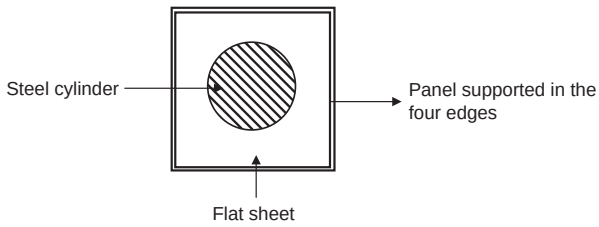

Figure 1. Geometry of the applied load in the FEM.

approximations and meshes but in this case foam panels were simulated. In order to do that, the relationship between Young's modulus and density for the foams under study was introduced in the analysis. In a third step, a variational analysis (goal-driven optimization) was performed in order to select the density and thickness of the panel with optimum performance (similar bending stiffness than that of the dense panel and minimum weight). The analysis was carried using a genetic multi-objective algorithm (MOGA), which is able to optimize problems with continuous input parameters.

In all cases, the selected input parameters were the foam density, the foam Young's modulus and the sheet thickness. The response parameters were the maximum sheet deformation, the maximum stress and the sheet weight. The objective was to find out the panel (density and thickness) with a similar stiffness to that of the dense polyethylene panel and with a minimum weight.

RESULTS

Cellular Structure

Figure 2(a) shows the typical cellular structure of the inner part of one of the foams (density 550 kg/m^3). It can be observed that the foam has a very homogeneous closed-cell cellular structure. Cells with diameters lower than 50 μm are observed. In addition, the foams presented skin–core morphology as it can be appreciated in Figure 2(b) for the same material. The skin has a higher density than the core, giving materials with a spatial mass distribution, which optimizes physical properties and surface quality.

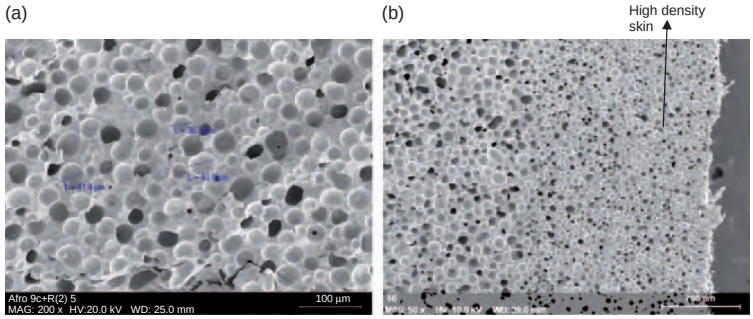

Figure 2. SEM micrograph of the inert part of one of the produced materials (density 550 kg/m^3).

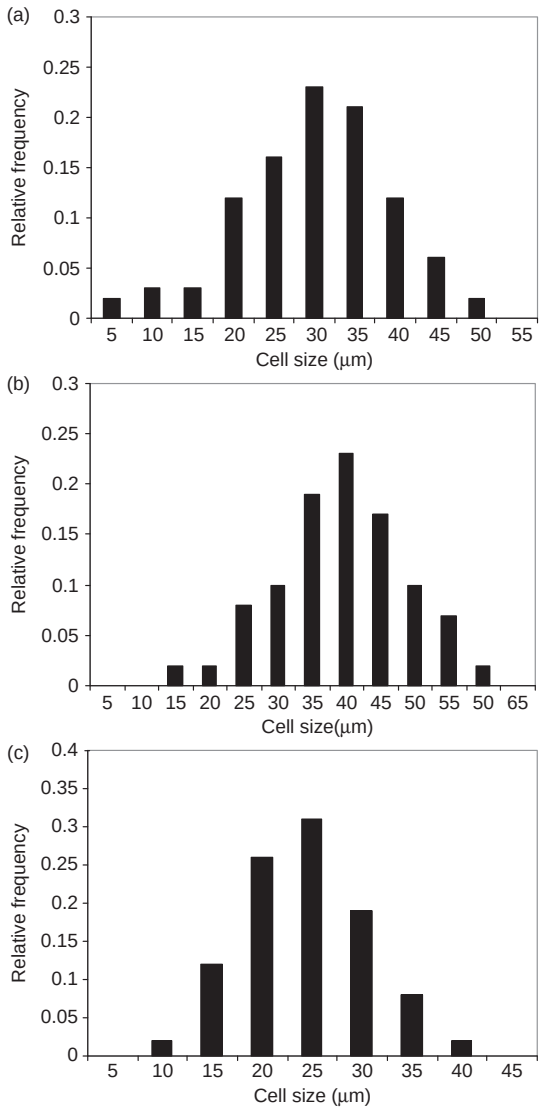

Figure 3. Cell sizes distribution of different samples: (a) density 550 kg/m^3, (b) density 750 kg/m^3, (c) density 730 kg/m^3.

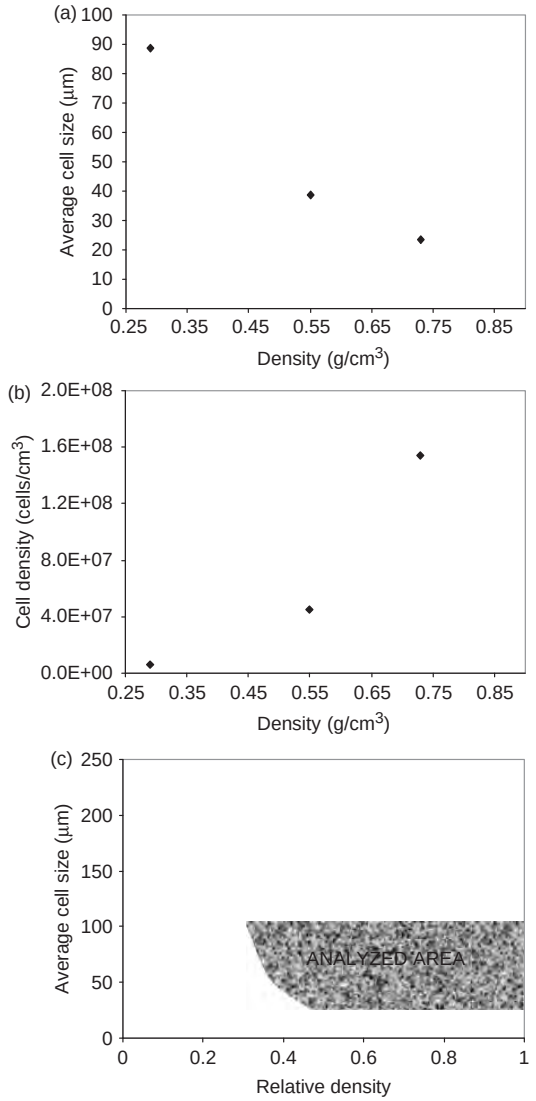

Figure 4. (a) Average cell size vs. density, (b) cell density vs. density, (c) density and cell size of the analyzed foams.

The cell size distribution of several materials is presented in Figure 3. It is seen that distributions are symmetrical with average values below 50 μm for foams of 500 and 750 kg/m^3.

Figure 4(a) and (b) summarizes several general trends of the average cell size, and cell density for some of the foams under study. As expected for foams produced using a chemical blowing agents [23] cell size is reduced and cell density is increased when density is increased. Appreciable values of cell density (higher than 10^8 cells/cm^3) were obtained for high-density foams. These values strongly decreased for the lower density foams.

By controlling the formulation of the precursor materials used for foaming it was possible to produce foams with relative densities in the range 0.27–0.92 and with average cell sizes in the range 25–100 μm, as it is depicted in Figure 4(c). The possibility of fabricating foams with a similar density but with a different cellular structure made possible analyzing independently the effect on both parameters in the mechanical response as it is explained in the next section.

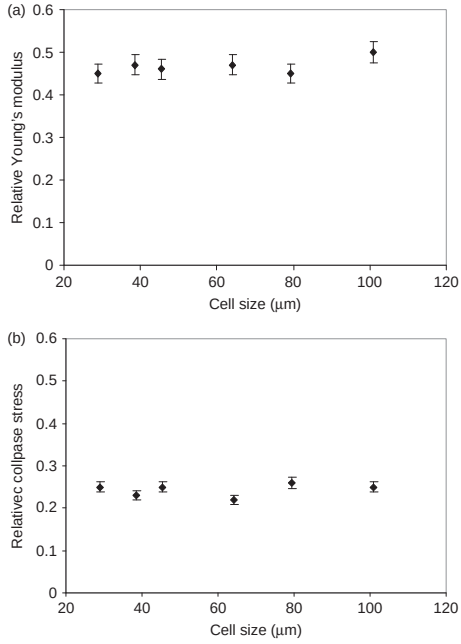

Figure 5. Relative Young's modulus and relative collapse stress as a function of cell size for foams with a relative density of 0.6.

Mechanical Properties

Figure 5 shows the Young's modulus and collapse stress of the foams as a function of cell size for a given relative density (0.60 in this case). Similar results were found for other densities. It can be observed that both parameters showed constant values in the cell size range between 30 and 100 μm. This result was also found for low-density foams [24]. It is an important finding from a practical point of view because it indicates that for materials working in the elastic regime it is not possible to improve the stiffness by only reducing the cell size.

As the mechanical properties did not show a dependency with cell size the average values of the Young's modulus for foams of a given density were obtained and analyzed as a function of the foams density. Figure 6 shows the experimental results compared with two lines that were

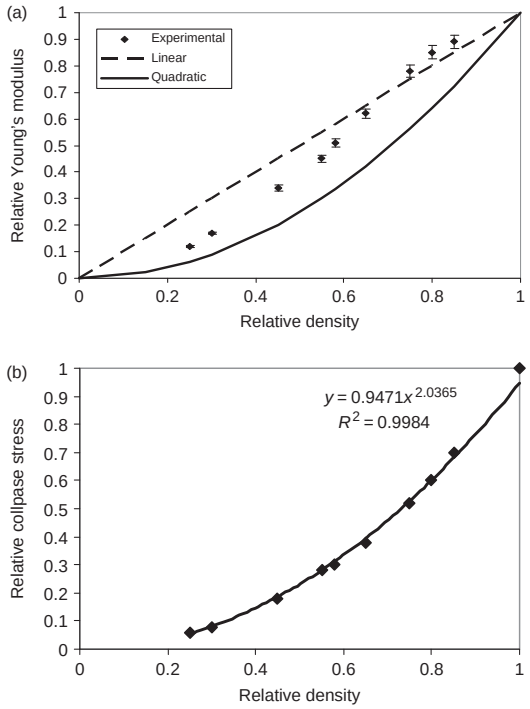

Figure 6. Relative Young's modulus and relative collapse stress as a function of density.

obtained using a potential law of relative Young's modulus versus relative density (Equation (2)) with exponent $n = 1$ and exponent $n = 2$. C was assumed to be 1 in these plots [20].

$$\frac{E_f}{E_s} = C\left(\frac{\rho_f}{\rho_s}\right)^n \tag{2}$$

where E_f and ρ_f are the foam Young's modulus and the foam density, respectively, and E_s and ρ_s are the modulus and the density of the solid material, respectively.

Values of n between 1 and 2 are typical for a wide amount of cellular materials [20], and therefore, it is expected that most foams, including the ones in this article, would have properties between these two trends.

The materials under study followed an approximately linear trend given by Equation (3).

$$\frac{E}{E_s} = \left[1.292\frac{\rho}{\rho_s} - 0.285\right] \tag{3}$$

A detailed analysis of Figure 6 shows different trends depending on the foam density. At high relative densities, the mechanical properties of the produced foams are slightly above the linear trend. This shows that in this density range the foams have very interesting mechanical properties. For relative densities below 0.7, the properties are between the linear trend and the parabolic one. For densities below 0.5 the properties are closer than to those of a potential law with exponent 2. Two different structural sources can be the origin of this nonunique trend with foam density. On the one hand, the different thickness of the skin for foams with different densities. Figure 7 shows that at low densities the skin seems to have a smaller density, which would reduce the mechanical properties. On the other hand, the different open cell

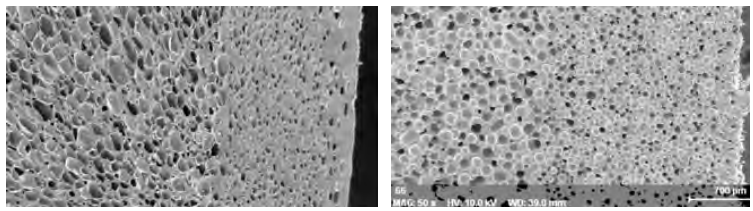

Density 730 kg/m^3 Density 550 kg/m^3

Figure 7. Presence of a more dense skin in samples with a higher density.

content of foams with different densities. As the low-density polyethylene of this study was not crosslinked, an increase of the open cell content in the materials was expected when the density was reduced and an increase of the open cell content will also reduce the foam stiffness [25].

The results for the collapse stress are given in Figure 6. It is observed that in this case a power law relationship with exponent 2 has been obtained in agreement with predictions for an elastic collapse of the cellular structure [20].

Table 1. Optimum design of the flat panel.

Material	Tickness (mm)	Density (kg/m^3)	Deformation (mm)	Stress (MPa)	Weight (kg)
Polyethylene solid	10	920	10.00	1.056	9.10
Polyethylene foam	18.927	316.5	9.85	0.294	5.99

FEM of the Foams Behavior in Flat Panels

Table 1 shows the results for the FEM comparing the behavior of a solid sheet with that of the optimum foam for this application (selected from those produced in the article). Both panels were selected with dimensions to assess an equal bending stiffness (the same deformation for a similar applied load). The panel produced from the solid material had a density of 920 kg/m^3 and a thickness of 10 mm and the optimum foam had a density of 310 kg/m^3 and a thickness of 18.9 mm. It was calculated (last column) that the panel produced with the foam has a smaller weight (5.99 kg in spite of 9.1 kg), therefore a 34% reduction in weight was obtained for a similar bending stiffness.

In addition, another advantage is that the maximum stress on the panel was much smaller for the cellular material than for the continuous solid material (Table 1 and Figure 8). In this case the reduction was much higher, from 1.06–0.29 MPa (a 72% reduction).

Finally, a map for panels with equivalent bending stiffness was obtained (Figure 9). In this diagram the mass of the panel is presented as a function of the foam density. Three types of materials are considered. First, ideal materials following a power law relationship between modulus and density with exponent equal to one; second, typical foams that is known to follow a power law relationship between modulus and density with exponent equal to two [20]; and third the

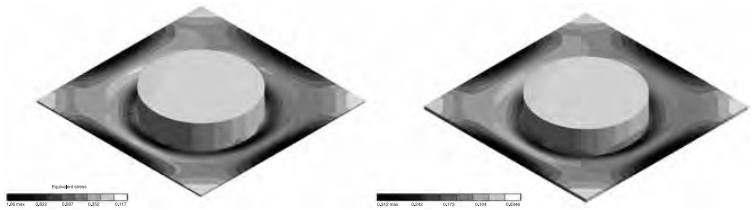

Figure 8. Equivalent stress distribution of (a) solid polymer (b) foam of 310 kg/m^3 in density.

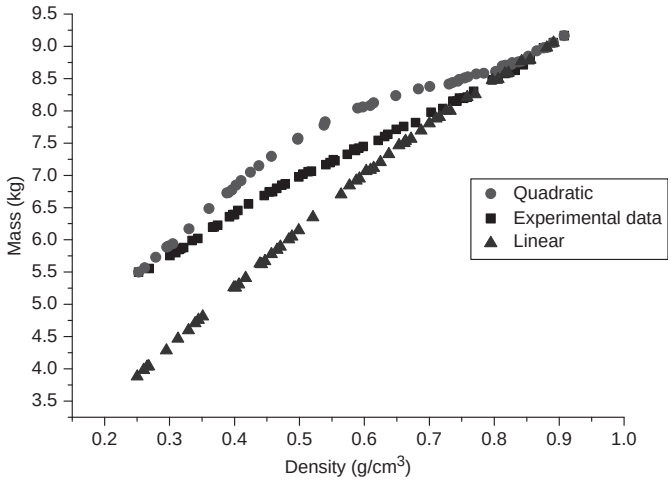

Figure 9. Mass of flat panels vs. foam density for panel with equal bending stiffness. The three curves correspond to: (linear) materials following a power law relationship with exponent equal to one, (quadratic) materials following a power law relationship with exponent equal to two, and (experimental data) the materials analyzed in this article that follow the relationships given in Equation (3).

materials analyzed in this article that follow the relationships given in Equation (3).

Several interesting conclusions are obtained. On the one hand it can be concluded that for panels loaded in bending, the minimum weight for a given stiffness is reached by using low-density foams; in other words, it can be said that for this geometry foams are stiffer materials than solids

at equivalent weight. On the other hand, the maximum weight reduction (minimum panel weight) is obtained for materials with a power law with exponent equal to one, followed by the materials in this study and the materials following a quadratic trend with density. The weights reductions for a relative density of 0.5 are: linear law 36%, experimental data 26%, quadratic law 17%. These data clearly point out the importance of producing foams in which the mechanical properties at low strains could take values close to the linear relationship. As it can be observed in the data, the materials produced in this article give very close weight reductions to the ideal trend for high-density foams and intermediate values between the optimum values and the ones obtained using the quadratic trend for mediums and lower density foams.

SUMMARY AND CONCLUSIONS

A collection of high-density polyethylene foams with cell sizes in the microcellular range have been produced. The cellular structure and compressive mechanical properties at low strains have been measured. The use of these products as materials for lightweight panels has been analyzed using FEM. The cellular structure of the foams was very homogeneous with cell sizes around 50 μm, the materials having a skin–core morphology. The cell size increased and the cell density decreased with a reduction of the density as it is expected for materials produced from a chemical blowing agent. Materials with different cell sizes for a given density were produced, but no improvement of the Young's modulus and the collapse stress was obtained using this strategy. The Young's modulus followed a linear trend with values slightly above the theoretical limit for relative densities above 0.7, which seems to be due to the presence of a thick skin. Using FEM it has been demonstrated that the materials can be used to produce lightweight structural panels. Weight reductions up to 34% can be reached using foams with densities in the range of 300 kg/m^3. In addition, FEM has allowed obtaining the weight reduction that could be obtained by using foams following a linear relationship between modulus and density.

ACKNOWLEDGMENTS

Financial assistance from the Local Government (Junta of Castile and Leon (VA047A07 and excellence group GR39)), Spanish Ministry of Education and Science and FEDER program (project MAT 2006 1614-C03-01) is gratefully acknowledged.

REFERENCES

1. Okamoto, K.T. (2004). *Microcellular Processing*, Munich, Hanser Publishers.
2. Park, C.B. (2000). Continuous Production of High-density and Low-density Microcellular Plastics in Extrusion, In: Lee, S.-T. (ed.), *Foam Extrusion: Principles and Practise,* USA, Technomic Publishing Company, USA, Chapter 11, pp. 263–305.
3. Colton, J. and Suh, N.P. The Nucleation of Microcellular Thermoplastic Foam with Additives: Part I: Theoretical Considerations, *Polym. Eng. Sci.*, 1987: **27**: 485–492.
4. Murray, R.E., Weller, J.E. and Kumar, V. Solid-State Microcellular Acrylonitrile-Butadiene-Styrene Foams, *Cell. Polym.*, 2000: **19**: 413–425.
5. Kumar, V. and Weller, J.E. A Process to Produce Microcellular PVC, *Int. Polym. Proc.*, 1993: **8**: 73–80.
6. Arora, K.A., Lessor, A.J. and McCarthy, T.J. Preparation and Characterization of Microcellular Polystyrene Foams Processed in Supercritical Carbon Dioxide, *Macromolecules*, 1998: **31**: 4614–4620.
7. Kumar, V., VanderWel, M., Weller, J.E. and Seeler, K.A. Experimental Characterisation of the Tensile Behaviour of Microcellular Polycarbonate Foams, *J. Eng. Mater. Technol.*, 1994: **116**: 439–445.
8. Wing, G., Pasricha, A., Tuttle, M. and Kumar, V. Time Dependent Response of Polycarbonate and Microcellular Polycarbonate, *Polym. Eng. Sci.*, 1995: **35**: 673–679.
9. Sun, H., Sur, G.S. and Mark, J.E. Microcellular Foams from Polyethersulfone and Polyphenylsulfone: Preparation and Mechanical Properties, *Eur. Polym. J.*, 2002: **38**: 2373–2378.
10. Sun, H. and Mark, J.E. Preparation, Characterization, and Mechanical Properties of Some Microcellular Polysulfone Foams, *J. Appl. Polym. Sci.*, 2002: **86**: 1692–1701.
11. Martini, J.E., Suh, N.P. and Waldman, F.A. (1984). US Patent 4473655.
12. Kumar, V. (2004). Microcellular Plastics, In: Eaves, D. (ed.), *Handbook of Polymeric Foams*, Chapter 10, UK, Rapra Technology.
13. Park, C.B., Behravesh, A.H. and Venter, R.D. Polymeric Foams: An Overview, In: Khemani, K.C. (ed.), *Polymeric Foams: Science and Technology*, Washington, DC, USA, ACS Symposium Series No. 669, pp. 1–7.
14. Seibig, B., Huang, Q. and Paul, D. Design of a Novel Extrusion System for Manufacturing Microcellular Polymer, *Cell. Polym.*, 2000: **19**: 93–102.
15. Bledzki, A.J., Kuhn, J., Kirschiling, H. and Pitscheneder, W. Microcellular Injection Molding of PP and PC/ABS with Precision Mold Opening and Gas Counterpressure, *Cell. Polym.*, 2008: **27**: 91–100.
16. Shimbo, M., Higashitani, I. and Miyano, Y. Mechanisms of Strength Improvement of Foamed Plastics having Fine Cells, *J. Cell. Plast.*, 2007: **43**(2): 157–167.
17. Shimbo, M., Baldwin, D.F. and Suh, N.P. (1999). Viscoelastic and Mechanical Behavior of Microcellular Plastics with Varying Cell Size,

In: *Proceedings of the Conference on Advances Technology on Experimental Mechanics*, pp. 309–313.

18. Puri, R.R. and Collington, K.T. The production of Cellular Crosslinked Polyolefins. 2. The Injection-Molding and Press Molding Techniques, *Cell. Polym.*, 1988: **7**(57): 219–231.
19. Eaves, D. (ed.) (2004). In: *Handbook of Polymeric Foams*, Chapter 8, UK, Rapra Technology.
20. Rodriguez-Pérez, M.A., del Carpio, M.A., Lopez-Díaz, J.F. and de Saja, J.A. (2006). Procedure to Produce Moulded Pipes with Cranial Microcellular Structure, Spanish Patent No. P200602638 (PCT Applied 2007).
21. Gibson, L.J. and Ahsby, M.F. (1997). *Cellular Solids, Structure and Properties*, UK, Cambridge University Press.
22. Rodríguez-Pérez, M.A., Velasco, J.I., Arencón, D., Almanza, O. and de Saja, J.A. Mechanical Characterization of Closed-cell Polyolefin Foams, *J. Appl. Polym. Sci.*, 2000: **75**: 156–166.
23. Rodríguez-Pérez, M.A., Almanza, O., Ruiz-Herrero, J.L. and de Saja, J.A. The Effect of Processing on the Structure and Properties of Mechanical Response of Polyethylene Foams 15 Crosslinked Closed Cell Polyethylene Foams, *Cell. Polym.,* 2008: **27**: 179–200.
24. Rodríguez-Pérez, M.A., González-Peña, J.I., Witten, N. and de Saja, J.A. The Effect of Cell Size on the Physical Properties of Crosslinked Closed Cell Polyethylene Foams Produced by a High Pressure Nitrogen Solution Process, *Cell. Polym.*, 2002: **21**: 165–194.
25. Rodríguez-Pérez, M.A. The Effect of Chemical Composition, Density and Cellular Structure on the Dynamic Mechanical Response of Polyolefin Foams, *Cell. Polym.*, 2002: **21**: 117–136.

7.4 Conclusions

A collection of high density structural polyethylene foams with cell sizes in the microcellular range have been produced using a novel procedure based on an improved compression moulding technique. This process allows controlling the foam density and the cell size in an independent way.

The cellular structure and compressive mechanical properties at low strains have been measured. The cellular structure of the foams was very homogeneous with cell sizes around 50 microns, having the materials a skin-core morphology. The cell size increased and the cell density decreased with a reduction of the density as it is expected for materials produced from a chemical blowing agent.

Materials with different cell sizes for a given density were produced, but no improvement of the Young's modulus and the collapse stress was obtained using this strategy. The Young's modulus followed a linear trend with values slightly above the theoretical limit for relative densities above 0.7, which seems to be due to the presence of a thick skin.

Using FEM it has been demonstrated that the materials can be used to produce lightweight structural panels and pipes. In panels weight reductions up to 34% can be reached using foams with densities in the range of 300 kg/m^3. In pipes weight reductions up to 40% can be reached using foams with densities in the same range.

8 Thermal properties and cellular structure

Resumen (Spanish):

En este capítulo se continua el estudio de los materiales celulares en base polietileno producidas con el método desarrollado para la presente tesis. Se estudia por un lado la estructura celular a la escala mesoscopica, analizando los gradientes de densidad presentes en la muestras y a escala microscópica, estudiando la estructura celular. Además se analiza la conductividad térmica de los materiales y se establece un sencillo procedimiento para determinar los gradientes de densidad presentes en los materiales mediante medidas de la conductividad térmica usando el método TPS (transient plane source method).

8.1 Introduction

The present section focus on the analysis of the skin-core morphology, cellular structure and thermal conductivity of the LDPE foams produced by the improved compression molding technology and presented in the previous chapter.

8.2 Thermal conductivity in foams

One of the most important functional properties of polymeric foams is their insulating capacity. Thus, the study of thermal conductivity in polymeric foams has become a subject of basic research for many years [1-4].

In order to measure the thermal properties of polymeric and metallic foams CellMat laboratory update a few years ago their measurement systems with the acquisition of a equipment based on the Transient Plane Source method (TPS)[4,5].

The main advantage of this technique is the possibility of measuring materials with very different thermal conductivity (from polymeric foams to metals). The second peculiarity of the system is that TPS locally measures the thermal conductivity of a volume of material next to the sensor, so it is possible to measure samples of various sizes and shapes as long as the heat flow during the experiment is enclosed within the volume to be measured[5]. Due to this it is possible to characterize small samples and localized areas of a given material.

Previous papers of our laboratory [4,6-8] prove that this measuring method is sensitive to the presence of defects and density gradients in cellular metals. As the produced LDPE foams showed a skin-core morphology it is expected a different thermal behavior of the area near the skin and the area in the centre. The measurements performed using the TPS has been analyzed taking into account this aspect.

It is known[1,4] that the thermal conductivity in polymeric foam can be separated into separate inputs for each mechanism of heat transfer, as is show in equation 8.1

$$\lambda = \lambda_s + \lambda_g + \lambda_c + \lambda_r \quad (8.1)$$

The four contributions to the heat transfer are λ_s that is the thermal conductivity for the solid phase, λ_g that is the thermal conductivity for the gas phase, λ_c that is the thermal conductivity by convection in the gas phase and λ_r that is the thermal conductivity by radiation.

Several authors have demonstrated [9] that the convection in the gas phase only occurs when the cells have diameters exceeding 4mm. As it has been showed in the previous chapters the produced foams have much smaller cell diameters the convection contribution can be neglected.

In addition the volume occupied by the polymer is very high (high relative density) compared with the common insulating foam[3]. Then given the high amount of polymer the emitted photons will be absorbed very quickly without being able to move a large distance. Then the radiative term will be also very small. It has been proved that this contribution is neglected for relative density above 0.1

In addition the volume occupied by the polymer is very high (high relative density) compared with the common insulating foam [3]. Then given the high amount of polymer the emitted photons will be absorbed very quickly without being able to move a large distance. Then the radiative term will be also very small. It has been proved that this contribution is neglected for relative density above 0.1[10].

The first objective of the paper included in this chapter is characterizing the thermal conductivity of the foams produced as a function of the relative density and analyzing the effects of density gradients on this thermal property

8.3 Nucleation and coalescence in cellular polymers

The improved compression molding technology allows producing foams with similar density but using different chemical compositions or processing parameters. This is an interesting option to perform scientific studies in several aspect connected to the foaming mechanisms and/or the physical properties. Part of the paper presented in this chapter is devoted to the analysis of the cellular structure of foams with similar relative densities but produced with different amounts of azodicarbonamide as chemical blowing agent. The results are useful to understand the role played by the residues of this blowing agent as nucleating sites for the cells and to analyze the coalescence phenomena taking place during foaming as a function of the final density and blowing agent concentration.

8.4 Paper: Density gradients, cellular structure and thermal conductivity of polyethylene foams producing with different amounts of chemical blowing agent.

Density gradients, cellular structure and thermal conductivity of polyethylene foams producing with different amounts of chemical blowing agent.

J.Lobos, J.A. de Saja, M.A. Rodrigez-Perez

Cellular Materials Laboratory (CellMat). Condensed Matter Physics Department, University of Valladolid, 47011 Valladolid, Spain.

Abstract

Foams of LDPE have been produced using the improved compression moulding technique (ICM) with relative densities from 0.3 to 0.7 and with different contents of chemical blowing agent (from 1% to 20%). The density gradients, cellular structure and thermal conductivity of the foams have been characterized. It has been proved that the density and the amount of CBA used have a significant influence on the cellular structure both at the mesoscale (density gradients) and at the microscale, (different cell sizes and cell densities). In addition, the thermal conductivity of the samples is very sensitive to the local structure in which the heat flow is located. The technique used to measure this property, the transient plane source method (TPS), allows detecting the presence of density gradients. A simple method to determine these gradients based on the thermal conductivity data has been developed.

1 Introduction

Polymeric foams can be defined as two-phase materials in which a gas is dispersed in a continuous macromolecular phase [1]. Due to their outstanding properties, thermoplastic foams have become essential items and although they are mainly used as thermal insulators or impact absorbing elements, they have found an application in almost every field, [2-4].

Since their development in 1940s, both scientific and industrial communities have focused their attention in the development of foaming technologies able to satisfy the growing demand of thermoplastic foamed products [3]. Nowadays, no single foaming method dominates thermoplastic foam manufacture, and both continuous and batch processes are operated using either chemical or physical blowing agents. The most commonly used foaming processes to produce thermoplastic foams are extrusion, injection moulding, compression moulding or batch foaming, (dissolution of a physical blowing agent at high temperature and/or pressure) [1, 5].

The election of the foaming process is conditioned mainly by the final application of the material which at the same time strongly depends on its relative density (i.e. the density of the foam divided by that of the corresponding solid). It is well known that foaming

process itself as well as the intrinsic characteristics of the polymeric matrix heavily determines the cellular structure of the foamed product [4, 5].

In the last years, CellMat laboratory has developed a new route to produce foams named improved compression moulding technique (ICM) [6-14]. In this route, foam density is controlled through the use of special moulds known as self-expandable moulds. Those moulds have the ability of applying and retaining pressure while the decomposition of the chemical blowing agent, subsequent dissolution of the gas phase and foaming. In addition, moulds are capable of controlling the expansion degree of the material hence regulating in a very accurate way both size and shape of the foamed part. The internal pressure of these moulds is determined by the amount of blowing agent in the precursor

One interesting aspect of this technique is that allows producing foams with the same density but very different cellular structures by modifying the chemical composition and/or the foaming parameters. Therefore, it is possible to produce interesting samples for scientific studies.

In the present paper foamed polyethylene samples are produced with different amounts of blowing agent (azodicarbonamide, from 1% to 20%). This allows obtaining a collection of samples with different cellular structures both at the mesoscopic and microscopic levels. The samples produced have been characterized by their relative density, thermal conductivity, cellular structure and X-ray radiographs. The main aim of the paper is gaining knowledge on the structure-property relationships for these materials and specifically in the dependence between the structure and the thermal conductivity of these materials.

2 Experimental

The raw materials used to produce the LDPE foams were:

1. Low density polyethylene (PE008) provided by Repsol Quimica with a melting temperature of 110ºC, MFI=4g/10min at 190ºC, density 923Kg/m^3.
2. Azodicarbonamide (AZO) provided by Uquinsa as blowing agent with an average particle size of 4.9µm.
3. Zinc oxide, Silox Active grade provided by Safin Alcan, used as catalytic of the chemical blowing agent
4. Stearic acid (Stearic Acid 301 supplied by Renichen) used as mixing processing aid.

The polymer, azodicarbonamide, stearic acid and zinc oxide were mixed, in the amounts described in Table 1, with a Haake torque rheometer type Rheodrive 5000 with type Rheomix 500 mixing head at 145ºC, 25 rpm, by 5 minutes with a total mass of 50 grams. The mixture was chopped in pieces of 2-8mm3 in volume (pellets) The homogeneity was checked by using three random samples of the mixture performing termogravimetry experiments.

Table 1: Composition of the foam precursors and the final residues of azodicarbonamide dispersed in the final foams.

	Afro-a	Afro-b	Afro-c	Afro-d	Afro-e	Afro-c+R
PE	98.6%	94.4%	89.3%	84.2%	79.3%	82.5%
AZO	1.2%	5.8%	10.5%	15.6%	20.5%	10.5%
AZO residue	-	-	-	-	-	6.6%
Octadecanoic acid	0.15%	0.15%	0.15%	0.15%	0.15%	0.15%
ZnO	0.05%	0.05%	0.05%	0.05%	0.05%	0.05%
Residues of azodicarbonamide in the polymer in the final foam						
	Afro-a	**Afro-b**	**Afro-c**	**Afro-d**	**Afro-e**	**Afro-c+R**
	0.8%	3.7%	6.8%	10.1%	13.2%	13.4%

The thermal decomposition of azodicarbonamide is produced at 210ºC without catalyser, 185ºC with 0.05% of ZnO[15,16]. During the decomposition the azodicarbonamide release 25.4% of its weight as gases at 190°C (N_2 71.9%, CO 26.3%, CO_2 1.4%, NH_3 0.4%) leaving 74.6% of solid residues in the polymer[16-18]. For the production of high density foams is enough to incorporate 1-2% of azodicarbonamide by weight in the polymer. However due to the special design of the moulds used in this paper, much higher amounts can be used to modify the cellular structure. Table 1 shows the azodicarbonamide amounts chosen (from 1 to 20%). Afro-c+R is a special composition with 10.5% of azodicarbonamide, plus 6.6% of azodicarbonamide residues The residues of azodicarbonamide were produced by heating the blowing agent at 190°C for 10 minutes. This material was produced to have the same amount of solid residues than Afro-c but a very different pressure during the foaming process.

The Improved Compression Moulding (ICM) route comprises the following steps. A certain amount of pellets are introduced in the mould (23mm in diameter, 27.5mm in height) and subjected to both temperature (T_P=120°C) and pressure (P_p=5Tn) to assure a good compaction of the pellets with the objective of producing the precursor material (Figure 1) .The density of the precursors were between 925kg/m^3 to 957kg/m^3 depending the amount of azodicarbonamide in the composition.

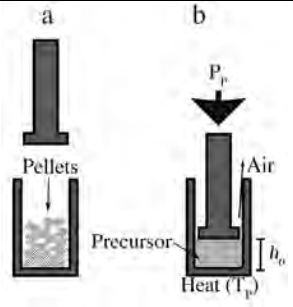

Figure 1: Compression of the pellets for the production of the precursors.

During the second and final step (Figure 2a-c) the precursor is introduced in the foaming mould (23mm in diameter and 27mm in height) which is located in a press for foaming. An initial pressure (P_0=15Tn) is applied while the mould is heated until the foaming temperature (T_F=190°C), Figure 2b. As the temperature increases, the blowing

agent starts decomposing and the pressure inside the mould increases up to a higher value (P_F). After a certain time (t_F=900s), when the blowing agent is fully decomposed, and PF stabilizes, (does not continue increasing), the pressure of the press is released allowing the polymer to expand until to a desired volume, Figure 2c. The mould was cooled by water spray and air in 300 seconds to reach room temperature (26°C).

The final foam had 23 to 25 mm in height, and 22.5mm in diameter. Figure 1d. The characterization of the density was performed by using the hydrostatic weighing density kit of the balance Mettler Toledo AT261. Relative density (density of the foam divided the density of solid precursor) is used in the paper to make comparisons between materials. X-ray radiographies were used to analyse possible density gradients in the materials.

Once the density is measured the top of the sample was cut at the same height for all the samples(18 mm),Figure 2e. The top part (7 mm thick) was used to characterize the cellular structure by using SEM micrographs using a JEOL JSM-820 microscope, after fracturing the samples previously cooled in liquid nitrogen. The SEM images were analyzed using the software ImageJ to obtain the cellular parameters of the foam. The bottom part of the samples (18 mm thick) was used to characterize their thermal properties by the Transient Plane Source (TPS) method.

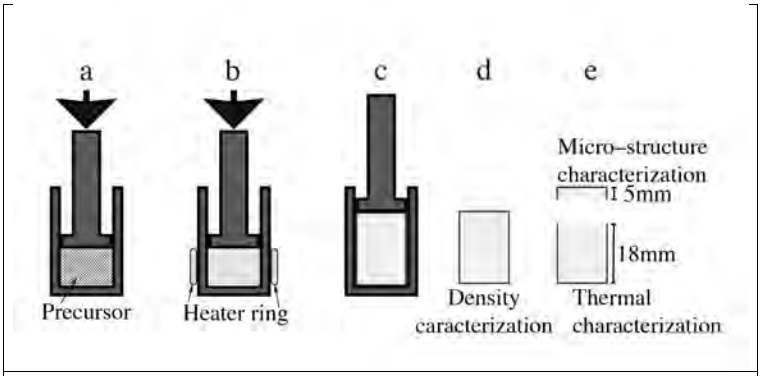

Figure 2: (a-c) Diagram of the ICM foaming steps. (d) Sample used to measure density. (e). Samples used to characterize the cellular structure and thermal conductivity.

In the TPS method, a round and plane heat source is used. It behaves as a transient plane source working simultaneously as a temperature sensor. This element consists of an electrical conducting pattern of thin nickel foil (10μm thick) in the form of double spiral, inserted between two insulating layers made of Kapton (70μm thick), so the final sensor thickness is 150μm. The TPS element is located between two samples with both sensor faces in contact with the two sample surfaces. The two necessary samples for this technique were chosen with similar density and same composition. To perform the experiments a constant electric power is supplied to the “hot-disk” sensor. The increase in temperature $\Delta T(t)$ is directly related to the variation in the sensor resistance R(t) by the equation[19]:

$$R(t) = R_0[1 + \alpha\Delta T(t)] \quad \text{(eq. 1)}$$

where R_0 is the disc resistance at the beginning of the recording (initial resistance) and α is the temperature coefficient of resistance of the nickel foil.

Assuming an infinite sample and the conductive pattern being in the XY plane of a coordinate system, the temperature rise at a point (XY) at time t is obtained by solving the equation for the heat conduction, which relates change in temperature with time.[19-21] In the particular case of our sensor geometry, n concentric ring sources, the spatial average $\overline{\Delta T(\tau)}$ can be obtained through the equation:

$$\overline{\Delta T(\tau)} = P_0\left(\pi^{3/2}a\lambda\right)^{-1} D(\tau) \quad \text{(eq.2)}$$

where P_0 is a Bessel function, D(τ) is a geometric function characteristic of the number n of concentric rings and ΔT(τ) is the temperature increase of the sensor expressed in terms of only one variable τ , defined as:

$$\tau = \left(\frac{t}{\theta}\right)^{1/2} ; \theta = \frac{a^2}{k} \quad \text{(eq. 3 and 4)}$$

Where t is the measurement time from the start of transient heating, θ is the characteristic time, which depends on parameters of both the sensor and the sample, a is the sensor radius and k is the thermal diffusivity of the sample. Thermal conductivity can be obtained by fitting the experimental data to the straight line given by Eqn(1), and thermal diffusivity is calculated from Eqn(3) taking into account the θ value determined experimentally.

The measurements of the thermal properties were performed with two samples of the same relative density, as it is shown in the figure 3. The samples were characterized in two different areas, the inner part (Figure 3a) and the outer bottom area (Figure 3b).

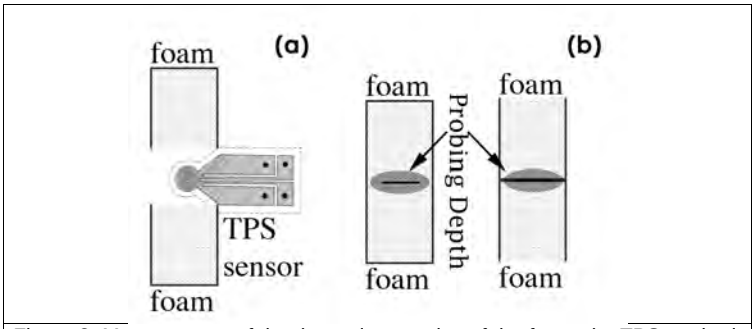

Figure 3: Measurement of the thermal properties of the foams by TPS method. The TPS sensor is placed between to foams of the same relative density and produced using the same pellets. The sensor heats the foams by a 'power output' inside the volume delimited by the 'probing depth'. For each couple of samples the experiments were done in two different configurations.

a)Measurement in the foam core. b)Measurement performed in the outer bottom surface (skin).

A sensor of radius 3.189 mm was chosen. The samples were set ensuring that the boundary conditions to perform the transient plane source experiments were verified (Eqn (2) and (3)). Output power (W) selected was 0.02 W and total measurement time (t) was 20s for all analysed samples. At least five measurements were carried out for each configuration. The probing depth was between 3,5and 4,2 mm in the core and between 3,2 and 3,8 mm in the skin.

3 Results and Discussion

3.1. Density gradients

Figure 4 shows the X-ray radiography of one of the samples (relative density 0.5) and the density as a function of the position (distance from the skin in the direction of the cylinder diameter) for this specific material. Density was calculated from the X-ray image [22]. It is clear from the analysis that there is significant density gradient, density near the surface is close to 600 kg/m^3 and in the core is around 375 kg/m^3. Density reaches a constant value for distances around 7 mm. This type of density gradient was observed both in the thickness direction and in the diameter direction and for all the samples under study.

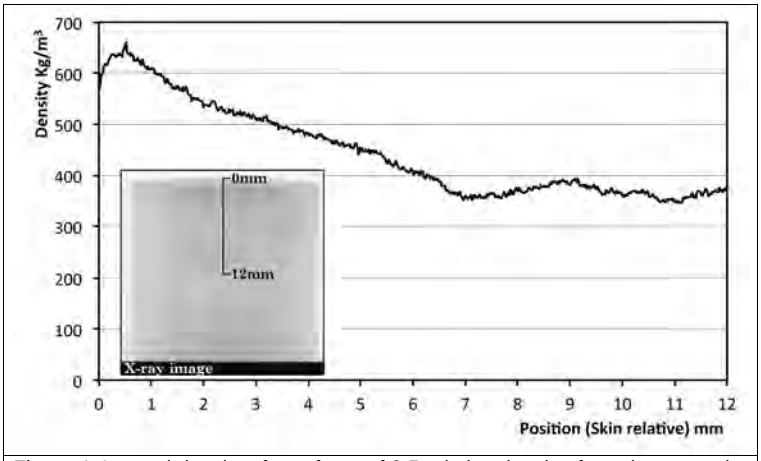

Figure 4: Internal density of one foam of 0.5 relative density, from the top to the centre of the foam in the direction of the axis of the cylinder. The density is obtained by the intensity of grey in the X-ray image.

At the micro-scale the same type of effect is observed (Figure 5). Figure 5 shows a micrograph of a foam with a relative density of 0.5. The cell size is clearly smaller in the area close to the skin, indicating a higher density in this area. It is also clear that there is a progressive change of the cellular structure from the skin to the core.

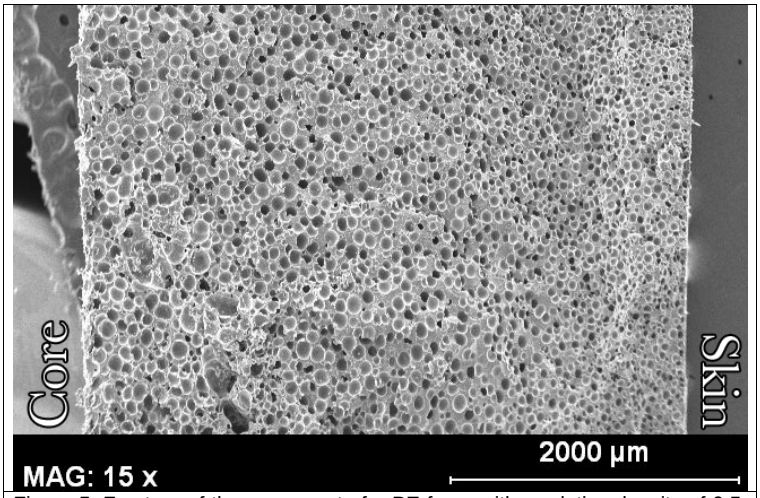

Figure 5: Fracture of the upper part of a PE foam with a relative density of 0.5. The axis of the cylinder is between the words 'Skin' (surface of the foam) and 'Core' (internal part of the foam)

3.2. Cellular structure.

Taking into account the previous density and cellular structure gradients, the comparative study of the cellular structure of foams produced with different amount of blowing agents and bulk densities were performed for samples cut from the inner part of the foam.

The cellular structure is clearly modified when the density is changed. Figure 6 and table 2 shows the SEM images and cellular characteristics of the centre of the foams for three objective densities when the same amount of blowing agent is used. (10.5%).

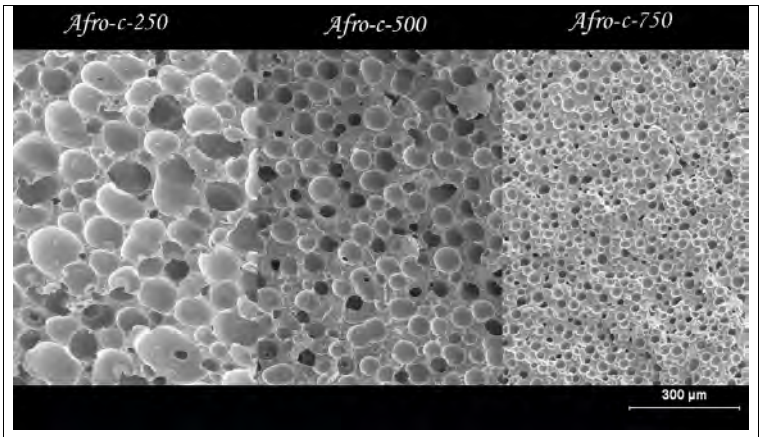

Figure 6: SEM images of the cellular structure of foams produced with the same amount of blowing agent and three different relative densities.

Table 2: Relative density, cellular diameter, cell density of foams, nucleating sites (N.P/cm3) and number of nucleating sites needed to produce a cell (N.P/cell) produced with a CBA content of 10.5% and different relative densities.

Afro-c	CBA content	ρ (relative)	Cell size (µm)	Cell density/cm^3	N.P/cm^3	N.P/cell
(250)	10.5%	0.29	88.77	6.70E+06	1.01E+09	150.1
(500)	10.5%	0.51	38.60	4.91E+07	1.01E+09	20.1
(750)	10.5%	0.73	21.94	1.86E+08	1.01E+09	5.4

As expected the cell size of the foam is reduced when the porosity of the foam is reduced (higher density); the SEM images show a significant degree of cell coalescence for low densities. Assuming that the residues of the CBA act as nucleating sites for the cells it is possible to calculate the Nucleation sites density (N.P/cm3 in the table 2) [23]. Starting from this value and dividing it by the cell density we have determined the number of nucleating sites that are needed to produce one single cell in the final foam. For the high density foams the coalescence is low, only 5.4 nucleating sites are needed to create one cell, there almost no coalescence. This value grows for the medium density foam (20.1) and is around 30 times larger for the low density foams.

On the other hand, figure 7 and table 3 shows the effect of the CBA content on the cellular structure of foams with the same relative density (0.5).

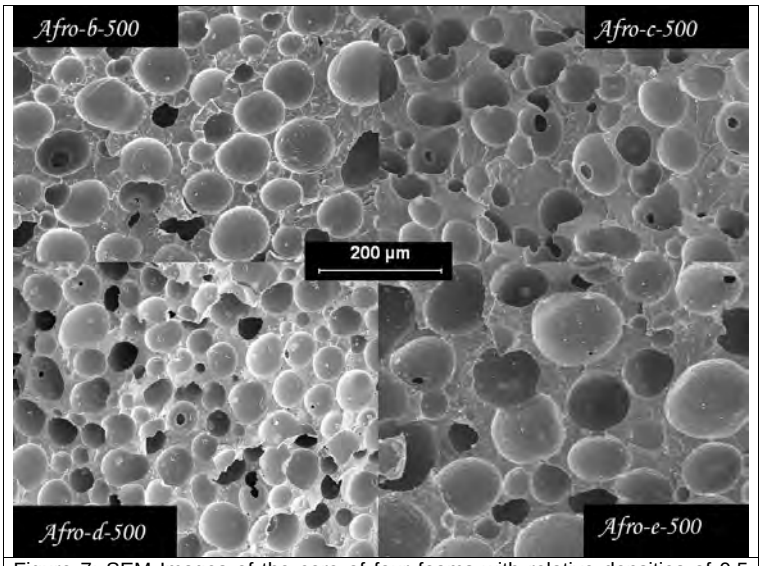

Figure 7: SEM Images of the core of four foams with relative densities of 0.5 and different amounts of CBA.

Table 3: Relative density, cell diameter, cell density, nucleating sites (N.P/cm^3) and number of nucleating sites needed to produce a cell (N.P/cell) for the foams of medium relative density 0.5

(500)	CBA content	ρ (relative)	Cell size (µm)	Cell density/cm^3	N.P./cm^3	N.P/cell
Afro-a	1.2%	0.61	100.9	5.98E+05	1.15E+08	192.2
Afro-b	5.8%	0.53	79.4	5.42E+06	5.56E+08	102.4
Afro-c	10.5%	0.51	38.6	4.91E+07	1.01E+09	20.1
Afro-d	15.6%	0.46	45.5	3.32E+07	1.49E+09	45.0
Afro-e	20.5%	0.45	64.1	1.21E+07	1.96E+09	162.0
Afro-c+R	2*10.5%	0.56	29.0	1.05E+08	1.72E+09	19.1

The results show that and increase of the CBA content up to 10% allows a significant reduction of the cell size and an increase of the cell density. The cell size is reduced from 100 microns for the material produced with 1.2% of CBA to around 40 microns for the material containing 10% of CBA. The cell size slightly increases for the materials containing 15 and 20% of azodicarbonamide. Interestingly the material produced with 10% of active CBA and 10% of residues of the CBA shows the lower cell size and higher cell density. The obtained results can be explained taking into account several simultaneous effects. On the one hand, it is clear that the blowing agent residues act as nucleating sites for the cells. On the other hand, increasing the amount of CBA up to 10% seems to have a positive effect on the foam stability, in fact the number

of nucleating sites to create a cell (N-P) is reduced for this CBA content. This effect deteriorates for higher pressures.

3.3. Thermal Conductivity

Figure 8 shows the experimental values of the thermal conductivity of the foams as function of the density, both of them relatives (i.e the real value was divided by the value of the solid material). Experimental values for the solid PE were 923Kg/m^3 and 0,378 W/mK.

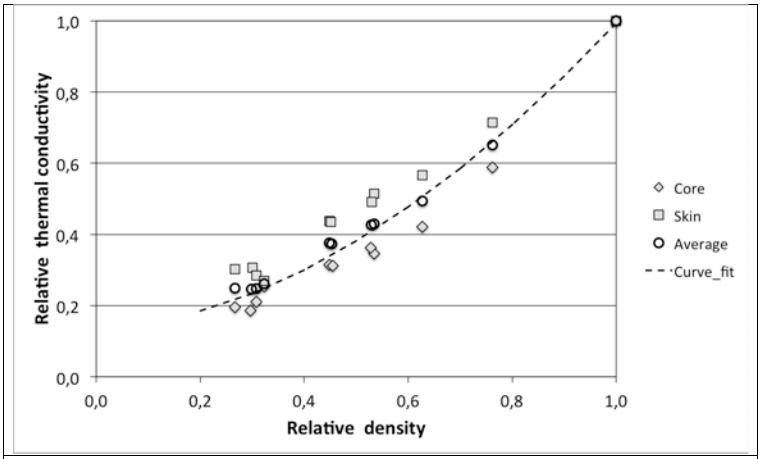

Figure 8: Relative thermal conductivity of the foams under study as function of the relative density.

For each density two data are included in the figure. The data for 'core' and the 'skin' are plotted as it was described in figure 3. The average of these two data is also included in the figure 8.

Ashby introduced a model to study the evolution for any physical property of a foamed material with density. This equation for the thermal conductivity would be as follows[2]:

$$\frac{\lambda}{\lambda_s} = \xi_1 \left(\frac{\rho}{\rho_s}\right)^n \qquad \text{(eq. 5)}$$

Lambda (λ) is the thermal conductivity of the foam; λ_s is the thermal conductivity of the solid material, the density of the material is ρ and the density of the polymer (923 Kg/m^3) is ρs. The constants ξ1 and n depend on the microstructure of the foamed material. The previous equation has to be modified when the gas contribution phase can not be neglected as in the case of polymeric foams. To include the thermal conductivity of the gas phase equation 5 is modified as follows.

$$\frac{\lambda}{\lambda_S} = \xi_1 \left(\frac{\rho}{\rho_s}\right)^n + \xi_2 \left(1 - \frac{\rho}{\rho_s}\right)^n \qquad \text{(eq. 6.2)}$$

This equation has a new constant ξ_2 that is related with the contribution of the thermal conductivity of the gas phase. The experimental data, were fitted to equation 6. The best fitting was for n=1.6±2, ξ_1=0.99±0.04 and ξ_2=0.15±0.08. The relative conductivity of the polymer is 1 (0.378W/mK), and the relative conductivity of the gas (Air) is 0.07 (0.026W/mK).

The fitting for equation 3.2 reproduces very well the average data obtained for the 'skin' and 'core' of the foams. Taking into account that the probing depth of the TPS measurements was lower than the effective distance in which the density reach a constant value it is possible using the fitting of the data to calculate an average value of the density in the area in which the thermal conductivity is measured. Figure 9 shows this idea with one example. For the foam with a bulk relative density of 0.53 (494kg/m^3), the data of thermal conductivity of the skin area can be understood if we assume an average density of the skin of 0.636 (587kg/m^3) and the conductivity of the core can be understood if the density of this area is 0.459 (423kg/m^3). Therefore the density gradient for this specific material can be obtained as the difference between the two previous values.

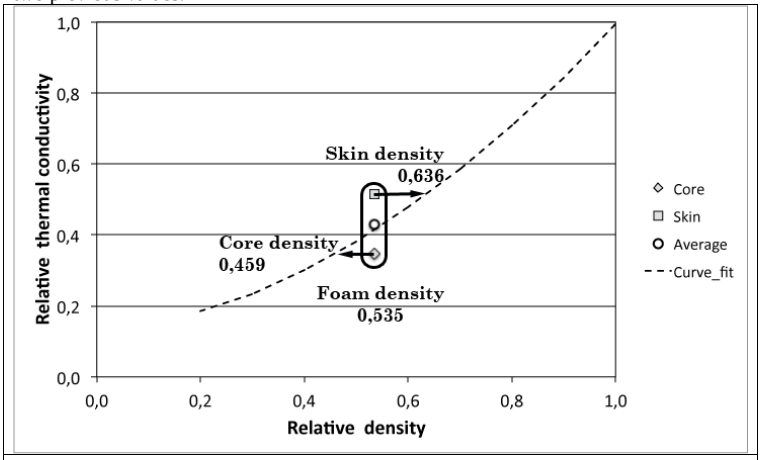

Figure 9: Different densities on the foams calculated using the thermal conductivity results.

The previous procedure was used for the foams with relative density 0.5 and 0.2 produced with different amounts of CBA (figure 10).

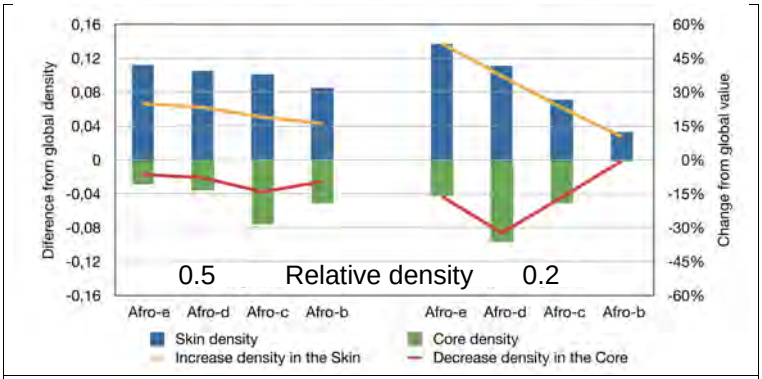

Figure 10: The columns show the difference between the density of the skin (Blue) ad the bulk density and he density of the core density (Green) and the bulk density. The yellow line shows the increase in density in the Skin, and the red line shows the decrease of density in the Core.

In general terms it is clear that the increase in density from the bulk macroscopic density in the skin is larger than the reduction observed for the density of the core. This is logical taking into account the lower thickness of the skin area. For the samples of medium density (relative density 0.5) the differences between the higher density in the skin and lower density in the core is almost constant with a slight reduction when the amount of azodicarbonamide is reduced. This means that the density gradient is almost constant. For the samples of low density (0.2 relative density) there is a clear dependency with the CBA content. The density gradient is higher for the foams produced with higher amounts of azodicarbonamide. This effect can be confirmed by observing the cellular structure of one of these materials (figure 11). It is possible to observe that due to the foaming process and the pressures generated by the gas several cells are crushed near the skin increasing the density in this area.

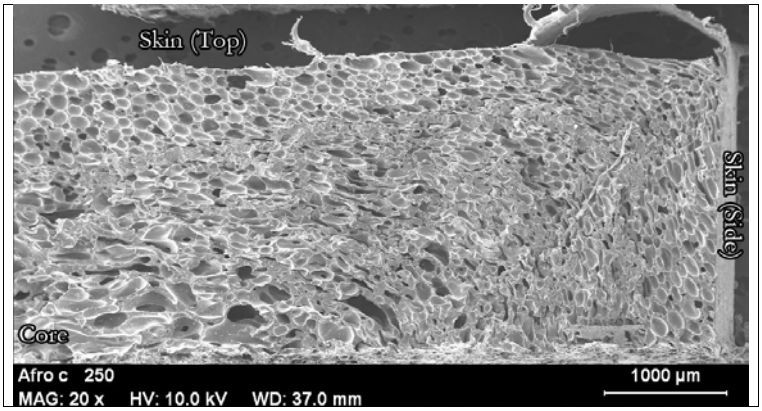

Figure 11: Sample with a relative density of 0.2 and produced with 10.5% of azodicarbonamide. Near of the skin the cellular structure shows a regular structure, 500 μm from the skin several cells are crushed in the direction from core to skin. In the core the cells are 4 times larger than in the skin.

As it was described in the experimental procedure the foams were produced in 1200 seconds with 900 second of heating and 300 of cooling. When the foam is cooled in the mould the exterior part is solidified first, the core of the foam is still in the molten state, with a large amount of gas inside. Due to this and for the low density foams with high amount of blowing agent the cells are deformed near the skin increasing the density. In addition, the core has more time to produce coalescence of the cells and the cell diameter is larger. The high pressure inside the plastic induces a higher amount of polymer along the walls of the mould.

4 Summary and conclusions.

A collection of LDPE foams with different densities have been produced using different amounts of chemical blowing agent. Due to the special features of the improved compression moulding technique it has been possible to produce foams with constant density and different cellular structures.

The cellular structure at the mesoscopic and microscopic scale has been evaluated showing the presence of a skin-core morphology for the foams and the strong effect of the residues as azodicarbonamide as nucleating sites for the cells. It has been proved that an optimum amount of blowing agent (10%) exists when the target is the reduction of the cell size. For this specific content the strong nucleation promoted by the blowing agent residues is combined with a stabilization of the cellular structure due to the pressure generated on the mould.

The characterization of the local thermal conductivity by using the TPS method has allowed establishing the relation between density and thermal conductivity for these materials and taking into account this dependency it has been possible to determine the global density gradient produced during processing. It has been proved that density gradients are more intense when low density foams are produced and when higher amounts of CBA are used.

Acknowledgements

Financial support from the Spanish Ministry of Science and Innovation and FEDER funds (MAT2009-14001-C02-01 and MAT 2012-34901) and the Junta of Castile and Leon (project VA174A12-2) are gratefully acknowledged.

References

1. M.A. Rodríguez-Pérez. Advances in Polymer Science, 184, 97-126, 2005.
2. L. Gibson, F. Ashby. Cellular Solids. Structure and Properties. 2nd Edition. Cambridge University Press, United Kingdom, 1997.
3. R. Gendrom, (Editor) Thermoplastic Foam Processing. Principles and Devlopment. CRC Press, Boca Raton, Florida, 2004.

4. D. Klempner, V. Sendijarevic. Handbook of polymeric foams and foam technology. 2nd Edition. Hanser Publishers, Munich, 2004.
5. D. Eaves. Handbook of polymeric foams. Rapra Technology. United Kingdom, (2004).
6. M.A. Rodríguez-Pérez, J. Lobos, C.A. Pérez-Muñoz, J.A. de Saja, L. González, B.M.A. del Carpio. Cellular Polymers, 27, 347-362, 2008.
7. M.A. Rodríguez-Pérez, J. Lobos, C.A. Pérez-Muñoz, J.A. de Saja. Journal of Cellular Plastics, 45, 389-403, 2009.
8. S. Román-Lorza, M.A. Rodríguez-Pérez, J.A. de Saja. Cellular Polymers, 28, 249-268, 2009.
9. S. Román-Lorza, M.a. Rodríguez-Pérez, J.A. De Saja, J. Zurro. Journal of Cellular Plastcis, 10. 1-21, 2010.
10. S. Román-Lorza, J. Sabadell, J.J. García-Ruiz, M.A. Rodríguez-Pérez, J.A. de Saja. Materials Science Forum, 636/637, 98-205, 2010.
11. M.A. Rodríguez-Pérez, R.D. Simoes, C.J.L. Constantino, J.A. de Saja. Journal of Applied Polymer Science, 212, 2324-2330, 2011.
12. M.A. Rodríguez-Pérez, R.D. simoes, S. Román-Lorza, M. Alvarez-Lainez, C. Montoya-Mesa, C.J.L. Constantino, J.A. de Saja. Polymer Engineering and Science, 52, 62–70, 2012.
13. C. Saiz-Arroyo, J.A. de Saja, M.A. Rodríguez-Pérez. Polymer Engineering and Science, 52, 751–759, 2012.
14. C. Saiz-Arroyo, J.A. de Saja, J.I. Velasco, M.A. Rodríguez-Pérez. Journal of Materials Science, 47, 5680-5692, 2012.
15. C.P. Park. Polyolefin Foams. In: Handbook of Polymeric Foams and Foam Technology, D. Klempner, K.C. Frisch, Eds., Hanser, Munich, 1991.
16. J. H. Exelby, R. R. Puri, D. M. Henshaw and R. F. Grossman. "Formulating Expanded Products, in Handbook of Vinyl Formulating", Second Edition (ed R. F. Grossman), John Wiley & Sons, Inc., Hoboken, NJ, USA. 2007.
17. F. Hidalgo “Design of the optimized parameters for the production process of crosslinked polyolefin foams by compression molding” Ph.D. Thesis, Valladolid 2008 (Spanish).
18. Dongjin Semichem Co., Ltd; “Unicell foaming agents” printed 22 February 2003.
19. S. E. Gustafsson. Review of Scientific Instruments 62, 797–804, 1991.
20. M. Gustavsson, E. Karawacki, and S. E. Gustafsson. Review of Scientific Instruments 65,3856–3859, 1994.
21. M.A. Rodríguez-Pérez, J.I.Velasco, D.Arencón, O.Almanza, J.A. de Saja, J. Appl. Polymer Sci, 75, 156-166, 2000.
22. E. Solórzano, J. Pinto, S. Pardo, F. Garcia-Moreno, M.A. Rodriguez-Perez. Polymer Testing, 32, 321–329, 2013
23. J. S. Colton, N. P. Suh.Polymer Engineering & Science 27, 493–499, 1987.

8.5 Double pressure drop

During the research presented in this section some samples were produced by using two different pressure drops Figure 8.1. A first opening to let the foam reach the half of the volume to grow, then stop in an intermediate position by 10sec (Figure 8.1b) and finally a second pressure drop to reach the final expansion. (Figure 8.1c).

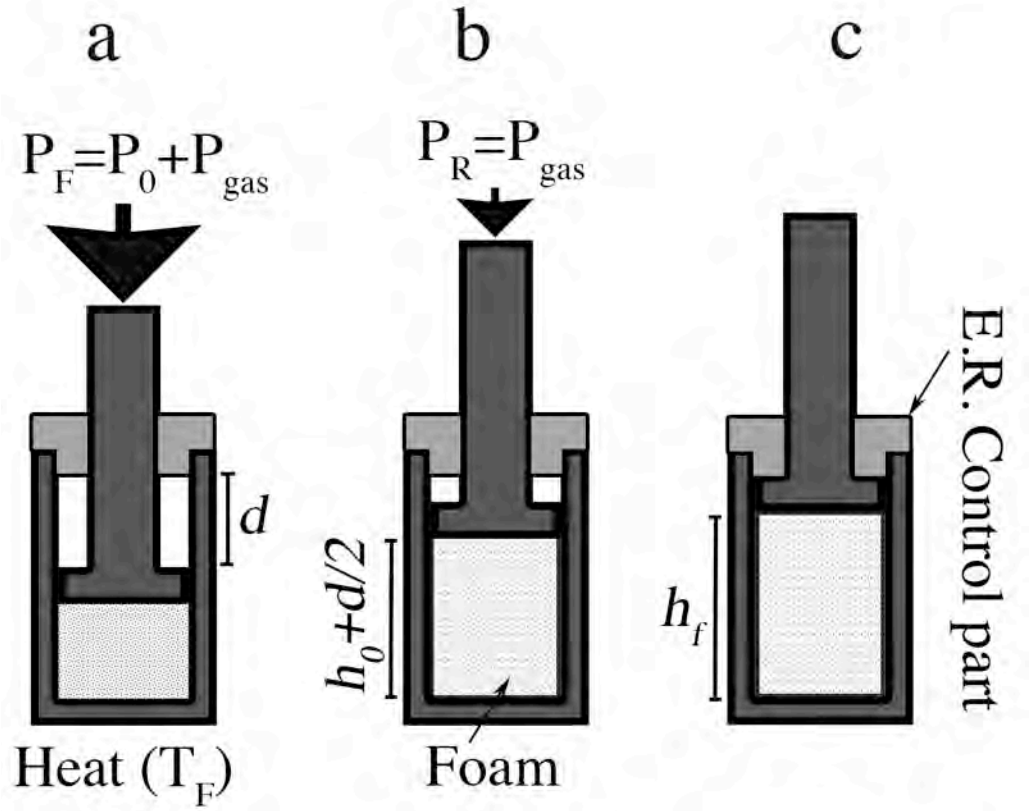

Figure 8.1: *Double pressure drop to produce the foam materials. In some samples not presented in the last paper the piston was opened in two steps. (b) One release to the half of the volume (c) wait 10sec and fill all the volume.*

The samples with double pressure drop had a unique cellular structure as can be seen in Figure 8.3. The cellular structure has two different pores distributions. One of them are larger and the other is smaller but the sizes are regular for the two sizes distribution.The simple experiments show an interesting new application of ICM, related with the production of foams with a bimodal celular structure due to a double nucleation process.

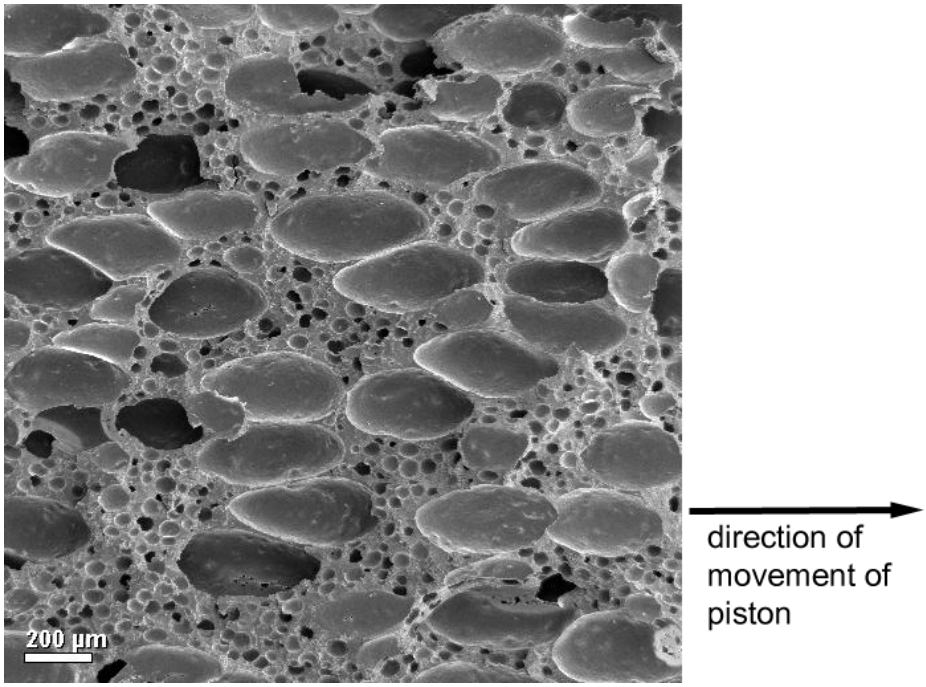

Figure 8.3: *SEM image of a foam with 0.5 relative density and 10% of azodicarbonamide content, foamed with a double pressure drop. The cellular structure of the foams produced by the double nucleation had a double pore size distribution with high regularity of sizes of the two types of cells.*

8.6 Conclusions

The most remarkable contribution of this research was developing the Improved Compression Molding Route (ICM). In the previous chapter we showed that the foams produced by this route could be use as structural support. One of the reasons is the presence of a skin-core morphology. This last chapter has been useful to understand the mechanisms creating this specific morphology.

Due to applied pressure gases coming from decomposition of the blowing agent are dissolved in the molten polymer(Figure 8.4a). Nucleation takes place when the pressure is released mainly in the areas where the residues of the blowing agent are located. The foams growths until the piston reach the maximum height. (Figure 8.4b). The spread water with air cooled quickly the mould and the surface of the foam but the inner part is still melted and the pressure due to the high amount of CBA causes the densification of the external parts creating the skin (Figure 8.4c). Also that molten polymer inside

of the foam had more time to coalescence giving as a result larger cells (Figure 8.4d).

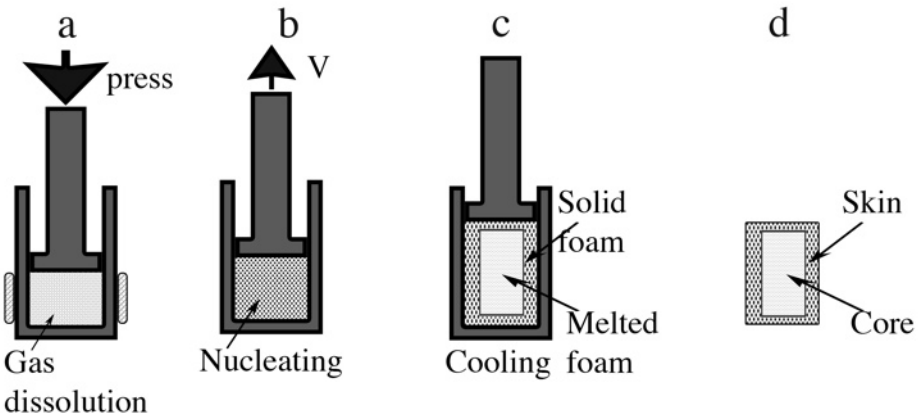

Figure 8.4: *Foaming process of the foams by improved compression molding route: (a)The gas liberated by the blowing agent is dissolved in the polymer. (b) The nucleation is produced in all the precursor when the pressure is released.(c) the foam near the mould walls is frozen by the cooling process. The internal part of the foam is still melted; the pressure due to the high amount of CBA creates the skin-core morphology. In addition coalescence occurs in the inner part (d) As result the foams had a differentiated internal structure a skin near the walls and a lower density with cells of larger sizes in the centre.*

The ideal amount of azodicarbonamide to reduce the cell size is near of 10%. That amount of blowing agent is the optimum to inverse nucleation rate with low coalescence.

The measurements of the thermal conductivity by the TPS method are sensitive to the local density in the area near the sensor. The density gradients in the samples can be estimated by measuring the thermal conductivity.

8.7 References

[1]. Gibson L.J. and Ashby M.F. "Cellular solids", Cambridge, UK: Cambridge University Press, 1997.

[2]. R.C Progelhof, J.L. Throne and R.R. Ruetsch, R. R. Polymer Engineering & Science ***16****, 615, 1976 .*

[3]. D. Klempner and K.C. Frisch, K. C. (Editors) "Handbook of Polymeric Foams and Foam Technology" Hanser 1991.

*[4]. O.A. Almanza, M.A. Rodríguez-Pérez, and J. A. De Saja. Journal of Polymer Science Part B: Polymer Physics **38**, 993, 2000.*

*[5]. M. Gustavsson, E. Karawacki, and S. E. Gustafsson. Review of Scientific Instruments **65**, 3856, 1994.*

*[6]. E. Solórzano, M. A. Rodríguez-Pérez, J. A. Reglero, J. A. de Saja. Journal of Materials Science **42**, 2557, 2007.*

*[7]. E. Solórzano, J.A. Reglero, M.A. Rodríguez-Pérez, D. Lehmhus, M. Wichmann, J.A. de Saja. International Journal of Heat and Mass Transfer **51**, 6259, 2008.*

*[8]. E. Solórzano, M. A. Rodriguez-Perez, J. A. de Saja. Advanced Engineering Materials **10**, 371, 2008.*

[9]. J.P. Holman, "Heat Transfer", McGraw-Hill, New York, 1981.

*[10]. E. Solórzano, M.A. Rodriguez-Perez, J. Lázaro, J.A. de Saja. Advanced Engineering materials **11**, 818, 2009.*

9 Conclusiones

9.1 Introducción

En esta tesis se han estudiado en dos tipos de materiales porosos y a pesar de tener diferentes matrices (matriz metálica para los materiales tipo lotus y polimérica para las espumas termoplasticas) la caracterización celular y tratamiento teórico de ambos materiales ha sido equivalente.

El principal objetivo de la tesis era acercar los valores mecánicos de rigidez y resistencia de los materiales celulares a los de los materiales estructurales no porosos usados en la actualidad, con el objetivo final de sustituir los materiales no porosos por otros espumados con el consiguiente ahorro de peso y de coste. En las gráficas 9.1 y 9.2 se pueden ver los resultados de las propiedades mecánicas elásticas (módulo de Young) y plásticas (Límite elástico) para todos los materiales estudiados Como referencia para los materiales metálicos se incluyen los valores del cobre. Las espumas poliméricas se comparan con el mismo material sólido, para este caso se incluyen los materiales celulares de diferentes densidades.

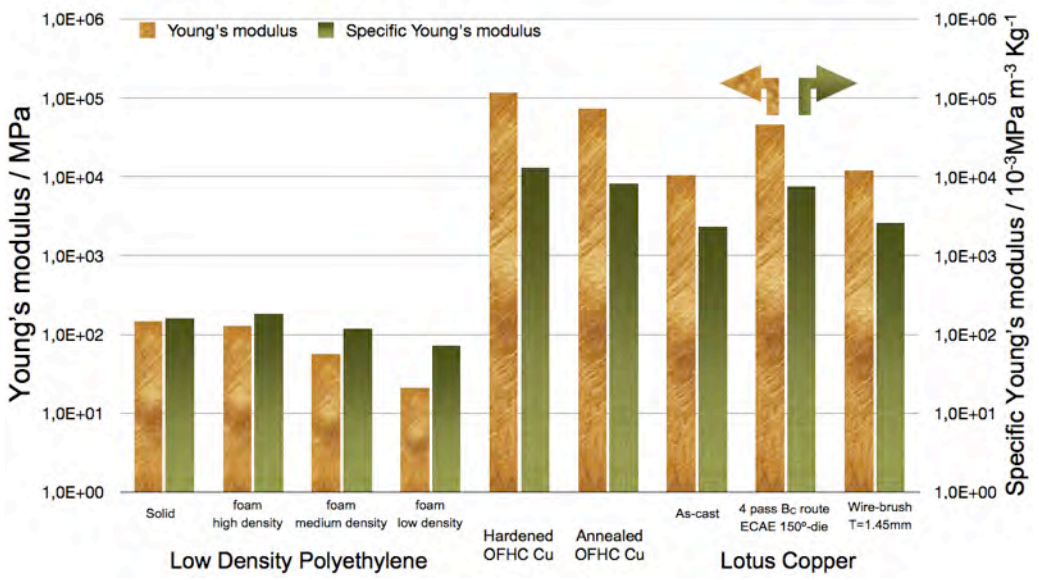

Gráfica 9.1: *Módulo de Young y módulo de Young especifico para algunos de los materiales estudiados en la presente tesis.*

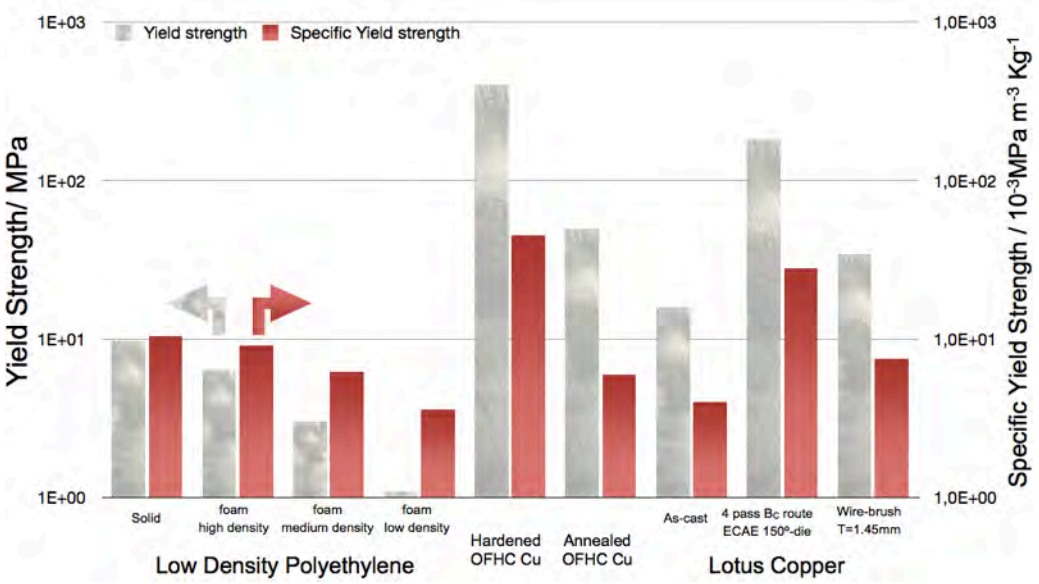

Gráfica 9.2: *Límite elástico y limite elástico especifico para algunos de los materiales estudiados en la presente tesis.*

En la comparación entre los materiales poliméricos y metálicos se puede ver como el módulo de Young de los segundos es entre 15 y 1000 veces superior en todos los casos. Aunque en el módulo de Young especifico se reducen esas diferencias a solo entre 3 y 83 veces superior.

Para el límite elástico de los materiales se conservan esas diferencias pero no son tan acusadas ya que entre el polietileno de baja densidad solido y los materiales metálicos el límite elástico de los metálicos solo es superior entre 2 y 40 veces. Pero el limite elástico especifico para los materiales metálicos no forjados (Annealed OFHC Cu y As-cast lotus copper) es inferior al limite elástico especifico para el polietileno sólido, incluso al especifico de las espumas de polietileno de alta densidad y media densidad.

En la presente tesis se han producido y caracterizado los siguientes materiales:

- Cobre poroso tipo lotus producido mediante moldeado en fundido (mold casting technique). La porosidad de estas muestras era de 47.5±2.4% (densidad relativa 0.48) y el diámetro medio 144µm.
- Cobre poroso tipo lotus producido mediante la técnica de fundición continua (continuous casting technique). La porosidad de estas muestras era de 46.3±0,4% con un diámetro medio de 338µm.

- Espumas microcelulares de polietileno producidas mediante moldeo por compresión mejorado (improved compression molding). La densidad relativa de estas espumas estaba entre 0.27 y 0.92 (73% y 8% de porosidad) mientras que el diámetro medio de celda oscilaba entre 90µm para las espumas de 80% de porosidad y 30µm para las espumas de 20% de porosidad.

Se recogen a continuación las conclusiones obtenidas para ambos tipos de materiales.

9.2 Metales porosos tipo lotus

Como se puede ver en las gráficas 9.1 y 9.2, las muestras de cobre poroso tipo lotus (as-cast) tienen unas propiedades mecánicas, módulo de Young especifico 26 veces inferior y límite elástico especifico 10 veces inferior, muy reducido frente a un metal forjado de referencia como puede ser el cobre libre de oxigeno (Hardened OFHC Cu). Incluso, debido al proceso de enfriamiento del cobre poroso tipo lotus, sus propiedades mecánicas son inferiores a cuando la muestra de referencia es sometida a un proceso de recocido donde se aumenta el tamaño de grano de la muestra (Annealed OFHC Cu). En particular el módulo de Young especifico es 16 veces inferior y límite elástico especifico 1,6 veces inferior. Las muestras celulares tipo lotus producidas por moldeado en fundido y fundición continua tenían las mismas propiedades mecánicas. Estas muestras fueron sometidas a dos procesos distintos de forjado en frío para mejorar la microestructura de matriz metálica. Se han obtenido las siguientes mejoras:

- La superficie de las muestras producidas mediante moldeado en fundido fueron procesadas por un cepillo de alambres (wire-brush) para mejorar las propiedades mecánicas del conjunto.
- El procesado por wire-brush refinó el tamaño de los cristales de cobre en la superficie, hasta 20~60µm de profundidad, como se esperaba en un proceso del tipo NS·SPD. El tamaño de grano promedio se redujo desde varios milímetros a unos 150 nanómetros con 200 mm^{-1} de velocidad de rotación por milímetro (300 nanómetros cuando el proceso fue realizado a 100mm^{-1}).
- El límite de comienzo de la deformación plástica fue incrementado con el proceso de wire-brush especialmente cuando los parámetros de procesamiento eran 3750rpm y 100 mm^{-1}. En ese caso, todos los poros estaban cerrados por la deformación de la superficie.
- Dado el reducido tamaño de la capa deformada la densidad relativa de las muestras se mantiene casi inalterada.

- La dureza Vickers en la superficie aumentaba cerca de 5 veces cuando las muestras eran procesadas a 5.000 rpm y 200 mm^{-1}.
- El limite elástico de las muestras depende de la microestructura original del cobre y de la microestructura de la capa deformada, así la mejora de la resistencia a la fluencia de las muestras dependerá inversamente del espesor de las muestras procesadas, ya que el tamaño de la capa deformada solo depende del proceso de cepillado. En las gráficas 9.1 y 9.2 se muestran la mayor mejora conseguida por la muestra de espesor 1,45 mm, con un aumento de 46% del límite de elasticidad específico. En las muestras de mayor espesor, 3,74 mm de grosor, sólo se aumenta un 3% el límite de elasticidad específico.
- Las muestras producidas mediante la técnica de fundición continua fueron procesadas por ECAE con un ángulo en el canal de 150°. El paso de la muestra a través del ángulo introduce deformaciones en la microestructura metálica que mejora sus propiedades.
- El ángulo de 150° del canal reduce la porosidad de las muestras una media aproximada de un 7% en cada paso, tras 4 pasos la porosidad de las muestras se ha reducido un 23%.
- El límite elástico especifico se incrementó cerca de 10 veces cuando las muestras de cobre poroso tipo lotus fueron procesados por ECAE con un ángulo en el canal de 150 ° por ruta C. El aumento fue ligeramente menor cuando la ruta era A o Bc.
- Las muestras procesadas por ECAE alcanzan el 60% del límite elástico específico de la muestra de referencia de cobre OFHC.
- Por el procesado por ECAE el módulo de Young especifico aumenta hasta alcanzar el del cobre de referencia templado (Annealed OFHC Cu) y alcanzar el 60% del módulo de Young de la muestra de referencia de cobre OFHC.
- En las muestras procesadas, la dureza Vickers muestra una clara dependencia entre la posición relativa de ese punto con el del ángulo.
- La dureza Vickers más alta, 2 veces superior a la original, se consigue por la ruta C en el lado que pasa por el interior del ángulo, después de 4 pasos.
- El proceso por ECAE no afectó al tamaño de grano del cobre. Por lo que se puede observar los defectos introducidos se acumulan en la red cristalina del metal sin estabilizarse en la formación de nuevas fronteras de grano.

9.3 Materiales celulares en base polietileno

Para fabricar las espumas de polietileno microcelular se desarrollo un nuevo procedimiento. En esta tesis se presentan las primeras espumas producidas con el "moldeo por compresión mejorado". Las principales conclusiones obtenidas son las siguientes:

- La nueva tecnología de fabricación permite fabricar materiales con celdas de tamaños por debajo de las 100 micras en un amplio rango de densidades y utilizando un matriz polimérica semicristalina y no reticulada.
- Las muestras de las espumas de PE presentan diferencias en la densidad en la superficie de las espumas (piel) y el centro de las espumas (núcleo) creando una estructura celular similar a la del hueso.
- Las muestras de la mayor densidad presentar un valor inesperadamente alto del módulo de Young, más alto que el exponente n = 1, considerado como límite teórico para este tipo de materiales. Efecto que puede ser debido a la orientación de las cadenas de polímero durante la formación de espuma o a la piel que presentan estos materiales.
- Para las espumas de densidad media-alta el módulo de Young en relación con la densidad de las muestras tiene un exponente de n = 1. Cuando la densidad disminuye, los valores para el módulo de Young se acercan al exponente n=2.
- El límite de elasticidad se ajusta a la ecuación de Ashby con un exponente de n=2 para todas las muestras, independientemente del tamaño medio de celda o la cantidad de azodicarbonamida utilizada para producir la espuma.
- Los residuos de la azodicarbonamida son puntos de nucleación adecuados para producir la espuma mediante una nucleación heterogénea.
- Todas las muestras estudiadas tenían un diámetro medio celular inferior a 100µm. El tamaño promedio mínimo de celda se consiguió en las espumas de alta densidad (densidad relativa 0.8) con diámetros celulares ligeramente superiores a las 30µm.
- La coalescencia crece rápidamente cuando tratamos de hacer espumas de densidad más baja, debido a la baja viscosidad del polietileno fundido y la inexistencia de un mecanismo de estabilización.
- Mediante la simulación por elementos finitos tomando como modelo las espumas producidas, un panel espumado (en el rango de los 300Kg/m^3) puede lograr soportar la misma carga que un panel del polímero sólido ahorrando un 34% del polímero, así mismo una tubería espumada (en el rango de los 300Kg/m^3) puede ahorrar un 40% del material usado para que una tubería solida soportase la misma carga.
- Se ha observado que al aumentar la cantidad de agente espumante en las espumas aumenta el gradiente de densidad entre la piel y el núcleo de las espumas producidas para una misma densidad global.
- Los residuos del agente espumante (Azodicarbonamida) son puntos de nucleación para las celdas.
- La caracterización de la conductividad térmica mediante el método TPS ha permitido establecer la relación entre la densidad y la conductividad térmica de estos materiales, y teniendo en cuenta esa dependencia ha sido posible determinar el gradiente de densidad global que se consigue con el método de compresión mejorado.

9 Conclusions (translation)

9.1 Introduction

In this thesis we have studied two types of porous materials (lotus type porous metals and microcellular materials produced from polyethylene) and despite having different type of matrices the cellular characterization and theoretical treatment of both materials have been the same.

The main objective of this thesis is to approximate the mechanical values of stiffness (Young' modulus) and strength of cellular materials to that of non-porous structural materials used today with the ultimate objective of replacing the non-porous materials by cellular materials with consequent weight and cost reduction. Figures 9.1 and 9.2 show the results of Young's modulus and yield strength for the main materials produced in this investigation. OFHC copper is included as a reference for metallic materials. Polymeric foams are compared with the solid polyethylene used as matrix.

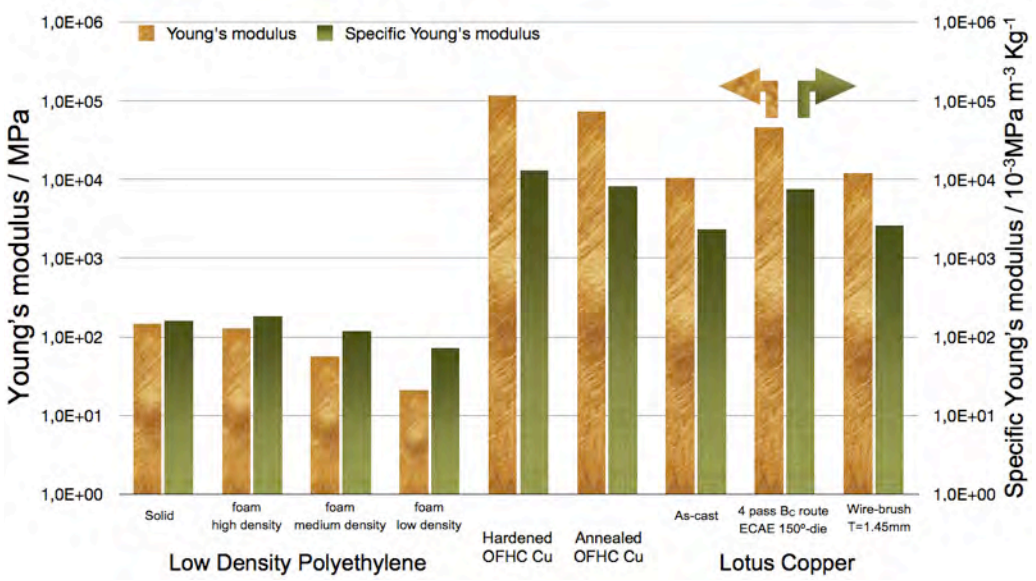

Figure 9.1: *Young's modulus and Specific Young's modulus for the main materials studied in this research.*

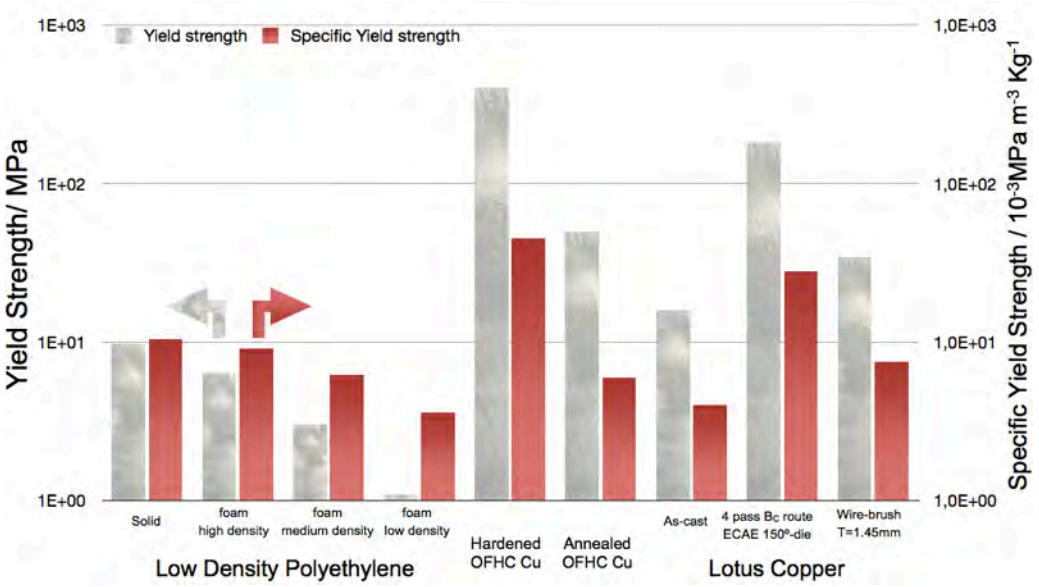

Figure 9.2: *Yield strength and Specific Yield strength for some materials studied in this research.*

The Young's modulus of the metals is between 15 and 1000 times higher than that of the polymers. The differences are reduced for the specific Young's modulus to values between 3 and 83 times.

The yield strength of the metallic materials is also higher than that of the polymeric ones, but the differences are reduced to only between 2 to 40 times. However, the specific yield strength for the cast metals (Annealed OFHC Cu and As-cast copper lotus) is lower than the specific yield strength of some of the polymeric materials, in particular the bulk polyethylene, the high density foam and the medium density foam.

During the present thesis the following materials have been produced and characterized:

- Lotus-type porous copper was produced by mold casting technique. The porosity of these samples was 47.5±2.4% (relative density 0.48) and the average diameter 144µm.
- Lotus-type porous copper was also produced by continuous casting technique. The porosity of these samples was 46.3 ± 0.4% with an average cell diameter of 338µm.
- Polyethylene microcellular foams were produced by using the new technique named improved compression molding. The relative density of these foam was between 0.27 and 0.92 (73% to 8% porosity) while the

average diameter ranged from 90µm (for foams of 80% porosity) to 30µm (for foams of 20% porosity).

The main conclusions obtained for each type of materials are summarized in the following paragraphs.

9.2 Lotus metals

As it can be seen in Figures 9.1 and 9.2 samples of lotus type porous copper (as-cast) have mechanical properties lower than that of the metal used as reference (oxygen-free high thermal conductivity copper (OFHC Cu)). The specific Young's modulus is 26 times lower and specific yield strength is 10 times lower. Even, due to the cooling process used to produce the lotus-type porous copper, their mechanical properties are lower than the annealed samples of OFHC Cu; specific Young's modulus is 16 times lower and specific yield strength is 1.6 times lower. The mechanical properties of the samples produced by the mold casting technique and the samples produced by continuous casting technique are almost the same. These samples were subjected to two different forging processes to improve the metallic matrix microstructure obtaining the following improvements:

- The surface of the samples produced by the mold casting technique were processed by a wire-brush technique to improve the mechanical properties of the samples.
- As it was expected for a NS·SPD technique, the wire-brush refines the grain size of copper from the surface until 20µm to 60µm in depth,. The average grain size was reduced from several millimeters to just 150 nanometers when a rotational speed per millimeter of 200mm^{-1} was used (300 nanometers when the speed was 100mm^{-1}).
- The yield stress increased especially when processing parameters were 3750rpm and 100mm^{-1}. In that case all the pores were closed by the deformation of the surface.
- Given the limited size of the deformed layer relative density of the samples remains almost unchanged.
- The Vickers hardness in the surface was improved by wire-brush. The improvement was near 5 times when the wire-brush was performed at 5000 rpm and 200mm^{-1}.
- The yield strength of the samples depends on the original microstructure of the copper and the microstructure of the deformed layer. In fact, the improvement of the yield strength of the samples depends inversely on the thickness of the processed samples. Figures 9.1 and 9.2 show that the best improvement obtained using samples of 1.45 mm in thickness was 46% in

the specific yield strength. The thicker sample, 3.74 mm thick, only shown an increase of 3% in specific yield strength.

- The samples produced by the continuous casting technique were processed by ECAE with a die angle of 150°. The passage of the sample through the angle introduces distortions in the metal microstructure. These modifications improve the mechanical properties
- The channel angle of 150° reduces the porosity the samples about 7% in each step (average value). After 4 steps porosity of the samples was reduced by 23%.
- The yield strength was increased near 10 times when de samples of the lotus copper were processed by by route C. The increase was slightly lower when the routes used were A or Bc.
- The samples of lotus-type porous copper processed by ECAE reach 60% of specific yield strength and specific Young's modulus of the reference sample (OFHC copper).
- Vickers hardness shows a clear dependence with the position in the sample with respect to the angle of the ECAE die.
- The highest Vickers hardness, 2 times higher than that of the reference, is achieved by the route C (after 4 passes) on the side that passes through the inside of the angle.
- The ECAE process did not affect the grain size of lotus copper. The defects introduced by ECAE process remain in the metal lattice without forming new grain boundaries.

9.3 Polyethylene foams

A new process was developed to produce the polyethylene microcellular foams. This thesis presents the first foams produced with the process now called "improved compression molding". The main conclusions obtained are:

- The novel developed technology allows producing cellular materials withe cells below 100 microns, in wide density range and using a noncross-linked semicrystalline matrix.
- The produced PE foams present differences in density on the surface of the foams (skin) and the center of the foams (core). Therefore, they can be considered as structural foams with a bone-like structure.
- The samples with the highest densities present an unexpected high value of Young's modulus, exponent higher than n = 1 (theoretical limit). This is due to the orientation of the polymer chains during foaming and the presence of a solid skin.

Conclusions

- The Young´s modulus maintain an exponent of n=1,for the high density and medium foams. When the density decreases, the values for Young's modulus are close to the line for the exponent n = 2.
- The yield strength did present an exponent n=2 for all the samples, regardless of the average cell size or quantity of azodicarbonamide used to produce the materials.
- Azodicarbonamide residues are good nucleating agents to form the foam in an heterogeneous nucleation process.
- All samples tested had an average cell diameter lower than 100µm . The minimum average cell size (30 µm) was achieved for foams with high densities (relative density 0.8)
- Coalescence grows rapidly when the foams density is reduced, due to the low viscosity of the molten polyethylene and the absence of stabilization mechanisms.
- Using FEM it has been demonstrated that the materials can be used to produce lightweight structural panels and pipes. In panels weight reductions up to 34% can be reached using foams with densities in the range of 300 kg/m^3. In pipes weight reductions up to 40% can be reached using foams with densities in the range of 300 kg/m^3.
- It has been proved that density gradients are more intense when low density foams are produced and when higher amounts of CBA are used.
- The residues of the chemical blowing agent used (azodicarbonamide) are nucleating sites for the cells
- The characterization of the local thermal conductivity by using the TPS method has allowed establishing the relation between density and thermal conductivity for these materials and taking into account this dependency it has been possible to determine the global density gradient produced during processing.